UNIVERSITY OF SOUTHAMPTON

FACULTY OF PHYSICAL AND APPLIED SCIENCES

Electronics and Computer Science

The cell-free expression of ion channels and electrophysiological measurements in interdroplet bilayers

by

Mark Samuel Friddin

A thesis submitted in partial fulfillment for the degree of Doctor of Philosophy

May 2014

UNIVERSITY OF SOUTHAMPTON

ABSTRACT

FACULTY OF PHYSICAL AND APPLIED SCIENCES
Electronics and Computer Science

Doctor of Philosophy

THE CELL-FREE EXPRESSION OF ION CHANNELS AND ELECTROPHYSIOLOGICAL MEASUREMENTS IN INTERDROPLET BILAYERS

by Mark Samuel Friddin

Ion channels are membrane proteins of interest for medical research and drug discovery, however a major bottleneck in obtaining functional measurements is the requirement to over-express the channel *in-vivo*. Cell-free (CF) protein expression is an alternative *in-vitro* approach capable of expressing proteins from a supplied DNA template - the method is fast, requires minimal apparatus and can be stabilised for the expression of membrane proteins by the addition of lipids or detergents. One drawback is the expense of commercial CF systems, however this can be economised by performing the reaction in microdroplets. This is attractive as microdroplets immersed in lipid-oil can be manipulated into contact to form a lipid bilayer, potentially allowing for ion channel expression and characterisation to be fully coupled. This study addresses the feasibility of achieving this goal by first investigating the stability of interdroplet bilayers formed in the presence of pre-incubated CF systems. Under these conditions the bilayers failed in $<$10 min, however a combination of diluting the mixture and adding vesicles was found to enable measurements of $>$30 min. The CF expression of the small prokaryotic potassium channel KcsA was then verified, in addition to the pore domain region of the eukaryotic hERG channel, where 20 ng/μl-74 ng/μl was expressed depending on the reaction conditions. Single-channel currents were subsequently obtained in interdroplet bilayers formed directly from the CF mixture, indicating that the channels were capable of self-inserting into the bilayer for measurements in both cases. The findings of this study support the feasibility of coupling the CF expression and electrical characterisation of ion channels in microdroplets and represent a progression toward the development of a high-throughput platform for screening novel pharmaceutical compounds.

Contents

Nomenclature

APS	Ammonium persulfate
ATP	Adenosine triphosphate
BLM	Bilayer lipid membrane or Black lipid membrane
BODIPY	Boron-dipyrromethane
BSA	Bovine serum albumin
CAD	Computer aided design
CECF	Continuous exchange cell-free
CF	Cell-free
CFCF	Continuous flow cell-free
CMC	Critical micellar concentration
D-CF	Detergent assisted cell-free
DEP	Dielectrophoresis
DHB	Droplet-hydrogel bilayer
DIB	Droplet interface bilayer
DOPC	1,2-dioleoyl-*sn*-glycero-3-phosphocholine
DPhPC	1,2-diphytanoyl-*sn*-glycero-3-phosphocholine
eGFP	Enhanced green fluorescent protein
GFP	Green fluorescent protein
GPCR	G protein coupled receptor
GTP	Guanosine triphosphate
GUV	Giant unilamellar vesicle
HEPES	4-(2-hydroxyethyl)-1-piperazineethanesulfonic acid
hERG	The product of the human ether-à-go go-related gene
HRP	Horseradish peroxidase
IPTG	Isopropyl β-D-1-thiogalactopyranoside
KcsA	Potassium crystollographically-sited activation channel
kDa	Kilo Dalton
L-CF	Lipid assisted cell-free
LOC	Lab on a chip

mRNA	Messenger ribonucleic acid
Ni-NTA	Nickel-nitrilotriacetic acid
NTP	Nucleoside triphosphate
P-CF	Precipitate assisted cell-free
PBS	Phosphate buffered saline
PCR	Polymerase chain reaction
PDMS	Polydimethylsiloxane
PEG	Polyethylene glycol
PMMA	Poly (methyl methacrylate)
POPE	1-palmitoyl-2-oleoyl-*sn*-glycero-3-phosphoethanolamine
POPG	1-palmitoyl-2-oleyl-*sn*-glycero-3-phospho-(1'-rac-glycerol)
PURE	Protein synthesis using recombinant elements
RAM	Regulated attachment method
RNA	Ribonucleic acid
SDS PAGE	Sodium dodecyl sulfate polyacrylamide gel electrophoresis
TEA	Tetraethyl ammonium
TEMED	Tetramethylethylenediamine
tRNA	Transfer ribonucleic acid
αHL	α-Haemolysin

Declaration of Authorship

I, Mark Samuel Friddin, declare that the thesis entitled *The cell-free expression of ion channels and electrophysiological measurements in interdroplet bilayers* and the work presented in the thesis are both my own, and have been generated by me as the result of my own original research. I confirm that:

- this work was done wholly or mainly while in candidature for a research degree at this University;
- where any part of this thesis has previously been submitted for a degree or any other qualification at this University or any other institution, this has been clearly stated;
- where I have consulted the published work of others, this is always clearly attributed;
- where I have quoted from the work of others, the source is always given. With the exception of such quotations, this thesis is entirely my own work;
- I have acknowledged all main sources of help;
- where the thesis is based on work done by myself jointly with others, I have made clear exactly what was done by others and what I have contributed myself;
- parts of this work have been published as: (Friddin et al., 2013a,d,c,b) and (Friddin et al., 2012)

Signed:.....

Date:.....

Acknowledgements

I owe much gratitude to the many people who have helped me along this journey, only a few of which I can mention in this short acknowledgement. Recognition should first go to my supervisors Dr. Maurits de Planque and Professor Hywel Morgan for offering me this opportunity and for their guidance throughout the course of this study. The Engineering and Physical Sciences Research Council (EPSRC) are also acknowledged for providing the funding required for this PhD. This work would also not have been possible if it were not for the help of project collaborators, Dr. Philip Williamson, Dr. Natalie Smithers, and Maïwenn Beaugrand from the Centre for Biological Sciences. I would also like to thank Katie Chamberlain for fabricating the planar microelectrodes used in this study and the rest of the Hybrid BioDevices Group for constantly offering guidance, advice and camaraderie. In addition, I am especially grateful to all of the people I lived with and got to know during my three years in Southampton - your friendship, counsel and banter was invaluable. I would also like to thank my friends from home for their support throughout this process, particularly to Declan and Sara for helping with the proofreading of this thesis. Finally, I would like to thank my parents, sisters and family for always encouraging me to succeed.

For Booba,

Chapter 1

Introduction

1.1 Objectives and outcomes of the PhD study

The purpose of this doctoral study was to determine the feasibility of coupling the cell-free (CF) expression and electrical characterisation of ion channels in microdroplets. A fundamental requirement to achieve this was to first demonstrate that interdroplet bilayers could be stabilised in the presence of a CF mixture to enable the measurement of single-channel currents. The next priority was to verify the CF expression of ion channels without the use of isotopic labels and to identify the key parameters that influence the protein yield. Further to addressing the bilayer stability and confirming protein expression, the final objective of this study was to determine whether CF expressed ion channels could spontaneously self-insert into an interdroplet bilayer for electrophysiological characterisation, directly from the CF expression mixture, without any purification or reconstitution.

The stability of interdroplet bilayers formed in the presence of a CF mixture is studied in Chapter 4, where electrophysiological screening of three different commercial CF mixtures allowed for the components of the systems responsible for destabilising the membrane to be identified. Stabilisation of the bilayer was achieved by diluting the system and adding vesicles, allowing for electrical measurements to be obtained for a minimum of 30 minutes.

The cell free expression of ion channels is shown in Chapter 5 by protein gel electrophoresis of purified KcsA obtained from a CF mixture supplied with the KcsA DNA template. The same method was also used to show the CF expression of the pore domain of the eukaryotic hERG channel as verified by Western Blotting.

Interestingly it was found that adding vesicles or increasing the amount of DNA supplied to the CF system led to a significant increase in the amount of KcsA expressed, however the same effect was not found with the hERG construct.

In Chapter 6 it is shown that single channel currents of KcsA and the hERG pore domain are obtained when an interdroplet bilayer is formed with a 2 μl droplet of buffer and a 2 μl droplet of the unpurified CF expression mixture incubated with the relevant DNA template. This outcome indicates that ion channels expressed *in situ* can spontaneously self-insert into interdroplet bilayers for electrophysiological measurements, without the need for protein purification or reconstitution.

The findings presented in Chapters 4, 5 and 6 support the concept of coupling the expression and characterisation of ion channels in microdroplets and provide preliminary data for conditions that support spontaneous channel insertion in combination with bilayer survival.

1.2 Novelty and contributions of the PhD study

The novel aspects of the research presented in this study are:

- The stability study of interdroplet bilayers formed in the presence of three commercial CF systems and their respective components. All three systems were found to destabilise the interdroplet bilayer. However, the cell-lysate fraction was identified to cause bilayer rupture while the reaction mixture caused elevations and spikes in the bilayer current. It was found that diluting the CF system 10x and adding vesicles to the reaction mixture enabled stable current measurements to be obtained for experiments lasting 30 minutes.
- Single-channel electrophysiology of cell-free expressed ion channels by direct incorporation into interdroplet bilayers. The CF expression of KcsA and the novel hERG$_{S5-S6}$ pore domain construct, was verified by purification followed by SDS PAGE. It was shown that single channel measurements could be obtained in interdroplet bilayers formed directly from each sample without purification or reconstitution. This shows that spontaneous-insertion of cell free expressed ion channels into interdroplet bilayers is a general phenomenon that is not specific for the small viral potassium channel Kcv (Syeda et al., 2008).

1.3 Scientific Relevance

This section outlines the motivations for studying ion channels and explains the limitations in obtaining measurements using conventional techniques. The rationale for using the cell-free method and the incentives for miniaturisation are then introduced before the ideal of coupling the expression and characterisation of ion channels in microdroplets is discussed.

The medical relevance of membrane proteins

Membrane proteins (Fig 1.1) are targets for approximately 50% of all drugs and account for ∼25% of all polypeptides encoded in the human genome (Overington et al., 2006). Yet despite their clinical significance, difficulties in expressing and purifying sufficient amounts of membrane proteins for analysis has resulted in a bottleneck in structural and functional studies (Junge et al., 2011). Ion channels are an important class of membrane proteins that mediate ion flow across cellular membranes and are responsible for a number of processes including the excitability of neurons and the regulation of cardiac rhythm (Hille, 2001). Obtaining electrical measurements of ion channels is therefore essential for studying their roles in normal physiology and for understanding their function in ion channel-related diseases, known as channelopathies (Celesia, 2001; Abraham et al., 1999). For this purpose the model potassium channel KcsA is studied, in addition to KvAP and the pore domain region of the eukaryotic hERG channel

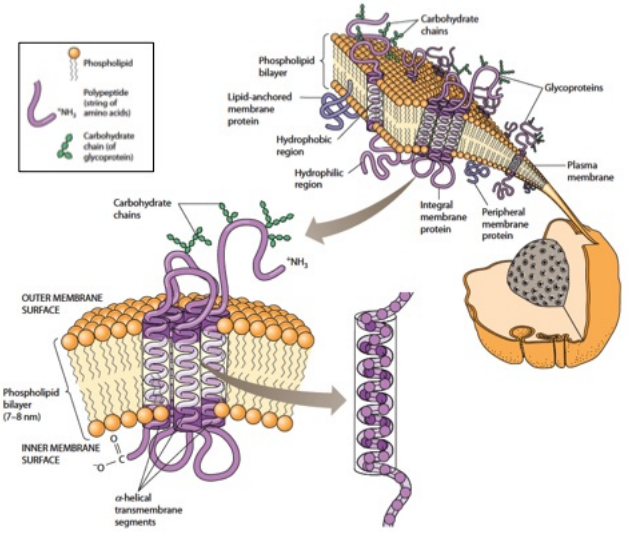

Figure 1.1: The cell membrane. The image illustrates a highly active cell surface that is densely populated by different types of membrane proteins. The figure was obtained from Hardin et al. (2011).

Conventional methods for studying ion channels

Ion channels can be characterised at a single-channel level with a number of electrophysiology techniques. These include patch clamping, where a glass pipette makes a seal with a cell membrane, or bilayer lipid membranes, where purified ion channels are introduced into an aperture-suspended bilayer of synthetic lipids. The first method requires precise positioning and clamping of the glass pipette over a small membrane patch, while the second method requires protein purification, reconstitution into proteoliposomes and incorporation into the lipid bilayer (Fig 1.2). Both methods require over-expression (an induced increase in the natural level of protein expressed by the cell) to generate sufficient amounts of the channel of interest, which may be toxic to the cell, leading to a substantial reduction in the process yield. This demands that the whole process be performed on a scale of several litres to obtain sufficient amounts of protein to study. This requires several days work and a substantial molecular biology infrastructure, which limits the throughput of ion channel research (Demarche et al., 2011).

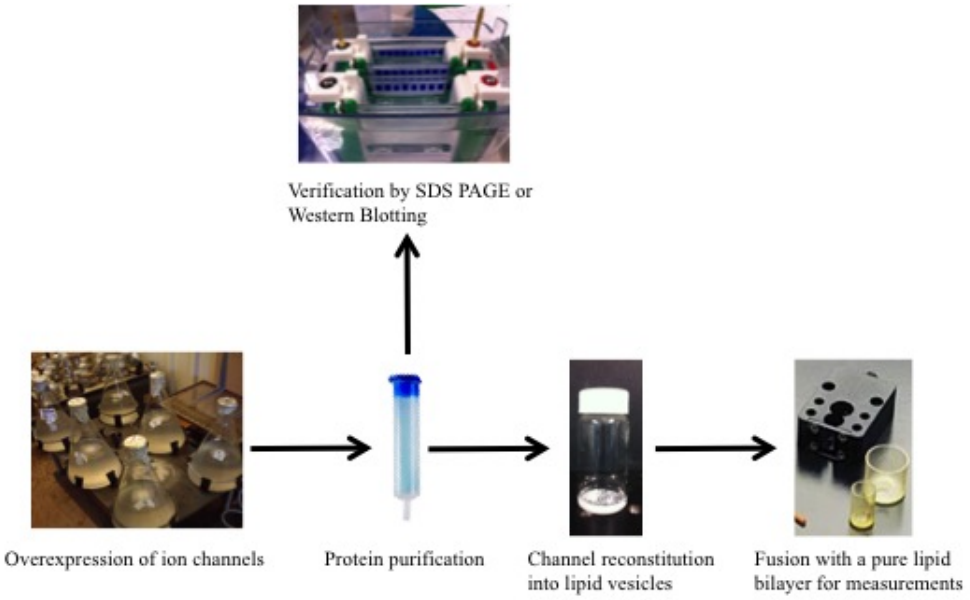

Figure 1.2: The conventional approach for expressing ion channels for electrophysiological measurements in BLMs. E.coli cultures are grown in litre scales for IPTG induced overexpression from a channel encoding plasmid. Further to centrifugation the cells are homogenised and the protein purified using an affinity chromatography column. SDS PAGE and/or Western blotting are typically used to verify the presence of the ion channel of interest. The protein is then reconstituted into lipid vesicles, which are subsequently fused with a BLM for electrical measurements. The entire process can take several weeks. The images are taken from Biontex (USA) and Warner Instruments (USA).

Electrophysiology of cell free expressed ion channels in microdroplets

Cell-free (CF) protein expression (Fig 1.3 a)) is an alternative *in vitro* method for producing proteins that works by adding a DNA template to a mixture of the essential components required for protein expression (Whittaker, 2013). The method is fast, commercially available and is continuously accessible, allowing detergents or lipid vesicles to be freely added for stabilising the expression of membrane proteins (Katzen, 2008; Junge et al., 2011). One drawback of the CF method is the expense of the systems, however this can be economised by performing the reaction in microlitre volumes. Performing the reaction on this scale is also interesting as it is possible to form a lipid bilayer by placing two aqueous droplets into contact inside a well of lipid-oil (Bayley et al., 2008). This presents the opportunity to express ion channels in the proximity of a lipid bilayer, which is desirable as it may allow for the entire process of ion channel expression and characterisation to be fully coupled (1.3 b)). This would be particularly useful for the development of miniature high throughput screening platforms, capable of testing the response of ion channels against arrays of novel pharmaceutical compounds.

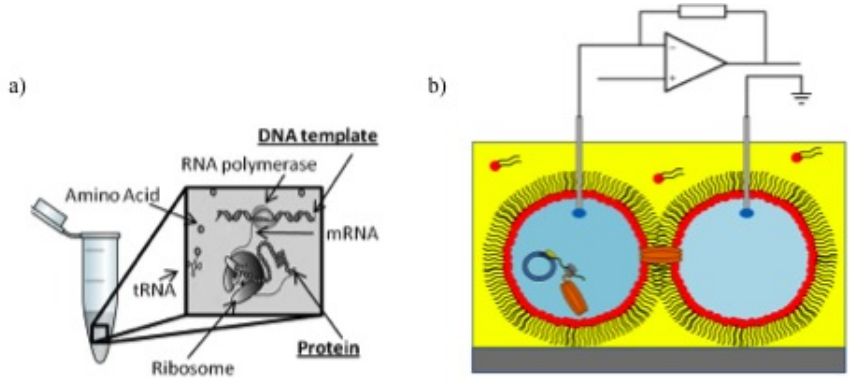

Figure 1.3: Cell free protein expression and coupled expression/characterisation. a) Cell-free protein expression is an *in-vitro* method of expressing proteins from a user supplied DNA template. The mixture contains all of the consumables and cellular apparatus required for the transcription and translation of DNA into proteins. b) An interdroplet bilayer can be formed by manipulating two aqueous microdroplets into contact inside a well of lipid-oil. If one droplet contained the CF expression mixture supplied with a DNA template for an ion channel it is possible that Ag/AgCl electrodes inserted into each droplet could allow for single channel measurements to be obtained as the channel is expressed.

.

Chapter 2

Literature and background

This chapter details the theoretical background behind the study and is supported by a review of the relevant literature. The chapter is split into four parts, where the first part provides an introduction to obtaining electrical measurements of ion channels using both the patch-clamp method and the model membrane method. The recent innovations towards developing high-throughput methods are then presented, followed by an introduction to the concept of obtaining electrophysiological measurements from bilayers formed using microdroplets immersed in lipid oil. The conventional methods used to express ion channels are then discussed in the third section of the chapter before achievements and observations using the cell-free method are detailed. The chapter concludes with a general description of ion channels followed by a summary of the specific characteristics reported in the literature for the KcsA, KvAP and the hERG channel.

2.1 Ion channel electrophysiology

Electrophysiology is a field of biophysics concerned with the study of the electrical properties of biological components such as tissues and cells. While the subject dates back to the late 18th century when Luigi Galvani discovered bioelectricity (Piccolino, 1998), the field as it is known today has largely evolved from the more recent era of classical biophysics (1935-1952) (Hille, 2001). This period is famous for research using the squid giant axon to investigate the ionic theory of membrane conduction and the electrophysiology of action potentials. Critically it was shown that the movement of ions were responsible for changes in membrane potential (inside potential - outside potential) and that the permeability of the plasma

membrane to Na^+ ions changes during the action potential which was recorded for the first time (Hodgkin and A.F, 1945; Curtis and Cole, 1940, 1942). These results were obtained by measuring the change in membrane potential at different locations along the squid giant axon when a current in the form of an electrical stimulus was applied. The invention of the voltage clamp technique in 1949 was a significant advancement as it allowed for ionic currents to be measured under a predefined membrane potential (Hille, 2001; Hodgkin et al., 1952; Maramont, 1949). The setup consisted of an intracellular electrode, a follower circuit to measure the membrane potential, a feedback amplifier to correct any difference between the recorded voltage and preset value and a second intracellular electrode to supply any subsequent current. Through keeping the membrane potential constant Hodgkin and Huxley were able to outline the ionic basis of the action potential earning them the Nobel Prize in Physiology or Medicine in 1963 (Hille, 2001).

2.1.1 Theoretical background

An open ion channel can allow the movement of ions into or out of the cell at a rate of over 10,000,000 ions per second (Hille, 2001), giving rise to cellular excitation required for the generation of an action potential. This movement of free charges in a conducting medium can be described as an electrical current, where one ampere equates to a steady flow of charges at a rate of one coulomb per second. In the case of potassium ions, a mole of KCl contains one mole of K^+ cations and a mole of Cl^- anions. By definition, one mole of any given substance contains 6.022 x 10^{23} number of particles, the charge of a proton is 1.16 x 10^{-19} C and the multiplication of these two values, the charge on Avagadro's number of elementary charges, is known as the Faraday constant (F), which is approximately equal to 10^5 C/mol. In the case of divalent cations, the charge is 2F while in monovalent anions the charge is -F. These terms allow Ohms law to be applied to ion channel studies, where the ionic current passing through the channel is equal to the conductance of the channel multiplied by the voltage difference across the conductor. As the cell membrane comprises of an insulating lipid bilayer separating two aqueous compartments, it is also possible to view this structure as a capacitor. These properties allow biophysicists to model the properties of membranes and channels with equivalent circuit diagrams (Hille, 2001). The circuit in Fig 2.1 for example reflects both the membrane capacitance and the ion channel conductance. The conductance is represented as a product of a voltage gradient across the membrane

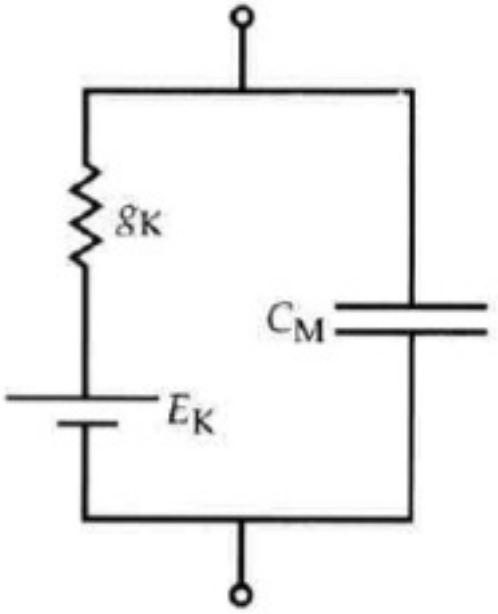

Figure 2.1: A model membrane circuit. The circuit is an electrical representation of an ion channel inserted into a cell membrane. The capacitor reflects the membrane capacitance (C_M), the resistor represents the conductance of the ion channel conductance (gK) and the battery depicts the membrane potential. The figure is taken from (Hille, 2001).

due to a concentration of ions generating an electromotive force (EMF) and the conductance of the channel is represented by a resistor. Using this circuit, the current-voltage relationship of ion channels can be represented.

It therefore stands to reason that electrophysiological recordings can be obtained by placing an electrode either side of the bilayer and measuring either the membrane potential or the transmembrane current. The latter can be achieved using silver/silver chloride (Ag/AgCl) electrodes, a standard non-polarised electrode (exhibiting no double layer capacitance) that is more practical to use than either the classic Hg/HgCl or calomel electrode. The electrode works when in contact with solution containing chloride (e.g. KCl), where the Cl atoms in the AgCl crust can be exchanged just like metal atoms in contact with a salt of that metal, allowing the Ag/AgCl electrode to effectively behave as a chlorine electrode in a salt of chlorine. The potential is determined by the concentration of Cl^- in the solution and can be calculated using the Nernst equation.

2.1.2 The patch clamp method

One method to record single-channel currents is to carefully press a glass micropipette with a small tip diameter of ∼1 μm against the surface of a cell such as a neuron as illustrated in Fig 2.2. A high resistance seal is formed between the pipette and the plasma membrane by applying suction, allowing the membrane patch to be electrically isolated from the rest of the cell surface. Any channels present in the membrane patch can be studied in the intact cell, or the membrane patch can be removed by drawing the pipette away, allowing for the investigator to have access to the cytosolic side of the membrane. In either case, a Ag/AgCl electrode inserted inside the pipette and a second Ag/AgCl electrode connected to ground allows for the voltage across the membrane to be maintained using an amplifier containing a voltage clamp feedback circuit. The voltage clamp then measures any changes in the transmembrane current, arising due to openings and closings of ion channels residing in the isolated membrane patch. This method, invented by Neher and Sakmannin in 1976, allowed the first experimental verification of ion channels by demonstrating single channel currents of the acetylcholine receptor (Neher and Sakmann, 1976). This achievement led to their award of the Nobel Prize in Physiology and Medicine in 1991. While the patch clamp method is considered the gold standard for obtaining single-channel measurements, the method suffers from low-throughput and practical difficulties. This has motivated the commercial development of automated platforms for performing electrophysiological measurements in mammalian cell lines and oocytes. These include both single and multichannel systems that essentially replace the top down access to cells via micropipettes with a bottom up configuration to enable compatibility with plate or chip-based formats (Fig 2.3). This is most typically achieved using planar-array based approaches, referring to the use of multi-well configurations to enable multiple recordings in parallel (Laszlo et al., 2003). The Ion Works HT system was the first screening platform to become widely available (Schroeder et al., 2003). The first-generation system used a 384-well PatchPlate, with each well containing a single 1-2 μm wide micropore in the glass substrate for patching a cell (Fig 2.3 a)). A more recent evolution of the platform obtained simultaneous recordings from 64 cells per well (Fig 2.3 b)) and termed the process population patch clamp (Finkel et al., 2006). A key advantage of this method is that it allows for multi-well averaging to overcome typical well-well variability observed with the single hole approach (John et al., 2007), however a major drawback is the absence of perfusion capability. The first planar-array based system to enable giga-ohm seal patch-clamp electrophysiology on-chip was

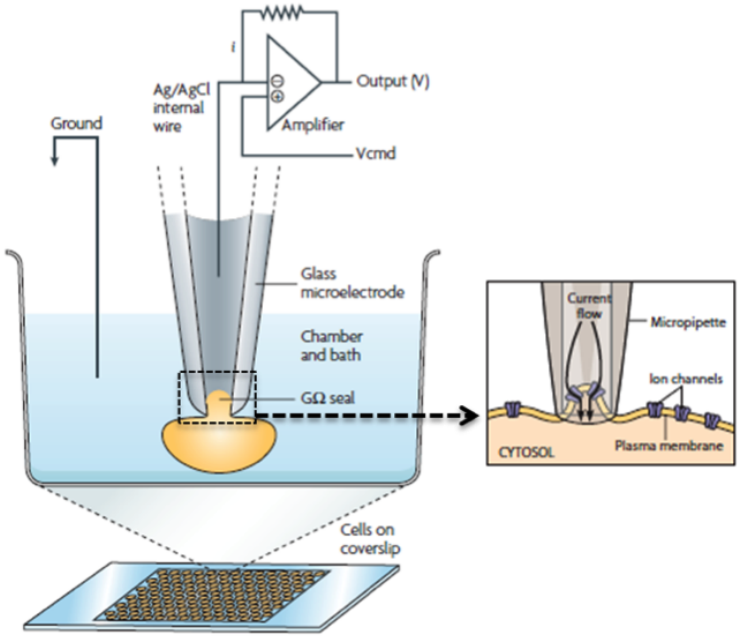

Figure 2.2: The Patch-Clamp method for obtaining measurements of ion channels. Cells containing the over-expressed channel of interest are supplied suspended in a bath solution. A glass micropipette with a $\sim$3 μm opening is positioned on to a cell using micromanipulators, a giga Ohm seal is created by applying suction, electrically isolating the ion channels inserted in the membrane patch from the rest of the cell membrane (insert). A patch clamp amplifier connected to Ag/AgCl electrodes inserted into the micropipette and the bath facilitates electrical measurements by maintaining the membrane potential and detecting any small changes in the transmembrane current. The figure is adapted from Dunlop et al. (2008); Hardin et al. (2011).

the Patch Xpress (Molecular Devies, USA), illustrated in Fig 2.3 part c) (Tao et al., 2004; Xu et al., 2003). The 'seal chip' used in the platform enabled fluid exchange using pumps. The QPatch is a similar platform and was the first to enable microfluidic flow capabilities for fluid exchange in their QPlate modules shown in Fig 2.3 part d) (Asmild et al., 2003; Mathes, 2006). The Patchliner system extended this microfluidic capability to facilitate fluid exchange on both the extracellular and intracellular side on a glass chip, the NPC16 chip used in the platform is shown in Fig 2.3 part e) (Farre et al., 2007). The recently developed CytoPatch robotic platform is shown in Fig 2.3 part f). The examples provided highlight the diversity in approaches that have been used to develop automated devices to patch clamping, however one general drawback is that each platform still requires a supply of cells. While Xenopus oocytes, are both mechanically and electrically stable, large in size and readily available (Cens and Charnet, 2007), the requirement to prepare cells for each individual ion channel remains limiting to the

potential throughput of the method. This makes automated patch clamp platforms closer to a 'chip in a lab as opposed to a lab on a chip. Additional practical limitations of the patch clamp system also include the inability to control the lipid composition of the membrane, the dependence of the channel incorporating into the patched region of the membrane, and the unavailability of ion channels that do not reside on the outer cell surface.

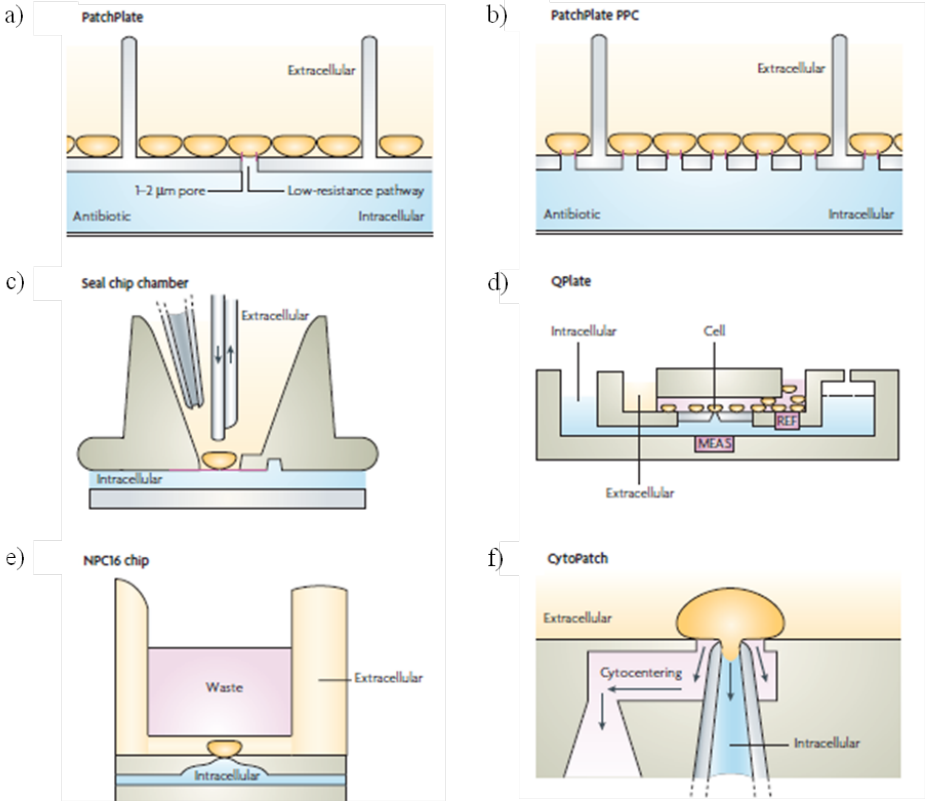

Figure 2.3: Cross sectional schematics of chips and flow channels used in automated patch clamp electrophysiology platforms. a) One well of the 384-well PatchPlate used in the IonWorks HT system. b) The second generation PatchPlate capable of 64 recordings per well. c) The seal chip chamber used in the PatchXpress system, capable of obtaining giga Ohm seals and fluid exchange using pumps. d) The QPlate used in the QPatch system, where MEAS and REF refer to the measurement and reference electrodes respectively. e) The NPC16 chip used in Patchliner NPC16 facilitates fluid exchange of both the intracellular and extracellular compartments using microfluidics. f) The CytoPatch chip used in the robotic CytoPatch system. The figure emphasises the diverse approaches undertaken to miniaturise and automate methods in pach clamping. The figure is adapted from Dunlop et al. (2008).

2.1.3 Electrophysiology using planar lipid bilayers

A model membrane system, classically referred to as a black lipid or bilayer lipid membrane (BLM), is an alternative method for performing ion channel electrophysiology that does not require sophisticated micromanipulators, nor the maintenance of cells for patch recordings. The method works by assembling an 'artificial' lipid bilayer formed from a predetermined mixture of phospholipids. Further to the fusion of ion channels, electrophysiological measurements of the membrane can be achieved using a voltage-clamp, similar to as described in section 2.1.2 for the patch clamp. The Montal Mueller method and the painting method (described in section 3.2.3) are the most established methods for forming planar lipid bilayers across pre-formed apertures (Montal and Mueller, 1972). The Montal Mueller (Fig 2.4) method comprises of two chambers part filled with electrophysiology buffer and separated by an aperture made from a hydrophobic material such as Teflon. A monolayer of lipids are formed in each aqueous chamber by applying lipids in a volatile solvent such as chloroform and waiting for the solvent to evaporate (Fig 2.4 a)). By raising the buffer in both chambers above the aperture (Fig 2.4 b)-c)) a lipid bilayer can be formed by 'folding' (Fig 2.4 d)). The painting method is similar to the Montal Mueller method except that the lipids

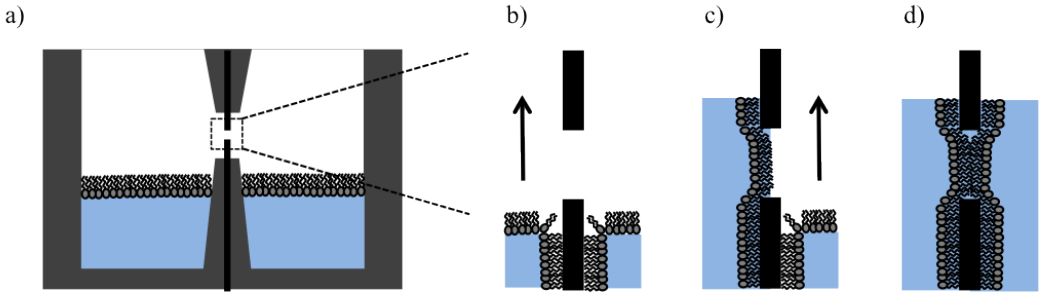

Figure 2.4: The Montal Mueller method for the formation of planar lipid bilayers. a) A small aperture engineered in Teflon separates two aqueous compartments containing buffer with a monolayer of lipids deposited on top. b)-c) Promoted by the lipophilic Teflon surface, a monolayer is formed across each side of the aperture by 'folding'. This is achieved by adding buffer to each compartment to raise each volume above the aperture. d) The formation of a monolayer either side of the bilayer leads to the formation of a lipid bilayer.

are directly applied to one side of the immersed aperture and bilayer formation is achieved by raising and lowering the buffer (section 3.2.3). The lipid bilayers formed using both methods typically contain a small solvent annulus. Ag/AgCl electrodes inserted into each compartment allow for single channel recordings to be

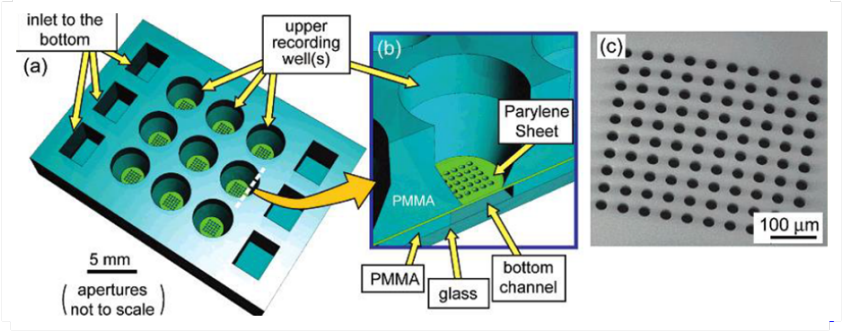

Figure 2.5: A lipid bilayer array chip. a) An overview and b) close up of the device showing a thin sheet of parylene with microfabricated apertures sandwiched between two PMMA plates. The lipid bilayers were formed across the apertures shown in c) by filling the upper wells with buffer before introducing buffer with DPhPC into the bottom channel. The figure was obtained from Le Pioufle et al. (2008).

obtained provided the investigator can supply and incorporate an ion channel into the lipid bilayer for analysis (Demarche et al., 2011). A similar method of bilayer formation involves the addition of liposomes to the system, allowing the amount of organic solvent to be reduced further (Schindler, 1980). Planar bilayers formed over micro-engineered apertures have been widely reported in the literature. These have been fabricated in silicon containing apertures 25-200 μm in size forming POPC bilayers lasting a maximum of 8 hours by etching (Peterman et al., 2002), in glass by ion-track etching (1-50 μm) using DPhPC(Fertig et al., 2001), in PMMA using POPC (50 μm) (Sandison and Morgan, 2005) and polycarbonate films containing 15 μm apertures (OShaughnessy et al., 2007) by laser microablation. This platform used POPC to make bilayers that were stable from 15 minutes to an hour. Apertures have also been reported in Teflon (2-3 μm) by piercing with a heated tip and painting with DPhPC-solvent solution (Kitta et al., 2009). Microfabricated apertures have also been engineered in array platforms (Le Pioufle et al., 2008) and inside microfluidic devices (Suzuki et al., 2004), as illustrated in Fig 2.5.

2.1.4 Electrophysiology using microdroplets

Recent innovative adaptations to the planar bilayer method have included the use of microdroplets and hydrogels, which effectively replace one or both of the aqueous compartments in the Montal Mueller method. One report, for example, describes the formation of free-standing Droplet Hydrogel Bilayers (DHBs) by depositing an aqueous 1 μl droplet on top of a DPhPC solution covering a 100 μm

aperture pressed onto a hydrogel. Single-channel recordings of the BK-channel, the ryanodine receptor channel and the nicotinic receptor channel were reported using this technique (Ide and Ichikawa, 2005). In an adapted method reported by the Wallace group at Oxford, DHBs were formed without an aperture where an aqueous droplet was placed on top of a hydrogel immersed in a DPhPC-decane solution (Thompson et al., 2007). The same group also reported the direct detection of membrane channels from gels by rolling 200 pl droplets over the gel in oil using a micromanipulator (Heron et al., 2007), a schematic for the platform is shown in Fig 2.6. DHBs formed this way were reported to be stable for weeks. The Schmidt group from the University of California have also reported a novel method of lipid bilayer formation using sessile droplets controlled by automated liquid-handling robotics (Fig 2.6 b). Bilayer formation is achieved using a customised Ag/AgCl pin which collects droplets from sample wells and delivers them to measurement wells containing an organic phase on top of an aqueous phase. As the droplet is immersed in the oil a monolayer of lipid is formed around its surface from DPhPC vesicles accumulating at the surface, when the droplet meets the monolayer of lipid separating the organic and aqueous phase a lipid bilayer is formed. To allow for electrical recordings each well on a 384 well plate was modified to contain a 200 μm Ag/AgCl electrode (Poulos et al., 2010). The setup has been shown to run unattended for up to 27 hours. The concept of forming bilayers using droplet interfaces immersed in lipid-oil has already been introduced in section 1.3. Forming bilayers this way is popular since the method is highly amenable to miniaturisation and high-throughput applications. The latter has been demonstrated in principle by Holden et al. through the construction of bionetworks from nanoliter water droplets (Holden et al., 2007; Hwang et al., 2008). A platform capable of high-throughput electrophysiological screening for blockers of the potassium channel Kcv was later reported by Syeda et al. (2008). whereby the protein was also produced using CF expression (Syeda et al., 2008). High-throughput screening was achieved by moving the droplet expressing Kcv into contact with different droplets each containing different blockers (Fig 2.6 c)). In another approach, the Leo group at Virginia Tech report the physical encapsulation of interdroplet bilayers using a PMMA device containing adjacent wells fixing the position of droplets in oil (discussed in detail in section 3.2.4). This was demonstrated with 2 and more droplets forming portable and durable DIB networks (Sarles and Leo, 2010a). A simplified PDMS platform was documented by the same group where the novel feature, reported as the regulated attachment method, allows for the lipid bilayer (DPhPC) to be controllably reconstituted using a deformable flexible aperture. By applying a controlled pressure to either

side of the device the aperture can be controllably opened, allowing for bilayer size to be dictated (Sarles and Leo, 2010b). Bilayers formed in this way are stable for a number of hours and are discussed in detail in section 3.2.4. In another report from the group non-invasive measurement techniques are discussed

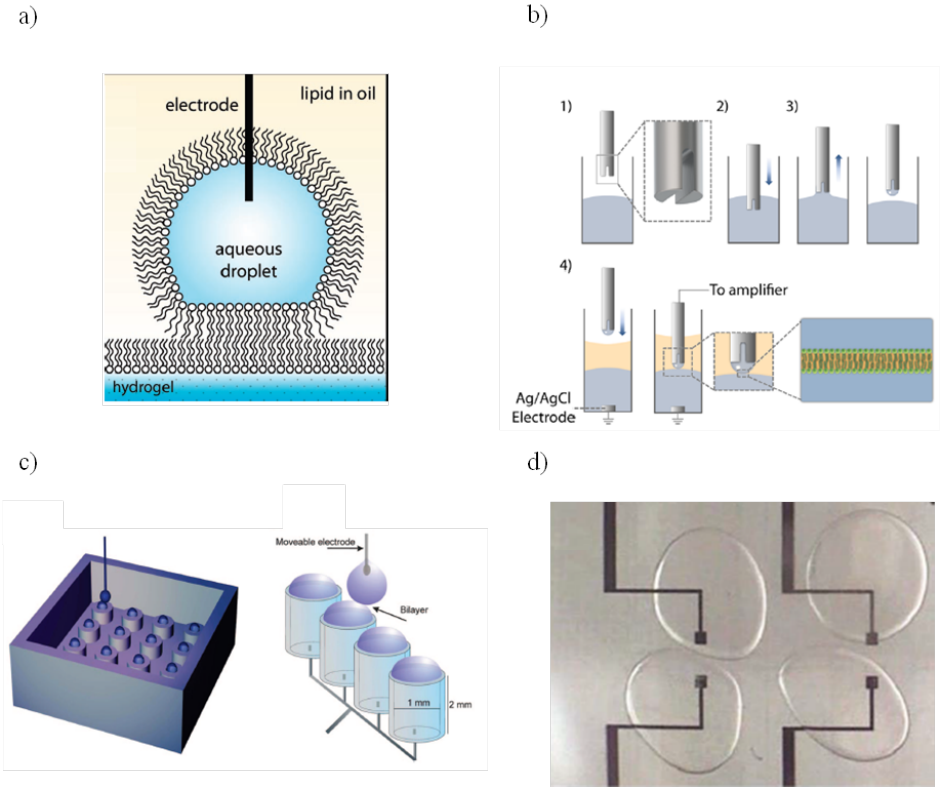

Figure 2.6: Electrophysiology using microdroplets. a) A schematic of a droplet hydrogel bilayer, where a droplet is placed on top of an agarose hydrogel while immersed in a well of lipid oil. An electrode in the droplet and an electrode in the hydrogel allow for single channel measurements to take place. The image is taken from Heron et al. (2007). b) Automatable lipid bilayer formation using sessile droplets, 1)-3) A pin tool connected to a servo is dipped into a well of aqueous buffer, removing a droplet in the process. 4) The pin moves the droplet to a second well containing lipid-oil on top of a volume of buffer. Precisely lowering the droplet to the oil-water interface leads to the formation of a lipid bilayer. The figure was taken from Poulos et al. (2010). c) An array of channel blockers in aqueous droplets were positioned in wells and submerged in oil. Interdroplet bilayers were formed with a second droplet containing the ion channel by placing the two droplets into contact. Manipulating the droplet into contact with other blockers in the array and taking electrophysiological measurements allowed the blockers to be screened. The image was obtained from Syeda et al. (2008). d) Droplets manipulated into contact to form an interdroplet bilayer using an electrowetting platform. The image was obtained from Poulos et al. (2009).

for performing electrophysiology on interdroplet bilayers. Here it was shown that electrophysiological measurements could take place using a single droplet pierced with an Ag/AgCl electrode and an adjacent agar coated electrode (Creasy and Leo, 2010). Manipulating droplets into contact using electrokinetics is an alternative method for forming interdroplet bilayers (shown in section 3.2.5.3). This has been demonstrated by Aghdaei et al. (2008) by moving 2 μl droplets into contact within an asolectin n-decane solution using DEP at 12 V with a 2 kHz sinusoidal wave. Bilayers formed this way were stable for $\sim$20 hours (Aghdaei et al., 2008). The novelty of this work is both the fabricated electrokinetic chip and the subsequent control of droplet motion without the need for manual dragging.

Electrokinetics has also been used to modulate the size of interdroplet bilayers by altering the contact angle between droplets using electrowetting (Punnamaraju and Steckl, 2011). In this example, a hydrophobic layer of the fluoropolymer Fluoropel was deposited on an Al_2O_3 dielectric layer on top of an ITO coated glass substrate and droplets pierced with an electrode were immersed in oil containing POPC/DPhPC. A similar device has also been reported by Poulos and co-workers (Poulos et al., 2009) except integrated Ag/AgCl electrodes were incorporated into the device (Fig 2.6 d)). Interdroplet bilayers, also referred to as Droplet Interface Bilayers (DIBs), have been reviewed by Bayley (Bayley et al., 2008).

2.1.5 Controlled delivery of proteins to lipid bilayers

Initially described by Woodbury (Woodbury and Miller, 1990; Woodbury, 1999) using Cl^- channels from *Torpedo californica* and later refined by De Planque et al. using β-amyloid peptide (de Planque et al., 2006), the controlled delivery of ion channels to lipid bilayers can be achieved by functionalising reconstituted proteoliposomes (section 2.2.5 with nystatin A1 trihydrate (antifungal) and ergosterol (a sterol component of yeast and fungal cell membranes). The two together form a small conductive pore which allows for fusion events to be observed when performing electrophysiology with an ergosterol deficient bilayer. Nystatin-ergosterol vesicles carrying the protein of interest are introduced to a lipid bilayer where the nystatin-ergosterol complex is introduced in its active form. The complex almost immediately disassociates as the ergosterol diffuses along the membrane and the conduction decays. If performed successfully, this method should indicate vesicle fusion by a short current spike and leave the ion channel of interest in the lipid bilayer ready to be studied. The technique has also been demonstrated to deliver the bacterial K^+ channel KcsA on-chip from

falling droplets (Zagnoni et al., 2009) and the bacterial Na^+ channel NaChBac into planar bilayers (Studer et al., 2011).

2.2 Ion channel expression for electrophysiological measurements

2.2.1 The expression of ion channels *in vivo*

Acquiring ion channels for electrical measurements may be achieved by isolation from native membranes, overexpression in cell lines or by CF protein expression. While high numbers of nicotinic acetylcholine receptors of the electric organ of Torpedo Californica can be found natively in in the plasma membrane (Kistler and Stroud, 1981), this is extremely uncommon. Overexpression is instead required for ion channels that are natively present in low numbers at the cell surface. This can be achieved using a variety of prokaryotic or eukaryotic hosts (Junge et al., 2008), where features of the expressed proteins such as their toxic effect on the cell and requirements for posttranslational modifications are deciding factors.

In general, a plasmid vector containing the DNA encoding the protein of interest is introduced into a host cell by transformation. The cells are grown in a nutrient broth containing one, or a mixture of antibiotics specific to the vector used such that all cells that do not contain the vector are rendered unviable. The cells are grown to a specific point before overexpression is triggered, usually through the addition of IPTG. The cells are later separated from the medium by centrifugation, sonicated in PBS to homogenise and spun again at high speed to pellet the membranes. At this stage a solubilisation buffer containing detergents is typically added before the protein is purified.

2.2.2 Ion channel purification

A C- or N- terminal amino acid tag included in the overexpressed protein to allow it to be specifically isolated from the thousands of proteins present in the cell lysate. This is commonly achieved using agarose beads functionalised with a Ni-nitrilotriacetic acid (NTA) resin that is specific for the amino acid tag. Typically, the beads are washed and incubated with the cell-lysate overnight in a cold room before the suspension is loaded onto a column. The column is normally

washed several times before the beads are eluted in 50 - 250 mM concentrations of imidazole in PBS and titrated to pH 7.4. At this stage the presence of the protein of interest may be inferred by running an SDS PAGE gel and confirmed by performing a Western Blot.

2.2.3 Sodium dodecyl sulphate polyacrylamide gel electrophoresis (SDS PAGE)

SDS PAGE is a frequently used method for separating proteins by size (Laemmli, 1970). The technique essentially involves the use of the detergent SDS to impart a negative charge onto denatured proteins, which are subsequently loaded onto a polyacrylamide gel immersed in buffer. A potential applied across the gel induces the migration of proteins down the gel by electrophoresis. The polyacrylamide matrix causes larger proteins to migrate down the gel slower than small proteins, leading to protein separation. The proteins are later visualised by staining, which is commonly achieved using Coomassie Brilliant Blue. The stain binds to the proteins present on the gel, revealing a series of bands after the excess stain is removed by destaining. The gel is later imaged for analysis, where the molecular weight of the proteins present on the gel can be estimated by comparing them to a known standard that is usually run on an adjacent lane. An overview of the method is shown in Fig 2.7.

2.2.4 Western blotting

Western blotting is a technique that allows for specific proteins to be identified using the amino acid affinity tag described in section 2.2.2. The method works by running a SDS PAGE gel of the sample before a Western transfer is performed to remove proteins from the gel onto a piece of nitrocellulose paper. The paper is subsequently blocked in BSA to prevent non-specific binding before an antibody containing specificity for the amino acid affinity tag is introduced. The antibody is subsequently probed with a second antibody that is specific for the first, but also contains a detectable signal, either an infra-red dye for detection by infra-red or horseradish peroxidase for detection using chemiluminescence. The observed signal allows the presence of the expressed ion channel to be verified.

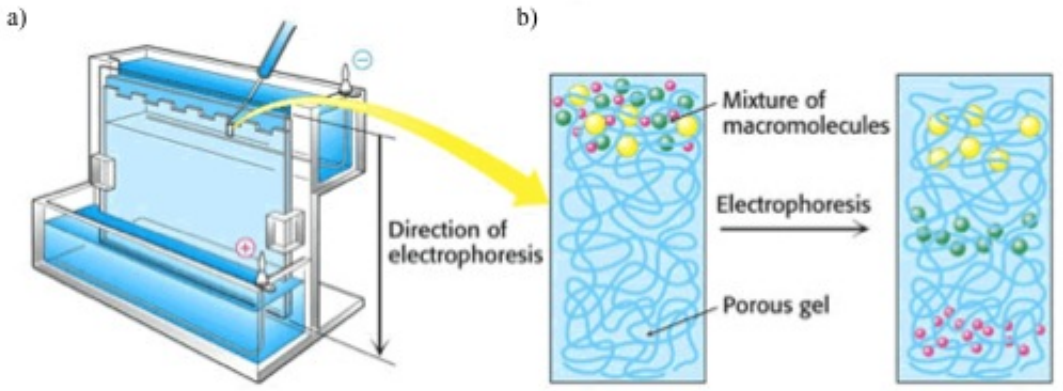

Figure 2.7: The SDS PAGE method for protein separation. a) A mixture of denatured protein, mixed with SDS is loaded onto a polyacrylamide gel immersed in electrolyte buffer. The SDS imparts a negative charge on the denatured proteins, causing them to move uniformly down the gel upon the application of a potential. b) The porous polyacrylamide gel causes large proteins to remain at the top of the gel while smaller proteins run to the bottom. The gel is subsequently stained and imaged for analysis. The figure was obtained from Hardin et al. (2011).

2.2.5 Protein reconstitution

Once SDS PAGE and/or Western blotting confirm the presence of the channel, the final step in the process prior to obtaining electrophysiological measurements is to reconstite the protein into liposomes for fusion with the bilayer (Demarche et al., 2011). This is possible using dialysis, where the dilution of detergent to values below the critical micelle concentration results in the disintegration of micelles into detergent monomers that can be easily removed (Seddon et al., 2004). An alternative method for detergent removal is hydrophobic absorption using Biobeads SM-2. These polystyrene beads are 750 μm in size with pores of 90 Å. Detergent removal is achieved through the interaction of the hydrophobic detergent tail with the hydrophobic surface of the bead (Seddon et al., 2004). These processes performed in the presence of lipids facilitates the conversion of micelles into proteoliposomes by gradually exchanging detergent for lipid. During this transition, detergent removal initially causes the transformation of small micelles into larger micelles before becoming bent to form curved mixed micelles. Further detergent removal leads to the formation of detergent-saturated vesicles which extend in size through fusion and lipid exchange mechanisms culminating in the formation of unilamellar liposomes typically 200 nm in diameter (Rigaud et al., 1998). The size of the liposomes can be tuned by extrusion, or reduced less

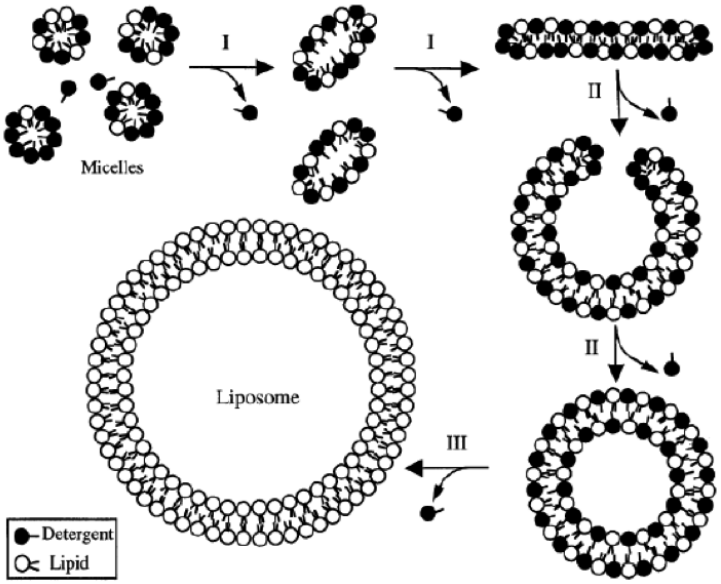

Figure 2.8: Translational states in the reconstitution of liposomes from micelles. I) Detergent removal initially causes small micelles to fuse forming larger micelles and eventually forming curved mixed micelles. II) Further detergent removal forms detergent saturated vesicles which expend in size through fusion and lipid-exchange mechanisms which ultimately leads to the formation of unilamellar liposomes (III). The figure is taken from Rigaud et al. (1998).

controllably by sonication. A schematic of the different aggregational states and micellar-lamellar phase transformations is shown in Fig 2.8.

2.3 Cell-free protein expression

Cell-free protein expression is an alternative *in-vitro* method for expressing proteins, which works by supplying a DNA template to a system containing the ribosomal machinery and reagents required for protein expression. For this to take place, ribosomal components are typically isolated by high-speed centrifugation and stabilised (Kigawa et al., 2004). This is a key component of commercial products where the exact protocol determines the activity of the lysate.

The development of CF systems has largely been motivated by the bottleneck in producing sufficent amounts of protein using *in-vivo* methods. This has lead to the development of CF systems that are now capable of producing milligrams of protein within 2-3 hours independent of the need for cells or a significant molecular biology infrastructure. The method also provides the freedom to add components

such as isotopic labels, detergents or lipids to the reaction mixture at any time, where the labels are useful for NMR structure studies, while the surfactants can stabilise the CF expression of membrane proteins (Schwarz et al., 2008).

CF protein expression has been known since the 1950s when several independent laboratories reported the continuation of protein synthesis in disrupted animal cells and cell extracts (Spirin and Swartz, 2008). This was later demonstrated with disrupted bacterial cells and led to the identification of the ribonucleoprotein fraction, the ribosome, being the core protein-synthesising component of a cell (Roberts, 1958). This discovery led to the assembly of the first cell-free (CF) protein expression systems consisting of cell extract, amino acids, ATP and GTP (Lamborg and Zamecnik, 1960; McQuillen et al., 1959; Schweet et al., 1958; Tissieres et al., 1960). These early systems allowed for the mechanisms for protein expression to be studied, but were only capable of translating endogenous mRNA. This was overcome in 1961 by Nirenberg and Matthaei who were able to remove endogenous mRNA without any damage to the ribosomal extract, allowing for the expression of exogenous mRNA (Matthaei and Nirenberg, 1961). This accomplishment led to the deciphering of the genetic code, an achievement for which Nirenberg was awarded the Nobel Prize in Physiology or Medicine in 1968.

The capability of CF systems to express proteins based on a DNA template was also demonstrated in this period through the development of bacterial CF systems containing endogenous RNA polymerases. Such systems were termed coupled transcription-translation systems as the rates of both mechanisms were coupled since elongating mRNA is simultaneously translated by ribosomes using this method (Matthaei and Nirenberg, 1961; Byrne et al., 1964; DeVries and Zubay, 1967; Lederman and Zubay, 1967). This was much more recently achieved in eukaryotic systems by the introduction of exogenous RNA polymerases such as T7 and SP6 isolated from bacteriophages. Although in this case the rate of transcription greatly exceeds the rate of translation, as such these systems were coined combined transcription-translation systems (Baranov and Spirin, 1993; Craig et al., 1992). These first generation CF systems were functional but limited by low yields due to their short periods of activity spanning less than 1 hour. This inhibition was due to the accumulation of waste products and the rapid depletion of the high-energy nucleotide triphosphate (NTP) pool by NTPases and NTP dependent-metabolic reactions (aminoacylation and ribosome function) (Spirin and Swartz, 2008).

To increase the lifetime of the system, a solution proposed by Spirin and co-workers was to alter the mechanics of the CF reaction, moving away from containing the reaction mix in a fixed test tube volume (or batch format) and introducing the continuous-flow cell-free (CFCF) translation system (Spirin, 2004). This system relied on the continuous supply of materials and metabolic energy into the reaction vessel and the continuous removal of reaction by-products (inorganic phosphates, nucleoside monophosphates and polypeptide products) from the reaction mix. The latter was achieved using a porous (ultrafiltration or dialysis) membrane to retain the high molecular weight protein synthesising components while being permeable to the low molecular weight waste products. It is documented that this technique extends the reaction time by 20 hours and increases the product yield by two orders of magnitude. However, the operational complexities of the CFCF method made it impractical and motivated the development of the semi-continuous or continuous exchange cell-free (CECF) method. Instead of using active pumping,

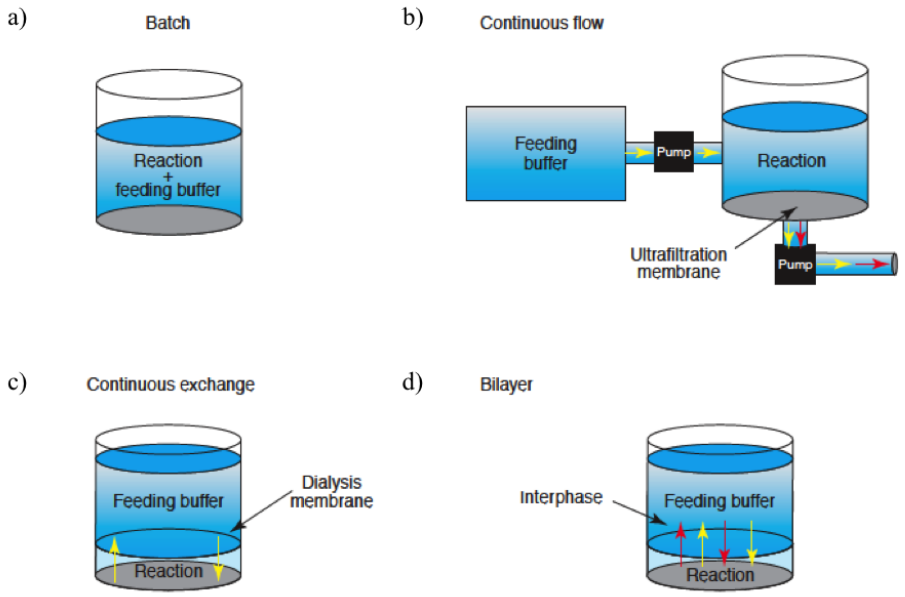

Figure 2.9: Different formats for performing cell-free protein expression. a) The batch format comprising the reacting mixture and the feeding buffer in a single vehicle. b) The continuous flow system consisting of a pump feeding the reaction mixture with feeding buffer and a pump removing waste products permeating an ultrafiltration membrane. c) The continuous exchange platform removes the need for pumping and relies on the diffusional exchange of nutrients and waste products into and away from the reaction mixture using a dialysis membrane to separate the compartments. d) The CECF principle can also be applied using a lipid bilayer in place of the dialysis membrane. The figure was taken from Katzen et al. (2005).

the CECF method exploits the passive (diffusional) exchange of CF substrates and low molecular weight products across a porous barrier separating the reaction mixture and the feeding buffer, extending the reaction lifetime of the system (Chekulayeva et al., 2001) and rendering it more applicable to miniaturised and automated high-throughput applications (Spirin, 2004). In addition to various types of dialysis membrane, the CECF principle has also been demonstrated using Sephadex granules, gel capsules and phase boundaries to separate the CF reaction mix and the feeding solution (Spirin and Swartz, 2008; Noireaux et al., 2005).

2.3.1 State of the art in CF protein expression

Founded on first generation systems there are now a variety of commercially available coupled and combined CF protein expression systems based on bacterial and eukaryotic extracts including E.coli, Insect, Wheat Germ and Rabbit Reticulate Lysate. In addition there also exists the selectively constructed PURE (Protein synthesis Using Recombinant Elements) system, a minimal reconstitution comprising of only 32 purified factors isolated from E.coli (Schwarz et al., 2008). The challenge is therefore not to produce CF expression systems but instead to use them effectively and sustainably on miniature platforms to produce correctly folded proteins of interest; a task which is no small feat for synthesising membrane proteins which require assistance to achieve their correctly folded conformations. Achieving the sustainable synthesis of soluble proteins has been well documented by the Noireaux group who have demonstrated the CF expression of green fluorescent protein (GFP) inside lecithin vesicles (1-50 μm in diameter) and the prolonged expression of the same product using vesicles supplied with the DNA for the expression of the bacterial toxin alpha haemolysin (αHL). This was accomplished using vesicles immersed inside an aqueous feeding solution (Fig 2.10 a)), where it was shown that the addition of αHL pores to the vesicles extended the longevity of expression from 20 to 100 hours (Fig 2.10 b)). This improvement was a result of the enhanced permeability of the vesicles to low molecular weight consumables due to αHL insertion (Noireaux and Libchaber, 2004; Noireaux et al., 2005). The progress made by the Noireaux group is part of a larger objective to construct an artificial cell based on gene expression inside vesicles. Working toward this goal the group have published several functionalities of CF systems including specific protein degradation, the development of an active membrane and the expression of a three gene genetic circuit behaving as a switch (Noireaux et al., 2005). The next challenges are to achieve vesicle division, develop a DNA

program and to efficiently express then insert membrane proteins into the lipid bilayer (Noireaux et al., 2011).

Compared to soluble proteins the advances in developing sustainable expression platforms for insoluble proteins has been comparatively modest despite significant improvements. Such progress has come in the form of different expression modes, applicable to both batch and CECF systems, for stabilising the expression of insoluble proteins and assisting protein folding. These techniques can be separated into precipitate forming CF expression (P-CF), detergent based CF expression (D-CF) and lipid assisted CF expression (L-CF) (Junge et al., 2011; Schwarz et al., 2008; Sobhanifar et al., 2010; Katzen et al., 2009) as illustrated in Fig 2.11. Protein precipitation occurs immediately after translation using the P-CF mode where precipitates are usually solubilised within a few hours using selected detergents (Klammt et al., 2005). Alternatively, protein expression can take place in the presence of selected detergents in the D-CF mode where protein products are inserted into micelles provided the concentration of the detergent exceeds the critical micelle concentration (CMC) (Junge et al., 2011). Once the reaction has completed, the reaction mix containing the proteomicelles can be applied to a

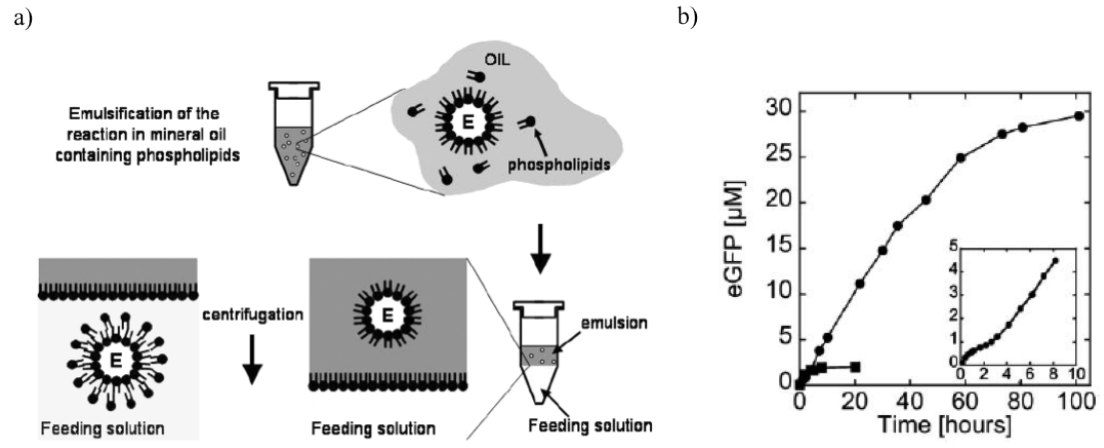

Figure 2.10: Cell-free expression in vesicles and extended expression. a) The CF reaction is emulsified in oil containing phospholipids where aqueous compartments containing the CF extract (E) are stabilised with a monolayer of lipids at the oil-water interface. The emulsion is placed on top of the feeding solution and a monolayer of lipids form at the biphasic interface. Vesicles form when micelles are forced through the monolayer upon centrifugation. They are subsequently recovered from the feeding solution. b) Kinetics of expression of HL-GFP inside a vesicle showing prolonged expression in vesicles containing HL. The filled squares are without αHL and the insert shows the first 10 hours of the expression. The figure was taken from Noireaux et al. (2005).

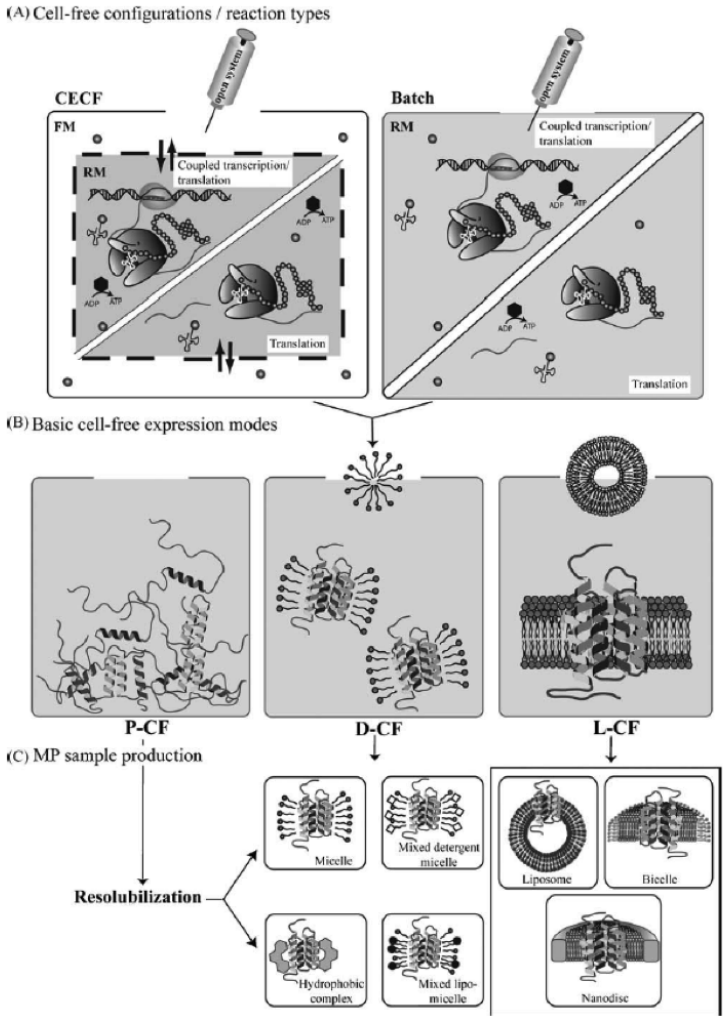

Figure 2.11: Different modes of CF protein expression. Protein is expressed either in batch format or using the CECF format with either coupled transcription/translation or translation. Membrane protein is either expressed without any hydrophobic agents (P-CF mode) or in the presence of detergents (D-CF mode) or lipids (L-CF mode). A host of samples can be prepared directly from D-CF and L-CF expression or through resolubilisation using P-CF expression. FM is feeding mix, RM, Reaction mix. The image is taken from Junge et al. (2011).

purification column or reconstituted to form proteoliposomes. Expressing proteins in the presence of lipids in the L-CF method is discussed in the next section.

2.3.2 Spontaneous channel insertion into vesicles

Interestingly, when liposomes are added to the cell-free reaction mixture, spontaneous reconstitution has been demonstrated for a variety of cell-free expressed membrane proteins, including stearyl-CoA desaturase, glucan synthase, ATP

synthase, DesK thermosensor, endothelin receptors A and B, bacteriorhodopsin, connexin-43, aquaporin Z, and the ion channels Kcv and KcsA (Goren et al., 2009; Periasamy et al., 2013; Matthies et al., 2011; Martín et al., 2009; Proverbio et al., 2013; Kalmbach et al., 2007; Moritani et al., 2010; Hovijitra et al., 2009; Syeda et al., 2008; van Dalen et al., 2002). Given that incorporation of protein into the liposome cannot be facilitated by translocon components as these are not present in the lysate, it has been speculated in the absence of a comprehensive study that the presence of detergents, trace amounts of native lipids, or a close ribosome-liposome proximity aid protein insertion in the lipid bilayer of the liposomes (Katzen et al., 2009; Junge et al., 2011; Roos et al., 2013). In principle, the bilayer self-insertion of

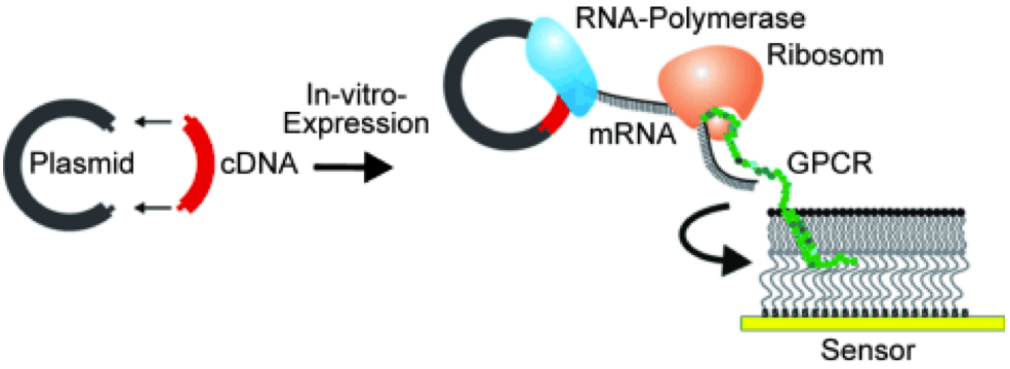

Figure 2.12: Spontaneous bilayer insertion of CF expressed membrane proteins. The figure illustrates the lipid association of CF expressed membrane proteins, where a G protein coupled receptor (GPCR) is shown to self-insert into a tethered lipid bilayer co-translationally. The image is taken from Robelek et al. (2007).

cell-free expressed membrane proteins can be exploited as a purification method for ion channel electrophysiology, as demonstrated in a small number of recent studies (Varnier et al., 2010; Berrier et al., 2011; Price et al., 2011; Robelek et al., 2007; Yildiz et al., 2013).

For example, large unilamellar vesicles containing the self-inserted ion channels VDAC or MscL have been purified from the expression mixture by density gradient centrifugation and subsequently fused with giant unilamellar vesicles (GUVs). The resulting proteoGUVs could be patch-clamped with planar aperture chips and single-channel current recordings of VDAC and MscL were obtained (Varnier et al., 2010; Berrier et al., 2011). Gradient-purified MscL-proteoliposomes have also been employed to deliver channels to an aperture-suspended bilayer, enabling single-channel MscL recordings with the aperture suspended lipid bilayer method (Price et al., 2011). Interestingly, direct incorporation of membrane proteins in the 'measurement bilayer' has been achieved for expression mixture-exposed

solid-supported bilayers (Fig 2.12), specifically for the odorant receptor OR5 and the transmembrane domain of the hERG potassium channel, enabling optical characterisation of ligand binding without protein purification (Robelek et al., 2007; Yildiz et al., 2013).

2.3.3 Cell-free protein expression in microsystems

CF expression of soluble proteins in microsystems has been largely achieved in the form of microchambers or microwells arranged into an array, a format of interest due to its overlap with protein microarray technology. CF protein expression has been reported using sub-microlitre volumes on chips containing nanowells (Angenendt et al., 2004) and in picolitre volumes within cylindrical PDMS chambers 10 μm in diameter and 15 μm deep (Kinpara et al., 2004). Here 250,000 PDMS chambers were made on a single, sealed device using a patterned silicon wafer as a master. A PDMS-glass microreactor array device with embedded temperature control has also been reported by the Fujii Group. The platform (Fig 2.13) comprised of PDMS reactor chambers 125 nl in volume bonded to the surface a patterned ITO glass substrate making the heaters and temperature sensors (Yamamoto et al., 2002). The hybrid platform was recently evaluated and demonstrated to express a variety of soluble proteins on-chip at 37 °C (Klammt et al., 2005). Albeit in larger 13 μl chambers milled into acrylic,

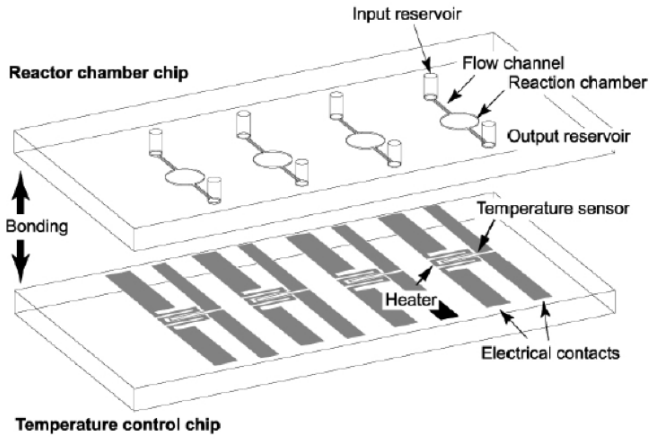

Figure 2.13: PDMS-glass microreactor array with embedded temperature control. The device is comprised of a 500 μm thick PDMS reactor chamber chip bonded to an ITO patterned, glass temperature control chip. The electrode width for the heaters was 100 μm and 60 μm for the temperature sensors. The image was taken from Yamamoto et al. (2002).

CF expression has also been demonstrated in an array format to detect toxins through synthesis inhibition (Mei et al., 2005). Arrays have also been formed in a single chamber by adsorbing proteins onto a functionalised surface. This has been demonstrated using CF expression to form tagged proteins which adsorb to a pretreated microtiter plate in situ forming an array (He and Taussig, 2001). The method known as Protein in-situ Array (PISA) is discussed along with other CF based array technologies in a recent review (He and Wang, 2007).

On-chip platforms capable of facilitating CECF expression have also been reported. These include a PDMS microreactor consisting of two chambers separated by dialysis membrane (Hahn et al., 2007), an array device containing nanoporous membranes and microchannels (Mei et al., 2010), and a microchannel array platform which supplies a small volume of feeding solution to a reaction mix using passive pumping (Khnouf et al., 2009).

The expression of water-insoluble proteins such as membrane proteins has been less frequently reported in microsystems. One publication from the Bayley group at Oxford describes a method for expressing αHL or the small viral potassium channel Kcv inside microdroplets in oil in the presence of an array of channel blockers (Figs 2.6). It was shown that the water soluble αHL could be expressed

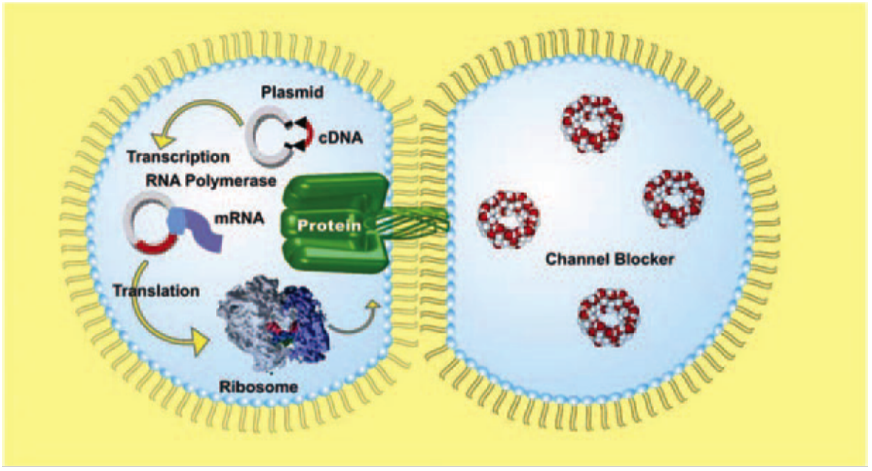

Figure 2.14: αHL expression in the presence of an interdroplet bilayer and a known channel blocker. DPhPC vesicles supplied to a droplet containing the CF expression mixture, and a droplet containing the channel blocker result in the formation of a monolayer around each droplet surface. An interdroplet bilayer is formed by positioning the droplets into contact using a micromanipulator. The image shows composition of each droplet forming the interdroplet bilayer, where one droplet contains the cell-free mixture and the αHL DNA required, while the opposite droplet contains a channel blocker. The image was taken from Syeda et al. (2008).

and inserted into the interdroplet bilayer directly from a droplet of the CF mixture without the requirement for incubation (Fig 2.14). However, the same effect was not observed for Kcv, where a lag time in the expression of the full-length protein was found to exceed the lifetime of interdroplet bilayers formed in the presence of the Promega E.coli T7 S30 CF system. The authors speculated that the presence of PEG and lipid components in the Promega system may be responsible for this instability, and reported that the bilayers were found to last for 0.7 hours on average, compared to 8.7 hours using the PURE system. Yet protein expression was not observed at room temperature for the PURE system, which instead required incubating with the Kcv DNA template for 1 hour at 37 °C prior to bilayer formation (Syeda et al., 2008). A separate report details the use of a CECF microwell array platform to express both the proton pump bacteriorhodopsin and the lipid binding ApoA lipoprotein (Khnouf et al., 2010).

2.4 Ion channels

The cell membrane is a dynamic environment that is host to a wide range of membrane proteins responsible for several critical functions of the cell, including the transportation of ions, small molecules and macromolecules between the cell interior and exterior. Ion channels (Fig 2.15 a)) are integral membrane proteins that form ion conducting pores which transverse the lipid bilayer to selectively allow ions to pass from one side to the other by opening and closing (gating). Ion channels differ vastly in their size, selectivity for ions (e.g. sodium, potassium, and chloride), and the triggers that cause them to gate. Such triggers include sensitivity to the transmembrane voltage, pH, or the presence of a ligand, causing the channel to open and close by adjusting the conformational state of its subunits. The subunits are individual membrane-spanning alpha helical proteins, which assemble with other identical or homologous (structurally similar) proteins to form a pore. In this context, voltage-gated potassium channels are multimeric proteins consisting of four subunits, while voltage-gated sodium channels from eukaryotes are one large (monomeric) protein comprised of four connected domains. In both kinds of channel, each subunit or domain contains six transmembrane alpha helices, referred to as S1-S6 (Fig 2.15 b)). Typically, S1-S4 form the voltage sensor which is loosely linked to S5-S6, forming the central pore domain and the selectivity filter (Bezanilla, 2005; Sigworth, 1994). The size of the central pore domain and the way it interacts with ions gives rise to the selectivity of the channel. This is a result of precisely positioned oxygen atoms in amino acids lining the centre of the

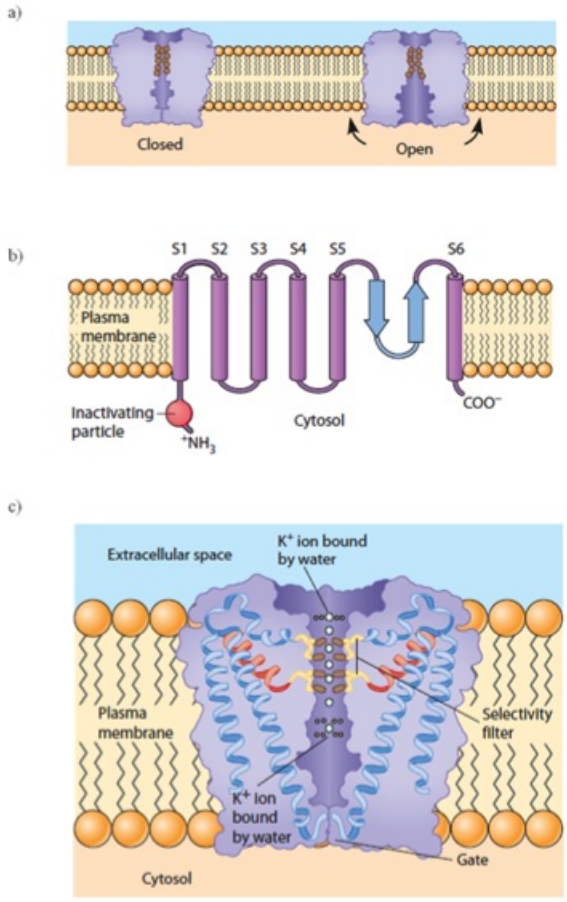

Figure 2.15: The structure and function of ion channels. a) Ion channels are integral membrane proteins that open and close depending on the conformational state of the channel subunits. b) The typical domain structure of an individual subunit contains six transmembrane helices, S1-S6. S1-S4 form the voltage sensor while S5-S6 are responsible for the pore domain and selectivity filter. c) The pore structure of a channel showing Potassium ions losing their waters of hydration as they pass the channel. Only two of four subunits are shown. The image was obtained from Hardin et al. (2011).

channel that interact with ions as they move through the selectivity filter, allowing them to give up their waters of hydration (Fig 2.15 c)). The level of precision of the positioning of the oxygen atoms is such that slightly smaller sodium ions can only interact with one of the oxygen atoms on one side of a potassium channel, rendering it energetically unfavorable for the sodium ion to give up its waters of hydration and enter the channel.

Voltage-gated ion channels play key roles in the generation of action potentials, defined as momentary but sizable electrical depolarisation and repolarisation events of the neural plasma membrane, caused by an influx of sodium ions and

the subsequent efflux of potassium ions. This mechanism is responsible for cell-cell communication in neurons, while in other cells such as muscle cells, the action potential is the first step in a cascade of events leading to muscle contraction. Such responsibility links defects in voltage-gated ion channels with human neurological diseases. Individuals carrying mutations in certain potassium channels for example suffer from a defect in muscle coordination known as ataxia, while one form of epilepsy is caused by a mutation in one specific voltage-gated sodium channel. Other conditions associated with faulty ion channels include muscular dystrophy, cystic fibrosis, osteoporosis and malignant hyperthermia (George, 2005; Celesia, 2001). The connection with ion channels and disease make them interesting targets for research, where small ion channels such as the KcsA from *Streptomyces lividans* have been extensively studied to reveal some of its principle structural and functional characteristics.

2.4.1 KcsA

The KcsA channel is the subject of many biophysical studies as it was the first ion channel to have its structure solved to a resolution of 3.2 Angstroms by X-ray crystallography (Doyle et al., 1998). This revealed that the channel forms a tetramer with each subunit having two transmembrane helices and a cytoplasmic domain that contains 35 amino acids at the C-terminus (Doyle et al., 1998; Cortes et al., 2001). Interestingly, the negatively charged amino acids comprising the cytoplasmic domain have recently been shown to be responsible for the pH sensing capability of the KcsA channel (Hirano et al., 2011). Single channel measurements of KcsA reveal that it is a proton-activated potassium channel (Cuello et al., 1998), which shows permeability to potassium ions, rubidium ions, ammonium ions and titanium ions, but is impermeable to sodium ion, lithium ions and cesium ions (LeMasurier et al., 2001). KcsA is known to exhibit asymmetric characteristics, where protons cause the channel to gate on the cytoplasmic side but not on the extracellular side of the membrane (Heginbotham et al., 1999). The cytoplasmic side of the channel is also susceptible to blockade by tetraethylammonium (TEA) (Heginbotham et al., 1999), an effect that has been shown to have complex voltage dependence (Kutluay et al., 2005). The single channel gating characteristics of KcsA are the subject of intense debate. Original observations of the channel reconstituted into proteoliposomes and fused into planar lipid bilayers revealed a channel conductance of 42 pS, and a less frequently observed larger opening with a conductance of 90 pS (Schrempf et al., 1995). The observation of dual conductance

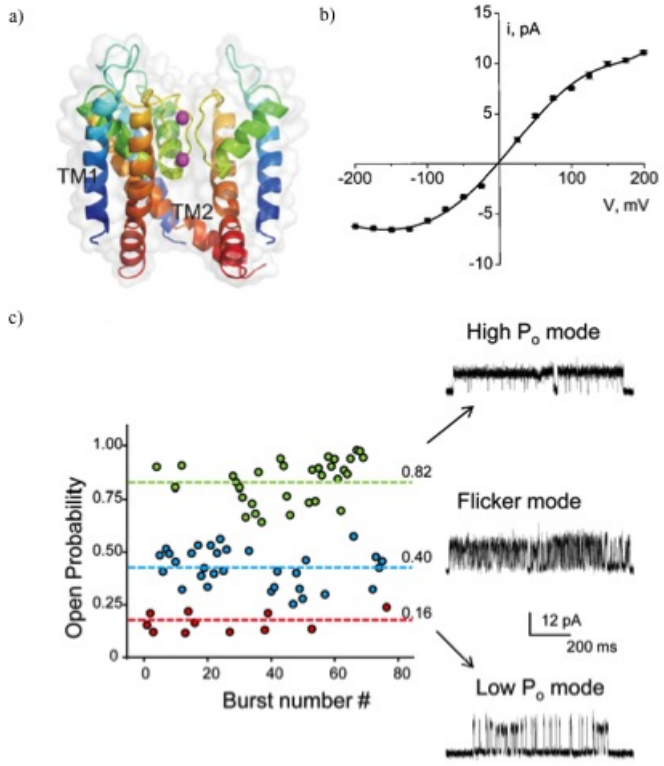

Figure 2.16: The KcsA channel. a) The KcsA channel in the open state with one subunit removed for the purposes of clarity (Cuello et al., 2010). b) The current voltage relation for KcsA in symmetrical 100 mM KCl, showing slight outward rectification (LeMasurier et al., 2001). c) Bursts of channel activity with different open probabilities leading to three different modes of gating, the high P_o mode, the flicker mode and the low P_o mode (Chakrapani et al., 2007).

states was also reported using asolectin or DOPE: DOPS planar lipid bilayers by Cuello, who identified a small conductance state of 70 pS and a more frequently seen larger conductance state of 135 pS (Cuello et al., 1998). Here it was also noted that the channel displayed considerable voltage dependence, with higher single-channel activity at negative potentials. In symmetric 100 mM KCl, KcsA was also shown to exhibit open-channel rectification by the observation of openings with conductances of 56 pS and 31 pS at 200 mV and -200 mV respectively. However it was noted that no low magnitude events were detected as reported previously (Heginbotham et al., 1999). The same results were also reported by LeMasurier, who observed the appearance of excess noise in channel openings that was notably worse at negative potentials (LeMasurier et al., 2001). In a more recent description of single channel KcsA currents, using the inside-out patch clamp method with symmetrical conditions of 200 mM KCl, KcsA was reported to have a single channel conductance of 70 pS at 100 mV (Chakrapani et al.,

2007). In this work, the intraburst open probabilities of the gating events were measured and three distinct populations reported, including a low P_o mode, a flicker mode and a high P_o mode (Fig 2.16 c)). These different gating modes gave rise to three distinctly different types of opening events, where the low P_o mode is characterised by few brief openings of a few milliseconds, the flicker mode is depicted by rapid gating, while in the high P_o mode the channel remains in the open position with short closing and opening events (Chakrapani et al., 2007). It was also found that the open probability of the channel increases ∼30-fold between pH 5.5 and 3.0, which is the first quantitative measurement of the pH dependency of the channel (Chakrapani et al., 2007).

2.4.2 KvAP

The first structure of a voltage-gated potassium channel, termed KvAP, from the hyperthermophilic archeabacterium *Aeropyrum pernix* (Ruta et al., 2003) was determined by crystallising the channel as a complex with a monoclonal Fab fragment attached to its voltage sensors (Jiang et al., 2003). This revealed that tetrameric KvAP contains a canonical pore (S5-S6) surrounded by voltage sensors, comprising of four membrane spanning helical segments (Jiang et al., 2003). Here, S3 consists of two helices referred to as S3a and S3b, where S3b forms a helix-turn-helix with the N-terminal half of S4. This is called the voltage-sensor paddle and resides on the outer perimeter of the channel (Jiang et al., 2003; Long et al., 2005, 2007). Single channel measurements of the full length KvAP channel in planar lipid bilayers, composed of POPE: POPG with a symmectric KCl concentration of 150 mM on both sides of the bilayer, revealed a single channel conductance of 170 pS when a voltage step was applied (Ruta et al., 2003). The channel was also found to be strongly selective for potassium ions over sodium ions, thus exhibiting functional properties similar to eukaryotic voltage-gated potassium channels. This preservation of function reflects structural conservation in the voltage sensor as revealed by specific, high affinity interactions with tarantula venom toxins (Ruta et al., 2003). In a separate study, measurements were also obtained by patch clamping giant DPhPC unilamellar vesicles containing KvAP. Under symmetric conditions of 100 mM KCl, channel openings and closings were observed with a conductance of 100 pS when the holding potential was suddenly raised to 100 mV (Aimon et al., 2011). It was also observed that the channels were highly selective for potassium over sodium and had a tendency to open more with increasing voltage (Aimon et al., 2011). KvAP gating has also been shown to

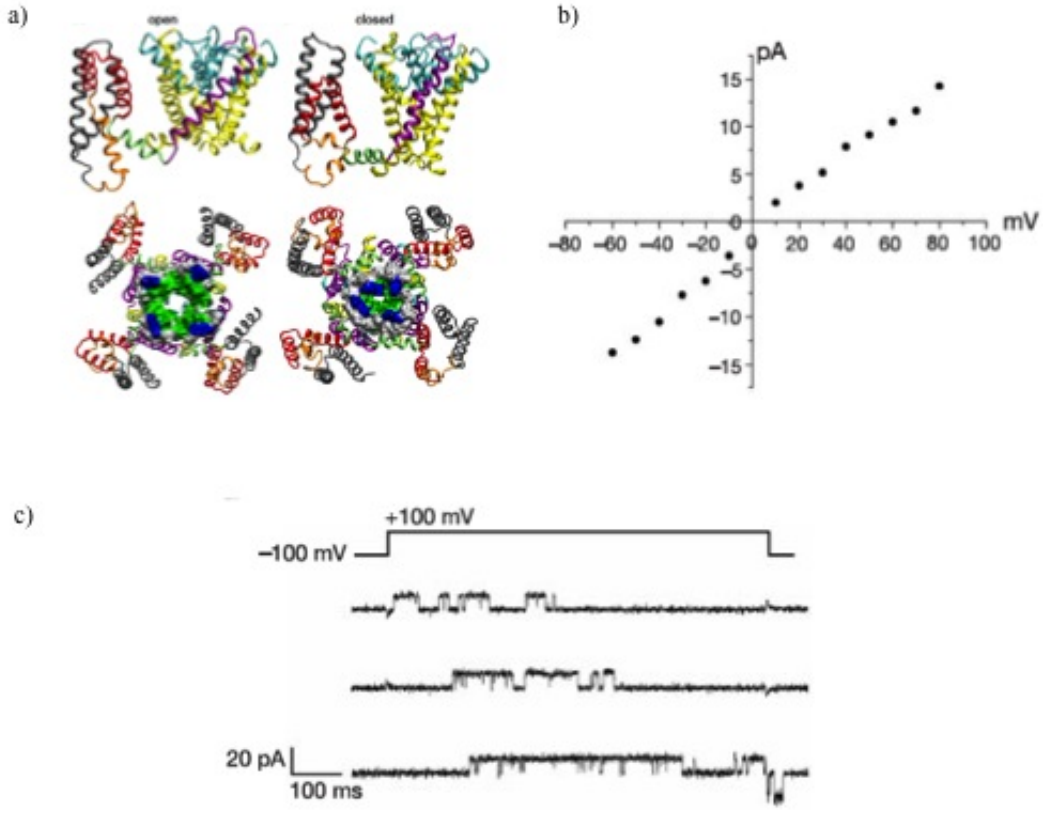

Figure 2.17: The KvAP channel. a) The pore domain and a single voltage sensor in the open and closed state, viewed from the side (top) and from the top (bottom). S1 and S2 are grey, S3a is orange, S3b-S4 is red, the S4-S5 linker is green, S5 is purple, the P-helix is cyan and S6 is yellow (Schow et al. 2012). Single-channel measurements were obtained from reconstituted protein in planar POPG : POPE bilayers in b)-c). b) Single-channel current of the KvAP channel as a function of voltage, c) Single-channel measurements at 100 mV. The voltage step used to trigger the openings is shown at the top of the traces. The figures are taken from Schow et al. (2012); Ruta et al. (2003).

depend on the properties of the lipid membrane (Schmidt et al., 2006; Schmidt and MacKinnon, 2008), where the channel was shown to respond differently in bilayers containing POPE:POPG compared to those formed of DPhPC (Schmidt et al., 2009). Specifically it was observed that the channels activated at more negative voltages in POPE:POPG bilayers and displayed a slower rate of recovery from the inactivated state.

2.4.3 Kv11.1 (hERG)

The human Ether-à-go-go Related Gene (hERG) [1] encodes the pore-forming subunit of the Kv11.1 delayed rectifier potassium channel. The protein comprises of 1,159 amino acids (Warmke and Ganetzky, 1994), forming 6 transmembrane segments, S1-S6, with S1-S4 forming the voltage sensor domain and S5-S6 along with the intervening pore loop contributing to the pore domain. Similar to KvAP, the channel forms a tetramer with a pore domain from each of the four subunits lining the ion conduction pathway. In addition to the membrane-spanning region, the hERG proein contains large cytoplasmic NH2-terminal and COOH-terminal domains, where the PAS domain of the former is a characterising feature of the ether-a-go-go subfamily of voltage-gated potassium channels (Warmke and Ganetzky, 1994) and the cyclic nucleotide binding domain (cNBD) of the latter is homologous with hyperpolarisation activated channels. The hERG channel is expressed in the heart, brain, smooth muscle, endocrine cells and a variety of tumour cell lines in humans (Vandenberg et al., 2012). The medical relevance of the channel arises since mutations in the gene are known to cause chromosome 7-assisted long QT syndrome (Curran et al., 1995), a cardiac repolarisation disorder that predisposes affected individuals to rapid irregular heartbeats that can lead to fainting and sudden death. In addition, blockade of the channel by a wide range of prescription medications can also cause drug-induced QT prolongation with an increased risk of sudden cardiac arrest. This discovery has resulted in the pharmaceutical industry performing cardiac safety screening for hERG channel activity in the early stages of developing novel pharmaceutical compounds (Sanguinetti and Tristani-Firouzi, 2006).

While the hERG channel is well-characterised for macroscopic currents, there are few reports detailing single channel characterisation. The first single-channel currents of the hERG channel were by Kiehn et al, achieved by inserting hERG RNA into *Xenopus oocytes* and obtaining electrical measurements using the standard two electrode patch clamp technique (Kiehn et al., 1996). Channel activity was only apparent during repolarisation and the single channel conductance was measured to be 7.0, 10.1 and 13.7 pS when the KCl concentrations in the pipette were 50, 100 and 300 mM respectively (Kiehn et al., 1996). In a separate study, using a similar method with 120 mM KCl in the pipette, a

[1] The hERG gene is the human homologue of the Ether-à-go-go gene found in Drosophila. The name à-go-go was coined in the 1960's by William Kaplan, who observed that flies carrying mutations in this gene had shaky legs when anaesthetised with ether and likened the effect to a type of dancing popular at the time at the Whisky A-Go-Go nightclub in West Hollywood, California.

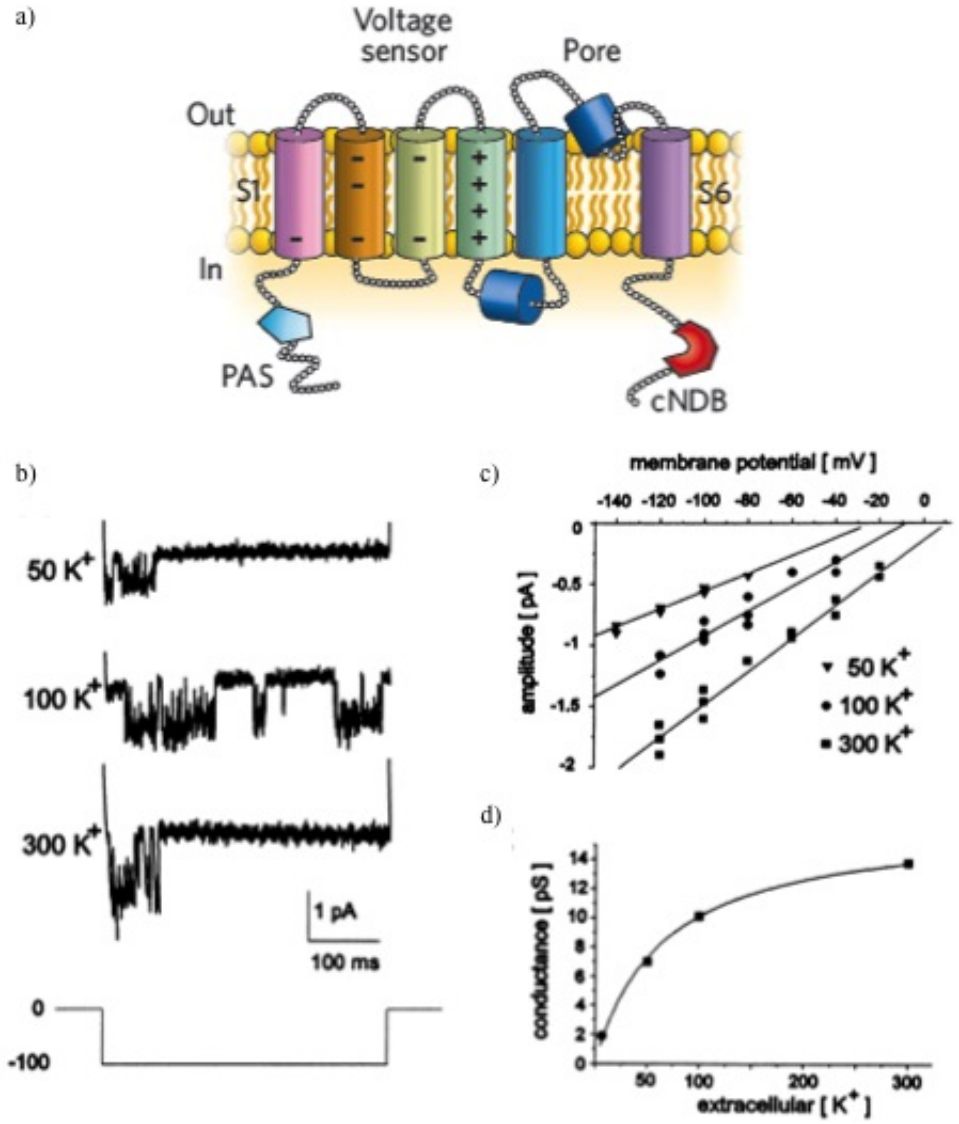

Figure 2.18: The hERG channel. a) A diagram of a single hERG subunit containing six alpha helical transmembrane domains, S1-S6. Features highlighted include the S4 domain which contains multiple basic (+) amino acids and the acidic Asp (-) residues in S1-S3, which can form salt bridges with specific basic residues in S4 during gating. The figure was taken from (Sanguinetti and Tristani-Firouzi, 2006). b) Single channel gating under the applied voltage step with different concentrations of potassium in the patch pipette. c) The amplitude of the observed channel openings plotted against the holding potential applied for each salt concentration. d) A plot of the channel conductance against the extracellular potassium concentration. Part a) was obtained from (Sanguinetti and Tristani-Firouzi, 2006)) and parts b)-c) were taken from Kiehn et al. (1996).

conductance of 12.1 pS was measured between test potentials of -50 and -110 mV. It was also reported that the probability of channel openings was low at positive test potentials (40 to 80mV) and the slope conductance was calculated to be 5.1

pS (Zou et al., 1997). In addition, the authors also showed channel blocking by MK-499, which they suggest occurs on the cytoplasmic side of the membrane (Zou et al., 1997).

2.5 Summary

Ion channels are membrane proteins of interest for medical research and drug discovery as outlined in section 1.3. This chapter begins by introducing the conventional methods for obtaining ion channel measurements (outlined in section 1.3) before a comprehensive review of contemporary approaches is presented. These include automated patch-clamp platforms, planar bilayer arrays and the use of interdroplet bilayers for performing electrophysiology. These configurations are of particular interest to this study for the purpose of developing a high-throughput screening platform as explained in section 1.3. The chapter continues to explain all of the steps involved in obtaining ion channel measurements from *in-vivo* expressed protein, previously summarised in Fig 1.2. This clarifies the advantages of the CF method, which is explained together with the current state-of-the-art in the field. Here, the phenomenon of self-insertion of CF expressed membrane proteins into lipid bilayers is reviewed in detail alongside a summary of the achievements made in performing CF expression in microsystems. The chapter concludes by outlining the general structure and function of ion channels, together with specific details of some of the characteristics of the channels investigated as part of this study. Such topics are important for developing a microdevice capable of the coupled expression and characterisation of ion channels as explained in sections 1.1 and 1.3.

The structure of this chapter is replicated in Chapter 3 where the specific methods used for expressing proteins and obtaining ion channel measurements are explained in further detail.

Chapter 3

Methods and preliminary work for cell-free expression and ion channel measurements

This chapter is split into two parts, detailing all of the materials and methods required to: 1) express a protein *in-vitro* using CF protein expression (as outlined in section 2.3) and 2) to form lipid bilayers and to obtain single-channel measurements using electrophysiology (as explained in section 2.1). The first section begins with a brief overview of the processes used by project collaborators to prepare the DNA templates used in this study, before the details concerning the preparation of the CF expression are presented. A summary of the methods used to verify the CF expressed protein is then provided. The section concludes by showing some preliminary data to demonstrate that the expression system functioned correctly. This is achieved by showing the CF expression of green fluorescent protein (GFP), while also highlighting the problem of identifying CF expressed proteins from the residual proteins present in the CF system. The second section begins by describing the assembly of a conventional electrophysiology system for aperture-suspended lipid bilayers. The section then continues to show the fabrication and setup of a flexible PDMS substrate akin to a version previously presented in the literature (section 2.1.4) that was shown to be capable of forming and regulating the size of interdroplet bilayers (Sarles and Leo, 2010b). This method was particularly interesting for the purpose of this study as control of the bilayer area may be beneficial for stabilising interdroplet bilayers formed in the presence of a CF system, a problem which has been introduced in section 1.1 and section 2.1.4. The third method involves the use of electrokinetic droplet

manipulation to form droplet interface bilayers, as discussed in section 2.1.4. The device used was previously developed in the Morgan group (Aghdaei et al., 2008) and represents a basic unit of a digital microfluidic system that could be scaled to form a high-throughput screening platform as introduced in 1.3. Lipid bilayers have been formed in all three systems, with or without ion channel recordings using KcsA proteoliposomes, and the advantages and disadvantages of each system are discussed.

3.1 Methods for cell-free protein expression

This section outlines all of the materials and methods required to express proteins using commercial CF expression systems.

3.1.1 Template preparation

Here, the preparation of the different DNA templates that were used in this study are described. All DNA templates were prepared by collaborators.

Green fluorescent protein plasmid

The control template supplied with the Roche RTS100 System (5PRIME GmbH, Germany) was the source of the GFP DNA used in this study. The GFP gene was supplied pre-inserted into the pIVEX 2.3d vector (Fig 3.1 a)) and amplified in E.coli by Dr. Natalie Smithers (University of Southampton). The DNA was

a) b)

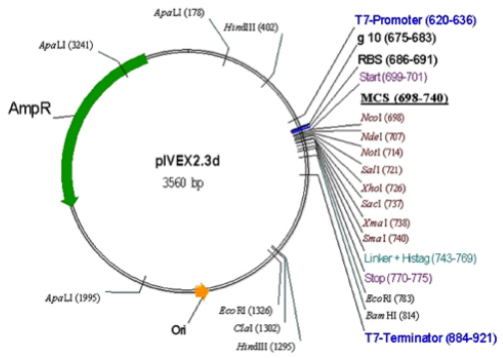

GFP:
M S K G E E L F T G V V P I L V E L D G D V N G H
K F S V S G E G E G D A T Y G K L T L K F I C T T
G K L P V P W P T L V T T F S Y G V Q C F S R Y P
D H M K Q H D F F K S A M P E G Y V Q E R T I F Y
K D D G N Y K S R A E V K F E G D T L V N R I E L
K G I D F K E D G N I L G H K M E Y N Y N S H N
V Y I M A D K Q K N G I K V N F K I R H N I E D G
S V Q L A D H Y Q Q N T P I G D G P V L L P D N H
Y L S T Q S A L S K D P N E K R D H M I L L E F V
T A A G I T H G M D E L Y K

Figure 3.1: The Green fluorescent protein DNA plasmid. a) The vector map of pIVEX 2.3d (image taken from 5PRIME GmbH, Germany). b) The amino acid sequence of the GFP protein.

introduced into E.coli and grown in broth containing ampicillin, allowing only the cells expressing the DNA template to grow. The cells were then harvested and the DNA was purified using standard methods. The final eluate was suspended in 10 mM Tris-Cl nuclease-free solution, pH 8.5 and the DNA concentration was determined using a NanoDrop Spectrophotometer. The amino acid sequence for wild-type GFP is given in figure 3.1 b).

KcsA plasmid

The DNA encoding KcsA was provided by Professor Tony Lee (University of Southampton). The DNA was supplied pre-inserted into the pQE32 vector and hosted in M15 cells as described previously (Marius et al., 2012). The KcsA was excised from the pQE32 vector and appropriate restriction sites were introduced to the gene by PCR (Dr. Natalie Smithers). The DNA was subsequently cut, amplified with the pEcoli-Cterm 6xHN vector (Figure 3.2 a)) using PCR and ligated. The DNA was inserted into E.coli and grown in broth containing ampicillin. The cells were harvested and the DNA was purified using standard methods. The final DNA concentration was determined using a NanoDrop Spectrophotometer and the sequence was confirmed by a commercial sequencing service. The amino acid sequence for wild-type KcsA is supplied in Fig 3.2 b). A modified pEcoli plasmid was also constructed for the production of non-tagged KcsA.

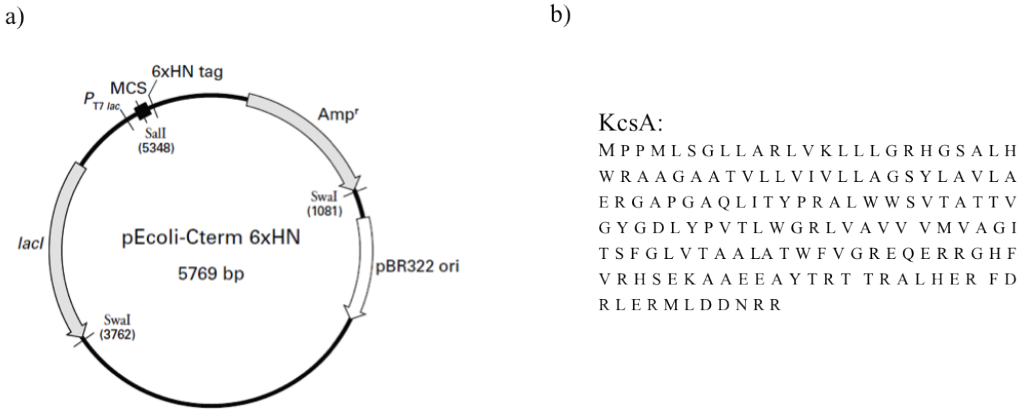

Figure 3.2: The KcsA DNA plasmid. a) The vector map of pEcoli-Cterm 6xHN (image taken from Clontech Laboratories, USA). b) The amino acid sequence of the KcsA monomer.

KvAP plasmid

The KvAP plasmid, encoding the full-length wild type protein (amino acid sequence shown in Fig 3.3 b)), was obtained from a stock of pre-transformed cells

stored in glycerol from previous work (Rogers, 2010). The original DNA sequence, inserted into the pQE-60 vector (figure 3.3 a)), was a gift from Professor R. MacKinnon. The plasmid was inserted into XL-1 Blue cells in order for the *in-vivo* expression of the vector to be inducible by IPTG. The cells were grown in 1 L of nutrient broth containing 1 mg/ml ampicillin and 0.0025 mg/ml tetracycline. The XL-1 Blue cells were resistant to tetracycline, while the vector encoded resistance for the ampicillin, ensuring that only the cells encoding the plasmid were allowed to grow. The cells were later harvested and the DNA was purified using standard methods. The DNA concentration of the final eluate was determined using a NanoDrop Spectrophotometer.

a)

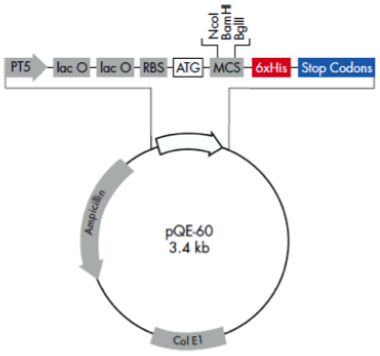

b)

KvAP:
MARFRRGLSDLGGRVRNIGDVMEH
PLVELGVSYAALLSVIVVVVEYTMQ
LSGEYLVRLYLVDLILVIILWADYA
YRAYKSGDPAGYVKK TLYEIPALVP
AGLALLIEGHLAGLGLFRLVRLLRF
LRILLIISRGSKFLSAIADAADKIRFY
HLFGAVMLTVLYGAFAIYIVEYPDP
NSSIKSVFDALWWAVVTATTVGYG
DVVPATPIGKVIGIAVMLTGISALTL
LIGTVSNMFQKILVGEPEPSCSPAKL
AEMVSSMSEEEFEEFVRTLKNLRRL
ENSMKLVPRGSRS

Figure 3.3: The KvAP DNA plasmid. a) The vector map of pQE-60 (image taken from the German Research Centre for Environmental Health, Germany.) b) The amino acid sequence of KvAP.

hERG$_{S5-S6}$ plasmid

The full-length hERG plasmid was provided by Dr. Philip Williamson through a collaboration with Professor Isabelle Marcotte (Université du Québec à Montréal). The hERG$_{S5-S6}$ plasmid (UniProtKB entry Q12809, residues 540-673) was prepared by Andre E. Gravel under the supervision of Jason C. Young (McGill University). The DNA fragment was inserted into a pProEX HTa vector (Fig 3.4 a)) with a Trc promoter sequence (Invitrogen Life Technologies, UK) by Maïwenn Beaugrand (University of Southampton). The cells were subsequently grown in ampicillin and harvested before the DNA was purified. The final eluate was analysed using a NanoDrop Spectrophotometer (Maïwenn Beaugrand).

a)

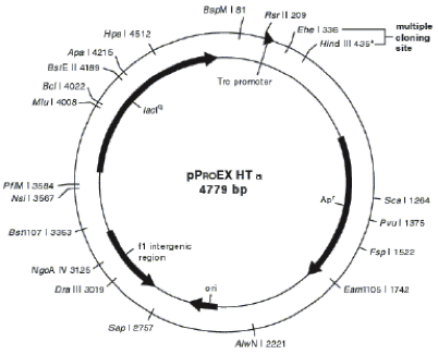

b)

hERG$_{S5\text{-}S6}$:
D R Y S E Y G A A V L F L L M C T F A L I A
H W L A C I W Y A I G N M E Q P H M D S R
I G W L H N L G D Q I G K P Y N S S G L G G
P S I K D K Y V T A L Y F T F S S L T S V G F
G N V S P N T N S E K I F S I C V M L I G S L
M Y A S I F G N V S A I I Q R L Y S G T A R Y

Figure 3.4: The hERG$_{S5-S6}$ DNA Plasmid. a) The vector map of pProEX HTa (image taken from Life Technologies, USA). b) The amino acid sequence of the hERG$_{S5-S6}$ pore domain.

3.1.2 GFP and KcsA protein

The GFP plasmid and the KcsA plasmid detailed in section 3.1.1 were separately expressed in E.coli culture and purified to obtain His-tagged GFP and KcsA protein (Dr. Natalie Smithers, University of Southampton). These proteins were used as positive controls on SDS PAGE gels as detailed in sub-sections 3.1.13, 5.1.1 and 5.1.2.

3.1.3 Unilamellar vesicle formation

The desired amount of lipid in chloroform was added to a glass vial. The lipids were typically a 1:1 (w/w) mixture of 1,2-dioleoyl-*sn*-glycero-3-phosphocholine (DOPC) and 1-palmitoyl-2-oleoyl-*sn*-glycero-3-phospho-(1'-*rac*-glycerol) (POPG) (Avanti Polar Lipids, AL, USA). The chloroform was evaporated under a stream of nitrogen to form a dry lipid film, which was placed inside a vacuum desiccator for $\sim$1 hour to remove any residual solvent. Subsequently, 1 mL of electrophysiology buffer pH 7 was added to the lipid film, which was then resuspended using a vortexer. The resulting dispersion of multilamellar vesicles was freeze-thawed five times and then passed 21 times through a polycarbonate filter with 100 nm pores (Avanti Polar Lipids, AL, USA) to obtain large unilamellar vesicles.

3.1.4 The cell-free reaction

The L1130 E. coli T7 Extract System for Circular DNA (Promega, USA), the EasyXpress Protein Synthesis Kit (Qiagen Ltd, UK), the Expressway Cell-Free E. coli Expression System (Invitrogen Life Technologies, USA), and the Promega L1110 S30 T7 High-Yield Protein Expression System (Promega, USA) were prepared as directed by the manufacturer, with the exception that the distilled water component in the reaction mixture was replaced with electrophysiology buffer (150 mM KCl, 10 mM HEPES, pH 7.0). Typically for the L1130 system, equal volumes of two minus amino acid solutions were first mixed by pipetting before 5 μl of the mixture was added to 20 μl of the reaction S30 pre-mixture. 15 μl of the cell extract was then added, followed by 9 μl of nuclease free water supplemented with buffer. The desired amount of DNA was typically prepared to 1 μl and added last to control the initiation of the reaction, with the only exception being when vesicles were added to the CF mixture. In this instance, the vesicles were added last, inside the 9 μl volume used to dilute the CF mixture, and the DNA was the penultimate component to be added. The final volume of all of the CF reactions was 50 μl, and is commonly referred to as one volume of the CF reaction in the later chapters. The CF mixture was used without incubation in Chapter 4 and at 30 °C for 2 hours in Chapters 5 and 6, with or without agitation as specified. The CF reactions were kept on ice before use.

3.1.5 Protein purification using Ni-NTA affinity chromatography

Ni-NTA agarose beads (Qiagen, UK) from 40 μl of as-supplied bead slurry were equilibrated and resuspended in 50 μl wash buffer (20 mM imidazole in phosphate buffered saline (PBS)) according to the instructions from the manufacturer. The affinity bead dispersion was then added to 100 or 150 μl of a completed cell-free reaction mixture, followed by overnight incubation under agitation at 4 °C. Beads were then washed with four bead volumes of wash buffer, before elution with stepwise increases in imidazole concentration: 0.1, 0.5 and 1 M imidazole in PBS with 5% glycerol. Finally, the beads were resuspended in 50 μl PBS. For purifications where the pooled eluates were to be used as an electrophysiology sample all elution buffers were supplemented with electrophysiology buffer (150 mM KCl, 10 mM HEPES, pH 7.0) and the 1 M imidazole elution step was replaced with more 0.5 M imidazole elutions. 15% SDS-PAGE gels were prepared

as described in the next section. 25 μl of the first bead wash and 50 μl of the final bead wash plus each of the bead imidazole eluates were mixed with 10 μl β-mercaptoethanol-containing loading buffer and denatured at 99 °C for 3 minutes. 50 μl of each sample (30 μl for the first bead wash) was loaded on the gel for gel electrophoresis. The gels were stained and imaged as described in the next subsection and were dried in cellophane for long-term storage using a gel dryer (Bio-Rad Laboratories, UK).

3.1.6 Gel electrophoresis

15% Tris-Glycine SDS PAGE gels were prepared using the mini-PROTEAN system (Bio-Rad Laboratories, UK) as shown in Fig 3.5 a). For one 15% gel, 1.87 ml of Millipore water was mixed with 1.02 ml of 1.5 M Tris-HCl, pH 8.8 and 60 μl of 10% SDS. 2.97 ml of polyacrylamide was then added, followed by 3 μl of TEMED and 72 μl of 25% APS. The gel was cast inside the fume hood and left to set for 15 minutes underneath a small volume of isopropanol, used to create a smooth interface for the adhesion of the stacking layer. This was prepared by mixing 1.02 ml of Millipore water with 960 μl of 1 M Tris-HCl pH 6.8, 360 μl of polyacrylamide, 2.5 μl of TEMED and 12 μl of 25% APS. The stacking layer was cast on top of the

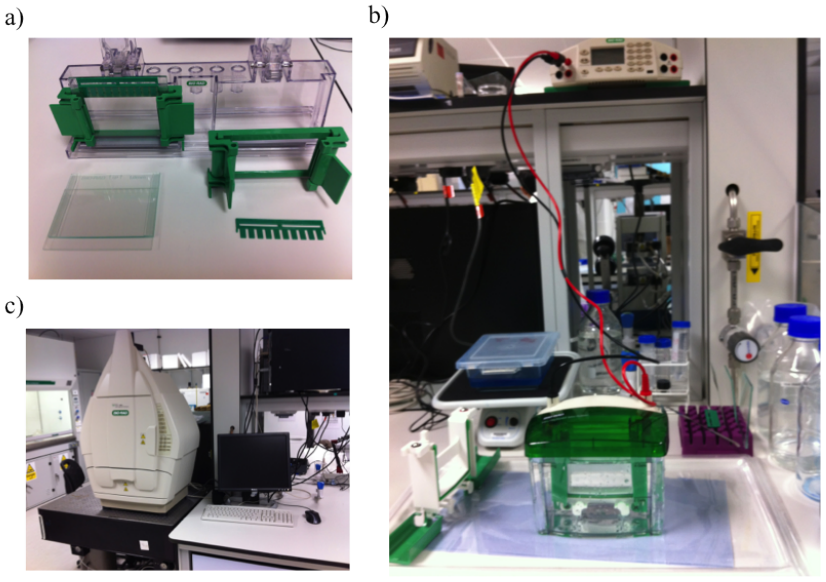

Figure 3.5: The SDS PAGE assembly. a) The gel is poured between two glass plates clamped together and inserted into a casting stand. b) The glass plate containing the gel is loaded into the electrode assembly and secured inside the gel tank filled with running buffer. c) The Gel Doc imager for photographing destained SDS PAGE gels.

resolving gel once the isopropanol was removed and a gel comb was inserted for the creation of the wells. The comb was removed once the gel had set and the gel was transferred to the gel tank (Fig 3.5 b)). This was filled with ∼1 L of running buffer containing 0.62 mM Tris-HCl, pH 8.3, 72 g of glycine and 5 g of SDS. Prior to loading, the desired volume of each sample was pre-mixed with loading buffer containing β-mercaptoethanol. The loading buffer was typically prepared to 5x to maximise the volume of sample loaded and contained 10% (w/v) SDS, 30% (w/v) Glyercol, 0.02% bromophenol blue, 0.25 M Tris-HCl, pH 6.8, and 5% β-mercaptoethanol. The samples were then denatured for 3 minutes at 99 °C and loaded onto the gel. 15 μl of See Blue Plus 2 (Life Sciences, USA), was loaded in the first lane and used as a molecular weight standard. The gels were typically run for 75 minutes at 150 V prior to staining with Coomassie Brilliant Blue for 10 minutes. Gels were then destained in 1 L of 5% methanol and 7.5% acetic acid. Destained gels were imaged with a Gel Doc XR imager (Bio-Rad Laboratories, UK) and analysed with Image Lab software (Bio-Rad Laboratories, UK). The gels were either disposed of in a dedicated bin for incineration or dried between two sheets of cellophane for long-term storage. For the purposes of approximating the mass of proteins loaded onto the gel, a standard gel was run containing 5.0 μg to 0.1 μg of BSA (Sigma Aldrich, USA). The 15% gel shown in Fig 3.6 a), was Coomassie stained and imaged under different exposure times ranging from

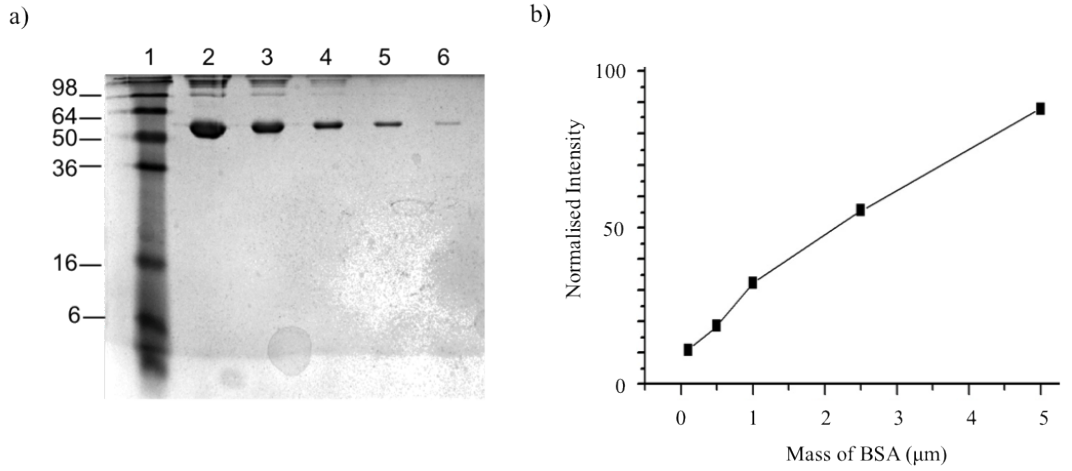

Figure 3.6: SDS PAGE standard gel containing BSA. a) 5.0 μg, 2.5 μg, 1.0 μg, 0.5 μg and 0.1 μg was loaded onto the gel in lanes 2-7 respectively and run for 75 minutes at 150 V. After Coomassie staining the gel was imaged under different exposure times and analysed using imageJ. The average of 5 measurements taken for the background was subtracted from measurements of each band and plotted as shown in part b). The figure shows one method for approximating the amount of protein loaded onto an SDS PAGE gel.

0.041 s to 0.06 s. The gel was analysed using ImageJ, where the intensities of the bands was recorded and normalised against an average of 5 measurements for the background. The data were plotted as shown in Fig 3.6 b), and repeated for each exposure time. An approximation of the amount of protein loaded onto a gel imaged with the same exposure time was determined by reading the value off the graph.

3.1.7 Western blotting

SDS PAGE gels were run for the CF expressed proteins as described in the previous section and supplied to collaborators for Western Blotting. Dr Natalie Smithers performed Western blots of CF expressed GFP and KcsA, while Maïwenn Beaugrand performed the Western blots for CF expressed KvAP and hERG$_{S5-S6}$. A piece of nitrocellulose paper was cut and dampened with transfer buffer (50 mM tris-HCl, 50 mM glycine, 800 ml methanol and 3.2 L of water) together with two sets of filter paper attached to pads. The gel was sandwiched in this setup as illustrated in Fig 3.7, with the nitrocellulose paper on the anode facing side of the gel. The setup was immersed in a transfer tank filled with running buffer and connected to a power pack. The Western transfer was run for 2 hours at 100 V. For CF expressed GFP and KcsA (section 5.1.1), the Western blot was attempted without protein purification from the CF system. After Western transfer the nictrocellulose paper was blocked overnight on a rotating platform in 0.1% (v/v) tween, 5% (w/v) milk in PBS at 4 °C. The nitrocellulose was then washed for

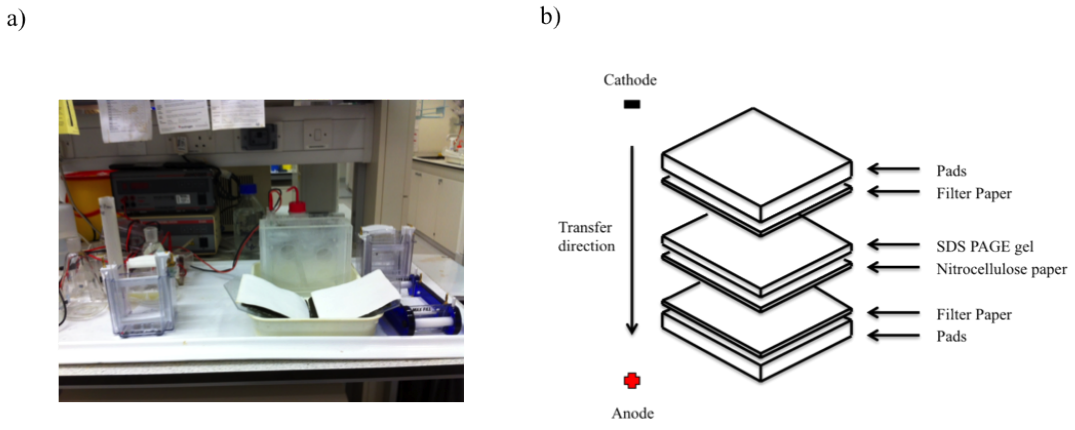

Figure 3.7: The Western transfer setup. a) The Western Transfer apparatus including the two sets of pads and filter paper and a tank containing the electrodes. b) A schematic diagram of the fundamental components required for Western transfer.

1 hour in a solution containing 0.1% tween (v/v), 5% milk and the rabbit anti-HN primary antibody (RayBiotech, USA) prepared to a final concentration of 1 μg/ml in PBS. The antibody solution was then removed and the nitrocellulose paper was briefly soaked in water, which was then replaced with wash buffer containing 5% BSA in PBS. The nitrocellulose was left soaking in the wash buffer on the rotating platform for 10 minutes before the wash buffer was replaced with fresh solution. This was repeated a total of three times. The nitrocellulose paper was then incubated with a solution containing a horseradish peroxidase (HRP) conjugated goat anti-rabbit secondary antibody (RayBiotech, USA), prepared at 1:3000 dilution in PBS containing 5% BSA, 0.1% tween. The nitrocellulose paper was then dried and transferred to a darkroom for chemiluminescent imaging using photographic paper. Briefly, the Thermo SuperSignal West Dura ECL detection reagent (Life Technologies, USA) was prepared as directed by the manufacturer and deposited on the nitrocellulose paper. The photographic film was exposed to the nitrocellulose for 30 seconds in a small light-proof box. The film was subsequently developed using standard developer solutions.

For CF expressed KvAP (section 5.2.1) and hERG$_{S5-S6}$ (section 5.3.1), the protein was purified from the CF system as described in section 3.1.5, before the SDS PAGE gel used for the Western transfer was run. After the transfer was complete, the nitrocellulose paper was blocked in Odyssey blocking buffer for 1 h. The primary monoclonal anti-polyhistidine antibody (Sigma-Aldrich Company Ltd., UK) was diluted as directed by the manufacturer and poured over the nitrocellulose paper. The paper was incubated with the primary antibody under light agitation for 1 h prior to being washed three times with PBS. The Quick Western Kit - IRDye 680RD (LI-COR) was used for detection. The detection solution was prepared according to the manufacturers instructions and incubated with the paper for 1 h. The nitrocellulose paper was finally washed three times with PBS and transferred to a Li-Cor Odyssey infrared imaging system.

3.1.8 Protein reconstitution

Protein reconstitution was performed using SM-2 BioBeads (Bio-Rad, USA). To activate the beads, 2 g were weighed out inside a beaker and washed with analytical grade methanol for 30 minutes using a magnetic stirrer. The beads were allowed to settle, the methanol poured away and the volume replaced with 150 mM KCl, 10 mM HEPES, pH 7.40 electrophysiology buffer. The beads were washed for 30 min using a magnetic stirrer, before the dispersion was allowed to settle. The

floating beads were discarded and the buffer replaced with a fresh solution. This was repeated three times to ensure that the methanol was completely removed. The washed beads were stored in buffer at 4 °C until use.

The desired quantity of lipid was prepared in a glass vial by making a lipid film, as described in the section 3.1.3 for the formation of unilamellar vesicles. 1 ml of electrophysiology buffer containing 40 mM b-D-octyl-glucoside was added and the solution was sonicated in short bursts lasting 1-2 min. The protein of interest was then transferred to the mixture to give a molar ratio of lipid:protein of 10,000:1. To initiate protein reconstitution, the buffer was removed from the washed BioBeads and 80 mg were added to solution. The absorption of the detergent by the BioBeads, resulted in the transformation of micelles to proteoliposomes, as is indicated by the clear solution changing to form a cloudy emulsion. The sample was carefully removed from the beads after 1 h and added to a fresh 80 mg of beads for a further hour, after which the reconstituted protein was again removed and transferred to a fresh eppendorf tube. The sample was either kept on ice and used immediately or stored at -20 °C.

3.1.9 The cell-free expression of green fluorescent protein and detection using fluorescence microscopy

The proceeding subsections in this chapter explain the methods used for expressing and detecting proteins, however it remains to be seen whether the commercial CF systems are compatible with the templates described in section 3.1.1. This is addressed in this subsection by demonstrating the CF expression of GFP using fluorescence microscopy.

Expression was performed as described in 3.1.4 using the Promega L1130 system and the Invitrogen ExpressWay system. Both systems were supplied with 1 μg of the GFP DNA template and run alongside controls containing no DNA (the volume was replaced with RNase-free water). The eppendorfs were snap-frozen using liquid nitrogen after incubation and thawed by hand for analysis, where 2 μl samples were prepared on a glass slide and imaged. Images were taken at multiple positions at x20 magnification with an exposure time of 10 sec using a FITC filter set. They were later analysed using ImageJ to determine the mean intensity of the fluorescence in selected areas, the size of which was kept constant for the purposes of consistency.

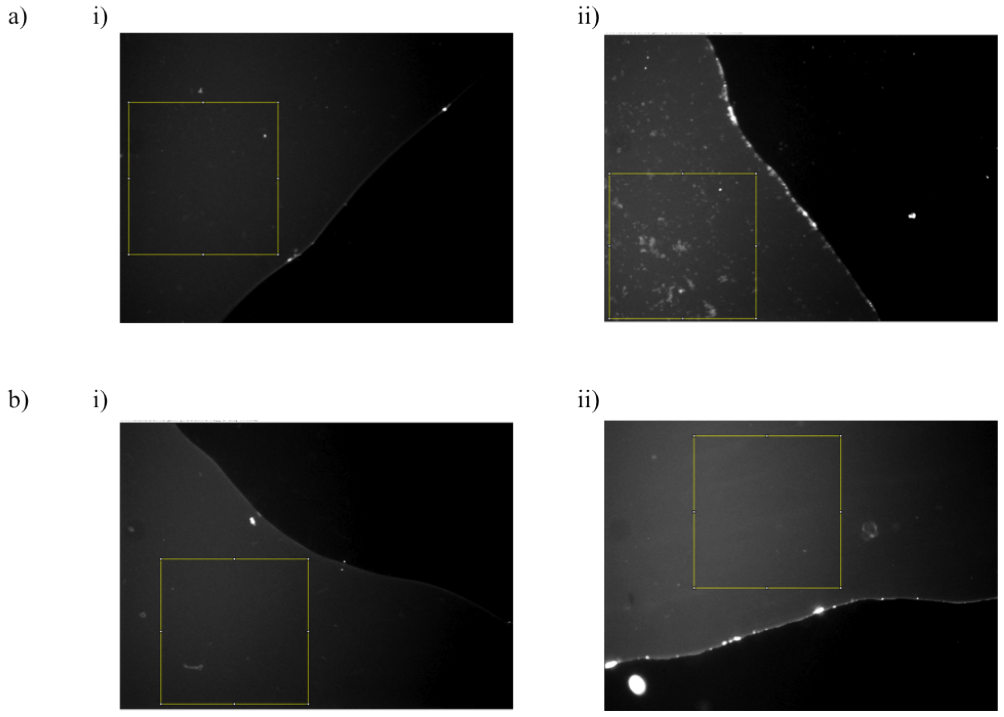

Figure 3.8: Fluorescent micrographs of cell-free expressed GFP. The eppendorfs were snap-frozen using liquid nitrogen after incubation and thawed by hand for analysis, where 2 μl samples were prepared on a glass slide and imaged. The Promega L1130 system is shown in part a) and the Invitrogen ExpressWay system in part b). The images were taken using a 20x objective using a FITC filter set and show the interface between a 2 μl volume of the sample and air. Control samples, containing no DNA are shown in i), while ii) shows samples containing 1 μg of DNA. The image area was 5.5 μm x 4.2 μm and the region used for image analysis is indicated with the yellow box. The appearance of a stronger fluorescent signal in the samples containing the GFP DNA indicate that the protein was successfully expressed

A representative image of a control sample (i) and a sample containing GFP DNA (ii) is shown for both CF systems in Fig 3.8, where the Promega system is shown in part a) and the Invitrogen system in part b). The images were all taken at the sample-air interface to show the fluorescence of the sample in contrast to the glass. The mean intensity for each image was averaged and is summarised in Table 3.1, the difference in average mean intensity from the control is also indicated. From the data and the selection of images in Fig 3.8, it seems clear that both of the cell-free systems exhibit background fluorescence, with the Invitrogen system exhibiting 4% more background fluorescence on average compared to the Promega L1130 system. The data also shows an 11% and a 10% difference in average mean intensity between samples supplied with DNA and those without, for the Promega

Table 3.1: A summary of the data obtained from Fig 3.8, showing the average intensity of fluorescent micrographs of two different CF expression mixtures incubated with and without the GFP DNA template. The data indicates that the protein was expressed in both instances.

	Average mean intensity with no DNA	$n =$	Average mean intensity with GFP DNA	$n =$	Difference
Promega	88	4	99	4	11
Invitrogen	92	4	102	4	10

and Invitrogen systems, suggesting that some GFP has been expressed. Here, the relatively small difference between the samples may be attributed to the fact that only a small amount of GFP was present in the sample. This stands to reason as a typical 50 μl reaction is only expected to yield 50-250 ng of protein (Promega, 2009), meaning that a 2 μl sample could have contained between 2-10 ng of GFP.

In summary, the data suggests that GFP was successfully expressed, indicating that the two CF systems are compatible with the supplied GFP DNA template detailed in section 3.2. This is important to know before expressing more troublesome proteins like ion channels, which are expected to be harder to express and detect due to their insolubility in water and lack of a fluorescence signal.

3.1.10 The cell-free expression of GFP and real time measurements using a plate reader

In the previous section analysis of CF expressed GFP was performed using fluorescence microscopy. While this data allowed for the presence of the expressed protein to be confirmed, it did not give any indication of the reaction kinetics. This is interesting for providing some insight into how much protein is expressed over time and could be useful for estimating how long it might take for an ion channel to be expressed. This is relevant as it may provide some indication as to how long an interdroplet bilayer would need to be stable in order for the ion channel to be expressed and inserted into the bilayer for measurements. This section describes how these measurements were achieved using a 96-well plate reader equipped with fluorescence to monitor the expression of GFP.

A Greiner half-area 96-well plate (Greiner bio-one, Austria) was cleaned in RNase Zap (Life Technologies, USA), rinsed thoroughly in Milli-Q water and wrapped in blue roll for drying overnight. The Promega L1130 system was prepared in triplicate and scaled to 30 μl. Samples contained either; i) 1 μg of GFP DNA ii)

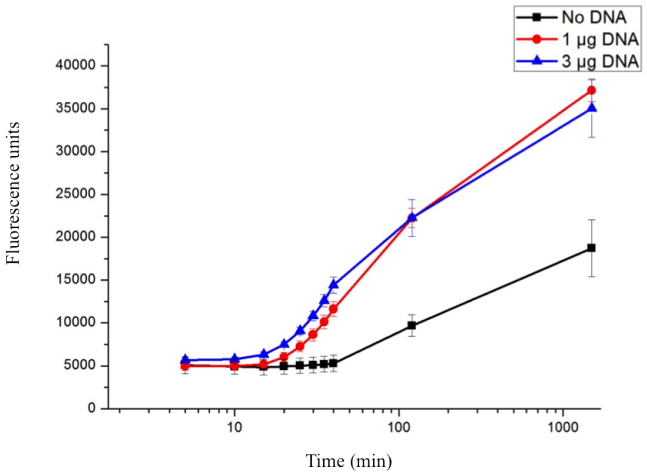

Figure 3.9: The cell-free expression of GFP and real-time detection using a plate reader. The CF reaction was prepared in triplicate on a 96-well place with 3 μg, 1 μg and no DNA as indicated. Measurements were taken every 15 minutes for 2 hours and again after a 24 hour incubation at 5 °C. Comparision of the amount of fluorescence detected for the samples containing DNA to the control with no DNA indicates that the expression of GFP was successful.

3 μg of GFP DNA and iii) no DNA (volume replaced using RNase-free water). Measurements were taken every 15 minutes for 2 hours and again after overnight storage in the cold room using the same gain settings.

The average of three data points for each condition is plotted in Fig 3.9. The data shows that the fluorescence of the samples containing 1 μg and 3 μg of DNA (indicated as red circles and blue triangles) rises rapidly before the rate of fluorescence increase gets smaller. In contrast, the sample containing no DNA is shown to exhibit only a negligable amount of fluorescence, until 100 minutes where a weak signal was observed. The expression of GFP is indicated by the average final fluorescence values, where the fluorescence of samples containing DNA is approximately twice the average value of those containing no DNA.

The data points in the control sample most likely arise from autofluorescence of the CF mixture as indicated in 3.1.9, while the reduction in the rate of protein expression is consistent with the exhaustion of metabolic precursor molecules as discussed in 2.3. The increase in the amount of fluorescence measured the next day is expected to be a due to the maturation of GFP overnight.

This data is useful to estimate the time required for a detectable amount of protein to be expressed, which appears to be ∼30 min.

3.1.11 Expression of GFP with fluorescent tRNA-lysine

It is clear from the data shown in this chapter that the commercial CF systems are capable of expressing GFP, however the methods presented thus far for protein detection are not suitable for CF expressed ion channels due to the lack of a fluorescence signal. The aim of this section is therefore to use CF expressed GFP to investigate other methods of protein detection. One strategy for achieving this is to supply the CF system with lysine transfer RNA labelled with the fluorophore BODIPY-FL and running the sample on an SDS PAGE gel. This allows for the fluorescent label to be incorporated into the CF expressed protein of interest, enabling the protein to be detected using a laser-based fluorescent scanner without the requirement for a C- or N- terminal affinity tag. This method also allows for the viability of identifying CF expressed proteins on SDS PAGE gels to be addressed, as the gel can later be stained and imaged.

The CF reaction was prepared and run in 50 μl volumes with 3 μg, 1 μg and no GFP DNA in triplicate as described in section 3.1.4, except that 3 μl of the BODIPY-FL tagged lysine transfer RNA (Promega, USA) was added with the nuclease-free water. As an additional control, an extra reaction was prepared containing 1 μg of the PinPoint control vector containing the chloramphenicol acetyltransferase gene fused to the pinpoint peptide sequence (Promega, USA). 5 μl of each sample was mixed with 7 μl of loading buffer (no β-mercaptoethanol), denatured for 3 minutes at 99 °C before 10 μl of each sample was loaded across two 10-lane, 15% 1.5 mm thick gels (prepared as described in section 3.1.6). $\sim$2 μg of recombinant eGFP protein (ThermoFisher Scientific, USA) was added as a positive control to estimate the position of the CF expressed GFP in the adjacent lanes. The gels were run for 1 hour and 15 min at 150V and imaged under UV light before staining with Coomassie blue.

The fluorescent band at $\sim$36 kDa in the gel images (indicated by the arrow) in parts a) and b) of Fig 3.10 show that the GFP was successfully expressed in lane 7 of gel a), and lanes 3, 4, 5 and 6 in gel b). This is inferred by the position of the positive control in lanes 2 of both gels, shown in red due to saturation of the instrument, and the absence of this band in all lanes that did not contain the GFP DNA template. The fluorescent signal in lane 2 is interesting, as the SDS present in the loading buffer should have denatured the GFP. This is relevant as it is then difficult to identify whether the GFP bands in the adjacent lanes are visible due to the fact that the protein has been expressed and not fully denatured, or whether the fluorescence signal is a result of the BODIPY-FL tagged lysine residue

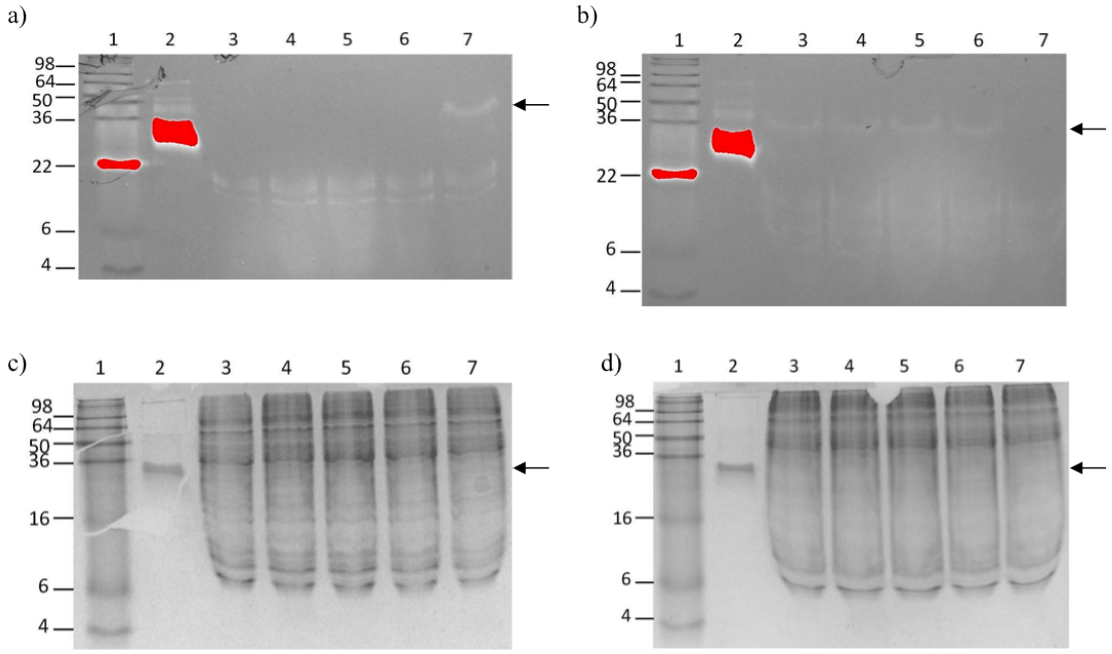

Figure 3.10: SDS PAGE gels of CF expressed GFP with BODIPY-FL tagged lysine tRNA. The gels were imaged under UV light, a)-b), and under white light after Coomassie staining, c)-d). In both gels, the molecular weight standard is shown in lane 1 and the recombinant eGFP protein in lane 2. In the gel shown in parts a) and c), lanes 3-5 contain the CF mixture with no DNA and the BODIPY-FL tagged lysine tRNA, while lanes 6, 7 and lane 3 of the gel in b) and d) show the CF mixture with tagged tRNA and 1 μg of GFP DNA. Lanes 4-6 of the second gel contain the CF reaction with 3 g of DNA with the BODIPY-FL tRNA, while lane 7 shows the CF reaction with the fluorescent label and the PinPoint DNA control vector supplied with the L1130 system. The data shows that CF expressed GFP was detected under UV light, but not after Coomassie staining. The position of GFP is indicated by the arrow.

incorporated into the protein. Yet the apparent absence of any fluorescence signal in lane 7 of gel b), containing the PinPoint DNA control vector, may indicate that the BODIPY-FL label is not detectable, although it is difficult to be certain that the protein was expressed. For this reason, and to determine whether CF expressed proteins could be detected without purification from a CF mixture, the gels were imaged under white light after Coomassie staining, as shown in parts c) and d) of Fig 3.10. Both of the gel images clearly show the molecular weight standard in lane 1 and the recombinant GFP protein in lane 2, where the position of the GFP is identical to the position of the fluorescent signal observed under UV light. The remaining lanes in both gels show a large number of proteins from the CF mixture, making it almost impossible to identify the protein of interest. This is an important observation as it is already clear from from the gel images in parts

a) and b) of Fig 3.10 that the GFP is present, meaning that in this instance, it is the method of detection (i.e. SDS PAGE with Coomassie staining) that is not suitable for identifying the CF expressed GFP. This would otherwise be difficult to determine without a fluorescence signal, as it would be difficult to confirm that the protein was expressed.

In summary, the data shows that GFP was expressed, however, the fluoresence exhibited by the positive control makes it difficult to determine whether the fluorescence observed for the samples was a result of the fluoro-tRNA label. This could have been verified by repeating the experiment without the fluorescent tag, introducing β-mercaptoethanol into the loading buffer to ensure complete protein denaturation or by attempting to express a non-fluorescent protein. In either instance, it is clear that Coomassie stained SDS PAGE gels containing the unpurified CF mixture are not useful for detecting CF expressed GFP.

3.1.12 Expression of KcsA with fluorescent tRNA-lysine

Further to the data presented in the previous section, the KcsA template engineered in 3.1.1 was supplied to the CF mixture supplemented with BODIPY-FL tagged lysine to determine whether the CF expressed protein could be identified.

Four CF reactions were prepared to a final volume of 50 μl. Two contained 1 μl of the BODIPY label and no DNA, one was mixed with 1 μg of GFP DNA and the remaining sample was supplied with 3 μg of KcsA DNA. In each case, the BODIPY label was added with the nuclease-free water that was used to adjust the final volume of the assay. Each sample was incubated as detailed in 3.1.4 and run on a 15%, 1 mm thick, 10 lane polyacrylamide gel as detailed in section 3.1.6 with 2.5 μl of each sample for 75 minutes at 150 V. The gel was imaged under UV light using a white light conversion screen and is shown in Fig 3.11. The bands at $\sim$17 kDa in lanes 2-6 and 9, are familiar from Fig 3.10 and, since lanes 2-4 contained no DNA, do not represent CF expressed protein. Instead, it is likely that these bands correspond to fluorescent proteins contained in the CF mixture, the presence of which has been indicated by previous data contained in Fig 3.8 and Fig 3.9. Lanes 5-7 shows samples supplied with the BODIPY label and the KcsA DNA template, however there appears to be no observable difference between these lanes and the control lanes 2-4. This suggests that either the KcsA protein cannot be detected or that no KcsA has been expressed. The absence of the low

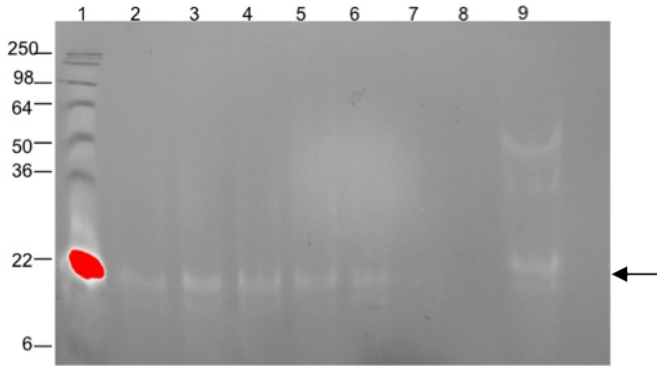

Figure 3.11: Cell-free expression of KcsA with incorporated BODIPY labeled lysine residues. Lane 1 contains the SeeBlue Plus 2 protein ladder, lanes 2-4 contain the negative control sample, the cell-free mixture with no DNA and 1 μl of the BODIPY label), Lanes 5-7 contain the CF system, 1 μl of BODIPY labeled lysine and 3 μg of KcsA encoding DNA, lanes 8 and 10 were empty, while lane 9 contained the CF system combined with 1 μl of the BODIPY label and 1 μg of GFP encoding DNA. The data show that no KcsA is detected. The gel was imaged under UV light. Saturation is indicated by red spots.

molecular weight proteins in lane 7 indicates that there was a pipetting error in the preparation of the sample. Lane 8 was left empty, while lane 9 contained the BODIPY label and 1 μg of GFP DNA template. The band observed at $\sim$40 kDa is higher than expected for GFP (27 kDa) but consistent with the data shown in the previous section, indicating that GFP has been expressed as observed in Fig 3.10. The arrow at $\sim$19 kDa indicates the region where the KcsA monomer would be expected.

The gel shows the CF expression of GFP, however no CF expressed KcsA is detected. It is unclear whether this infers that the KcsA was not expressed or whether the KcsA was expressed but did not incorporate the BODIPY label.

3.1.13 SDS PAGE of diluted CF expression mixtures spiked with KcsA protein

Experiments with GFP in the previous subsections have shown that commercial CF systems contain large quantities of proteins, leading to difficulties in identifying the CF expressed protein of interest by Coomassie staining (3.10). The ability to visualise the contents of the CF system on an SDS PAGE gel can be improved by dilution, however this will also dilute any CF expressed protein. The aim of

this section is thus to determine how much KcsA would be required for this to be achieved.

All samples contained 5 μl of 5x loading buffer, either 0.5 μl, 1.0 μl, 2.5 μl or 5 μl of the CF mixture, 0.1 μg, 0.5 μg, 1.0 μg or 2.0 μg of KcsA (prepared as described in 3.1.2 by Dr. Andy Powl, Birkbeck College) and were made up to a final volume of 12 μl using molecular biology grade water. 10 μl of each sample was loaded onto a 10% gel and run for 1 hour and 15 minutes at 150 V as detailed in section 3.1.6. Lane 2 of each gel contained 2.5 μg of KcsA, useful to identify the KcsA present in the adjacent lanes.

The gels shown in Fig 3.12 show two different sets of dilutions, where lanes 3-6 in part a) contain the CF mixture diluted 3.8x, while lanes 7-10 contain the CF mixture diluted 0.72x.

In both cases, the KcsA was added incrementally which, using the reference sample and the arrow provided as a guide, is just visible in lanes 3-6 but difficult to detect in lanes 7-10. Analysis of the gel suggests that the molecular weight of the reference sample in lane 2 is 13.5 kDa, while the bands in lanes 4, 5, and 6 were measured at 12.0 kDa, 11.9 kDa and 12.0 kDa respectively. Although these values are slightly lower than that measured for the control, the observation of increasing band intensity is convincing for the presence of KcsA. A plausible explanation for this is that the proteins in lanes 3-6 are running slightly further down the gel due to the effect of protein overloading.

The difficulty in identifying the KcsA in lanes 7-10 appears to be due to the higher concentration of the background proteins from the CF mixture. Bands similar in molecular weight to those highlighted in lanes 3-6 are highlighted in Table 3.2 however the absence of increasing band intensity relating to the increasing amount of KcsA is noticeable. This may indicate that the bands are not KcsA or that the high intensity of the bands already present in the CF system makes the difference in the bands of interest negligible. This clarifies that the level of dilution used for the samples in lanes 7-10 was inferior for the purposes visualising KcsA in comparison to the level of dilution used in lanes 3-6.

The gel containing the remaining two sets of samples, diluted 23x and 11.5x respectively is shown in Fig 3.12 b), where lanes 3-6 show the 23x diluted sample and lanes 7-10 contain the 11.5x diluted sample. As before, the KcsA was added incrementally in both sets of samples. The bands of interest are summarised in Table 3.2.

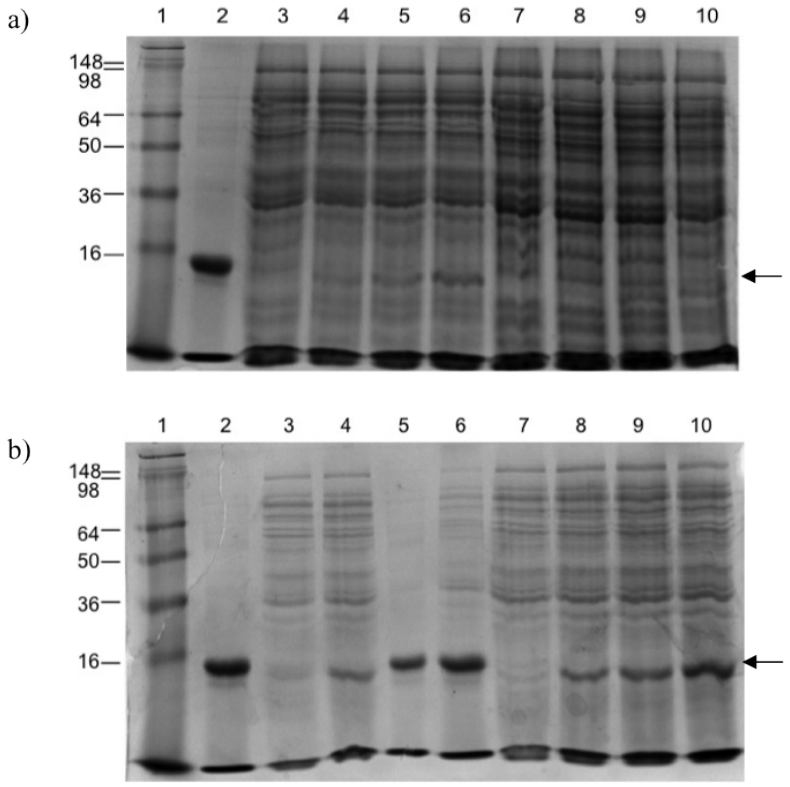

Figure 3.12: Detection of purified KcsA premixed with different dilutions of a cell-free system. Lane 1 of gel a) contains SeeBlue Plus 2, lane 2 contains 2.5 g of KcsA, lanes 3-6 contain the CF system diluted 3.8x laced with 83 ng, 416 ng, 833 ng and 1.66 g of KcsA. Lanes 7-10 contain the same quantities of KcsA as lanes 3-6 with the cell-free system diluted 0.72x. Lane 1 of gel b) contains SeeBlue Plus 2, lane 2 contains 2.5 g of KcsA, lanes 3-6 contain the CF system diluted 23x laced with 83 ng, 416 ng, 833 ng and 1.66 g of KcsA. Lanes 7-10 contain the same quantities of KcsA as lanes 3-6 with the cell-free system diluted 11.5x. The gels were run for 75 minutes at 150 V and Coomassie stained. The figure shows that it is difficult to detect the spiked KcsA with 0.72x dilution of the cell-free system compared to a 3.8x dilution where the KcsA can be identified from 416 ng.

It is interesting to observe that the KcsA appears to be detectable in both sets of dilutions at 83 ng, as shown by the bands lane 3 and lane 7. The molecular weights of the bands are 13.7 kDa and 13.3 kDa, which are within 1 kDa of 14.3 kDa measured for the reference sample. It stands to reason that the increased dilution enhances the visualisation of these bands, a notion that is supported by the fact that the intensity of band 17 in lane 3 is approximately three times more intense than band 18 in lane 7. By comparing the gels, it is also noticeable that the KcsA appears higher up the gel in Fig 3.1.13 b) compared to a), in line with higher dilution. This supports the inference regarding the effect of overloading

Table 3.2: Summary of the bands of interest extracted from Fig 3.12

Lane	Mol. Wt (kDa)	Relative front	Volume (int)	Mass loaded (μg)	Dilution Factor of Kit	Eq. Yield (μg/50μl)	Band %
Data from Fig 3.12 part a)							
1	16.0	0.63	1.7 x 10^6	N/A	N/A	N/A	9.9
2	13.5	0.69	6.9 x 10^6	2.50	N/A	N/A	49.9
4	12.0	0.73	0.5 x 10^6	0.42	3.80	8.30	2.0
5	11.9	0.73	0.7 x 10^6	0.83	3.80	16.70	2.6
6	12.0	0.73	1.4 x 10^6	1.66	3.80	33.20	6.1
7	12.8	0.71	0.7 x 10^6	0.08	0.72	0.87	3.1
8	12.0	0.73	0.7 x 10^6	0.42	0.72	4.20	2.8
9	11.6	0.74	0.6 x 10^6	0.83	0.72	8.30	2.3
10	11.6	0.74	0.6 x 10^6	1.66	0.72	16.60	1.8
Data from Fig 3.12 part b)							
1	16.0	0.63	2.8 x 10^6	N/A	N/A	N/A	13.2
2	14.3	0.66	6.9 x 10^6	2.50	N/A	N/A	42.8
3	13.7	0.68	0.8 x 10^6	0.08	23.00	8.30	5.8
4	13.6	0.68	2.0 x 10^6	0.42	23.00	41.60	13.8
5	15.0	0.65	3.7 x 10^6	0.83	23.00	83.30	30.8
6	14.8	0.65	6.1 x 10^6	1.66	23.00	166.00	39.9
7	13.3	0.69	0.3 x 10^6	0.08	11.50	4.15	1.6
8	13.5	0.68	1.6 x 10^6	0.42	11.50	20.80	8.3
9	13.6	0.68	2.3 x 10^6	0.83	11.50	41.65	11.0
10	14.0	0.67	4.5 x 10^6	1.66	11.50	83.00	18.0

and is useful to note for future experiments.

The molecular weight of the KcsA reference sample in lane 2 on both gels, recorded as 13.5 kDa in Fig 3.12 a) and 14.30 kDa in Fig 3.12 b) is close to the molecular weights of the KcsA measured in the spiked samples, ranging from 11.9 kDa to 15 kDa. This is convincing in terms of identifying the laced KcsA. In summary, the data shows that while dilution is advantageous, it will not be feasible to detect CF expressed KcsA using this method unless at least 4 μg of protein can be expressed to allow for sufficient dilution, which remains an ambitious target for one 50 μl volume of the CF system

3.2 Methods for bilayer formation and current measurements

This section explains the methods used for forming lipid bilayers and for obtaining ion channel measurements. The section is split into six parts, with the first subsection explaining the general amplifier setup, the second detailing the

formation of Ag/AgCl electrodes, the third describing the formation of aperture-suspended lipid bilayers, and the fourth discussing the use of the regulated attachment method for the formation of interdroplet bilayers. The fifth and sixth sections describe the formation of free-standing interdroplet bilayers using electrokinetic forces and by manual positioning.

3.2.1 Bilayer current amplifier

Bilayer current measurements were obtained using an Axon AxoPatch 200B Patch-Clamp amplifier (Molecular Devices, USA) connected to a Digidata 1440A digitiser (Molecular Devices, USA). The digitiser was connected to a PC via a USB connection, allowing for the amplifier to be controlled using pClamp (Molecular Devices, USA). The amplifier and digitiser were stored on the top of a steel storage cabinet (500 mm x 820 mm x 500 mm) used as a Faraday cage. The size of the cage allowed for a stereozoom microscope together with the relevant goniometer and translation stages to be inserted for work with microdroplets. The whole unit was connected to the ground port of the amplifier and placed on top of a Newport RS1000 optical table, which was separately grounded using the mains electricity supply. A retort stand fitted with a clamp was placed inside the Faraday Cage to hold the CV 203BU headstage (Molecular Devices, USA), which connected directly to the amplifier using a shielded cable. Single channel measurements were obtained at a sampling rate of 50 kHz, filtered using a 5 kHz low-pass 8 pole Bessel filter and later digitally filtered with a 1 kHz low-pass digital filter. Any additional filtering beyond this stage is indicated in the text. Capacitance measurements were obtained by applying a linear voltage ramp under conditions (triangle waveform; 500 Hz frequency, 1 mV peak-to-peak, i.e., $\pm$1V/s voltage ramp), where the measured current response (e.g., 100 pA) can be interpreted as the bilayer capacitance (e.g., 100 pF).

3.2.2 Silver/silver chloride electrodes

Ag/AgCl electrodes were made in pairs by electroplating in 0.1 M HCl, as illustrated in the schematic diagram in Fig 3.13. Two even lengths of silver wire (Goodfellow, UK) were cut, soldered into a simple electrical circuit and immersed in a container of HCl. Care was taken to ensure that the metal surface of the wire remained untouched and that both wires were lowered into the HCl to the same depth without touching each other. A Pt counter electrode was inserted into

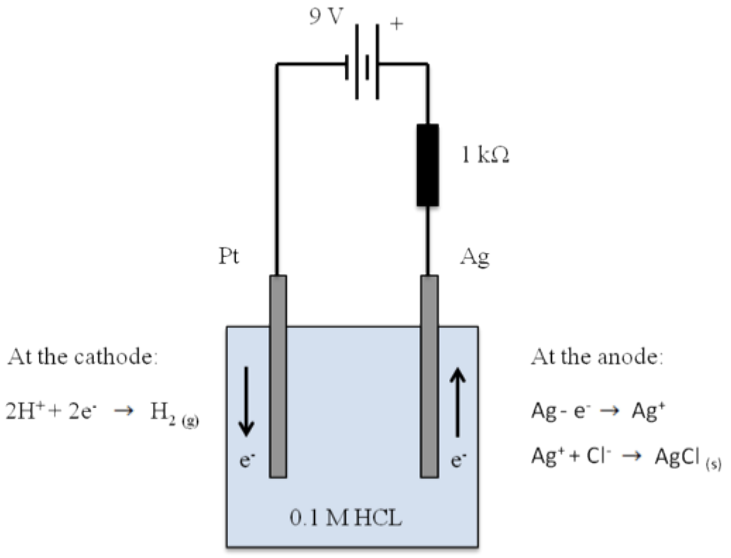

Figure 3.13: The formation of silver/silver chloride reference electrodes by electroplating. The schematic diagram represents a simple electrochemical circuit used for chlorinating two silver wires simultaneously in 0.1 M HCl. The dissolution of the HCl occurs at the cathode, resulting in the formation of H_2 gas, while at the anode AgCl rapidly accumulates on the surface of the anode

the HCl and a 9 V battery was attached for 30 seconds when using wire 250 μm thick, or 60 seconds with 500 μm thick wire. The current was limited by a 10 k resistor. Upon application of the electric field, the Ag wires rapidly darkened due to precipitation of insoluble AgCl salt on the anode surface while small bubbles of hydrogen gas emerged from the Pt cathode as a result of the dissociation of HCl.

3.2.3 KcsA electrophysiology with bilayer curvettes

The bilayer curvette system (Fig 3.14a)) is a conventional 2-part apparatus used to form planar lipid bilayers across a small pre-formed aperture either 150, 200 or 250 μm in diameter. The system consists of two chambers and a cuvette containing the preformed aperture. The cuvette fits precisely into one of the two chambers and is secured using a screw. For the purpose of this study, a cuvette made from Delrin was used with an aperture size of 150 μm. The system works by filling both chambers with 1 ml of buffer and painting a bilayer across the aperture. Ag/AgCl electrodes inserted into each compartment are connected to the amplifier to enable bilayer current and capacitance measurements. A schematic diagram of the setup is shown in Fig 3.14 part b) and a schematic of the assembly is shown in c). 20 μg of KcsA protein (prepared in section 3.1.2) was reconstituted into

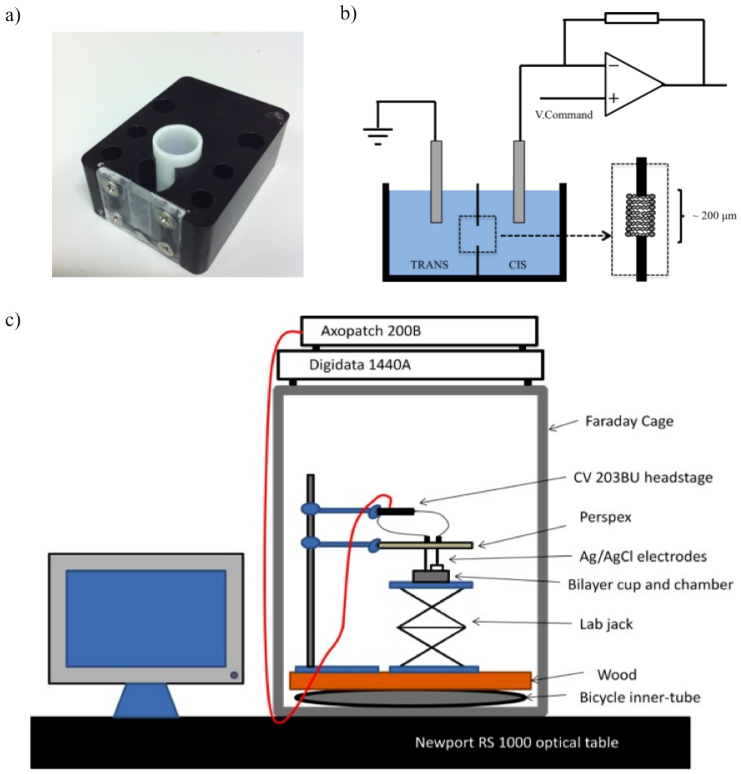

Figure 3.14: The bilayer cuvette method for planar bilayer formation. a) A photograph of the apparatus showing the bilayer curvette containing the preformed aperture and the bilayer chamber. b) A schematic diagram of the method, showing the insertion of Ag/AgCl electrodes in each compartment and the formation of a lipid bilayer across an aperture separating the two compartments. c) A schematic of the assembly, a bicycle inner tube was inflated and placed at the bottom of the Faraday cage to minimise vibrations. A piece of wood positioned on top of the bicycle tyre was used as a base to which a small lab jack was screwed. The bilayer cuvette system was fixed onto the lab jack via an acrylic stand, which was stuck onto the surface of the jack using a piece of double sided tape. A retort stand with two clamps was used to secure the acrylic electrode holder and the CV 203BU headstage.

DOPC/POPG vesicles as described in section 3.1.8. Pure POPG lipids were used to form the bilayer, prepared to a final concentration of 20 mg/ml in n-decane. The cis chamber was filled with 150 mM KCl, 10 mM HEPES pH 4.0 and the trans chamber filled with 150 mM KCl, 10 mM HEPES pH 7.40. The bilayer was formed by painting a small droplet of the lipid-oil solution over the aperture using a pipette tip, followed by raising and lowering the buffer contained in the trans compartment. Bilayer formation was indicated using capacitance measurements.

For ion channel measurements from reconstituted protein, a holding potential of 100 mV was applied and 2-5 μl of KcsA proteoliposomes was added into the trans

chamber. If no activity was observed after ∼10 min, the bilayer was broken and reformed by raising and lowering the buffer. This was repeated several times before more vesicles were added. All measurements were obtained using a sampling rate of 50 kHz and a low-pass 2 kHz Bessel filter.

Bilayer current measurements of reconstituted KcsA in the bilayer cuvette system are shown in Fig 3.15. A 30 s segment of a recording obtained at 100 mV is shown in a) where channel activity is indicated by a number spikes in the baseline of approximately the same intensity. The single-channel events are more clearly shown in the insert, revealing a number of non-periodic openings and closings in the baseline of approximately 8 pA and a baseline noise of ∼1 pA peak-to-peak. No channel activity was observed prior to the addition of vesicles. The histogram in b) of the figure shows a dense population of data points at ∼1.5 pA and a much smaller number of events at ∼9.5 pA. Single-channel analysis of the data indicates that the average opening amplitude was 6.8 ±0.64 pA, the dwell time was 4.15 ms and the opening probability was 0.21, results which fit closely with previously reported measurements for KcsA (LeMasurier et al., 2001).

A sample trace obtained at -100 mV is shown in part c) of the figure. In this instance, the channel openings are observed as negative spikes in the baseline, identified more clearly by the zoomed region. In this example, channel openings are associated with an increased amount of baseline noise, which is consistent with previous observations with recordings at negative potentials (Cuello et al.). The histogram in part d) of the figure reveals a very small population of data points at ∼-6 pA and a large number of points at ∼0.5 pA. Analysis of the burst shown in the figure revealed an average opening amplitude of -6.3 ±1.3 pA, a dwell time of 3.29 ms and an opening probability of 0.18. While slightly high, this figure for the average opening amplitude is close to what has been observed previously for KcsA in the literature (2.4.1) and still remains lower than the value obtained at 100 mV, indicating that the channel is displaying weak outward rectification, which is consistent with previous reports.

The measurement at 100 mV was repeated in part e) but with the concentration of KCl in the trans chamber increased to 750 mM. The 30 s trace shows that this resulted in single channel events with a greater opening amplitude than those shown in part a). The histogram in part f) shows a small population of data points at ∼27 pA and a dense number of points at ∼2.5 pA. Single channel analysis of the burst shown in the insert revealed an average opening amplitude of 22.51 ±2.42 pA a dwell time of 2.51 ms and an open probability of 0.13. These measurements

are in line with previous reports at high potassium concentrations (LeMasurier et al., 2001), however the channel openings were unexpectedly brief.

In summary, the data in this subsection verifies both the low-noise performance of the apparatus and the preparation of the His-tagged KcsA protein, expressed *in vivo* from the same DNA template used to supply the CF system in Chapters 5 and 6.

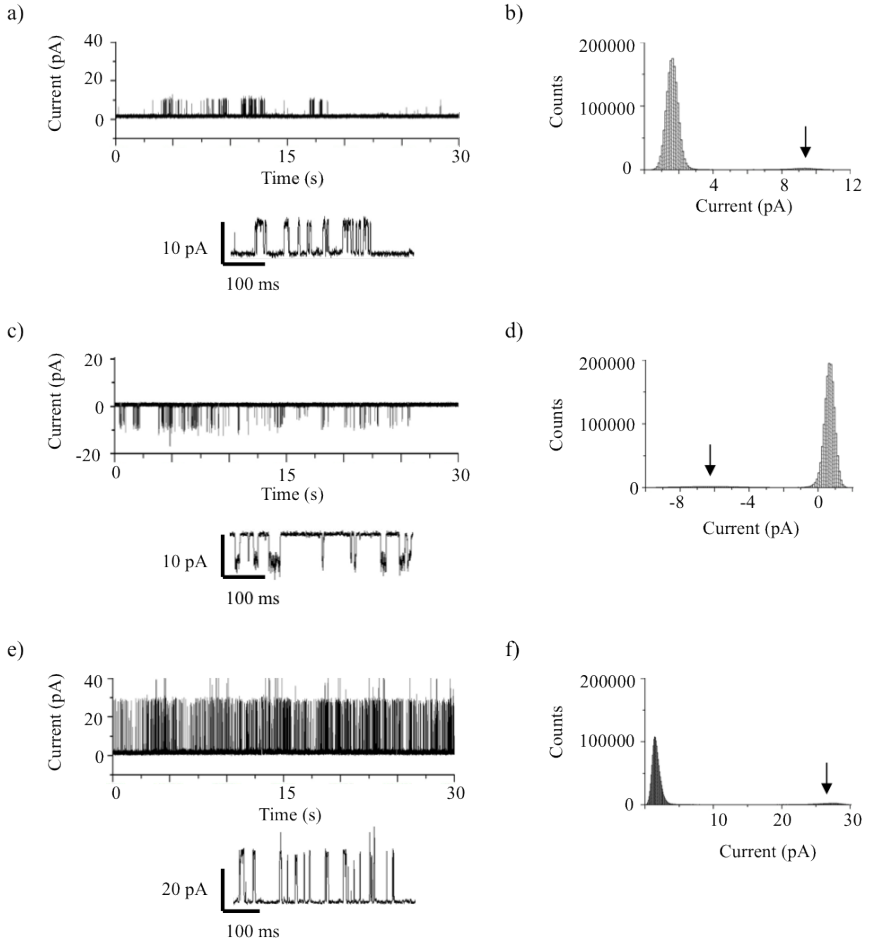

Figure 3.15: KcsA electrophysiology in bilayer cuvettes. Measurements of *in vivo* expressed and reconstituted KcsA were performed at a-b) 100 mV, c-d) -100 mV and e-f)) 100 mV with the KCl concentration of the trans chamber increased to 750 mM. The figure shows KcsA activity, verifying the KcsA preparation and the low-noise performance of the apparatus. The arrows in the histograms indicate the positions of small peaks.

3.2.4 Interdroplet bilayer formation using the regulated attachment method

The regulated attachment method (RAM) for forming lipid bilayers has been described previously using a flexible PDMS substrate (Sarles and Leo, 2010b) and is introduced in section 2.1.4. The device, shown in Fig 3.16 a)-b) essentially consists of a tablet-shaped piece of PDMS containing a well, with two smaller slightly overlapping wells in the centre. The well was filled with oil and a small volume of an aqueous vesicle dispersion was added to the small wells which are pierced with Ag/AgCl electrodes (Fig 3.16 c) part 1). Bilayer formation was achieved by manually compressing and releasing the device, causing the aperture separating two small chambers to close and open. This caused the initial volume of aqueous vesicles, enclosed by a monomer of lipids, to be split into two smaller droplets (Fig 3.16 c) part 2). The lipid bilayer is formed when the two droplets, now each encased by a monolayer of lipids, come into contact when the aperture opens (Fig 3.16 c) part 3). The extent of the aperture opening allows for the attachment of the two droplets, and thus the size of the lipid bilayer, to be regulated as shown in Fig 3.16 d).

This method of bilayer formation is interesting as the control over the bilayer size should allow the level of membrane incorporation to be dictated. Specifically, for the purposes of this project, this functionality may also be helpful for stabilising the bilayer in the presence of high concentrations of membrane perturbants, such as those expected to be present in a CF mixture (as introduced in section 2.1.4 and discussed in 4.4).

In this section, a customised version of the flexible PDMS device is engineered using 3D printed moulds. The data shown in the results and discussion section was obtained by an MSc student, Bandar Alfaifi, who was supervised as part of this study. Undergraduate students who worked on the project previously, found that it was easier to deform the PDMS substrate by rotating the device features by 90 degrees, resulting in the compression along the width of the device rather than the length. Moulds of both designs with different aperture sizes and a contraption for manually deforming the PDMS device were made for the MSc project student.

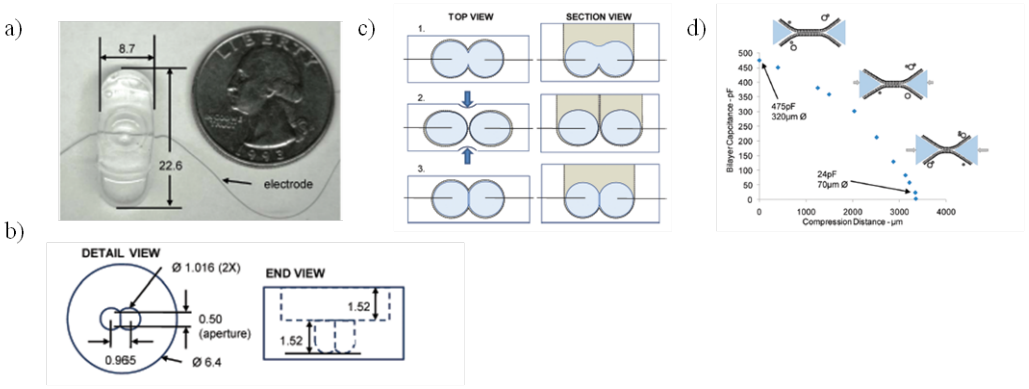

Figure 3.16: The Regulated Attachment Method for forming lipid bilayers. a) The flexible PDMS substrate consists of two small wells inside a larger well. A schematic representation is shown in b). Lipid bilayer formation is shown in part c) where part 1 shows a volume of aqueous vesicles immersed in oil inside the two overlapping small wells. Compression of the device, leading to the closure of the aperture and the separation of the two droplets is shown in part 2 of the scheme. Due to the formation of a lipid monolayer around each droplet, an interdroplet bilayer is formed when the device is released and the two droplets contact (part 3). The amount of contact formed between the two droplets, and thus the size of the resulting bilayer, can be controlled by regulating the release of the device after compression. This is demonstrated in part d) where the bilayer capacitance, obtained from the Ag,/AgCl electrodes inserted into the wells, is shown as a product of compression distance, resulting in interdroplet bilayers controllably ranging from 70 μm to 230 μm in size. Taken from Sarles and Leo (2010b).

3.2.4.1 Fabrication of a flexible PDMS substrate for interdroplet bilayer formation using RAM

In the original publication (Sarles and Leo, 2010b) the PDMS substrate was made using a double moulding process from an original device made in acrylic with a vertical end mill. Briefly, a PDMS negative of the acrylic part was made and used to cast the PDMS substrates used in the study. In this work, a one-step moulding process was used with moulds designed in 3D CAD (Fig 3.17 a)) and printed on an Objet 3D printer (Fig 3.17 b) i)). The moulds were designed to allow for the insertion of a piece of Perspex around the device features (Fig 3.17 b) i)) which was engineered on an Epilog laser cutter. The Perspex insert enabled substrates to be made with even side walls and regular depth. It also made the device easy to remove from the mould after casting and was modified with the laser cutter to include small holes to allow for the Ag/AgCl electrodes to be inserted during moulding.

Before casting the PDMS, the 3D printed moulds were treated with reactive oxygen plasma to render the surface more hydrophobic for the attachment of a silane. This was achieved using 2 μl of tricholorosilane (Sigma-Aldrich, USA), which was deposited on a glass slide with the moulds inside a vacuum desiccator. Uncured Sylgard 184 (Dow-Corning) PDMS (10:1 wt-wt ratio of base to curing agent) was prepared in a plastic cup and fully degassed inside a vacuum desiccator before being poured into the moulds shown in Fig 3.17 b) part ii). The moulds were transferred to a 90 °C oven, for 10 minutes and two pieces of silver wire were inserted into the mould using the holes engineered in the Perspex insert. The assembly was returned to the oven for a further 30 minutes before the wires were removed from the cast, which was released from the mould by removing the Perspex insert with a pair of pliers. The cast could then be easily 'popped out' of the Perspex for any excess PDMS to be removed using a scalpel before fresh Ag/AgCl electrodes were re-inserted into the device. Examples of two different designs of the PDMS platform fabricated using this method are shown in part c) of Fig 3.17, where the photographs to the left show the final device and the images in the middle focus on the centre of the substrate, highlighting the different positions of the two sets of wells. The images to the right of the image magnify the inner wells, allowing both the aperture and the position of the Ag/AgCl electrodes to be clearly visualised.

A device was also designed in 3D CAD and 3D printed for deforming the flexible PDMS substrate manually. The operating principle was that the amount of displacement could be controlled by two nylon screws that are tightened to deform the PDMS substrate, provided that it is securely clamped in position. The design, included in Fig 3.17 d) part i), shows a base plate containing a stage for the PDMS substrate to be positioned, two holes for screws, guides for the Ag/AgCl electrodes and some small pillars for securing a Perspex bracket. Soft print material was used inside the stage to promote adhesion with the PDMS device and adequate spacing was left for the movement of the screws. Some tolerance was also included to account for the PDMS expanding. The Perspex bracket, used to fasten the PDMS into position was made on an Epilog laster cutter. To maximise grip, the shape of the PDMS device was etched into the bottom surface of the bracket. Perspex was chosen as the build material over the 3DP print material for the brackets due to its mechanical strength (3D printed brackets tended to deform over time). The final assembled device is shown in Fig 3.17 d) part ii).

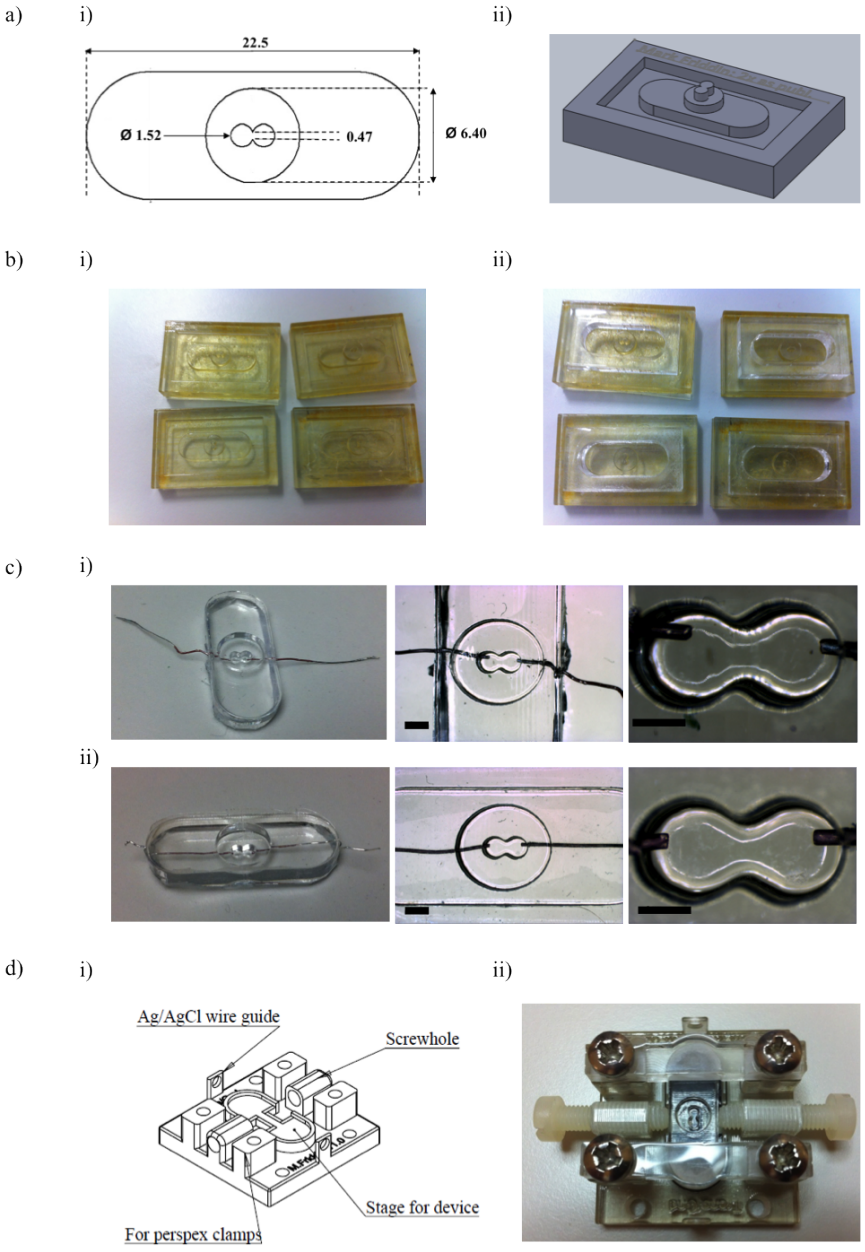

Figure 3.17: Fabrication and manual displacement of the flexible PDMS substrate. a) i) A CAD drawing for the PDMS substrate, showing two wells 1.52 mm in diameter, inside a larger well 6.40 mm in diameter. The total length of the cast was 22.5 mm. A 3D model of the mould is shown in ii). b) i) 3D printed moulds for casting the PDMS device with ii) Perspex inserts for controlling the device dimensions, inserting Ag/AgCl electrodes and easy release from the mould. c) Photographs and micrographs of PDMS casts made from two separate designs of the 3D printed moulds (scale bar = 1 mm). d) i) Design of the contraption for manual displacement of the PDMS device, using two nylon screws to displace the PDMS which is fixed in position using two brackets. ii) A photograph of the final device.

3.2.4.2 Lipid bilayer formation in RAM devices

Experiments were initially conducted using 5 μl of 150 mM KCl, 10 mM HEPES, pH 7.40 as the aqueous volume and 40 μl of 20 mg/ml asolectin in hexadecane as the oil phase. An interdroplet bilayer was formed by closing and releasing the aperture through manual compression of the PDMS substrate. The device was subsequently placed on the stage of a stereozoom microscope for imaging.

One problem with this method was the tendency of the PDMS to absorb the solvent, resulting in the oil escaping the well and the droplets merging. It was observed that the problem was worse when using decane instead of hexadecane and that immersing the PDMS casts in different solvents resulted in significant expansion of the devices. Devices soaked in decane were the most affected and were unusable, while those soaked in hexadecane were swollen but retained functionality. Subsequent experiments were therefore performed after pre-soaking the device for 24 hours in hexadecane. Interdroplet bilayers formed this way were found to last for several hours compared to 5-10 minutes without pre-soaking.

It was found that when the PDMS device was used with one droplet, as originally described, it took time for the aqueous volume to evenly disperse across both wells, as shown in Fig 3.18 a). One drawback of this method was that it was generally found to be more challenging to obtain an interdroplet bilayer in the centre of

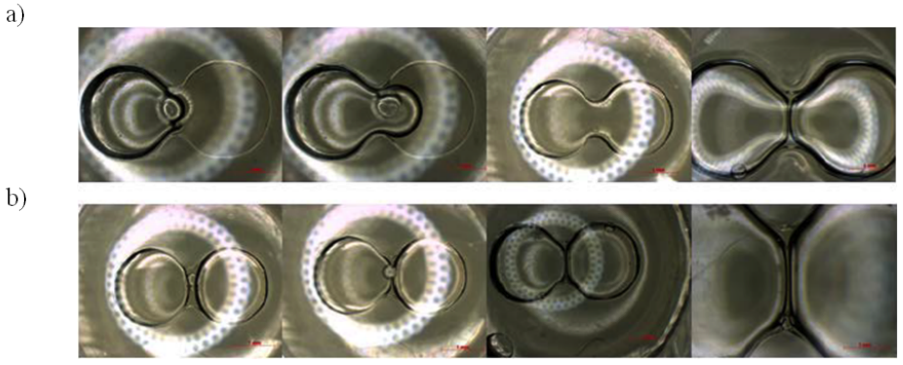

Figure 3.18: Interdroplet bilayer formation using the RAM method. a) An interdroplet bilayer is formed from a 5 μl droplet, which is dispensed into a well and allowed to spread across the surface. The droplets are separated by compression of the device, resulting in the closure of the aperture. An interdroplet bilayer is formed when the device is released. b) An interdroplet bilayer is formed when a 2.5 μl droplet was inserted into each well and left to form contact. The method shown in b) was found to be quicker and easier than in a). The diameter of the wells was 1.52 mm. The data in the figure was obtained from Alfaifi (2013).

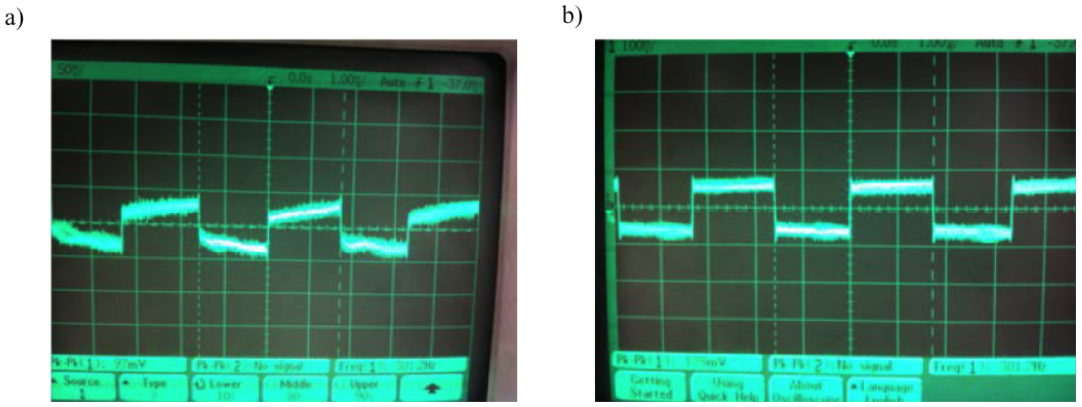

Figure 3.19: Capacitance traces of interdroplet bilayers formed using the flexible PDMS device. a) Interdroplet bilayers were initially found to be leaky after bilayer formation. b) After a few minutes the bilayer was found to stabilise, which was often associated with a small increase in the bilayer capacitance. The oscilloscope gridlines have spacings of a) 50 mV and 1 ms or b) 100 mV and 1 ms (Alfaifi, 2013).

the device. Instead, it was found to be simpler to form an interdroplet bilayer by pipetting two 2.5 μl droplets of buffer into each compartment, as shown in Fig 3.18 b). A key advantage of this method is that both droplets could have different compositions, yet this also meant that, under such conditions, the bilayer could not be reformed when the bilayer failed and the droplets fused.

An ID562 BLM amplifier (Industrial Developments Bangor, UK) and an oscilloscope were used for taking electrical measurements of the interdroplet bilayers via the inserted Ag/AgCl electrodes. A piece of tin foil was used for shielding the device. Bilayer capacitance measurements suggested that the interdroplet bilayers formed in the flexible device were initially leaky, indicated by the slant at the top and bottom of the capacitance trace as shown in Fig 3.19 a). This was found to stabilise after a few minutes (Fig 3.19 b)) but was typically associated with a small increase in the bilayer capacitance, from 97 pF shown in part a), for example, to 125 pF in part b). This corresponds to an increase in the approximate bilayer diameter from 157 μm to 178 μm.

As a result of this observation, the bilayer was given time to stabilise before attempting to modulate the bilayer area, which was initially achieved by compressing the PDMS substrate using the 3D printed manual manipulator described in section 3.2.4.1. Typically, a 2.5 μl droplet of buffer was dispensed into each well of a pre-soaked PDMS device and clamped into the manipulator. Once the bilayer capacitance had stabilised, one of the two screws was tightened, resulting in a reduction in the bilayer capacitance as shown in Fig. 3.20 a). In this example, a

bilayer capacitance of 125 pF (corresponding to an approximate bilayer diameter 178 μm) was obtained when the screws were tightened until the distance between them was 54.27 mm. The bilayer capacitance was found to increase to 1.97 nF (equivalent to an approximate bilayer diameter of 708 μm) when the distance between the screws was released to 56.46 mm, as shown in Fig 3.20 b). Although these experiments demonstrated that the bilayer size could be manually controlled, it was found that the range of bilayer sizes available was limited by the thread of the screws. This is highlighted in Fig 3.20 where it is shown that a change of only 2.19 mm, or approximately half a turn of the screw, led to a change of $\sim$530 μm in the bilayer diameter, indicating that a finer, more precise, method of compressing the PDMS was required.

To address the need for more accurate and quantifiable displacement of the PDMS device, the experiment was repeated using a SM325 motorised micro-manipulator fitted with a M3301EH electrode holder (World Precision Instruments, USA). The apparatus was controlled with a PC using Win-Commander software, allowing for precise movements of the manipulator to be defined. The setup for compressing the PDMS device using the motorised micro-manipulator was similar to the manual method except one of the screws was removed and replaced with the end of a paintbrush that was secured to the electrode holder. Displacement of the PDMS substrate was subsequently achieved by moving the paintbrush through the hole toward the device, i.e. increasing the compression distance. This method was found to be capable of achieving 10 different bilayer sizes ranging from $\sim$350 μm (600 pF) to $\sim$50 μm (46 pF) as shown in Fig 3.21.

While the data indicates that a greater range of bilayer sizes were achieved compared to those reported previously (Sarles and Leo, 2010b), there was no evidence to suggest that these bilayer sizes remained constant for a significant period of time, or after the application of a holding potential. This was indicated by the observation that capacitance values of bilayers formed using the RAM method did not remain constant and gradually increased with time. It is unclear whether this is an inherent feature of the system that was observed but not reported by the original authors or whether it originates from a problem with the method or an artefact in the design/fabrication of the device. One possibility for example was that the resolution limit of the 3D printing led to the incomplete formation of the aperture. This would, in principle, have required more force to close the aperture, which if applied unevenly could have given rise to a pressure gradient that might have forced the position of the bilayer to move to either side

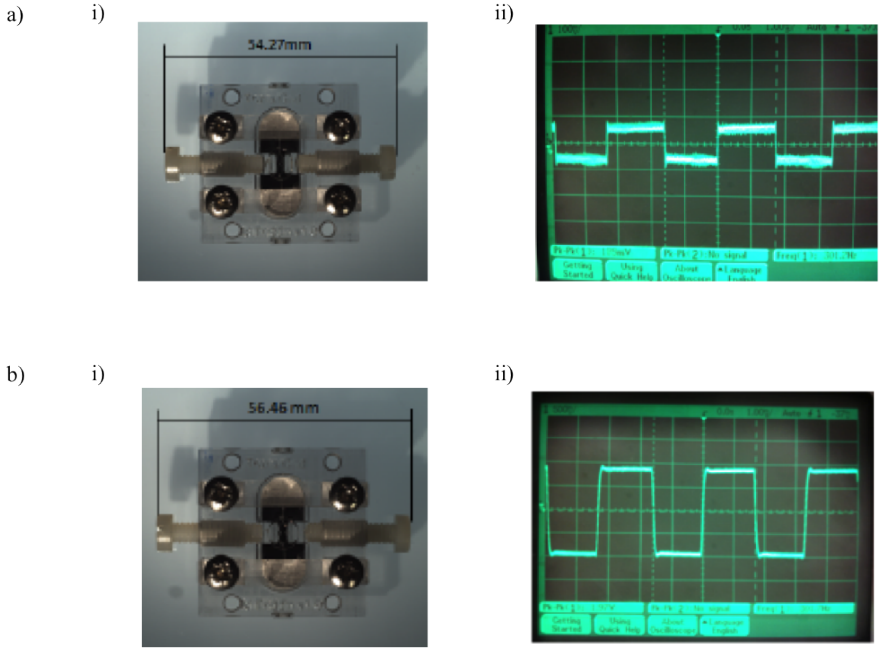

Figure 3.20: Bilayer modulation by manual displacement of the PDMS substrate. An interdroplet bilayer was formed from two 2.5 μl droplets of 150 mM KCl, pH 7.40 in the wells of a pre-soaked PDMS substrate filled with 20 mg/ml of asolectin in hexadecane. The substrate was clamped inside the manual manipulator and the screws were tightened once the bilayer capacitance stabilised. a) (ii) A capacitance of 125 pF was observed when the screws were tightened so that the distance between them was 54.27 mm (i). b) i) When the screws were loosened to a separation distance of 56.46 mm, a capacitance of 1.97 nF was measured (ii). The figure shows that the bilayer diameter was controlled by manual manipulation of the PDMS device, however the range of sizes available was limited by the thread of the screws. The oscilloscope gridlines have spacings of a) 100 mV and 1 ms or b) 500 mV and 1 ms. The data in the figure was obtained from Alfaifi (2013).

of the aperture where the level of attachment between the two droplets would no longer be regulated.

3.2.5 Interdroplet bilayer formation on a planar microelectrode array

A droplet dielectrophoresis device capable of forming interdroplet bilayers from 2 μl droplets immersed in lipid-oil has been developed previously by the Morgan group (Aghdaei et al., 2008; Aghdaei, 2011). The 20 x 20 mm device consists of 6 pairs of individually addressable microelectrodes (Fig 3.22 a)), however for the

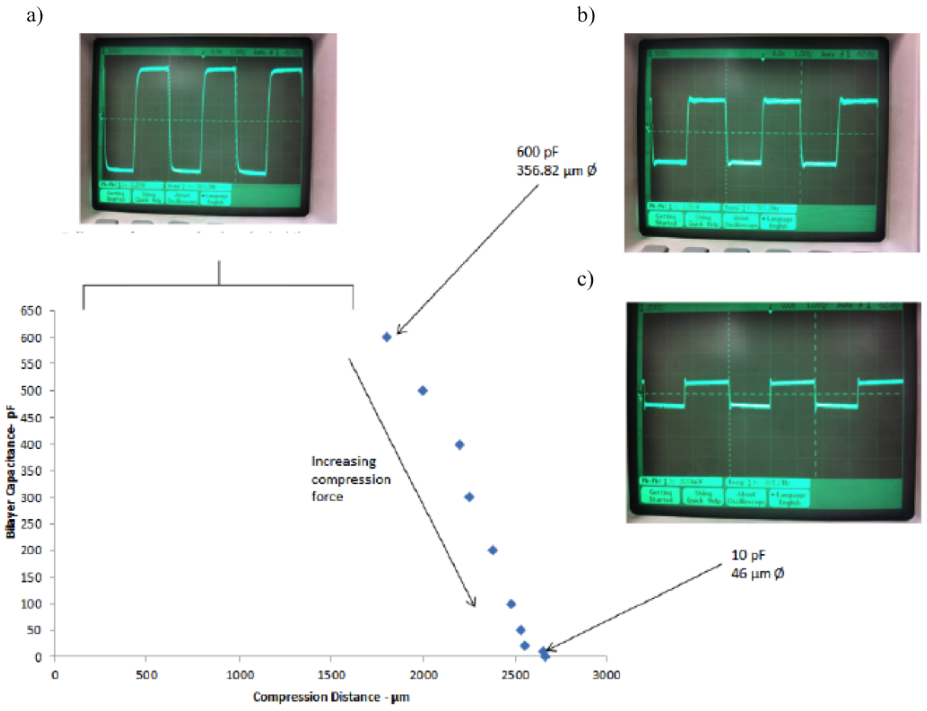

Figure 3.21: Bilayer modulation by motorised displacement of the PDMS substrate. An interdroplet bilayer was formed by pipetting two 2.5 μl droplets of 150 mM KCl, 10 mM HEPES, pH 7.40 into the wells of a pre-soaked PDMS device filled with 20 mg/ml of asolectin in hexadecane. The PDMS cast was clamped inside the manual manipulator compressed with the end of a paintbrush attached to a motorised micro-manipulator. The compression distance was controlled using a PC. a) When the aperture is fully open the bilayer capacitance was measured at 3.39 nF, which approximates to a bilayer diameter of 929 μm. b) When the compression distance was increased the bilayer capacitance reduced to 1.91 nF, indicating a bilayer with an approximate diameter of 697 μm. c) Further compression of the device resulted in a bilayer capacitance of 300 pF, equivalent to an approximate bilayer diameter of 276 μm. The data points show the reduction of the bilayer diameter with compression distance, from 356 μm to 46 μm. The figure was modified from Alfaifi (2013).

purpose of forming interdroplet bilayers with two droplets, only two pairs of the outer 1,1 and 4,4 electrodes are required (Fig 3.22 b)).

The microelectrode array described in Aghdaei et al. (2008) was fabricated by patterning an evaporated Ti/Pt layer (10/200 nm thick) by ion beam milling, before a 700 nm thick SU-8 insulating layer was applied. Droplet manipulation was achieved when a 2 kHz sinusoidal waveform, with a peak-to-peak intensity of 10 V, was applied to the outer electrodes 1,1 and 4,4, which captured the droplets and focused them toward the centre of the device. In this position the

two pairs of inner electrodes (2,2 and 3,3) were activated and agar coated Ag/AgCl electrodes were inserted into each droplet. The signal intensity was then reduced to 2 V peak-to-peak and the outer electrodes turned off, causing the droplets to move into the centre of device and make contact. The formation of an interdroplet bilayer was verified by capacitance measurements and the method was also verified by obtaining recordings of gramicidin and KcsA (Aghdaei et al., 2008).

The specific workings of the device are detailed in a previous study by Aghdaei (2011). Briefly, when a signal is applied, the SU-8 insulating surface becomes charged. The charge distribution is governed by the geometry of the microelectrodes, which were designed (Dr. Nicolas Green, University of Southampton) to generate a divergent electrical field that increases towards the centre of the device. The polar droplet becomes polarised in response to the electric field, resulting in the migration of charges and the formation of a dipole. A secondary effect, caused by the divergence of the electrical field then arises which causes in an imbalance of charges acting on the droplet and initiates droplet movement (Fig 3.22 d)). The droplet thus travels toward the centre of the device as dictated by the electrical field gradient.

3.2.5.1 Fabrication of planar microelectrode arrays

Devices were fabricated on 6″ glass wafers as described by Aghdaei et al, with minor modifications to the photoresist application. Electrode structures were formed by patterning an evaporated Ti/Pt layer (10/200 nm thick) by ion beam milling by Katie Chamberlain in the Southampton Nanofabrication Centre (SNC). Wafers were diced into 20 x 20 mm chips and cleaned with fuming nitric acid, acetone and isopropanol prior to overnight baking at 150 °C. A piece of Kapton tape was applied to protect the contact pads before spin coating Ti Prime adhesion promoter at 3000 RPM for 20 s and baking at 120 °C for 2 min. Two layers of the negative photoresist SU-8 2000.5 were then deposited by spin coating at 6000 RPM for 30 s, followed by soft-baking at 95 °C for 1 min. The SU-8 was cross-linked by flood exposure to UV light for 10 s at an intensity of 11.85 mJ/cm^2 , followed by post-exposure baking at 95 °C for 2 min, and by hard baking at 150 °C for 20 min. This procedure produced a 0.5 μm thick SU-8 film, verified using a profilometer, which served as the dielectric that is required for electrokinetic droplet manipulation on planar electrodes.

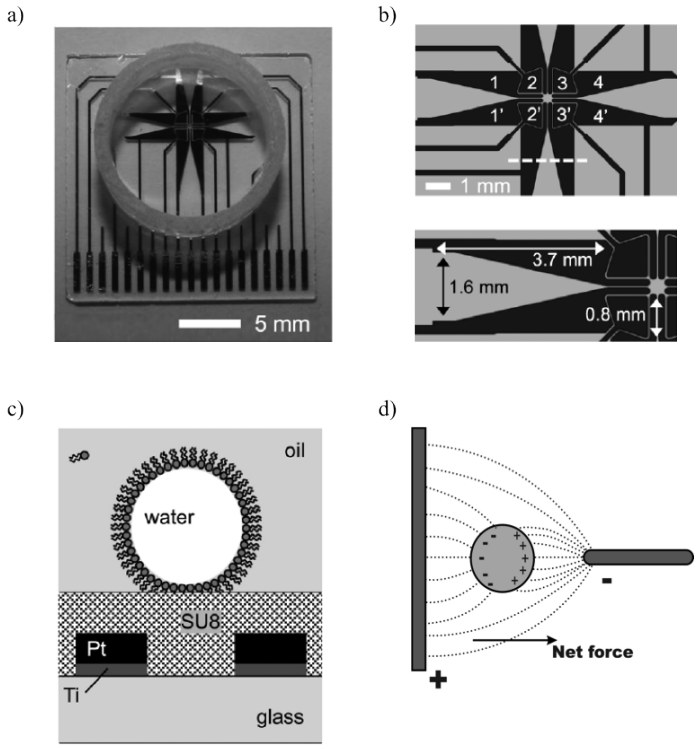

Figure 3.22: Planar microelectrode array for interdroplet bilayer formation. Bilayer formation is achieved by focusing the two droplets toward the centre of the device using the outer (1,1 and 4,4) electrodes before the inner (2,2 and 3,3) are used to position the droplets into contact. a) A photograph of the chip fitted with a reservoir glued onto the surface of the device. b) A schematic diagram of the chip, highlighting the four pairs of electrodes used for manipulating the two droplets into contact and a zoom of the electrode surface, indicating the sizes of key features. c) A cross sectional representation of the chip (indicated as the white dotted line in part b)), highlighting the surface profile of the device. d) The electrokinetic effect of dielectrophoresis, where particle motion is achieved as a result of the non-uniform electric field inducing an imbalance of charges acting on the particle. The image in part d) was obtained from Hughes (2000).

3.2.5.2 Fabrication of chip holders and oil reservoirs

Practical requirements for forming interdroplet bilayers using the droplet dielectrophoresis device include the need to fit a well capable of retaining the lipid-oil solution, a means of clamping or holding the device into place, and the ability to reversibly and reliably form an electrical connection with each channel of the device to the controlling electronics. This was achieved previously using a customised connector that screwed on top of the chip, positioned on a metal plate and secured to a large two axis goniometer stage. Alignment of the chip with the connector

was achieved visually and the oil was retained by gluing part of a 5 ml pipette tip to the chip surface. A ribbon cable attached the connector to a switchbox which was in turn connected to the output of a wideband amplifier, used to increase the intensity of signals generated by a function generator. An oscilloscope was used to verify the output.

A PCB was designed by Dr. Marta Lombardini (University of Southampton) to fit a surface SMT mount, one piece 20 pin connector (SEI Series, Samtec). 2 mm holes in the PCB were integrated into the design to match the 2 mm threaded holes positioned on each end of the connector. Matching holes were also included in the design for an alignment tray (Fig 3.23 a)), which was printed to position the electrodes in line with the connector. The assembly was secured together using 2 mm screws as shown in Fig 3.23 b).

In order to avoid the use of glue on the chip surface, two designs were made to secure the device and retain the oil. The first consisted of a PDMS cast made from a 3D printed mould (Fig 3.23 c)-d)), where the choice of material was motivated by the possibility of integrating microfluidics such as a droplet generator or channel. A mould was designed to include a frame for the chip to be inserted and a hole for the oil to be added (Fig 3.23 e)-f)). A housing was designed and 3D printed for the PDMS cast to be secured and to also allow for the chip/PCB assembly to be attached using the 2 mm screws (Fig 3.23 g)-h)). A 3D printed bracket was used to create a seal between the PDMS cast and the chip to prevent the oil from leaking (Fig 3.23 h)). One general observation was that it was difficult to keep the platform flat when using this setup, however the key limitation was the tendency of the PDMS to absorb the oil and become deformed, leading to leakage. This approach was abandoned after it was found that reducing the size of the well did not significantly improve the problem.

The second design incorporated the same chip/PCB assembly used for the PDMS setup (Fig 3.23 b)), however in this instance the alignment tray fitted into a recess designed into a 3D printed baseplate (Fig 3.24 a)). The plate was designed to fit onto a small GNL 20 dual axis goniometer stage (ThorLabs, Germany), and included two 1.8 mm holes positioned for the attachment of a 3D printed gasket (Fig 3.24 c)-f)).

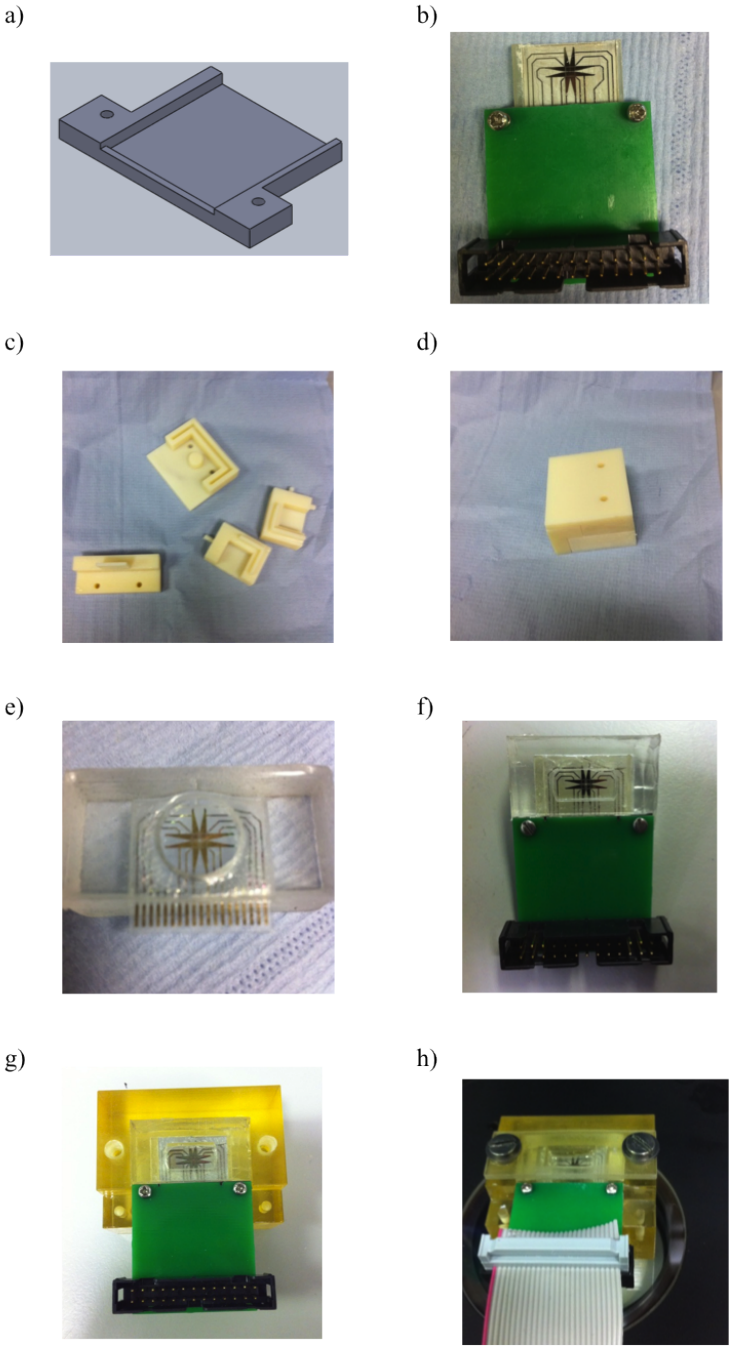

Figure 3.23: Fabrication of chip holders and oil resevoirs for the droplet dielectrophoresis device. An alignment frame for connecting the chip to the PCB was designed in 3D CAD (a) and printed. The two components connected via 2 mm screws (b). c)-e) A mould was designed in SolidWorks and printed for the purpose of making a PDMS cast with a reservoir for containing the oil. The alignment frame holding the chip and PCB assembly could be easily inserted into the PDMS cast (f), which fitted into a 3D printed housing (g). A 3D printed bracket was screwed on top of the assembly and used to clamp to seal the PDMS on top of the chip surface. This design was limited by the difficulty in keeping the chip flat and by the tendency of the PDMS cast to absorb the oil, leading to deformation of the cast and leakage.

The gasket was designed as a rectangular window that included a narrow trench, positioned in the centre of the frame and running alongside the bottom surface of the structure (Fig 3.24 b)). The trench was filled with a rectangular ring, designed in Solidworks and printed with the soft, Tango Black, build material. The concept was that the soft build material would extend beyond the bottom surface of the frame and form a seal with the surface of the chip (Fig 3.24 c)-d) & f)). The gasket was designed with two 2 mm holes to allow the assembly to be fitted to the 3D printed baseplate (Fig 3.24 a)).

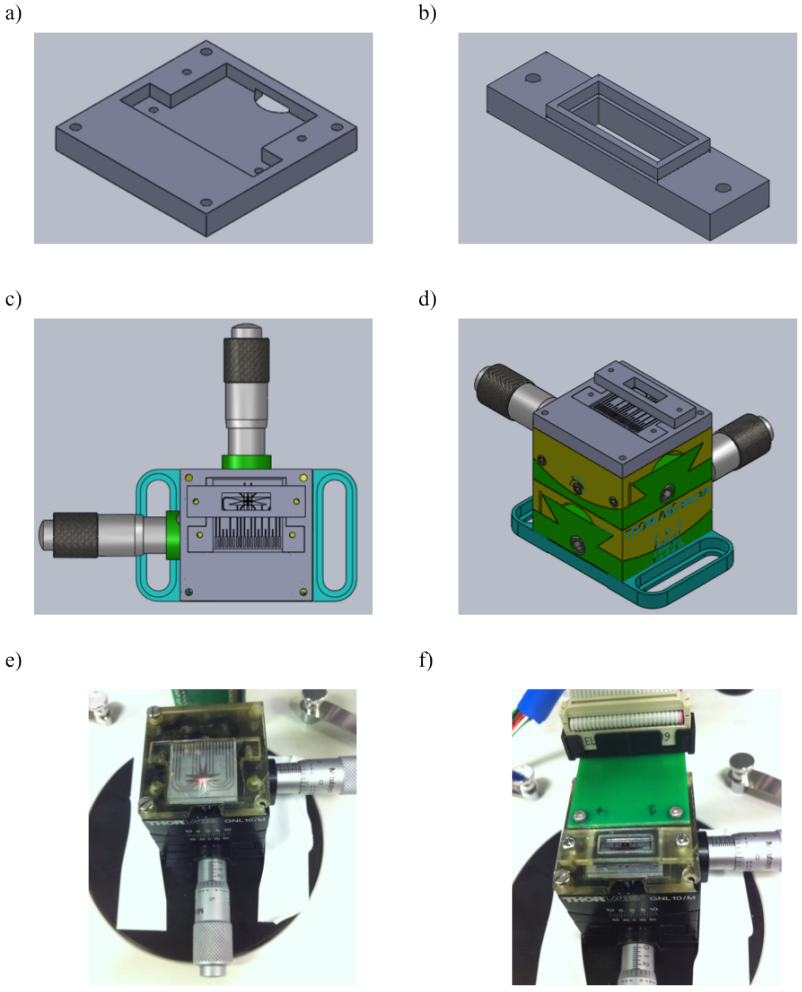

Figure 3.24: Fabrication of chip holders and oil reservoirs for the droplet dielectrophoresis device. a) A baseplate was designed and printed to house the alignment frame/chip/PCB assembly. b) A 3D printed gasket was engineered with a rectangular ring of soft build material extruded from the base to make a seal with the chip surface. The baseplate was fitted onto the top of a small dual axis goniometer stage (c)-f)) and fitted with the gasket which was designed to screw into the baseplate, forming a reservoir around the focusing electrodes (c),d) & f)).

It was found that the method worked well for retaining the oil but was not consistently reliable. For example, the setup would occasionally leak when the gasket was secured unevenly or as a result of the structure deforming under the applied stress from the screws. For this reason the 3D printed gasket was eventually replaced with a reservoir made from a pipette tip and glued to the chip surface as described by Aghdaei. While this method resulted in some spoiling of the chips, it was found to be the most reliable method for containing the oil.

3.2.5.3 Interdroplet bilayer formation using the planar microelecrode array

A schematic diagram of the apparatus used for forming interdroplet bilayers using the droplet dielectrophoresis device is shown in Fig 3.25.

For gramicidin measurements, 1 mg of gramicidin was dissolved in 1 ml of analytical grade ethanol and serial diluted to a final concentration of 1 ng/ml. The solution was subsequently diluted in buffer (150 mM KCl, 10 mM HEPES, pH 7.40) until the desired concentration was achieved. Alpha haemolysin was similarly prepared and the KcsA was used directly from the reconstituted sample used in 3.2.3.

A common problem when first attempting to achieve droplet motion was the observation of air bubbles emanating from the droplet. This was most likely caused by the hydrolysis of water into gaseous hydrogen and oxygen as a result of a hole in the SU-8 layer and the droplet coming into contact with an exposed part of the metalised chip surface. This explanation was supported by the observation of the bubbles appearing more rapidly when the intensity of the applied signal was increased and vice versa. To avoid damaging the spade shaped electrodes (See Fig 3.22 part b)), droplet motion was first developed using a similar chip with square shaped inner electrodes.

When investigating the problem it was established that the holes in the SU-8 layer occurred due to the SU-8 being deposited unevenly, either as a result of contamination of the chips before spin coating and/or from a problem with the spin coating process itself. The concern with the latter arose due to the unavailability of a chuck capable of spinning small wafer fragments. Several short-term solutions were tested, including 1) using a larger chuck with a 6″ plastic wafer to which the chip was stuck using dicing tape, and 2) positioning the chip directly on top of the rotor without a chuck at all (as suggested by Katie Chamberlain, University

of Southampton). Difficulties with the first method included positioning the chip in the centre of the 6″ wafer and removing the device from the tape, while the second method frequently caused vacuum failure of the spin coater, resulting in the chips flying off the rotor during processing. Despite this limitation, it was found that the overall quality of the SU-8 layer (identified as a reduction in the amount of hydrolysis observed) was significantly improved when this method was used in combination with placing the chips in clean petri dishes for overnight drying before the application of the resist. Here, it stands to reason that particles contained in the drying oven were accumulating on the chip surface and led to cracks in the SU-8 layer when it was deposited on top. Despite the problems encountered, some devices were successfully engineered this way without the vacuum failing and droplet motion was achieved without the observation of hydrolysis (Fig 3.26 a)-e)). The damage to the instrument was later fixed and an adequately sized

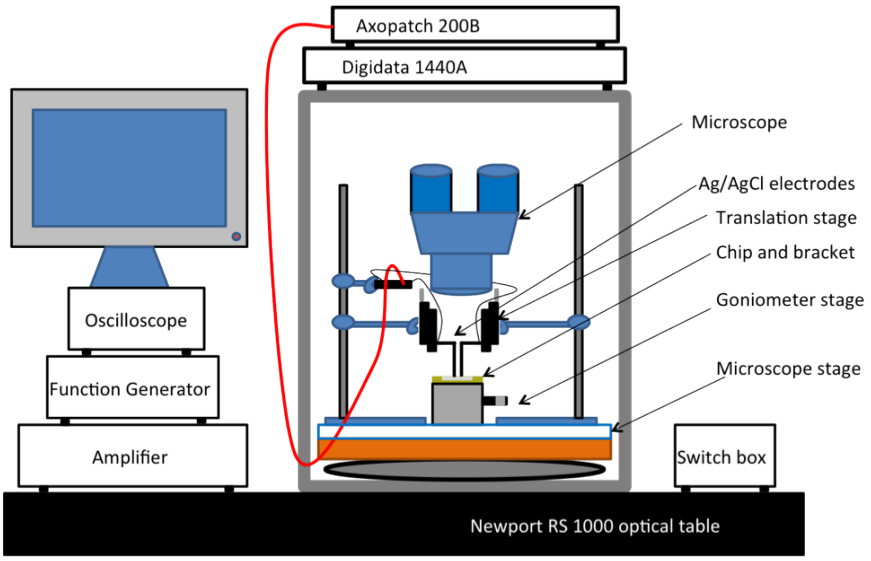

Figure 3.25: Schematic diagram for performing electrophysiology using the planar microelectrode array. An inflated bicycle inner-tube was positioned inside the Faraday cage underneath a piece of wood used as a base. The dual axis gonoimeter stage containing the assembled chip, PCB and gasket was secured in the centre of the cage, within the field of view of a stereozoom microscope. Retort stands with claps were positioned either side of the stage and clamped translation stages in place for lowering Ag/AgCl electrodes into the gasket. Gold plated wires connected the Ag/AgCl electrodes to the headstage which connected to the amplifier via a shielded wire. A ribbon cable connected the PCB attached to the chip to a switchbox, that was fed the output of an amplifier that was used to intensify the signal emitted by a function generator. The signal was verified using an oscilloscope and the output of the amplifier was controlled by a PC via a digitiser.

chuck was purchased for the spin coater.

Droplet motion was first achieved at 10 V, as described previously by (Aghdaei et al., 2008; Aghdaei, 2011) using the electrode array with the square focusing electrodes. During these experiments, it was generally observed that the droplet motion was more readily achieved once the device had been washed with the lipid-oil solution, that speed of the droplet motion increased when raising the peak-to-peak intensity of the applied signal, and that the design of the square focusing electrodes was more suited to moving a droplet from one side of the device to the other rather than bringing the droplets into contact in the centre of the device. Although this was still achievable as shown in Fig 3.26 e). With the setup functioning correctly, the chip was substituted for the design with the spade shaped focusing electrodes and the camera was removed from the microscope. This was necessary for removing the electrical noise that was detected in its presence during current measurements, which required the insertion of Ag/AgCl electrodes into each droplet.

The Ag/AgCl electrodes were inserted when the droplets were positioned stationary by the activation of both the inner and outer pairs of electrodes as described by Aghdaei et al. (2008). This was first attempted by lowering both electrodes into the oil using translation stages but was found to be problematic, largely due to the droplet moving and/or deforming to avoid being pierced by the wire. The problem was overcome by making the Ag/AgCl electrode tips more hydrophilic. This was achieved by coating the electrodes with 5% (w/v) agar, boiled until a thick syrup consistency was obtained and poured into a small petri dish that was used to dip the electrodes. It was important to get the right consistency of the agar, to evenly coat the electrodes, and to gauge the level of insertion required, as over inserting the electrodes restricted droplet movement. It was also found to be important to immediately hydrate the agar coating with buffer to ensure that the electrode successfully pierced the droplets.

With the Ag/AgCl electrodes inserted the droplets were brought into contact by lowering the peak to peak intensity of the supplied signal to 2 V and deactivating both sets of outer electrodes. Upon droplet contact, to avoid the droplets fusing, it was found to be important to slowly reduce the intensity of the applied signal before switching the electrodes off. The ribbon cable was then carefully removed from the switchbox and placed inside the Faraday cage, which was then closed for electrical measurements. Examples of electrical measurements of the droplets a) before contact, b) in contact and c) after fusion are shown in Fig 3.27. For 2

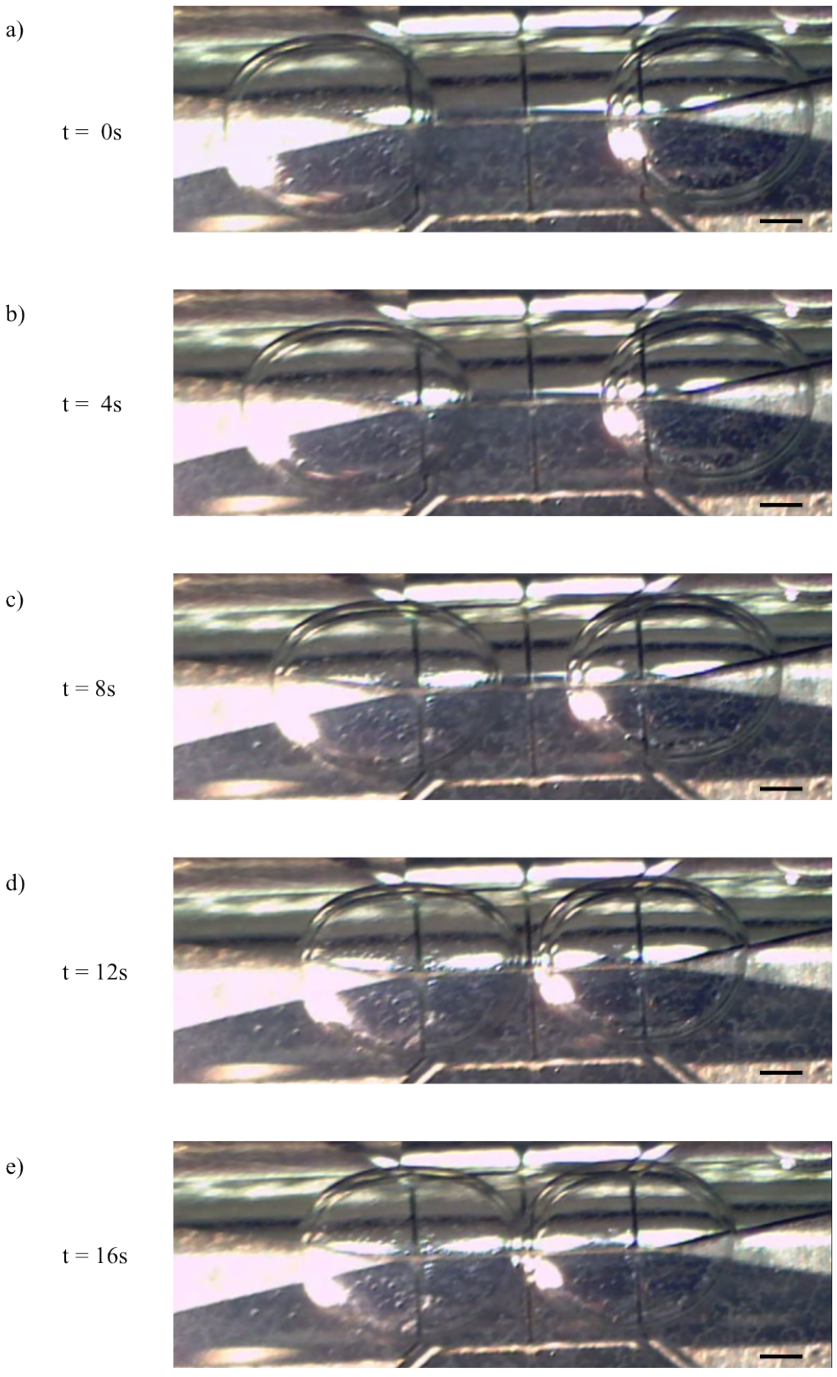

Figure 3.26: Interdroplet bilayer formation using the planar microelectrode array. A 2 μl droplet of buffer were dispensed on each of the two pairs of outer electrodes, activated by the application of a 2 kHz sinusoidal wave with a peak-to-peak intensity of 10 V. a)-b) The droplet is drawn towards the centre of the device where it starts to overlap the inner focusing electrodes. c) The droplets are held in position momentarily when both the inner and outer pairs of electrodes are activated. d)-e) The peak-to-peak intensity of the applied signal is lowered to 2 V and the droplets are brought into contact. (Scale bar = 100 μm).

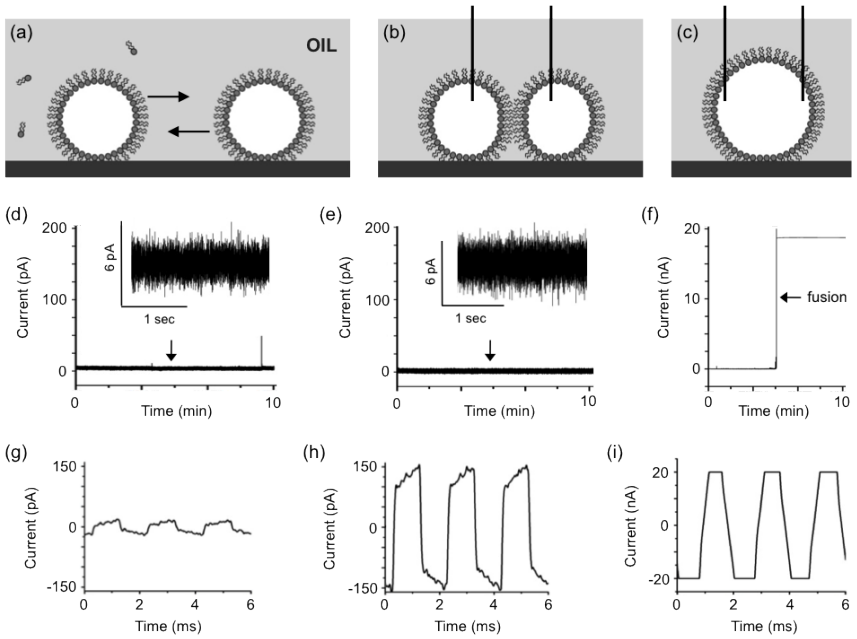

Figure 3.27: Electrical measurements of bilayers formed using the planar microelectrode array. Representative current traces (d)-(f)and capacitance traces (g)(i) are shown for three different scenarios: (d) and (g) the droplets are in close proximity but have not yet expelled the interdroplet oil layer, (e) and (h) a defect-free interdroplet bilayer has formed, and (f) and (i) the interdroplet bilayer has failed during the measurement, resulting in an open circuit and saturation of the amplifier (20 nA cut-off). The insets are an expansion of the region of the main trace marked with an arrow. Note that bilayer failure is apparent from both current and capacitance measurements, whereas interdroplet bilayer formation is only confirmed by an appreciable capacitance value, as calculated from the current response to a triangle-shaped voltage input.

μl droplets of buffer, separated on the microelectrode array, the transmembrane current was low (Fig 3.27 d)), with a peak-to-peak noise of $\sim$4 pA, and the initial capacitance was typically 60 pF (Fig 3.27 g)). This was found to increase with time to $\sim$150-300 pF (Fig 3.27 h)) when the droplets were brought into contact, indicative of an interdroplet bilayer with a diameter of 195-276 μm. Under these conditions, the baseline typically remained at 0 pA with a peak-to-peak noise of $\sim$6 pA (Fig 3.27 e), confirming that the bilayer had no defects. When the bilayer failed, resulting in the droplets fusing, both measurements saturated at 20 nA (Fig 3.27 i) & f)). These measurements confirm that an interdroplet bilayer was formed when the droplets were brought into contact on the planar microelectrode array.

The presence of the bilayer was also verified through measurements of the peptide gramicidin A, which forms a prototypical ion channel that is specific for monovalent cations. A key advantage of using gramicidin is that it does not

require reconstitution into proteoliposomes. 2 μl of gramicidin, diluted to 2 ag/ml in buffer, was placed onto the microelectrode array and brought into contact with a second 2 μl droplet of buffer inside a well of 20 mg/ml asolectin in n-decane. A sample recording (n=3) taken at 100 mV with a 2 kHz low-pass Bessel filter and filtered again using a digital 1 kHz low-pass filter is shown in Fig 3.28 a). The figure shows single openings and closings of approximately 1 pA in the baseline and also highlights a multiple opening where two channels were open at the same time. This is clear from a $\sim$1 pA opening in the baseline followed by a second $\sim$1 pA opening and two subsequent closing events of the same magnitude, events that were also described when the experiment was performed on the device previously (Aghdaei et al., 2008). Bilayer current measurements were also performed when one of the droplets contained 10 ng/ml of the pore forming toxin alpha haemolysin (αHL), a protein toxin that destroys cells by rendering their membranes permeable to ions.

A typical recording of this behaviour (n=3) is shown in Fig 3.28 b), where it is clear that the pore is fixed in a continuously open state once inserted into the membrane and is succeeded by several successive openings of $\sim$14 pA. Finally, the setup was also tested with an aliquot of reconstituted KcsA used in the bilayer cuvette method as detailed in section 3.2.3. In this instance, a 2 μl droplet of reconstituted KcsA in 150 mM KCl, 10 mM HEPES, pH 7.40 buffer was brought into contact with a second droplet containing the same buffer at pH 4.0 inside a well of 2 mg/ml POPG in n-decane. A sample measurement (n=5) at 100 mV is shown in Fig 3.28 c) where discrete openings and closings in the baseline are observed, as clarified by the magnified region of the recording. Analysis of the burst revealed an average opening amplitude of 5.9 $\pm$1.3 pA, a dwell time of 1.75 ms and an open probability of 0.062. The average amplitude of the openings was slightly less than what was measured (6.8 $\pm$0.64 pA) when the reconstituted protein was supplied to the bilayer cuvette system in section 3.2.3, however this might be accounted for by the difference in the peak-to-peak noise of the system.

In summary, this section shows that the planar microelectrode array was successfully assembled and used to form interdroplet bilayers. It is also shown that these bilayers exhibit similar properties to aperture-suspended lipid bilayers formed using the bilayer cuvette method, which matches previous observations (Bayley et al., 2008).

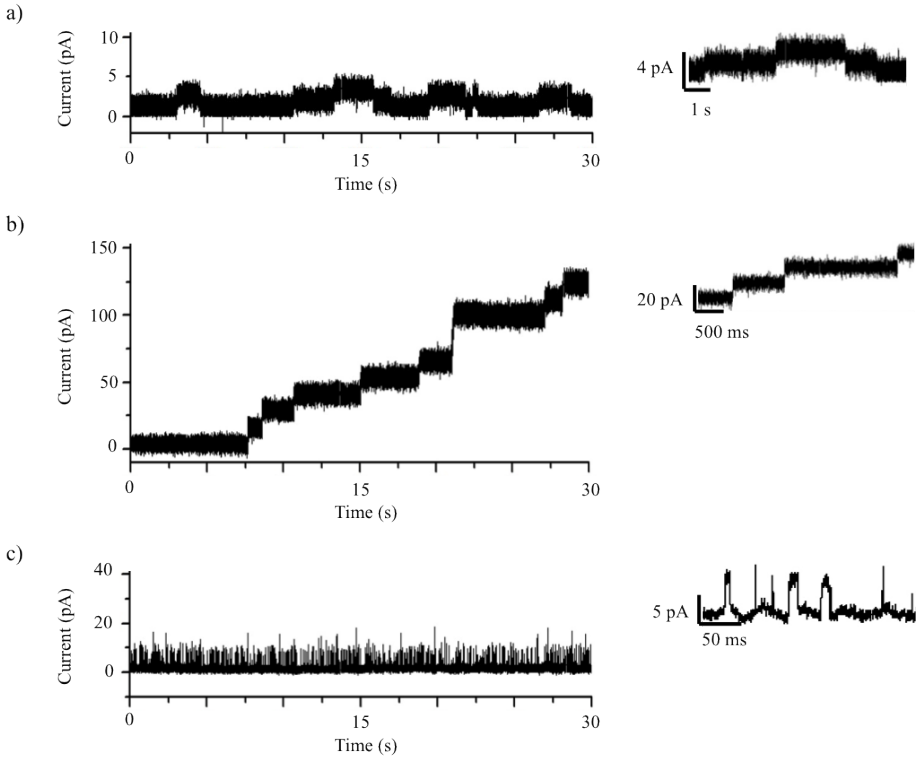

Figure 3.28: Measurements of bilayers formed on the planar microelectrode array. The image shows measurements when one droplet contained buffer with a) gramicidin, b) alpha haemolysin and c) reconstituted KcsA. The second droplet contained buffer at pH 7.40 in parts a)-b), and at pH 4.0 in c). The measurements show small, ∼1 pA, openings and closings in the baseline for gramicidin (a), continuous openings at ∼14 pA for alpha haemolysin (b) and brief openings at ∼6 pA for KcsA (c). The figure shows three distinctly different opening characteristics for each sample, verifying that the bilayer is successfully formed.

3.2.5.4 Electrokinetic versus manual interdroplet bilayer formation

While the droplet dielectrophoresis platform represents the state-of-the-art in interdroplet bilayer formation using a/c electrokinetics, the platform was also demanding in terms of fabrication, maintenance and repair. This motivated the use of a simpler and more reliable method of bilayer formation that did not involve electrokinetic manipulation. This was achieved by dispensing the droplets onto the tips of agar coated Ag/AgCl electrodes, lowering them into the oil and manually positioning them into contact by moving the retort stands. This method allowed for the SU-8 coated devices to be used repeatedly, without the need to continually strip and re-apply the insulating layer.

3.3 Summary

The methods described in this chapter are relevant to the work discussed in the following Chapters. The CF reaction (discussed in section 2.3 and explained in detail in section 3.1.4) and the preparation of vesicles (2.2.5/3.1.3) in combination with the formation of interdroplet bilayers (2.1.4/3.2) is important for both the study of bilayer stability in Chapter 4 and for obtaining single-channel measurements of CF expressed ion channels in Chapter 6. In addition the CF reaction and the preparation of vesicles in combination with protein purification (2.2.2/3.1.5) and gel electrophoresis (2.2.3/3.1.6) is also central to demonstrating the CF expression of ion channels in Chapter 5.

Chapter 4

Stability of interdroplet bilayers with cell-free expression mixtures

The formation of a stable and durable lipid bilayer is a fundamental requirement for achieving the coupled expression and characterisation of ion channels in microdroplets (section 1.1), however the stability of interdroplet bilayers formed in the presence of CF systems, which are known to destabilise the bilayer (Syeda et al., 2008), has not been comprehensively studied.

To this end, the stability of interdroplet bilayers formed between two droplets of pure buffer solution was studied in mixtures of different synthetic lipids, in addition to asolectin bilayers formed in the presence of different pH gradients. Further to demonstrating the stability of the bilayers, three different commercial CF mixtures and their comprising fractions were screened, followed by measurements of pure proteins, polymers and vesicles.

4.1 Interdroplet bilayers of asolectin

Interdroplet bilayers composed of asolectin, a lipid extract from soybean, were formed by manual manipulation of the droplets as described in section 3.2.5.4. This enabled the properties of the bilayer to be studied without electrokinetic forces and in the absence of a CF system. Two representative recordings of interdroplet bilayers formed this way are shown in Fig 4.1 a)-b), where in both examples the baseline is shown to be stable and close to 0 pA, with no significant leakage currents. The appearance of only a few of spikes in the baseline is shown in

both recordings, in addition to the fact that the interdroplet bilayers typically remained intact for the duration of the 30 minute measurements. This is inferred by a capacitance value of 200 pF shown in a) and 400 pF in b), corresponding to an approximate bilayer diameter of 225 μm and 320 μm respectively. From 39 recordings it was found that the interdroplet bilayers were stable on 31 occasions and failed 8 times with an average lifetime of 14 minutes. The magnified region shown for each example, where the arrow indicates the position of the insert in the recordings, also highlights the stability of the bilayers.

A similar result was obtained when the interdroplet bilayer was formed using electrokinetic forces, as shown in Fig 4.1 part c). This is shown by the stability of the baseline and emphasised by the insert. A capacitance value of 400 pF indicated that the bilayer remained intact for the duration of the recording and had an approximate bilayer diameter of 320 μm, slightly higher than the typical capacitance value of 150-300 pF (corresponding to an approximate bilayer diameter of 195-276 μm) observed over 28 separate recordings. From 34 independent measurements the interdroplet bilayers were found to fuse on 6 occasions with an average lifetime of 19 minutes.

In general, interdroplet bilayers formed with asolectin were found to be repeatedly stable and free of current spikes or high leakage currents. While such conditions are ideal for obtaining single channel measurements it is also beneficial to be able to control the exact lipid composition of the bilayer. This is a drawback of using asolectin since it contains a mixture of lipids and will inevitably lead to some variation in the bilayer composition. This is significant as previous studies have indicated that ion channel activity can be influenced by the presence or absence of particular lipids in the bilayer, as shown with POPG for KcsA (Marius et al., 2008). For this reason it was desirable to understand whether stable interdroplet bilayers could be formed using a well defined mixture of DOPC/POPG or pure POPG.

4.2 Interdroplet bilayers of synthetic lipids

The amount of lipid used for forming interdroplet bilayers with asolectin was used to guide the starting concentration of DOPC/POPG interdroplet bilayers, which were formed by manual manipulation as described in section 3.2.5.4.

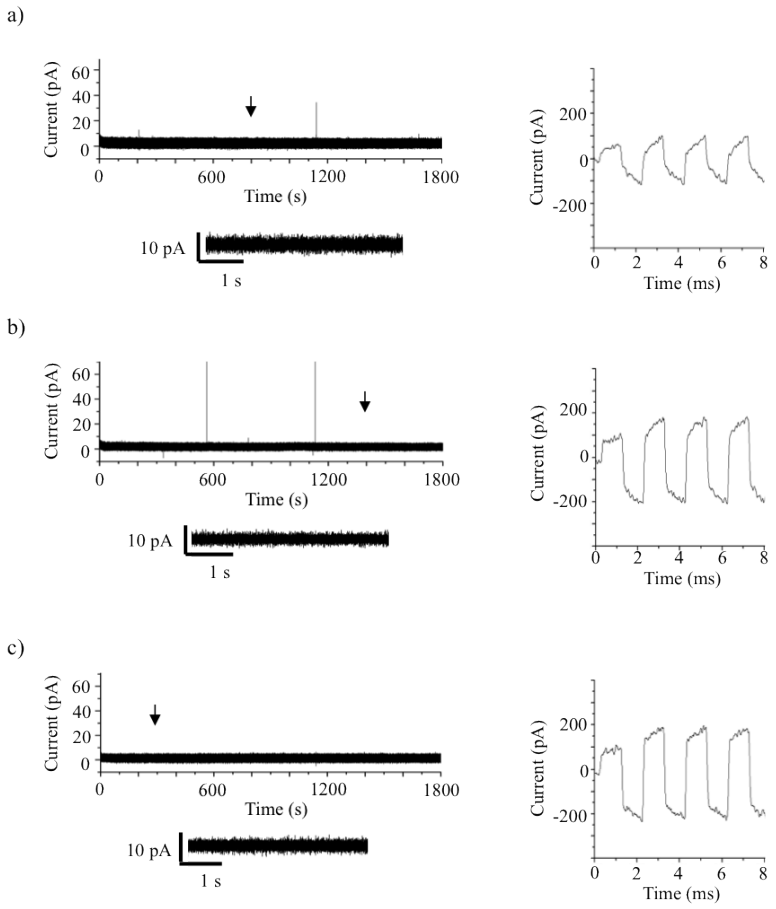

Figure 4.1: Electrophysiology of interdroplet bilayers formed with asolectin. The interdroplet bilayers were formed with two 2 μl droplets of buffer containing 150 mM KCl at pH 7.0 either manually a)-b), or using electrokinetic forces c). Measurements were obtained at 100 mV as described in section 3.2.1. The appearance of stable baselines in each part of the figure are highlighted by the magnified regions (indicated with an arrow), while the capacitance recordings confirm the bilayer remained intact at the end of the experiment. The data shows that interdroplet bilayers formed of asolectin were stable for the duration of the 30 minute recordings.

It was observed that an abundance of a white cloudy precipitate formed when a lipid concentration of 20 mg/ml was used, most likely caused by the presence of lipids in the lamellar phase as a result of the high lipid concentration. Under these conditions, the droplets spread across the surface, adopting a slug-like appearance that could not be penetrated by the Ag/AgCl electrodes.

The appearance of the solution improved when the concentration of the lipids was lowered to 13 mg/ml, with only a small amount of cloudy precipitate forming around the droplet surface. Under these conditions, the Ag/AgCl electrodes could

be inserted into the droplets when lowered into the lipid-oil and the droplets could also be manipulated more freely in solution compared to when 20 mg/ml was used.

The current measurement shown in Fig 4.2 a) is representative of three independent recordings. The measurement shows that the bilayer current starts at $\sim$ 0 pA for the first $\sim$3 minutes before a small leakage current is observed. From this point the bilayer current stays elevated above 0 pA and gradually rises, yet notably remains below $\sim$150 pA for the duration of the recording. It is also noticeable from the data that the baseline remains relatively unstable for the duration of the measurement, with occasional rapid fluctuations in the bilayer current leading to the occurrence of spikes and small steps in the recording.

The data is interesting as the leakage current is relatively small in magnitude, there were no high intensity (>300pA) spikes observed in the recording, and the bilayers remained intact for the duration of the 30 minute recording (n=3), as indicated by the capacitance trace. The square wave with a peak-to-peak amplitude of $\sim$350 pF, corresponding to an approximate bilayer diameter of 298 μm, disappeared when the droplets were manually separated. The data indicates that DOPC/POPG interdroplet bilayers can be formed with a lipid-out concentration of 13 mg/ml, but defects in the bilayer lead to a small leakage current which cause a degree of instability in the baseline.

The requirement of a stable baseline to clearly elucidate single-channel activity infers that the method requires further optimisation before bilayers of this composition are used for ion channel measurements. The experiment was susequently repeated with a lipid-oil mixture diluted to 8 mg/ml.

A representative measurement of three independent recordings is shown in Fig 4.2 b). The recording shows that the baseline stays much closer to 0 pA compared to the previous measurements, however it should be noted that this was not always repeatable as a recording with a similar leakage current to Fig 4.2 part a) was also obtained. Nonetheless, the data in this case indicates that the bilayer was still susceptible to destabilisation. This was indicated by the appearance of both low and high intensity spikes in the baseline, in addition to some deviations in the baseline current noted toward the end of the recording. The value of $\sim$550 pF obtained for the capacitance of Fig 4.2 b) indicates that the bilayer remained intact at the end of the experiment and had an approximate diameter of 375 μm. While this may be considered a particularly large bilayer, the data remains consistent with part a) where the interdroplet bilayers did not fuse (n=3).

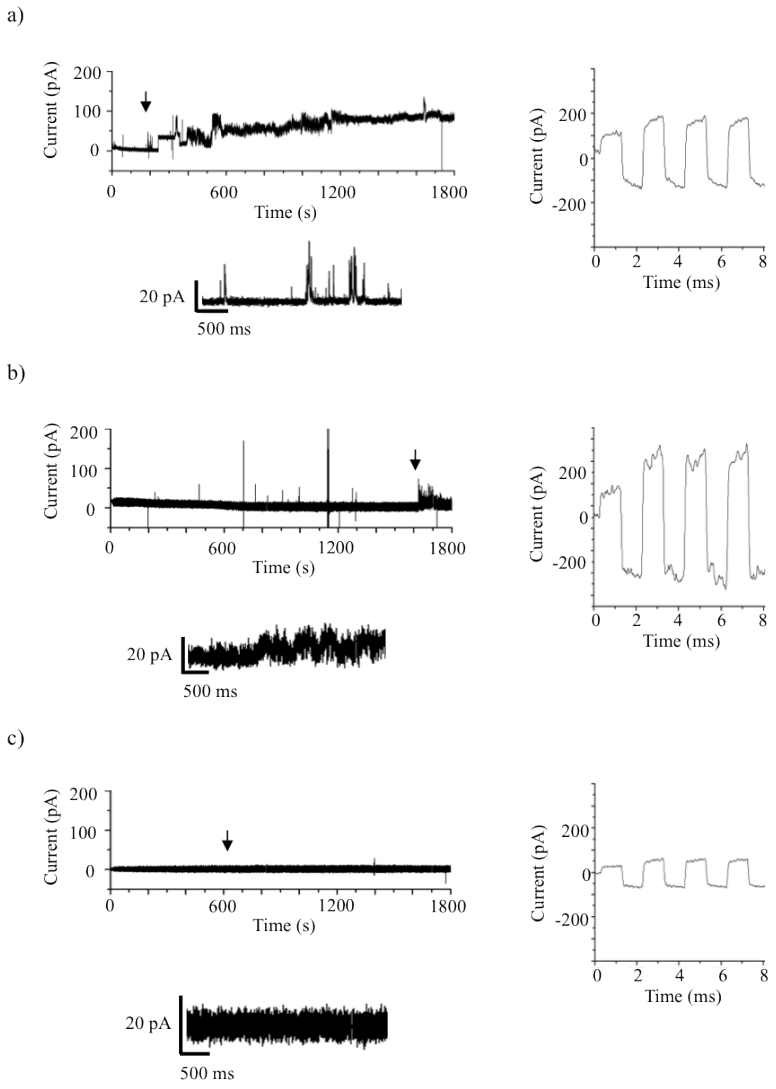

Figure 4.2: Electrophysiology of interdroplet bilayers formed from DOPC/POPG. Interdroplet bilayers were formed from two 2 μl of 150 mM KCl, pH 7.0 buffer in a) 13 mg/ml b) 8 mg/ml and c) 5 mg/ml of DOPC/POPG in n-decane. Measurements were obtained at 100 mV as described in section 3.2.1. The data was reduced 3x and filtered again with a 1 kHz low-pass filter for the purposes of demonstration. The figure shows that the interdroplet bilayers remained intact for the duration of the 30 minute recordings, as indicated by the capacitance measurements, however the stability of the baseline was not reproducable.

The recordings were similar in terms of their irreproducibility when the DOPC/POPG lipid stock was diluted to 5 mg/ml, however it was possible to obtain a stable bilayer as shown in part c) of Fig 4.2. The figure shows that the bilayer is stable with a very low leakage current, as indicated by the fact that the baseline is close to 0 pA. It is also notable that there are no current spikes in the measurement. The 125 pF was recorded for the bilayer capacitance as shown in c) , corresponding

to an approximate bilayer diameter of 180 μm. It is unclear whether the reduction of the bilayer diameter contributed to the stability of the interdroplet bilayer. However the data in parts a) and b) may indicate otherwise as the bilayer in b) was bigger than a) but exhibited greater stability.

While the interdroplet bilayers formed with DOPC/POPG were shown to repeatedly remain intact for the duration of the 30 minute recordings, obtaining measurements without observing bilayer instability was found to be less reproducible. Such destabilisation events, the intensity of which appeared to be lowered by a reduction in the amount of lipid used, are most likely the result of defects in the bilayer. The lipids were sonicated on ice in attempt to resolve the issue, however the problem of irreproducibility remained.

To address this further, the experiment was repeated with a lipid stock comprised only of POPG in decane. POPG was selected as its presence in the membrane has been shown to influence both the opening amplitude and open probability of KcsA (Marius et al., 2008). The data obtained with DOPC/POPG bilayers was used to influence the starting concentration of the POPG stock. The data from these experiments is shown in Fig 4.3, where the amount of lipid in the stock was a) 5 mg/ml, b) 0.5 mg/ml, and c) 0.1 mg/ml.

The measurements obtained using the 5 mg/ml lipid stock show that the lipid bilayers remained intact for the duration of the 30 minute recordings but exhibited destabilisation events similar to those observed with interdroplet bilayers formed from DOPC/POPG. The capacitance value for the interdroplet bilayer shown in the figure was 125 pF, indicating that the bilayer had an approximate diameter of 180 μm.

The bilayer was typically more stable when the lipid concentration was lowered to 0.5 mg/ml (n=3) however it was still common to observe small leakage currents as shown in Fig 4.3 part b). Under these conditions the interdroplet bilayers were again found to remain intact for the duration of the 30 minute recordings, as indicated by the capacitance value of 500 pF shown in b) part ii). This equates to a bilayer diameter of approximately 357 μm, which is slightly larger than typically expected, possibly accounting for the higher than normal peak-to-peak noise associated with the baseline.

The lipid concentration was subsequently lowered to 0.1 mg/ml to determine whether the bilayer stability could be improved. A representative measurement of these recordings (n=3) is shown in Fig 4.3 part c). The recording shows a stable

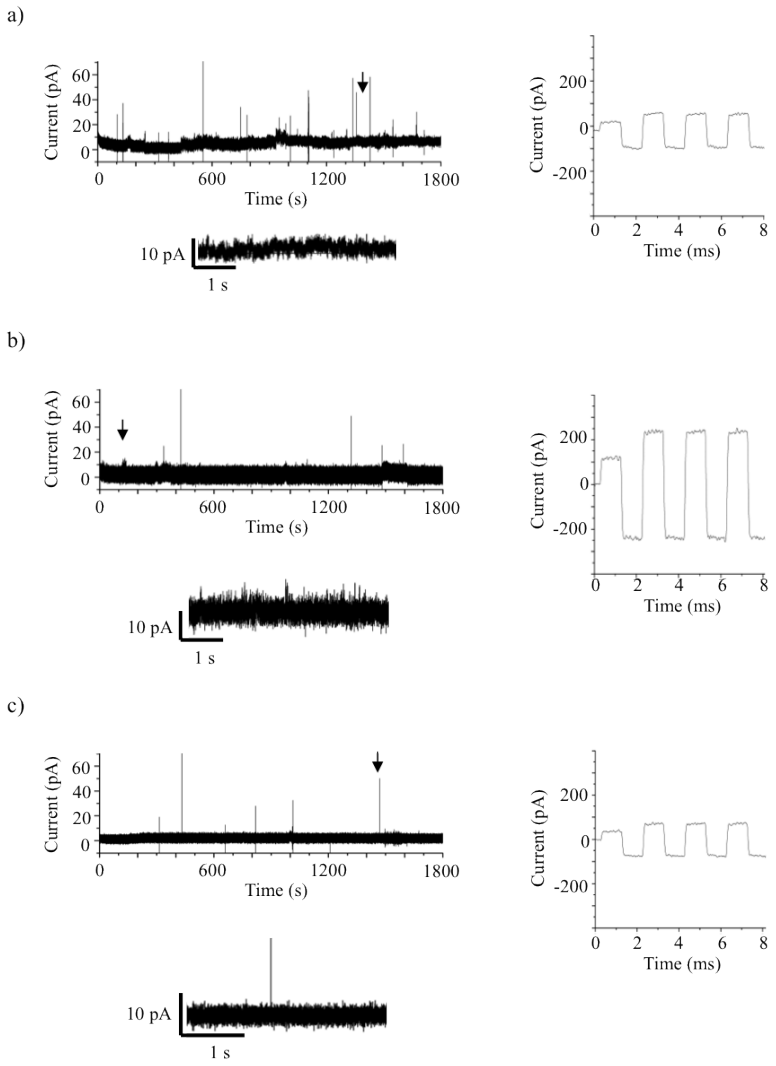

Figure 4.3: Electrophysiology of interdroplet bilayers formed from POPG. Interdroplet bilayers were formed from two 2 μl of 150 mM KCl, pH 7.0 buffer in a) 5 mg/ml b) 0.5 mg/ml and c) 0.1 mg/ml of POPG in n-decane. Measurements were obtained at 100 mV as described in section 3.2.1. The data was reduced 3x and filtered again with a 1 kHz low-pass filter for the purposes of demonstration. The figure shows that the interdroplet bilayers remained intact for the duration of the 30 minute recordings, however stable baselines were not repeatably obtained.

baseline containing less leakage currents by comparison to part b) of the figure, however a similar number of spikes are found in the baseline. It was also observed that the bilayer remained intact for the entirety of the 30 minute recordings as indicated by the capacitance trace in c) part ii) of the figure. The peak-to-peak intensity of the square wave was 150 pF, approximating to a bilayer diameter of 195 μm. The data shows that POPG can be used to form interdroplet bilayers which remain intact for over 30 minutes, however reproducibly obtaining stable

bilayers devoid of leakage currents or current spikes was found to be problematic. It is difficult to identify the origins of these destabilisation events, particularly since the lipid bilayer is a stochastic system in constant flux, manifested by the lateral diffusion of lipids (Jacobson et al., 1995). However it is plausible that the leakage currents arise from small defects in the lipid bilayer, while the current spikes could have a number of origins, including external electrical noise.

In summary, the data in this section shows that interdroplet bilayers can be successfully formed using asolectin, a mixture of DOPC/POPG and pure POPG lipids. In each case, the bilayers remained intact for the duration of the 30 minute recordings, however the measurement of stable baselines was found to be more reproducible with asolectin compared to the synthetic lipids.

This was unexpected because synthetic lipids are routinely used to form aperture suspended lipid bilayers (Marius et al., 2008). This difference in stability could be due to the size and shape of the lipid bilayer formed using the droplet method, where interdroplet bilayers are typically much larger than those formed across apertures.

4.3 Interdroplet bilayers with asymmetric pH

Obtaining stable baselines when both droplets contain buffer at different pH is a requirement for acquiring single-channel measurements of pH gated ion channels. Interdroplet bilayers of this nature have been reported in the literature (Aghdaei et al., 2008; Bayley et al., 2008) however to date there has been no detailed investigation in to the stability of these bilayers over time. This is important to understand for the purposes of this study as it is desirable for the bilayer to be stable for ∼30 minutes while a pH gated ion channel is expressed *in-situ* and inserted into the bilayer for electrical characterisation. The aim of this part of the study was therefore to determine whether interdroplet bilayers are stable when one droplet contains buffer at pH 4.0.

Interdroplet bilayers were formed by manual manipulation as described in section 3.2.5.4, in 20 mg/ml asolectin in n-decane. Current measurements were performed for 30 minutes under a holding potential of 100 mV (as detailed in section 3.2.1).

As shown in Fig 4.4 a), it was found that interdroplet bilayers with one droplet containing buffer at pH 7.0 and the other containing buffer at pH 4.0 rapidly failed

upon the application of the holding potential. This lead to the saturation of the baseline current and fusion of the two droplets, as indicated (*). The recording shows low-intensity destabilisation events in the baseline which appear as spikes <100 pA in intensity and small leakage currents (<10 pA) leading up to the point of bilayer failure. From 12 independent experiments, the bilayer was found to fail on each occasion with an average lifetime of 6 minutes. A similar result was observed when both droplets contained buffer at pH 4.0, however these conditions were less interesting since protein expression is unlikely to be sustained at low pH.

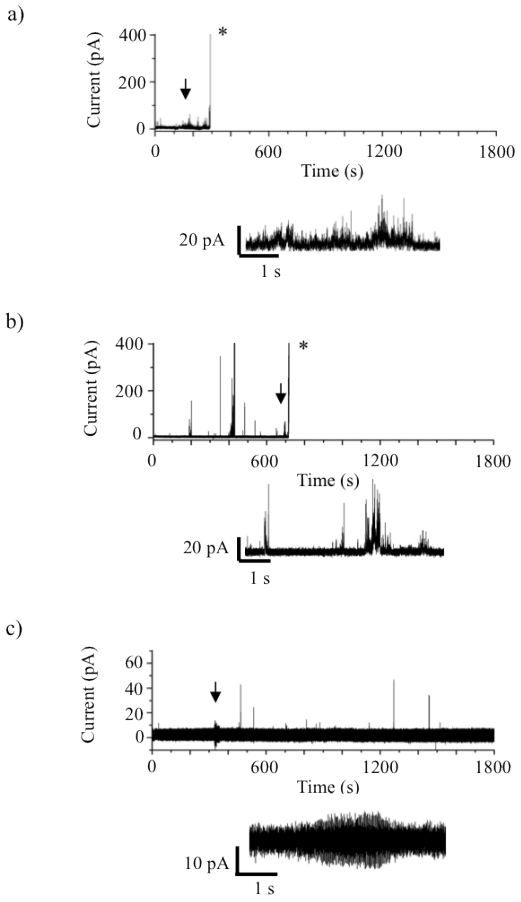

Figure 4.4: Interdroplet bilayers with asymmetric pH. Interdroplet bilayers were formed with one droplet containing 150 mM KCl buffered at pH 7 and a second droplet containing; a) 150 mM KCl buffered at pH 4.0, b) 150 mM KCl buffered at pH 4.5, and c) 150 mM KCl buffered at pH 5.0. The interdroplet bilayers were formed manually in 20 mg/ml asolectin in n-decane as described in section 3.2.5.4. Measurements were obtained at 100 mV as detailed in section 3.2.1. The data was reduced 3x and filtered again with a 1 kHz low-pass filter for the purposes of demonstration. The data shows that the lifetime of the interdroplet bilayers is significantly effected by the pH of the second droplet.

The data suggests that the low pH of the second droplet led to the destabilisaiton of the bilayer, an outcome that would be surprising as the same level of instability has not been reported for aperture suspended lipid bilayers under the same conditions (Marius et al., 2008)(Cuello et al., 1998)(Chakrapani et al., 2007).

To verify the pH dependence on the bilayer stability, the experiment was repeated with the second droplet containing buffer at pH 4.5. A representative measurement is shown in Fig 4.4 b), where some high intensity spikes are observed in the baseline before the bilayer fails. The magnified region also reveals some small leakage currents, where the current temporarily rises above 0 pA and several ∼100 pA intensity spikes are present in the baseline. From 6 independent experiments the interdroplet bilayers were found to fail on 4 occasions with an average lifetime of 10 minutes but were also found to remain intact for the duration of the 30-minute recordings on 2 separate occasions.

The data suggests that the higher pH of the droplet led to a significantly increased bilayer lifetime, an observation that was supported by the measurement of stable bilayers that did not fuse when the pH of the second droplet was increased to 5.0 (n=3). A representative recording of one of these measurements is shown in Fig 4.4 c), where only a small amount of noise is detected in the baseline, which is otherwise comparable to the data obtained at pH 7.0 in the previous subsection.

The data clearly demonstrates a pH dependent effect on the bilayer stability, however it still remains necessary to stabilise the bilayer at pH 4.0 in order to obtain measurements of pH gated channels such as KcsA. To achieve this, the experiment was repeated using higher concentrations of asolectin in n-decane.

The measurement in Fig 4.5 parts a)-b) clarifies the result when 20 mg/ml was used, where in part a) both droplets contained buffer at pH 7.0 and in part b) one droplet was substituted for a droplet containing buffer at pH 4.0. In line with what was observed in Fig 4.1 parts a) and b), the data in Fig 4.5 a) shows that the bilayer was stable and did not fail when both droplets contained buffer at pH 7.0. While Fig 4.5 b) shows that the bilayer fails after ∼5 minutes when the second droplet is replaced with buffer solution at pH 4.0.

The result when the lipid concentration was increased to 40 mg/ml is shown in parts c-d) of the figure, where the measurement shown with both droplets at pH 7.0 in part c) reveals a stable baseline with only a few low intensity (<20 pA) current spikes. Part d) is a representative recording of when the second droplet was substituted for buffer at pH 4.0 and shows that despite bilayer failure,the

lifetime of the bilayer appears to be improved by comparison to when 20 mg/ml of asolectin was used. This was inferred over 4 independent experiments where the bilayer fused on 2 occasions with an average lifetime of 20 minutes and was found to remain intact for the duration of the 30 minute recordings on 2 separate occasions. This is a significant improvement compared to the previous conditions, where the bilayer was shown to fail on each of the 12 measurements with an average lifetime of 6 minutes.

To identify whether the stability of the bilayer could be improved upon further, the experiment was repeated with the lipid concentration increased to 60 mg/ml. The data is shown in Fig 4.5 e)-f), where the control experiment with both droplets containing buffer at pH 7.0 is shown in e) and a measurement when one droplet contained buffer at pH 4.0 is shown in part f). Consistent with previous observations at lower lipid concentrations, the data shows that the

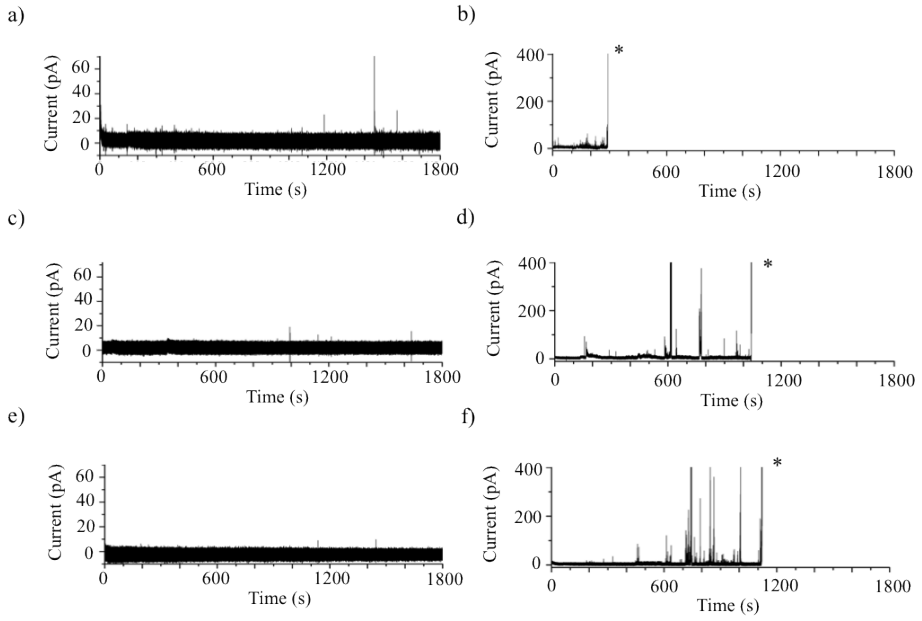

Figure 4.5: Stabilisation of interdroplet bilayers with asymmetric pH. Interdroplet bilayers comprising of one 2 μl droplet of 150 mM KCl buffer at pH 7.0 and either a second identical 2 μl droplet or a second droplet containing 150 mM KCl buffer at pH 4.0 were formed manually in 20 mg/ml (a-b), 40 mg/ml (c-d) or 60 mg/ml (e-f) of asolectin in n-decane. Bilayers of symmetric composition are shown in parts a), c) and e). Measurements were obtained at 100 mV as described in section! and, additionally, the data was reduced 3x and filtered again with a 1 kHz low-pass filter for the purposes of demonstration. Bilayer failure leads to saturation of the baseline current as indicated (*). The data shows that the lifetime of the interdroplet bilayers with asymmetric pH is significantly improved by increasing the amount of lipid supplied to the system.

Table 4.1: The stability of interdroplet bilayers formed with asymmetric pH and different lipid concentrations. The composition of the two droplets is shown together with the average lifetime of bilayers that failed within each 30-minute experiment.

Lipid out	Trans (ground)	Cis	$n =$	No.fused	Average lifetime (s)
20 mg/ml	150 mM KCl, pH 4.0	150 mM KCl, pH 7.0	12	12	6
20 mg/ml	150 mM KCl, pH 4.5	150 mM KCl, pH 7.0	6	4	10
20 mg/ml	150 mM KCl, pH 5.0	150 mM KCl, pH 7.0	3	0	-
40 mg/ml	150 mM KCl, pH 4.0	150 mM KCl, pH 7.0	4	2	20
40 mg/ml	150 mM KCl, pH 7.0	150 mM KCl, pH 7.0	3	0	-
60 mg/ml	150 mM KCl, pH 4.0	150 mM KCl, pH 7.0	5	2	20
60 mg/ml	150 mM KCl, pH 7.0	150 mM KCl, pH 7.0	3	0	-

baseline remained stable when both droplets contained buffer at pH 7.0 when 60 mg/ml of asolectin in n-decane was used. When the second droplet was substituted with a droplet containing buffer at pH 4.0, it was found that the interdroplet bilayers still had the propensity to fail, seemingly within a similar timeframe to what was observed when 40 mg/ml of asolectin in n-decane was used. From 5 independent measurements it was found that the interdroplet bilayers failed twice with an average lifetime of $\sim$20 minutes and remained intact for the duration of the 30 minute recordings on 3 separate occasions. The data from this section is summarised in Table 4.1.

In summary, the data in this subsection shows that interdroplet bilayers failed at 100 mV when one droplet contained buffer at pH 7.0 and when the second droplet contained buffer at pH 4.0. However it was found that the lifetime of the bilayer could be improved by supplying 60 mg/ml of asolectin to the decane solution. While destabilisation events were still found to occur under these conditions, the data shows that these events do not occur continuously throughout the recordings, indicating that it is possible to obtain single channel recordings of pH gated ion channels when interdroplet bilayers with asymmetric pH are used. This is assuming that the bilayer is not destabilised further by the presence of a CF system, a topic which is addressed in the next section.

4.4 The effect of cell-free expression mixtures and components on bilayer stability

As discussed in section 2.3.3, CF systems have been previously reported to destabilise interdroplet bilayers (Syeda et al., 2008), however a systematic study

was not undertaken. This is addressed in this section of the study, where the stability of interdroplet bilayers made of asolectin was investigated in the presence of different CF systems and their comprising fractions.

Interdroplet bilayers were formed using the electrokinetic method described in section 3.2.5.3 and the CF systems were prepared without incubation as outlined in section 3.1.4 with the DNA fraction replaced with 150 mM KCl buffer at pH 7.0.

Bilayer current recordings with a CF expression mixture in one droplet and buffer solution in the second droplet are shown in Fig 4.6 a)-c). It can be seen that the bilayer current is elevated, with a current baseline at ∼5-15 pA and with occasional bursts of short-lived current spikes (<20 ms lifetime and up to 80 pA amplitude). Similar irregular current bursts or current steps have also been observed for lipid bilayers in contact with pure buffer solution when the lipids are near their phase transition temperature (Blicher et al., 2009; Laub et al., 2012) and for bilayers in the presence of silica nanospheres (Klein et al., 2008; de Planque et al., 2011) and have been attributed to lipid packing defects.

The electrical recordings thus indicate that the structural integrity of the bilayer is compromised by exposure to each of the three CF expression mixtures. Bilayer rupture, observed as saturation of the baseline current, was usually preceded by more intense leakage current spikes of up to 0.5-1.0 nA. Based on at least three independent experiments (See Table 4.2), the lifetime of the interdroplet bilayers of asolectin lipids is on average reduced to 8 minutes in the presence of the L1130 mixture, and to less than 30 seconds for the EasyXpress and Expressway solutions. Hence, the lifetime of interdroplet bilayers in the presence of cell-free expression mixtures based on S30 lysates (Zubay, 1973) is too short to allow experiments with in situ expressed membrane proteins.

To identify the cause of the bilayer instability, which is unlikely to result from an osmotic imbalance because it was also observed when the same mixtures are present in both droplets, the various components that make up the cell-free protein expression mixtures were investigated. It is the S30 cell lysate, extracted from E.coli cell cultures, that contains the actual ribosomal machinery for translation of mRNA (Zubay, 1973; Kigawa et al., 2004; Zawada, 2012; Berrier et al., 2004). This is supplemented with T7 RNA polymerase for transcription of the user-supplied DNA to mRNA, and with a system for metabolic energy generation (referred to as premix or reaction buffer), for example based on pyruvate or creatine kinase enzymes (Kim and Kim, 2009), to sustain the transcription and

translation reactions. Because the various suppliers divided the key biomolecules over these premixed component fractions in different ways, the protein content of these various fractions were visualised by gel electrophoresis. Fig 4.7 shows that each of the three lysate fractions contains a large number of <150 kDa proteins, which is consistent with previous reports (Berrier et al., 2004). A band with a molecular weight corresponding to T7 RNA polymerase is visible for the Expressway enzyme mix in lane 8, whereas the remaining component fractions are either devoid of protein, or the protein concentration is too low to be detected by staining with Coomassie Blue.

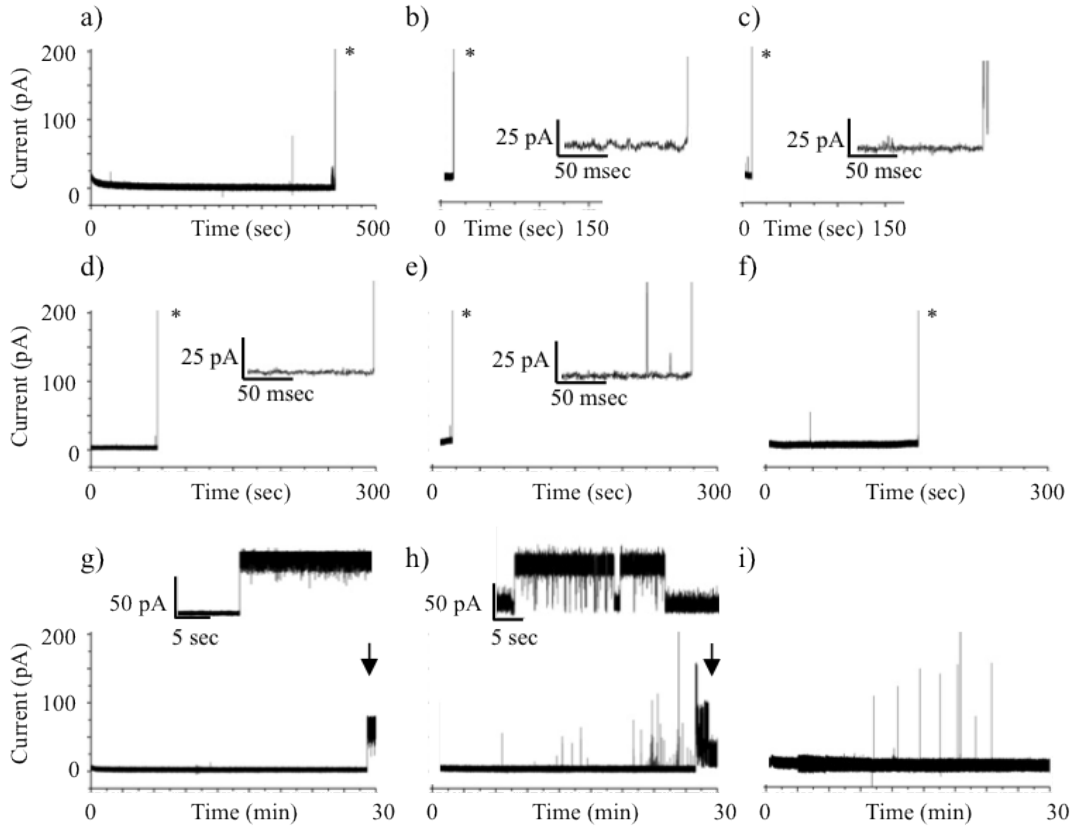

Figure 4.6: Electrophysiology of interdroplet bilayers containing different CF systems mixtures and selected fractions. (a-c) Current traces for L1130 (a), EasyXpress (b) and Expressway (c) complete reaction mixtures. (d-f) Current traces for L1130 (d), EasyXpress (e) and Expressway (f) lysate fractions, supplemented with buffer solution. (g-i) Current traces for L1130 (g), EasyXpress (i) and Expressway (j) metabolic energy supply fractions, supplemented with buffer solution. An abrupt rise in current at the end of a trace indicates bilayer failure (a-f); corresponding insets show details of the current trace immediately before bilayer failure. The insets are an expansion of the region of the main trace marked with an arrow while an asterisk signifies bilayer failure.

To investigate whether the bilayer destabilisation by the cell-free mixtures was due to a high protein concentration, the effect of the lysate fractions were studied alone. The lysates were diluted with buffer solution to achieve the same concentration as in the total expression mixture, and subsequently one 2 μl droplet of diluted lysate was placed in the oil reservoir and brought into contact with a 2 μl droplet of buffer solution using the electrode array. As shown in Fig 4.6 d)-f), the lysates did not give rise to bursts of bilayer current spikes, but bilayer destabilisation was evident from the decreased bilayer lifetime. In contrast to the total mixtures shown in Fig 4.6 a)-c) the average lifetime of the lysates by themselves was different for the three suppliers: 8 min for L1130 lysate and ∼30 seconds for EasyXpress and Expressway lysates. The absence of pronounced current spikes and the significantly increased bilayer lifetime observed with the L1130 lysate, suggest that it is not just the protein-rich lysate that contributes to the bilayer destabilisation by the complete CF expression solutions.

The 'energy mixture' fractions, which contain the components for metabolic energy generation, and sometimes also T7 RNA polymerase, were also investigated at a dilution corresponding to the concentrations in the total mixture. The bilayer current traces in Fig 4.4 g)-i) show low-intensity current spikes (up to 30 pA) as well as large current steps (∼75 pA amplitude with a lifetime of several

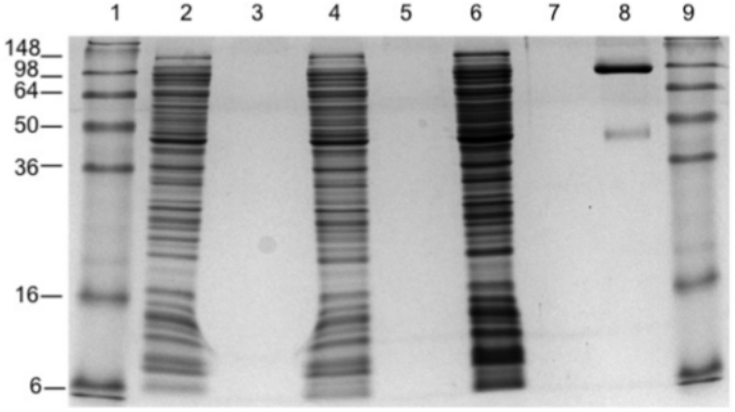

Figure 4.7: SDS PAGE of the protein content of various components of cell-free expression mixtures. The lanes are loaded as follows: 1) SeeBlue Plus 2 protein ladder with apparent molecular weights in kDa, 2) L1130 lysate, 3) L1130 reaction buffer, 4) EasyXpress lysate, 5) EasyXpress reaction buffer, 6) Expressway lysate, 7) Expressway reaction buffer, 8) Expressway T7 enzyme mixture, and 9) protein ladder. The 15% SDS-PAGE gel was run at 150 V for 75 mins in Tris-glycine buffer and stained with Coomassie Blue. The figure shows that the cell lysate fraction of the CF expression systems contain a large number of proteins.

Table 4.2: The stability of interdroplet bilayers formed with CF expression mixtures and components. The composition of the two droplets is shown together with the average lifetime of bilayers that failed within each 30-minute experiment.

Trans (ground)	Cis	$n =$	No.fused	Average lifetime (s)
Buffer	Buffer	34	6	1140
Amino Acids	Buffer	3	0	-
1 μg GFP DNA	Buffer	3	0	-
L1130 system	Buffer	8	8	499
L1130 lysate	Buffer	3	3	520
L1130 reaction mixture	Buffer	3	0	-
L1130 system	L1130 system	5	5	153
EasyXpress system	Buffer	12	12	19
EasyXpress lysate	Buffer	4	4	20
EasyXpress reaction mixture	Buffer	3	0	-
Expressway system	Buffer	9	9	15
Expressway lysate	Buffer	7	7	171
Expressway reaction mixture	Buffer	3	0	-

seconds), which are not evident for the total cell-free expression mixtures or for the lysate fractions. Despite these bilayer perturbations, the interdroplet bilayer remained intact for 30 minutes for all the three energy mixtures, at which point the measurement was terminated. It should be noted that the other fractions of the cell-free mixtures, such as the amino acids and the T7 RNA polymerase did not give rise to any bilayer perturbations or reduced bilayer lifetimes, and a control experiment with DNA plasmid also resulted in a bilayer current similar to that observed for pure buffer solution. A summary of the data obtained in this subsection is shown in Table 4.2.

In summary, this subsection shows that interdroplet bilayers become unstable and fuse within a few minutes when in the presence of a CF system. The possible causes of this instability are investigated in the next section.

4.5 Interdroplet bilayers formed of pure protein and polymers

In the previous subsection it was found that interdroplet bilayers failed rapidly when one droplet contained a CF expression mixture. It has been previously suggested that membrane destabilisation of CF systems to interdroplet layers could be due to polyethylene glycol (PEG) or E.coli lipids (Syeda et al., 2008), while the findings of the previous section also highlight the effect of high concentrations of

proteins. The aim of this section is to investigate the effect of these components on the stability of interdroplet bilayers. The effect of lipids is studied in the next section.

Polymer and proteins at different concentrations were all prepared in buffer solution (150 mM KCl, pH 7.4). Interdroplet bilayers were formed by manipulating a 2 μl droplet of the sample into contact with a 2μl droplet of buffer (150 mM KCl, pH 7.4) using electrokinetic forces as described in section 3.2.5.3. Current measurements were obtained under a holding potential of 100 mV as detailed in section 3.2.1.

Cell-free expression mixtures based on S30 cell lysates contain proteins at a concentration of ∼15 mg/ml (Patnaik et al., 1998; Freischmidt et al., 2010), which is estimated to be equivalent to ∼0.11 mM. BSA, a positively charged protein, and lysozyme, a negatively charged protein, were prepared at concentrations of 3 mM, 3 μM and 3 nM, for the effect of high concentrations of the protein to be compared with the effect of much lower concentrations, where the latter are closer to the typical range used for interdroplet bilayer experiments with ion channels. Measurements of bilayers formed between a droplet with a nM protein concentration and a droplet of pure buffer solution, depicted in Fig 4.8 a) and b), show a stable baseline as observed for pure buffer, and the bilayer remains intact for 30 minutes, after which the measurement was aborted. Similar results were obtained at a concentration of 3 μM. Interestingly at the higher concentration of 3 mM the two proteins have a different effect on the bilayer, as shown in Fig 4.8 b) and d).

The negatively charged BSA causes a small number of current spikes prior to failure of the bilayer, which happens before ∼65 sec on average (n=5), whereas the positively charged lysozyme causes a large number of high-amplitude (up to 1.2 nA) bilayer current spikes, but these do not lead to bilayer failure within the 30-minute measurement period (n=3). Thus, the effects of a high concentration of BSA and lysozyme are, respectively, reminiscent of the effect of cell lysates and energy mixtures shown in the previous subsection. The polymer PEG 8000 is added to cell-free reaction mixtures as a molecular crowding agent to compensate for the dilution of the pure S30 lysate, typically to a concentration of 4-5% (w/v) (Kigawa et al., 2004; Patnaik et al., 1998). The bilayer current was measured in the presence of 0.1 or 10% PEG 8000 on one side of the interdroplet bilayer and pure buffer solution on the other side. As shown in Fig 4.8 e),f), current spikes were observed for both polymer concentrations, but occurred more frequently, as

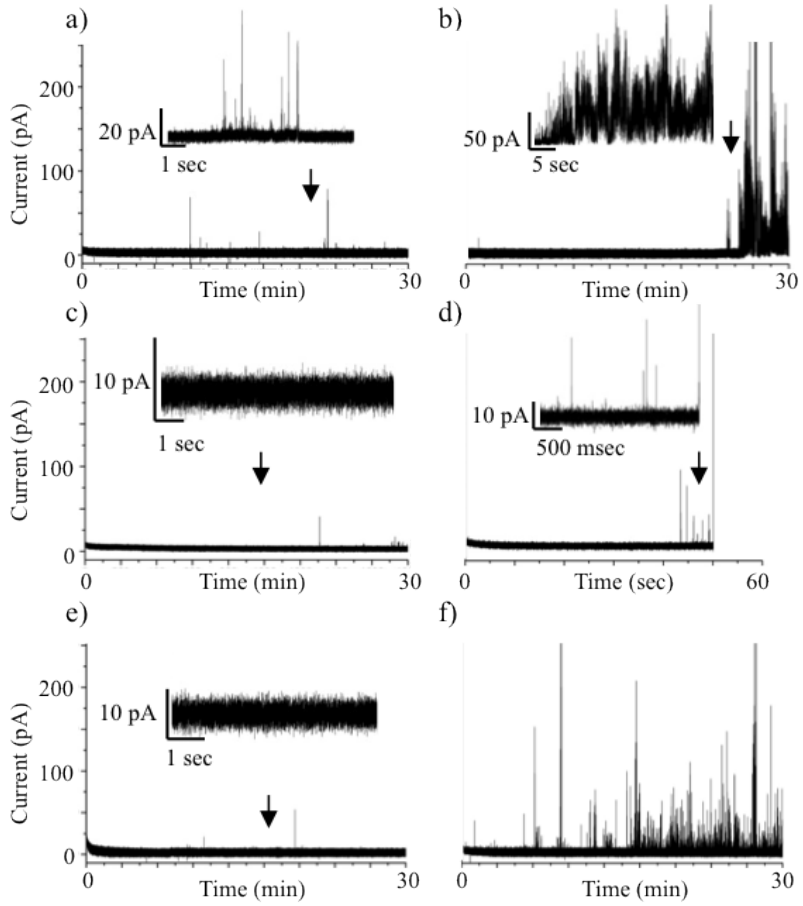

Figure 4.8: Electrophysiology of interdroplet bilayers in the presence of various concentrations of pure proteins and polymers. a) 3 nM lysozyme, b) 3 mM lysozyme, c) 3 nM bovine serum albumin, d) 3 mM bovine serum albumin e) 1% (w/v) poly(ethylene glycol) 8000, f) 10% (w/v) poly(ethylene glycol) 8000. The insets are an expansion of the region of the main trace marked with an arrow. Note that the large current fluctuations observed at the higher polymer (f) and lysozyme (b) concentrations indicate bilayer instability without bilayer failure, whereas the presence of 3 mM albumin (d) causes the bilayer to break within one minute.

prolonged current bursts, and with a higher amplitude (up to 800 pA) for the higher PEG concentration. However, for both polymer concentrations, the bilayer did not fail within 30 minutes (n=3). A summary of the data obtained in this subsection is shown in Table 4.3.

In summary, this subsection shows that proteins or PEG at the high concentrations typical for cell-free expression mixtures destabilise interdroplet bilayers, either by inducing transient defects manifested as current spikes, or by bilayer failure which is observed as current saturation and droplet fusion. However, elevated current baselines following current steps were not observed. It is possible that the current

Table 4.3: The stability of interdroplet bilayers formed in the presence of pure proteins and polymers. The composition of the two droplets is shown together with the average lifetime of bilayers that failed within each 30-minute experiment

Trans (ground)	Cis	$n =$	No.fused	Average lifetime (s)
3 nM BSA	Buffer	3	0	-
3 μM BSA	Buffer	5	0	-
3 mM BSA	Buffer	5	5	62
3 mM BSA	3 mM BSA	4	4	16
3 nM Lysozyme	Buffer	3	0	-
3 μM Lysozyme	Buffer	3	0	-
3 mM Lysozyme	Buffer	3	0	-
0.1 % (w/v) PEG,8000	Buffer	3	0	-
1.0 % (w/v) PEG,8000	Buffer	3	0	-
10.0 % (w/v) PEG,8000	Buffer	3	0	-

fluctuations observed with lysozyme indicate electrostatic interactions with the overall negatively charged asolectin bilayer, but it is difficult to explain the rapid bilayer rupture observed for BSA.

4.6 Stabilisation of interdroplet bilayers formed in the presence of CF systems

In the previous section, it was shown that high concentrations of proteins and polymers can destabilise interdroplet bilayers, a problem that must be resolved in order to achieve the coupled expression and characterisation of ion channels in microdroplets.

In this section, the stability of interdroplet bilayers formed in the presence of cell-free expression mixtures are studied in two ways: dilution of the cell-free mixture and addition of lipid vesicles. The latter approach also serves to establish whether bilayer destabilisation is a result of residual lipid molecules in the S30 lysates, discussed in the previous section. The rationale of supplementing the cell-free mixture with lipid vesicles is that additional lipid surface is provided, effectively lowering the concentration of undesirable membrane-associating molecules at the interdroplet bilayer. Also, when membrane proteins are expressed by cell-free expression (e.g. in glass vials), vesicles are commonly added to prevent aggregation of the produced proteins and to achieve protein incorporation in the vesicle bilayer for subsequent proteoliposome assays, as discussed in section 2.3.2.

DOPC/POPG vesicles were prepared as described in section 3.1.3 and added to the CF system in place of buffer. A 2 μl droplet of the sample was brought into contact with a 2 μl droplet of buffer (150 mM KCl, pH 7.4) using electrokinetic forces as described in section 3.2.5.3 and current measurements were obtained at 100 mV as outlined in section 3.2.1.

The L1130 cell-free mixture was supplemented with 0.05, 0.5 or 5 μg lipid (DOPC/POPG=1:1 (w/w)) per μl, which corresponds, respectively, to concentrations of 200-nm lipid vesicles of 0.2, 2.0 or 20 nM. Fig 4.9 (a-c) shows that the dominant features of the bilayer current in the presence of vesicle-supplemented cell-free expression mixture are current steps of up to 25 pA. Once the current has increased following a current step, the current noise increases significantly and appears as downward spikes, suggesting that there is a tendency for the bilayer to seal the defects that give rise to the elevated current. The current steps are also observed in the non-supplemented expression mixtures (Fig 4.6 a)-c)), but in the presence of the vesicles, the average lifetime of the bilayer was significantly increased, from 2-3 minutes (see above) to 22-28 minutes (n=3 for each lipid concentration). This lifetime is sufficiently long for various membrane protein assays, but the observed current steps indicate the bilayer will, to some extent, be permeable to ions, which can interfere with ion channel experiments.

It is interesting that these relatively well-defined current transitions were observed when lipid vesicles were added to the cell-free mixture, which could indicate that the current steps in the non-modified mixtures were indeed caused by residual E. coli lipids in the S30 cell lysates (Syeda et al., 2008). It is possible that these steps correspond to the fusion of vesicles with the interdroplet bilayer, with each vesicle carrying a large number of surface-associated molecules with bilayer perturbing properties, which gradually diffuse away after a vesicle-bilayer fusion event. In this scenario, increasing the vesicle concentration would reduce the amount of material associated with each vesicle and thus cause less bilayer perturbation, but in these experiments it was not possible to increase the amount of lipids while maintaining a homogeneous mixture. Instead, the concentration of expression-associated molecules was reduced by diluting the L1130 expression mixture 10-fold with buffer solution. This dilution by itself, without added vesicles, improved the bilayer stability significantly, enabling an average lifetime of 21 minutes (n=6), with only a few brief ($\sim$2 ms) elevations in the baseline (200-400 pA) prior to bilayer failure. Hence, a 10-fold reduction in the concentration of all the components of the cell-free mixture mitigates the destabilisation effect. In the presence of 0.2 nM vesicles, distinct bilayer current steps with associated

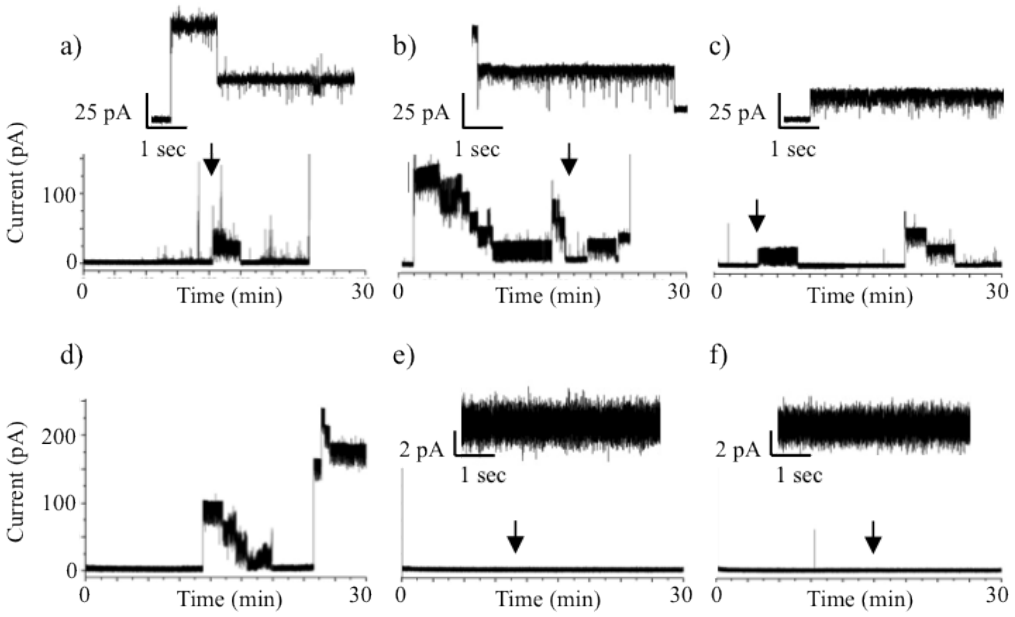

Figure 4.9: Electrophysiology of interdroplet bilayers in the presence of a non-diluted and diluted CF expression mixture, supplemented with lipid vesicles. (a-c) Standard, non-diluted, L1130 mixture with 0.2 nM (a), 2.0 nM (b) and 20 nM (c) lipid vesicles. (d-f) Ten-fold diluted L1130 mixture with 0.2 nM (a), 2.0 nM (b) and 20 nM (c) lipid vesicles. The insets are an expansion of the region of the main trace marked with an asterisk. The figure shows that dilution in combination with vesicle addition stabilises the interdroplet bilayer

elevated bilayer currents were apparent for the diluted expression mixture, but at higher vesicle concentrations the current baseline was identical to that observed for pure buffer solution (Fig 4.9 d)-f)), indicating that the interdroplet bilayer was free of defects, and the bilayers remained intact for the duration of the 30-minute measurements. Dilution in combination with vesicle addition thus enables a stable interdroplet bilayer as a matrix for insertion of cell-free expressed membrane proteins. A summary of the data obtained in this subsection is shown in Table 4.4.

In summary, the data in this subsection shows that a 10-fold dilution of the CF mixture and the addition of lipid vesicles improved the lifetime and stability of interdroplet bilayers formed in the presence of a CF expression system. Since cell-free expressed membrane proteins are known to insert into vesicles (as discussed in section 2.3.2) and proteoliposome fusion is a means of membrane protein delivery to lipid bilayers, (section 2.2.5) it is feasible that the proposed stabilisation strategy is compatible with incorporation of CF expressed membrane proteins into interdroplet bilayers.

Table 4.4: The stabilisation of interdroplet bilayers. The composition of the two droplets is shown together with the average lifetime of bilayers that failed within each 30-minute experiment

Trans (ground)	Cis	$n =$	No.fused	Average lifetime (s)
L1130 system & 0.2 nM of vesicles	Buffer	3	3	1341
L1130 system & 2.0 nM of vesicles	Buffer	3	3	1288
L1130 system & 20.0 nM of vesicles	Buffer	3	2	1614
L1130 system x 10 dilute	Buffer	6	4	936
L1130 system x 10 dilute & 0.2 nM of vesicles	Buffer	3	1	1117
L1130 system x 10 dilute & 2.0 nM of vesicles	Buffer	3	0	-
L1130 system x 10 dilute & 20.0 nM of vesicles	Buffer	3	0	-

4.7 Summary

As the effect of concentrated protein solutions in general, and of CF mixtures in particular, on lipid bilayers is not known (section 2.3.3) the interdroplet bilayer electrophysiology system described in section 3.2.5 was used to study the stability of bilayers exposed to different pre-incubated CF expression mixtures and their comprising fractions. This led to the identification of the cell-lysates and the energy mixtures being responsible for disrupting the membrane in section 4.4, where two distinctly different types of destabilisation were observed; 1) sudden bilayer failure and 2) current spikes and baseline fluctuations.

Sudden bilayer failure was also observed for high concentrations of BSA in section 4.5 where spikes in the baseline are also shown in representative concentrations of PEG. Baseline fluctuations similar to those observed in section 4.4 were similarly found when supplying vesicles to the system in section 4.6, yet vesicle addition coupled with a 10x dilution of the CF system led to the stabilisation of the bilayer, enabling measurements for longer than 30 minutes.

The stabilisation of interdroplet bilayers in the presence of the pre-incubated CF system is a milestone toward achieving the coupled expression and characterisation of ion channels, which could be realised if ion channels can be expressed by the CF system and can self-insert into the bilayer for characterisation.

Chapter 5

The cell-free expression of ion channels

As outlined in Chapter 1, the aim of this study was to determine whether the CF expression and characterisation of ion channels could be coupled in microdroplets. This motivated the study of the bilayer stability in the presence of the CF system in Chapter 4 where, to determine the intrinsic effect of the mixture on the bilayer stability, three commercial pre-incubated CF systems were screened without the addition of a DNA template. This led to the stabilisation of interdroplet bilayers through a combination of dilution and the addition of vesicles but did not address the ability of the CF systems to express ion channels.

The focus of this chapter is therefore to demonstrate and quantify the capability the CF system to express ion channels from the DNA templates engineered in section 3.1.1 and to determine the yield dependence on the presence of DNA and vesicles. This methodology is developed in the first part of the chapter for His-tagged KcsA and then applied to the full-length KvAP channel, a substantially larger channel containing an extramembranous domain, before being attempted with the hERG pore domain.

5.1 The cell-free expression of KcsA

This section details the CF expression of the KcsA channel, discussed in detail in section 2.4.1, and outlines the methods developed to verify that the protein was successfully expressed

5.1.1 Western blotting of cell-free expressed His-tagged KcsA

As shown in section 3.1.11, verifying the expression of KcsA is complicated by the number of proteins at high concentrations present in the CF system. This motivated the use of Western blotting (section 2.2.4) to identify CF His-tagged KcsA. Dr. Natalie Smithers performed the Western transfer, staining and imaging.

Eight CF reactions were prepared to 50 μl as detailed in section 3.1.4. Two contained no DNA, two contained 0.5 μg of KcsA DNA, two contained 1 μg of KcsA DNA while the two remaining reactions contained 2 μg of KcsA DNA. One of each sample was incubated at 37°C for 2 hours while the remaining sample for each condition was kept at room temperature. Three 1.5 mm thick 10 % gels were prepared as described in section 3.1.6, except a 5 well comb was used to allow for the entire 50 μl samples to be loaded.

The first gel contained 20 μl of SeeBlue Plus2 protein standard in the first lane while the second and third lanes contained purified His-tagged GFP and KcsA protein expressed *in-vivo*, prepared by Dr. Natalie Smithers as detailed in section 3.1.2. The GFP sample was prepared by taking 15 μl of the sample, adding 35 μl of nuclease free water and mixing with 50 μl of 5 x loading buffer. The concentration of the GFP protein was unclear since other proteins were present in the final eluate. The KcsA sample was prepared by taking 10 μl of the protein, adding 40 μl of nuclease-free water and 50 μl of 5 x loading buffer. The amount of the His-tagged protein loaded was 57 μg. Lane 4 contained the CF mixture with no DNA after 2 hour incubation at 37°C. This sample was mixed with 50 μl of 5 x loading buffer. The second gel contained 20 μl of SeeBlue Plus2 protein standard in the first lane, pre-mixed with 30 μl of nuclease free water as in the first gel. Lanes 2, 3 and 4 contained the CF mixtures containing 0.5 μg of KcsA DNA, 1 μg of KcsA and 2 μg of KcsA DNA respectively. Each sample was incubated at 37°C for 2 hours and loaded as described above with 50 μl of 5 x loading buffer. Lane 5 contained KcsA protein, prepared as in the first gel. The third gel was identical to the second gel except that the samples incubated at room temperature were used in lanes 2-4. The three gels were run together for 75 minutes at 150 V prior to Western transfer (as detailed in sections 3.1.6 and 3.1.7.

The Coomassie stained gels after Western transfer to the nitrocellulose paper are shown in parts a), c) and d) of Fig 5.1 where a)-b), c)-d) and e)-f) correspond to gels one, two and three respectively. Although each gel shows the almost

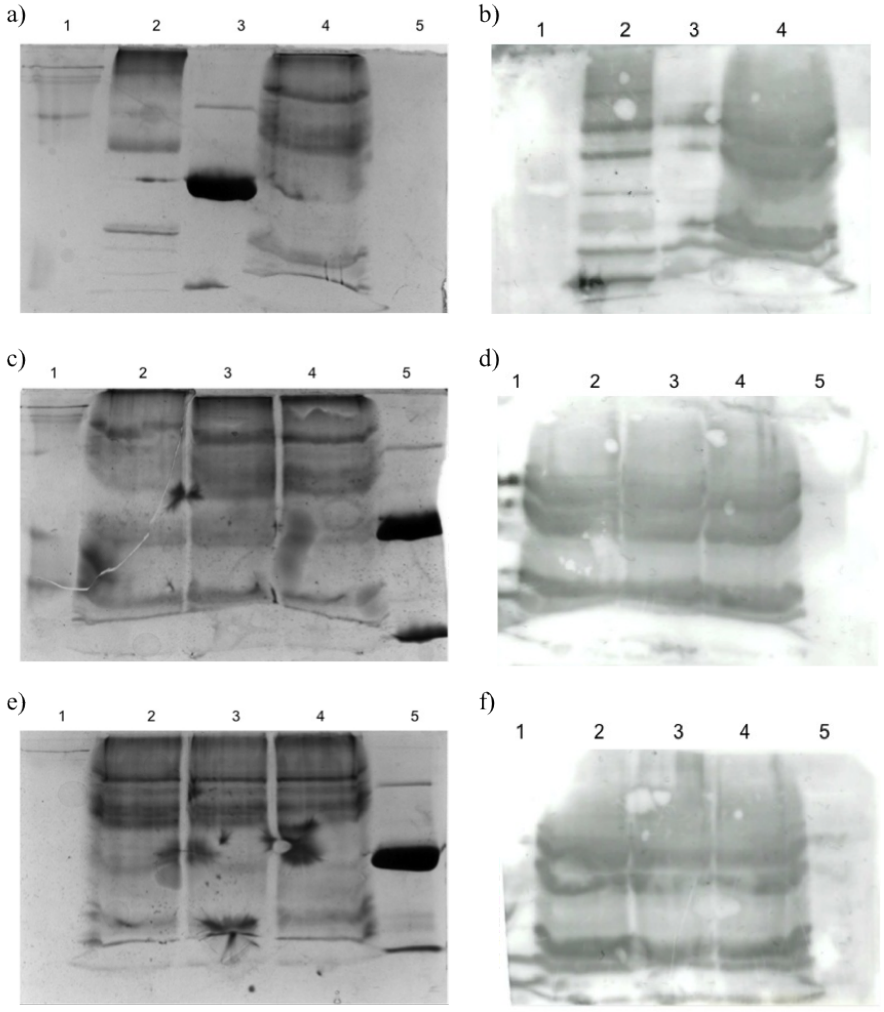

Figure 5.1: Western blot of CF expressed KcsA. Three SDS Page gels were run and transferred onto nitrocellulose paper for antibody detection. The SDS page gels are shown in parts a), c) and e) of Fig 5.3 while the photographic impression of the luminescence released by the bound secondary antibody is shown in parts b), d) and f). Lane 1 of all gels contained the molecular weight standard See Blue Plus 2. a-b) Lane 2 contained purified His-tagged GFP, lane 3 purified His-tagged KcsA and the cell-free mixture with no DNA after a 2 hour incubation at 37°C was loaded into Lane 4. c-d) Lanes 2, 3 and 4 contained the cell-free mixture with 0.5 μg, 1 μg and 2 μg of KcsA DNA respectively incubated at 37°C for 2 hours and Lane 5 contained purified KcsA protein. e-f) Was a duplicate of c-d) except the samples were incubated at room temperature. KcsA is not identified in either the samples or the control and the data shows a large amount of non-specific binding by the primary anti-HN antibody.

complete transfer of the protein ladder there remains a large amount of protein in the remaining lanes, indicating that not all of the protein was transferred to the nitrocellulose.

The imaged blotting paper from gel one is shown in Fig 5.1 a), where multiple proteins are detected in lane 2, containing the His-tagged GFP control compared to fewer in lane 3 containing the His-tagged KcsA control. As no DNA was supplied to CF mix in lane 4, no tagged proteins should be present. However the image shows that a huge number of proteins are detected as indicated by the luminescence spanning the entire lane, inside of which three pronounced bands are more clearly seen. This indicates that the primary anti-HN antibody is binding non-specifically to the protein sample, with the secondary antibody subsequently binding to the primary antibody leading to the signal observed. The same outcome was observed for the second and third gels as shown in Fig 5.1 c) and e), where all lanes containing the CF system display similar levels of non-specific binding.

This is interesting given the signal observed on the blotting paper in the lanes containing the CF system and most likely reflects the scale of the amount of protein loaded onto the gel, which may negatively influence the specificity of the binding of the primary antibody. With this in mind, the pieces of nitrocellulose were stripped of both antibodies, blocked with a higher concentration of milk and re-probed with the same primary antibody and an IR dye conjugated secondary antibody for direct imaging using a LI-COR ODYSSEY infrared imager. However no improvement was observed (data not shown), which again points toward the specificity of the primary antibody. One possibility could be that the huge number of proteins on the blotting paper compromise the specificity of the primary antibody, but this would then bring into question why no signal was obtained for the control sample. This may be explained by the gels in Fig 5.1 which show that a considerable amount of the control sample was retained on each gel and thus not transferred to the nitrocellulose.

In summary, the data shows that the CF protein expression product was not successfully detected using Western Blotting, indicating that protein purification may be required to identify the CF expressed protein of interest on an SDS PAGE gel, which is investigated in the next subsection.

5.1.2 Affinity-bead purification of cell-free expressed His-tagged KcsA

The presence of the His-tag introduced for Western Blotting also allows for the purification of CF expressed proteins using nickel beads functionalised with a nitrilotriacetic acid resin as explained in detail in Chapter 3, section 3.1.5. This

Table 5.1: Summary of the bands of interest extracted from Fig 5.2

ID	Lane	Band no.	Mol. Wt (kDa)	Relative front	Volume (int)	Band %
Lysozyme	1	7	16.0	0.77	2.4 x 10^6	18.4
KcsA monomer (control)	10	9	18.5	0.70	22.0 x 10^6	63.1
KcsA dimer (control)	10	7	35.3	0.390	1.5 x 10^6	3.1
KcsA tetramer (control)	10	5	64.6	0.16	8.5 x 10^6	24.3
KcsA monomer	9	18	18.3	0.71	2.1 x 10^6	6.1
KcsA monomer	8	11	17.9	0.71	0.9 x 10^6	8.4
KcsA monomer	7	14	17.1	0.74	2.3 x 10^6	9.6
KcsA monomer	6	13	17.1	0.74	0.5 x 10^6	2.4

subsection discusses the development of a method to purify CF expressed KcsA to enable clear visialisation of the protein on an SDS PAGE gel from the most economical amount of the CF system.

Two samples were prepared, one containing 1 μg of KcsA DNA (scaled to 150 μl volume) and one containing no DNA (scaled to 100 μl volume). The samples were incubated at 37 °C for 2 hours (as outlined in 3.1.4 before being terminated on ice. Purification was performed as detailed in Chapter 3, section 3.1.5 and SDS PAGE gels were run as discussed in section 3.1.6.

The destained gel is shown in Fig 5.2 a) where lane 1 contains 10 μl of the pre-stained protein standard, lanes 2-4 contain the bead washes, lanes 5-8 contain the bead elutions, lane 9 contains the material removed from the beads and lane 10 contains 57 μg of pre-purified KcsA used as a positive control, prepared as detailed in section 3.1.2 by Dr. Natalie Smithers. The regions of interest are highlighted by the arrows. The gel image reveals a large number of proteins washed off the beads in lanes 2-4 and the intensity of the bands appears to reduce from left to right as expected with successive washes. In lane 10 the KcsA monomer can be clearly seen as a distinct band at 18.5 kDa (band 9), the dimer appears at 35.3 kDa (band 7) and the tetramer is visible at 64.6 kDa (band 5). Looking across the gel from right to left, distinct bands in-line with the KcsA monomer can be clearly seen in lane 7 at 17.1 kDa (band 14), lane 8 at 17.9 kDa (band 11) and lane 9 at 18.3 kDa (band 18) with a fainter band observable in the same position in lane 6 at 17.1 kDa (lane 13). It is of note that the bands appear to be more intense than the background proteins and are not observable in the same position in the washes in lanes 2-4. The most pronounced band can be seen in lane 9, indicating that the KcsA was tightly bound to the Ni-NTA beads and not entirely removed by the elution buffer. The data is summarised in Table 5.4. By comparing lanes 6-9 with the closest equivalent in Fig 3.12, it is possible to get a rough estimation for the

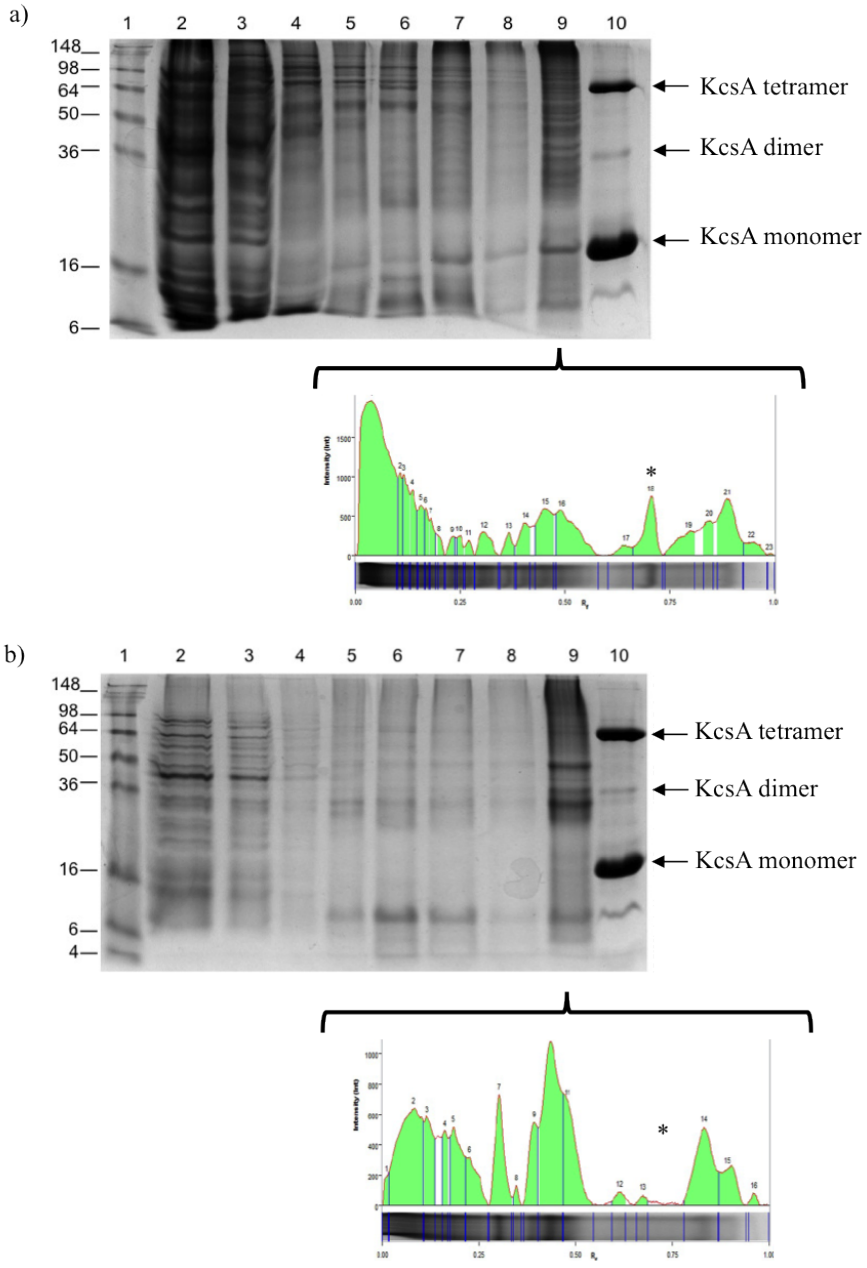

Figure 5.2: SDS PAGE of Ni-NTA purified CF expressed KcsA. The gel in part a) corresponds to the sample containing 1 μg of the KcsA DNA per reaction volume, where Lane 1 contains SeeBlue Plus 2, lanes 2-4 contain the bead washes, lanes 5-8 contain the bead elutions, lane 9 contains the material removed from the beads and lane 10 contains 57 μg of pre-purified KcsA. Part b) is a control with the same lane assignments as part a) except the CF mixture was not supplied with DNA. The positions of the KcsA monomer, dimer and tetramer are indicated in the figure by the arrows. The appearance of bands in lanes 7, 8 and 9 in line with the control at 18.5 kDa, that are not present in part b) where no DNA was added, indicates that KcsA was expressed.

amount of KcsA monomer detected on the gel in Fig 5.2 a). To achieve this, lanes were carefully selected containing a similar amount of background protein and a closely matching band volume for the KcsA monomer, where lanes 6-9 in Fig 5.2 a) most closely resemble bands 7, 8, 3 and 9 from Fig 3.12 b). This suggests that the amount of the KcsA monomer detected in lane 9 is ∼833 ng, in lane 8 is ∼83 ng, in lane 7 is ∼416 ng and in lane 6 is ∼83 ng.

The data in Fig 5.2 a) suggests that the KcsA has been successfully expressed, an outcome which is supported by part b) of the figure where no DNA was added and no bands were subsequently detected in the regions indicated by the arrows. It should however be noted that ∼1/3 less protein was loaded onto the gel as only two volumes of the CF system were used. It is also clear from the amount of residual protein on the gels in Fig 5.2 that the purification process requires further optimisation to allow for the protein of interest to be more clearly identified from the background noise.

The method was thus modified to include additional wash and elution steps at different imidazole concentrations and longer incubation times. To promote adhesion to the beads, the pH of the buffers used was not fixed. This was attempted with two CF reactions supplied with 1 μg of the KcsA DNA template per 50 μl reaction volume, run at a final volume of 200 μl and 50 μl. The reaction was incubated at 37°C for 2 hours, in Fig 5.2.

The gel image in Fig 5.3 a) shows the sample prepared to 4x volume, where the protein standard is loaded in lane 1, the first and last washes in lanes 2 and 3, followed by the elutions in lanes 4-9. The contents boiled off the beads was loaded in lane 10. It is clear from the gel image that far fewer proteins are detected in the elution lanes of the gel compared to Fig 5.2, which is positive considering that more of the CF system was used. Comparison of lanes 2 and 3, reveals a wide range of proteins at high concentrations in lane 2 compared to trace amounts detected in lane 3, indicating that the wash steps have been more successful at removing residual protein compared to the data in Fig 5.2 (equivalent lanes 2 and 4). This suggests that the modifications to the purification method successfully increased the amount of residual protein removed from the beads. The band with the greatest intensity in lane 10 was detected at 17.2 kDa (band 16), which is in line with what is shown in Fig 5.2 for the KcsA monomer. In terms of yield approximation, lane 10 in Fig 5.3 a) can be compared to lane 10 in Fig 3.12 b), suggesting that the total amount of the KcsA monomer detected is $\sim$ 1.6 μg, equating to ∼0.4 μg per 50 μl of the CF mixture since 4x volume was used.

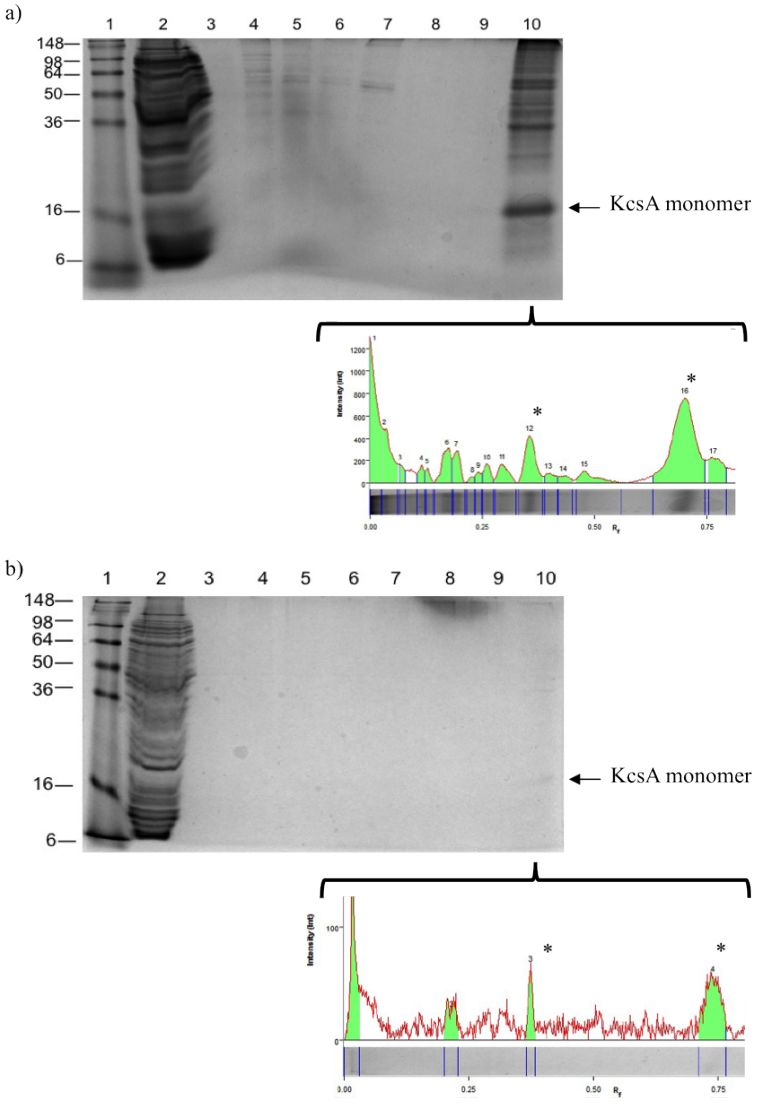

Figure 5.3: SDS PAGE of Ni-NTA purified CF expressed KcsA from different reaction volumes. The gel in part a) corresponds a sample prepared to 4x volume containing 1 μg of the KcsA DNA per reaction volume, where Lane 1 contains SeeBlue Plus 2, lanes 2-3 contain the first/final bead washes, lanes 4-9 contain the bead elutions and lane 10 contains the material boiled off the beads. Part b) has with the same lane assignments as part a) except the CF mixture was prepared to 1x volume. The position of the KcsA monomer is indicated in the figure by the arrow. The appearance a band at exactly 17.2 kDa in both gels is indicative of the presence of the KcsA monomer, while the visability of the bands indicates a optimum volume of 2x.

As the band relating to the KcsA monomer is distinguishable from the background proteins it is also possible to estimate the mass of the expressed monomer by comparing the band to the BSA standard discussed in section 3.1.6. This returned a value of $\sim$ 5 μg, equating to 1.25 μg per 50 μl of the CF mixture. Despite the

Table 5.2: Summary of the bands of interest extracted from Fig 5.3

ID	Lane	Band no.	Mol. Wt (kDa)	Relative front	Volume (int)	Band %
Data from Fig 5.3 part a)						
Lysozyme	1	7	16.0	0.73	1.3 x 10^6	15.0
KcsA monomer	10	16	17.2	0.70	4.4 x 10^6	33.6
Data from Fig 5.3 part b)						
Lysozyme	1	7	16.0	0.77	1.9 x 10^6	19.1
KcsA monomer	10	4	17.2	0.74	0.2 x 10^6	39.2

small discrepancy between the two estimations, it is clear that both values are significantly higher than the expected yield for the CF system (50 - 250 ng per 50 μl).

The results of the purification when 1x volume was used are shown in Fig 5.3 b), where the lane assignments are consistent with the previous gels in this subsection. Compared to the gel in part a), it is immediately clear that there is less protein on the gel under these conditions, which is expected considering that a smaller volume of the CF mixture was used. Notably a faint band at 17.2 kDa was detected in lane 10 (band 4), consistent with the position of the bands detected for the KcsA monomer, and is indicated by the (*) in the intensity plot supplied for lane 10 in Fig 5.3 b). Approximation of the yield of the expressed monomer was complicated in this instance as the intensity of the band was lower than the smallest sample detected in the BSA standard shown in 3.6, suggesting that the amount of protein present was between 50-100 ng. This range is deduced by the fact that 100 ng was the lowest detectable mass of protein in the standard run in Fig 3.6 where 50 ng was not detectable. This result falls inside the expected range for the yield of the CF system, but is not consistent with the approximation of the yield when 4x volume was used. This may be due to more significant losses of the CF expressed protein from the purification process, too much de-staining of the gel, or reduced yield as a result of contamination. The result may also indicate that the volume of the CF reaction also affects the final yield.

For high resolution imaging of the CF expressed KcsA, the reaction was repeated at 1x volume with 1 μg of the DNA template, alongside a control sample containing no DNA. The CF expressed protein was purified as described for Fig 5.3 b) and analysed with a Protein 230 chip using an Agilent Bioanalyzer. Using this method, all of the proteins are labelled on-chip using a proprietary fluorescent dye which, by comparision to the molecular weight standard, allows for quantification (Kuschel, 2000). To promote the release of the CF expressed KcsA, the pH of the final

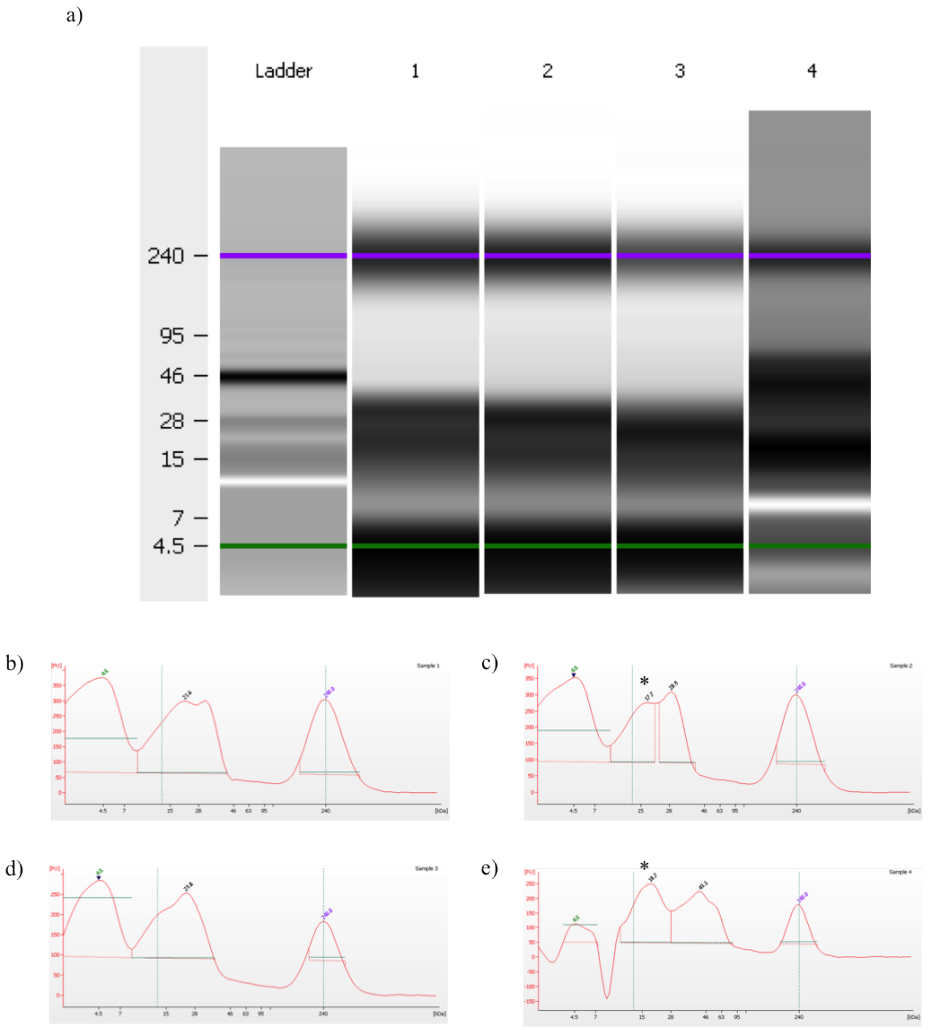

Figure 5.4: High-resolution imaging of CF expressed KcsA. 1x volume of the cell-free system was prepared with 1 μg of the KcsA DNA template, purified with slight modification to the optimised Ni-NTA method and analysed on a Protein 230 chip using the Agilent Bioanalyzer. a) An automatically taken high-resoloution gel image, showing the proprietary molecular weight ladder in the far left lane. The samples diluted 21.5x as directed by the manufacturer are in lanes 1 and 2 while lanes 3 and 4 contain the samples diluted 3x. DNA was added to the samples shown in lanes 2 and 4 , while lanes 1 and 3 contained no DNA. A substantial amount of protein is detected on the gel however individual bands are not resolved. The intensity of the staining in each lane is plotted in the electropherograms in parts b)-e) where a protein measuring 17.7 kDa is detected in part c), corresponfing to lane 3, while a protein measuring 18.7 kDa is detected in part e). These values are close to those observed previously for the monomer indicating that the KcsA has been successfully expressed. The yield approximation for the band in lane 2 equates to 3.15 μg per 50 μl of the CF system while the amount of KcsA in lane 4 is estimated at 1.32 μg per 50 μl of the CF system.

elution solution was buffered to pH 7.0. Samples were analysed as directed by the manufacturer, involving a 21.5x dilution, and with a lower 3x dilution in attempt to emphasise any proteins at low concentrations. The results in Fig 5.4 show the high-resolution gel image of the 4 lanes in part a) and the electropherograms of each lane in parts b)-e). The molecular weight standard is shown in the far left lane, where the intensity of the first and last band are used for internal calibration of the system. Lanes 1 and 2 contain the 21.5x diluted sample with lane 1 containing the control sample with no DNA. Lanes 3 and 4 contain the 3x diluted sample, where lane 3 contained no DNA. A considerable amount of staining is seen in each of the 4 lanes, the intensity of which is plotted in the electropherograms. Although clear bands are not visually distinguishable from the high-resolution gel image, the peaks are readily identifiable from the electropherograms, enabling two bands to be detected at 17.7 and 18.7 kD in lanes c) and e), which are not present in the lanes containing the control. These measurements are close to the values obtained for the KcsA monomer in Figs 5.2 and 5.3, indicating that the protein has been successfully expressed and detected.

One advantage of using the on-chip system is that it provides an estimation of the protein concentration, which is automatically approximated relative to the intensities of the first and last bands in the ladder. This returns a value of 63.1 ng/μl for the peak at 17.7 kDa in lane 2, equating to a total yield of 3.15 μg per 50 μl. The 18.7 kDa band in lane 4 is estimated at 188.9 ng/μl, which scales to 26.38 μg/μl accounting for the dilution and equates to 1.32 μg per 50 μl. A discrepancy between the two estimations is expected for different levels of dilution as indicated by the manufacturer. Noticeably, the on-chip approximations for protein yield are generally higher compared to previous estimations in this subsection. The exception is the 1.25 μg per 50 μl approximated for Fig 5.3 a), which is close to the value of 1.32 μg per 50 μl mentioned above for lane 4 of Fig 5.4. The overall higher approximations of the on-chip method could be a reflection of the direct method of staining, with no requirement for de-staining as with the Coomassie stained gels, however more repeats of the experiment would be necessary to support this inference and to validate the approximation supplied by the system. The ambiguity of the high-resolution gel image also indicates that the

Table 5.3: Summary of the bands of interest extracted from Fig 5.3

ID	Lane	Mol. Wt (kDa)	Relative concentration (ng/μl)	Band %
KcsA monomer	2	17.2	63.1	54.1
KcsA monomer	4	18.7	188.9	51.0

process requires further optimisation while in comparison, the conventional SDS PAGE gels shown previously allow for the purified protein to be clearly visualised provided the reaction is performed at a suitable volume.

In summary, the data in this subsection shows that the KcsA template engineered in section 3.1.1 was successfully expressed using a commercial CF expression system. The KcsA monomer was easily detected when the reaction was performed at 4x volume, but difficult when performed at 1x volume. This indicates that a compromise of 2x volume is sufficient and cost-effective for future experiments. By isolating CF expressed proteins from the CF mixture, this method also allows for the factors determining protein yield to be studied. This is addressed in the following subsections.

5.1.3 Dependence of KcsA expression yield on the amount of DNA template

Previous reports have shown that the final yield of the CF expression reaction is sensitive to the amount of DNA added to the system. This was shown with eGFP, where the amount of protein expressed was reported to increase by raising the amount of DNA supplied to the system from 0.03 μg/μl to 0.24 μg/μl (Roos et al., 2013). In contrast, when expressing the Firefly luciferase protein the amount of protein expressed was shown to rise and slowly fall between plasmid concentrations of 0.01 nM and 1 nM (Noireaux et al., 2005). These reports indicate that the amount of DNA supplied to the CF system has an influence on the protein yield and the purpose of this subection is to determine whether the same effect is observed with CF expressed KcsA.

The expression was performed at 37 °C for 2 hours using 2x volume with 0 μg, 3 μg and 6 μg of KcsA DNA per 50 μl of the CF system. The reactions were terminated on ice, purified as described in section 3.1.5 and run on SDS PAGE gels.

The gel image in Fig 5.5 a) shows the purified CF mixture where no DNA was added. Consistent with the previous gels, a large amount of residual protein is detected in lane 2 relating to the first wash, no proteins are detected in the elution lanes 4-9, while some residual protein was removed from the beads in lane 10. Here a small amount of protein ~36 kDa and above is observable, which is similar to the region where the KcsA dimer has been observed in Fig 5.2, however there are no detectable bands in the position for the KcsA monomer, at 19 kDa or below.

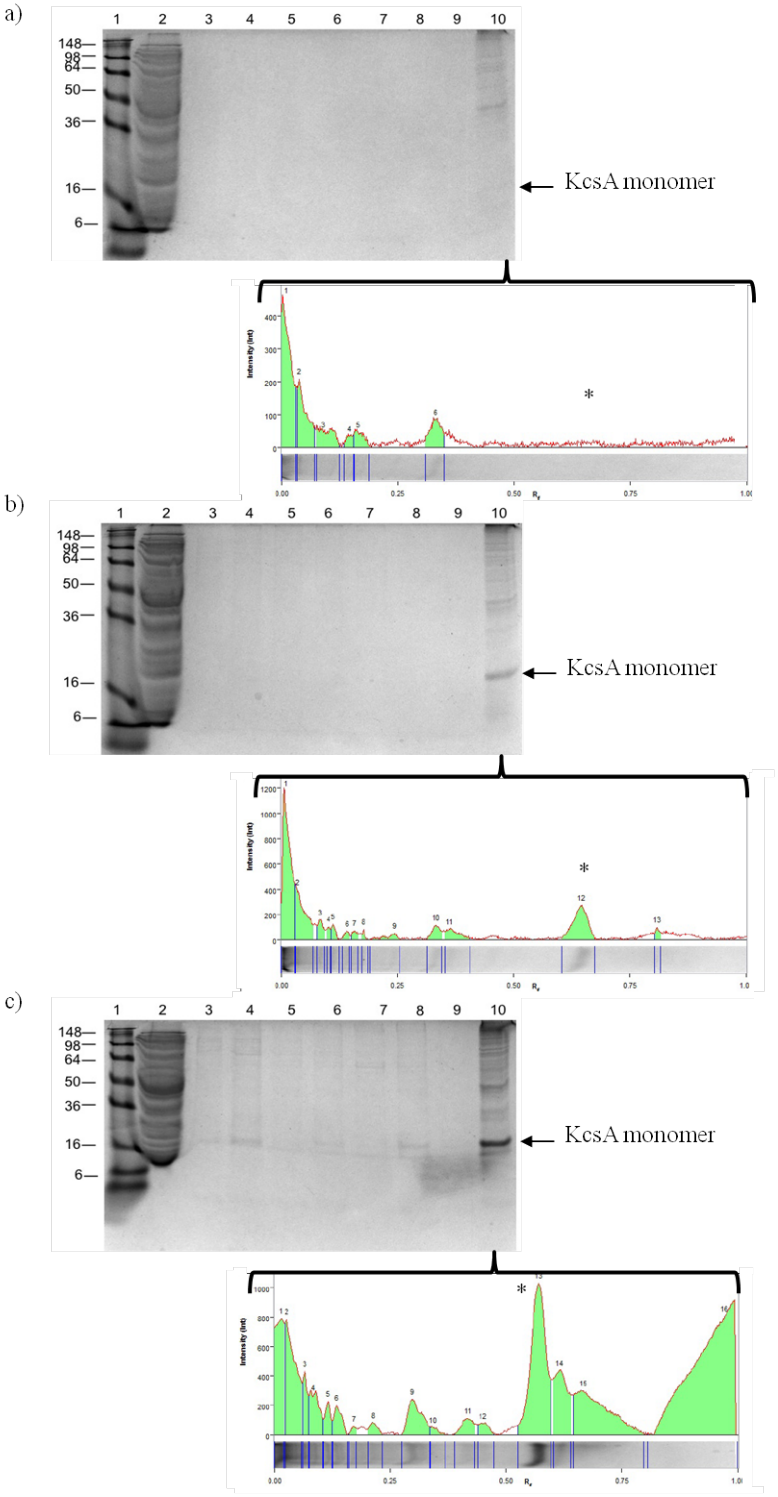

Figure 5.5: Dependence of the KcsA expression yield on the amount of DNA template. SDS PAGE of Ni-NTA purified CF expressed KcsA expressed in the presence of a) 0 μg, b) 3 μg and c) 6 μg of KcsA DNA. The appearance of an intensifying band at ~17 kDa is shown in parts b) and c) of the figure and indicated by the asterisk. The data suggests that more KcsA is expressed as the amount of DNA is increased to the system.

This is emphasised by the intensity plot of lane 10 shown in the figure, where the position expected for the KcsA monomer is indicated by the (*).

The SDS PAGE gel in Fig 5.5 b) shows the purified CF mixture when 3 μg of the DNA template was added to the system. The gel shows that several smaller proteins are detected in lane 10 compared to the control sample, as highlighted by the intensity profile. It is clear from both the gel and the intensity profile that the most distinct band in lane 10 is at ∼19.5 kDa (band 12), which is consistent with what has been observed for the KcsA monomer. The figure also shows a band at 39.5 kDa in lane 10 (band 11) which could be the KcsA dimer, however this is difficult to confirm as a protein of approximately the same size is also present in the control in part a).

ImageJ analysis of the gel suggested that the total amount of protein contained in lane 10 band 12 was ∼500 ng, corresponding to ∼250 ng per 50 μl of the CF system, a value which is in range of the upper limit specified by the manufacturer. This estimation is also supported by the observation that lane 4 of Fig 3.12 b), containing 0.416 ng of KcsA, has a comparable amount of residual protein on the gel and a similar band intensity to the band of interest in lane 10, band 12, of Fig 5.10. It is therefore reasonable to assume that the total amount of KcsA monomer on the gel is $\sim$ 0.5 μg. The result when 6 μg of the KcsA DNA template was supplied to the CF system is shown in Fig 5.5 c). It is clear from the figure that far more protein is detected in lanes 4-10 compared to parts a) and b). The most prominent band in lane 10 was band 13, marked on the intensity plot by an asterisk, where the band intensity is significantly higher compared to the equivalent band in Fig 5.5 b), indicating that more KcsA monomer has been expressed. This is also evident from the relatively large number of proteins detected in lanes 4-9, several of which appeared in line with band 13 in lane 10. Band 13 of lane 10, for example, is detected at the relative front position of 0.570 (17.0 kDa), compared to band 3 of lane 9 at position 0.576 (16.6 kDa), band 5 of lane 8 at 0.583 (16.2 kDa), band 5 of lane 6 at 0.573 (16.8 kDa), band 9 of lane 4 at 0.559 (17.8 kDa) and band 6 of lane 3 at 0.559 (17.8 kDa). The similarity of these positions together with the absence of any bands in the control sample in Fig 5.5 a) suggests that they are also the KcsA monomer.

ImageJ analysis of the bands suggests that the band at ∼17 kDa represents more than 5 μg of protein in lane 10, ∼0.85 μg in lane 8, ∼0.6 μg in lane 6 and ∼0.75 μg in lane 4, where the intensity of the band in lane 9 was difficult to measure due to the unexpected smear. These approximations suggest a total yield of more

Table 5.4: Summary of the bands of interest extracted from Fig 5.3

ID	Lane	Band no.	Mol. Wt (kDa)	Relative front	Volume (int)	Band %
Data from Fig 5.5 part b)						
Lysozyme	1	7	16.0	0.73	1.8 x 10^6	12.2
KcsA monomer	10	12	19.5	0.65	0.9 x 10^6	17.4
KcsA dimer	10	11	39.5	0.36	0.3 x 10^6	5.2
Data from Fig 5.5 part c)						
Lysozyme	1	7	16.0	0.59	2.3 x 10^6	12.9
KcsA monomer	10	13	17.0	0.57	3.0 x 10^6	16.2
KcsA monomer	9	3	16.6	0.58	0.6 x 10^6	2.7
KcsA monomer	8	5	16.2	0.58	0.2 x 10^6	1.6
KcsA monomer	6	5	16.8	0.57	0.1 x 10^6	1.4
KcsA monomer	4	9	17.8	0.56	0.4 x 10^6	10.5
KcsA monomer	3	6	17.8	0.56	0.1 x 10^6	2.0

than 7 μg, equating to $\sim$3.5 μg per 50 μl reaction, which is 14 x more than the expected yield specified by the manufacturer. Although this estimation appears high, the band intensity from the gel image also suggests that there is several μg of the monomer present in the lane.

In summary, the data confirms the expression of KcsA and indicates that the CF reaction exhibits DNA dependence, where more protein is expressed when more DNA is supplied to the system. This is interesting as controlling the amount of protein could be advantageous for obtaining single channel measurements.

5.1.4 Dependence of KcsA expression yield on the presence of lipid vesicles

As discussed in section 2.3.2, reports have shown that CF expressed membrane proteins are capable of co-translationally self-inserting into small unilamellar vesicles (Roos et al., 2013; Junge et al., 2008). This is interesting as it was also shown in section 4.6 that adding vesicles to the CF mixture assisted in the stabilisation of interdroplet bilayers. Yet it remains unclear what effect, if any, the presence of vesicles has on the CF expression of KcsA. The aim of this subsection is thus to identify the dependence of KcsA expression yield on the presence of lipid vesicles.

To determine this, three different concentrations (1, 10 and 100 μg/μl) of 200 nm POPC/POPG vesicles (1:1) by mass were added to the CF reaction, prepared (to 2x volume, with 1 μg of the KcsA DNA template. The reaction was incubated

at 37°C for 2 hours and terminated on ice. CF expressed His-tagged protein was purified as described in section 3.1.5 and run on an SDS PAGE gel as detailed in section 3.1.6.

Fig 5.6 a) shows the result when 1 μg of vesicles were added to the CF system. It seems apparent from the gel image in part a) that more KcsA was expressed compared to what has been previously obtained. This is indicated by the presence and intensity of the bands observed in the position expected for the monomer in lanes 4-9. Such bands were detected at 17.4 kDa (band 10), 16.6 kDa (band 10), 16.5 kDa (band 5), 16.8 kDa (band 10), 16.7 kDa (band 3) and 17.0 kDa (band 2), as summarised in Table 5.5. The bands all appear in line with the most prominent band in lane 10 (band 13), recorded at 18.0 kDa and indicated in the intensity plot for the lane provided in the figure by an asterisk.

ImageJ analysis suggests that the band in lane 10 represents more than 5 μg of protein with lane 9 containing $\sim$0.1 μg of protein, lane 8 containing $\sim$0.1 μg, lane 7 containing $\sim$0.7 μg of protein, lane 6 containing $\sim$0.65 μg, lane 5 containing $\sim$ 0.9 μg of protein and lane 4 containing 1.25 μg of protein. This totals to more than 8.7 μg of the KcsA monomer, which is the equivalent of $\sim$4.35 μg of protein per 50 μl of the CF mixture. While this figure is high, the intensity of band 13 in lane 10 is greater than observed in the previous gels, such that the amount of the KcsA monomer can only be estimated as greater than 1.66 μg. Lanes 4-7 however could be likened to lane 4 of Fig 3.12 b) which contained 416 ng of the KcsA monomer, while lanes 3, 8 and 9 appear closer to lane 3 of Fig 3.12 which contained 83 ng of the KcsA monomer. This suggests that approximately 1.9 μg of the KcsA monomer is present on the gel in lanes 3-9. While the approximation suggested by imageJ analysis seems high, it seems likely that the gel contains at least 5-6 μg of the KcsA monomer in total. This was unexpected since less DNA was used compared to the work in the previous subsection and yet it appears that more KcsA has been expressed, indicating that the supplied vesicles assisted in the expression as reported previously (Berrier et al., 2011) (Kalmbach et al., 2007).

Fig 5.6 b) shows the purification product when 10 μg of 200 nm POPC/POPG vesicles (1:1 by mass) were added to the CF reaction. There is a clear similarity between the gel image and that in part a), however from visual comparison it seems that slightly less of the protein of interest is detected in the elution lanes. The supplied intensity plot also infers this where the indicated peak at 18.5 kDa in lane 10 (band 14) is less intense than the corresponding band in part a).

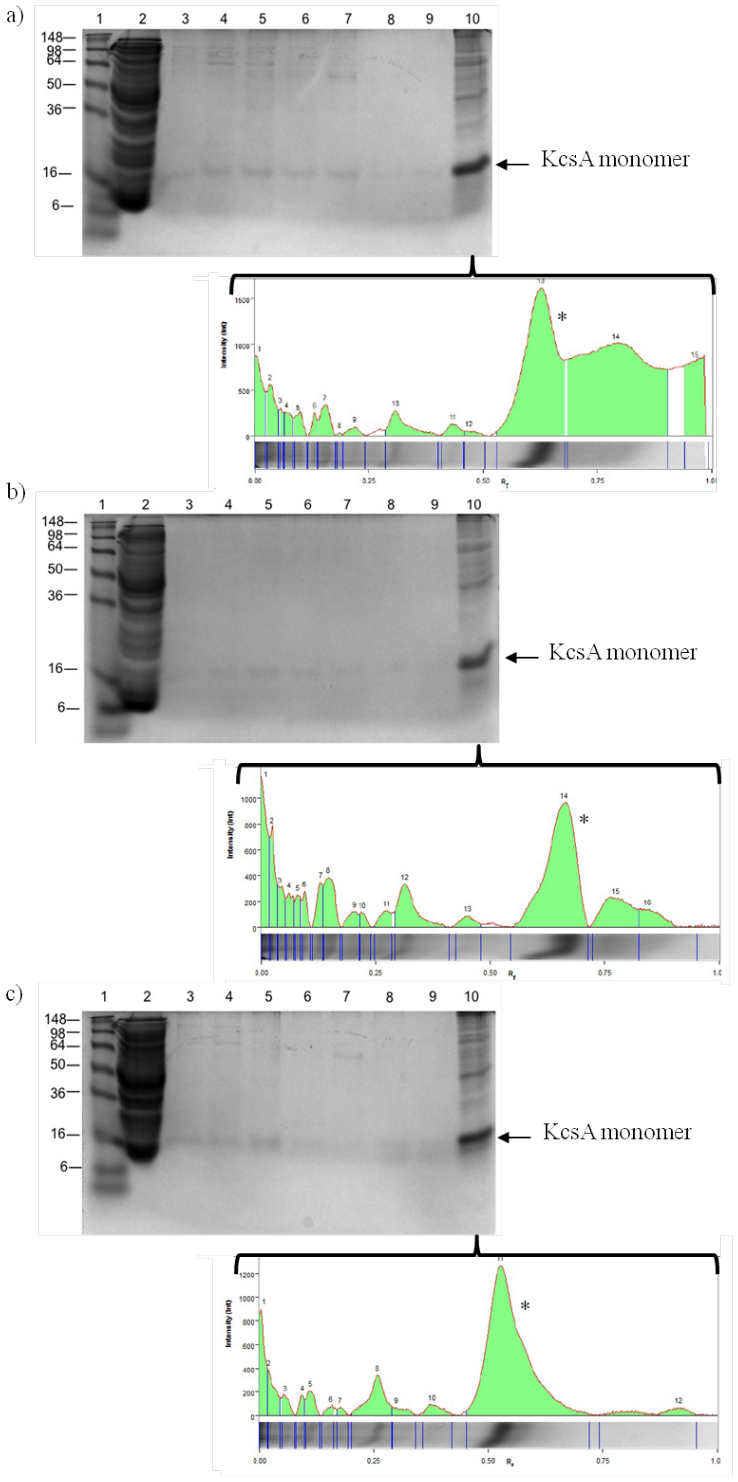

Figure 5.6: Dependence of KcsA expression yield on the presence of lipid vesicles. SDS PAGE of Ni-NTA purified CF expressed KcsA expressed in the presence of a) 1 mg/ml, b) 10 mg/ml and c) 100 mg/ml of 200 nm POPC/POPG vesicles. The appearance of intense bands at ∼17 kDa in lane 10 and several of the elution leanes in all three gels indicates that the presence of vesicles promotes the expression of KcsA, however the intensity plots in the figure indicate that the effect is not concentration dependent.

The prominent bands detected in lanes 4-9 on the gel were recorded at 16.6 kDa (band 10), 16.6 kDa (band 9), 16.7 kDa (band 9), 16.9 kDa (band 11), 17.1 kDa (band 10) and 17.8 kDa (band 5), values that are closely similar to those obtained for the KcsA monomer detected in the elution lanes in part a). The bands of interest detected on the gel are sumarised in Table 5.5.

Analysis of the gel using ImageJ indicated that there was more than 5 μg of protein at 18.5 kDa in lane 10, $\sim$0.1 μg in lane 7, $\sim$0.2 μg in lane 6, $\sim$0.4 μg in lane 5, $\sim$0.75 μg in lane 4 and $\sim$1 μg in lane 1. This suggests that the total amount of expressed protein is more than 7.45 μg, or more than 3.73 μg per 50 μl of the CF system. Lanes 3-9 can also be likened to lane 3 of Fig 3.12 b) which contained 83 ng of KcsA, while lane 10 seems to contain more protein than in lane 6 of the same figure, which had 1.66 μg of KcsA. It therefore seems plausible that the gel could contain $\sim$4 μg of the KcsA monomer. Despite some discrepancy between the two estimations, it seems clear that both methods return values which are slightly less than what was estimated for the previous figure when 1 μg of vesicles were added.

The result of the effect of adding 100 μg of vesicles to the CF expression reaction is shown from the SDS PAGE gel in Fig 5.6 c). The gel appears visually similar to the other gels in this subsection with the most distinct band in lane 10 inline with fainter bands in lanes 3-6 and lane 8. The most intense band in lane 10 (indicated on the intensity plot) was detected at 15.4 kDa, which is lower than the molecular weight obtained previously for the KcsA monomer. This was also the case for the bands detected in lanes 3-6 and lane 8, which measured at 14.7 kDa (band 5), 13.7 kDa (band 6), 13.3 kDa (band 4), 12.0 kDa (band 4) and 12.0 kDa (band 4) respectively. No low molecular weight bands were detected in lane 7 while the band in lane 9 appears further down the gel compared to the other bands summarised in Table 5.5. The consistency of the data indicates that the apparent reduction in the molecular weight measured for the KcsA monomer was due to an artefact in the running of the gel. This is supported by the observation that the molecular weight ladder has not run as far down the gel as seen in parts a) and b).

Estimations from the gel, shown in Fig 5.6 c), suggest there is >5 μg of protein in lane 10 of the figure, $\sim$0.7 μg of protein in lane 5, $\sim$0.8 μg in lane 4 and $\sim$1.5 μg in lane 3. This indicates that more than 8 μg in total, or $\sim$4 μg per 50 μl, of the protein of interest was expressed. Although this estimate seems high, most likely due to background staining, it is roughly in line with what was estimated for the other gels in this subsection. By comparing each lane to Fig 5.1, lanes 3-6

Table 5.5: Summary of the bands of interest extracted from Fig 5.6

ID	Lane	Band no.	Mol. Wt (kDa)	Relative front	Volume (int)	Band %
Data from Fig 5.6 part a)						
Lysozyme	1	7	16.0	0.67	1.4 x 10^6	17.1
KcsA monomer	10	13	18.0	0.63	10.0 x 10^6	30
KcsA monomer	9	2	17.0	0.65	0.2 x 10^6	2.9
KcsA monomer	8	3	16.7	0.66	0.1 x 10^6	1.7
KcsA monomer	7	10	16.8	0.67	0.1 x 10^6	5.9
KcsA monomer	6	5	16.5	0.66	1.7 x 10^6	11.2
KcsA monomer	5	10	16.6	0.66	2.3 x 10^6	13.6
KcsA monomer	4	10	17.4	0.64	0.5 x 10^6	4.8
KcsA monomer	3	7	16.7	0.66	0.3 x 10^6	2.9
Data from Fig 5.6 part b)						
Lysozyme	1	7	16.0	0.72	2.0 x 10^6	15.7
KcsA monomer	10	14	18.5	0.66	5.7 x 10^6	39.8
KcsA monomer	9	5	17.8	0.68	0.3 x 10^6	17.1
KcsA monomer	8	10	17.1	0.70	0.3 x 10^6	7.5
KcsA monomer	7	11	16.9	0.70	0.3 x 10^6	9.8
KcsA monomer	6	9	16.7	0.71	0.4 x 10^6	9.8
KcsA monomer	5	9	16.6	0.71	0.4 x 10^6	10.5
KcsA monomer	4	10	16.6	0.71	0.3 x 10^6	7.2
KcsA monomer	3	8	16.5	0.71	0.2 x 10^6	5.8
Data from Fig 5.6 part c)						
Lysozyme	1	7	16.0	0.52	2.1 x 10^6	22.4
KcsA monomer	10	11	15.4	0.53	9.0 x 10^6	66.3
KcsA monomer	8	3	12.0	0.56	1.1 x 10^6	23.2
KcsA monomer	6	4	12.0	0.56	0.6 x 10^6	41.0
KcsA monomer	5	4	13.3	0.55	1.5 x 10^6	48.6
KcsA monomer	4	6	13.7	0.54	1.8 x 10^6	69.5
KcsA monomer	3	5	14.4	0.54	0.5 x 10^6	64.8

and lane 8 look again to be between lanes 3 and 4, containing 83 ng and 416 ng of KcsA respectively, while lane 10 again appears incomparable, suggesting that more than 1.66 μg of the KcsA monomer was present as found in parts a) and b).

In summary, the data indicates that the CF expression of KcsA is enhanced in the presence of lipid vesicles, leading to an increase in the amount of protein expressed. While more experiments would be needed to draw a firm conclusion, the data does not indicate that this effect is dependent on the concentration of vesicles added.

5.2 Cell-free expression of full-length KvAP potassium channel

This subsection details the CF expression of the full-length KvAP channel, discussed in detail in section 2.4.2, and outlines the methods used to verify that the protein was expressed.

5.2.1 Western blotting of cell-free expressed His-tagged KvAP

The aim of this subsection is to demonstrate the CF expression of the full-length KvAP channel, using the same approach as shown in the previous section for KcsA.

The CF reaction was performed at 2x volume with 1 μg per volume of the KvAP DNA template discussed in section 3.1.1. The reaction was performed for 2 hours at 37 °C when using the L1130 system, and for 1 hour at 37°C under light agitation (1,200 RPM) using the L1110 system. His-tagged protein was purified as detailed in section 3.1.8 and run on an SDS page gel as detailed in section 3.1.6 and Western blotting was performed by Maïwenn Beaugrand, (University of Southampton) as described in section 3.1.7.

No protein of interest was detected when the KvAP was expressed using the L1130 system used previously for the expression of KcsA. This was most likely due to the fact that the pQE-60 vector encoding the KVAP gene contained a T5 promoter sequence while the expression system contained a T7 polymerase, binding specifically to T7 promoter sites. To account for this, the expression system was supplemented with endogenous RNA polymerase however this was also unsuccessful, possibly caused by an insufficient amount of polymerase supplied to the system as advised by the manufacturer.

Expression was subsequently attempted with the L1110 High Yield expression system, which despite being based on a T7 system, has been shown by the manufacturer to be compatible with a T5 promoter sequence. Fig 5.7 a) shows the destained gel containing protein purified from the CF expression reaction when 1 μg of DNA was added. The gel in part a) of the figure shows that a large amount of protein was washed off the beads in lane 2, while few proteins are detected

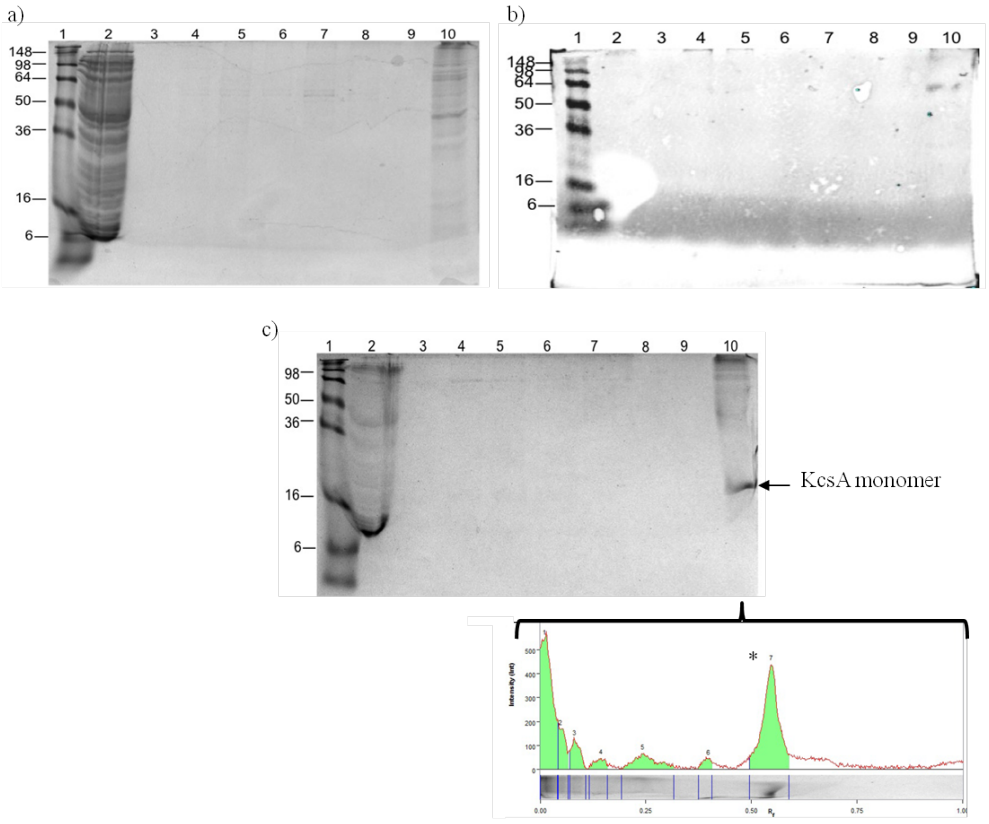

Figure 5.7: Western blotting of CF expressed KvAP. The CF reaction was performed for 1 hour at 37°C in duplicate under light agitation (1,200 RPM) using the L1110 system. His-tagged protein was purified in both cases and run on an SDS PAGE gel. One gel (a) was Coomassie stained while the other was used for Western Blotting. An image of the final blot is shown in part b). The figure shows that no KvAP was detected, however the CF system was shown to be capable of expressing the KcsA template in part c).

in the elution lanes 3-9. Proteins of high molecular weight are visible in lane 10 however nothing in the 28 kDa-38 kDa range expected for KvAP.

A Western Blot was performed with an unstained duplicate of the gel to help determine whether any KvAP was present. An image of the blot is shown in Fig 5.7 b), where the successful transfer of the molecular weight standard is visible in lane 1, however there is no indication of KvAP in any of the neighboring lanes, indicating that no protein was expressed.

It is unclear why the expression of KvAP was unsuccessful; one possibility is that there was a problem with the design of the DNA template or choice of vector, perhaps due to the position of the cloning site or due to the type of promoter sequence used. However it is also possible that there was a problem with the

Table 5.6: Summary of the bands of interest extracted from Fig 5.7

ID	Lane	Band no.	Mol. Wt (kDa)	Relative front	Volume (int)	Band %
Lysozyme	1	7	16.0	0.61	1.8 x 10^6	18.5
KcsA monomer	10	7	18.8	0.55	1.7 x 10^6	38.1

preparation of the DNA, possibly during purification. To confirm that the L1110 system was not responsible, the experiment was repeated with 2 μg of the KcsA DNA template used in the previous section. The data is shown in Fig 5.7 c) where it is clear that a pronounced band is present in lane 10 at ∼19 kDa as expected for the KcsA monomer. Analysis of the gel returned an approximate molecular weight of 18.8 kDa for the band which is detailed in Table 5.6.

In summary, the data shows that KvAP was not expressed with the L1110 system, indicating that the reaction conditions, the template design or the preparation of the DNA template require further optimisation for the KvAP to be expressed.

5.2.2 Dependence of KvAP expression yield on the amount of DNA template

In section 5.1.3 it was shown that increasing the amount of the KcsA DNA template supplied to the CF system mixture led to a higher yield protein being expressed. This subsection explores whether there is a similar trend between the amount of KvAP expressed and the amount of DNA supplied to the system.

The CF reaction was performed using 2x volume of the CF mixture and incubated with 6 μg of the DNA template per volume for 1 hour at 37 °C under light agitation (1,200 RPM). His-tagged protein was purified as described in section 3.1.8 and run on an SDS page gel as detailed in section 3.1.6

The data in Fig 5.8 shows the result of the experiment, where it is clear that there no distinct bands of high intensity in any of the elution lanes (3-10). This indicates that under these conditions, the expression of the KvAP template was not dependent on the amount of DNA supplied to the CF system.

5.2.3 Dependence of KvAP expression yield on the presence of lipid vesicles

This part of the study explores whether the CF expression of KvAP can be assisted by the addition of vesicles to the reaction mixture, as observed in section 5.1.4 for KcsA. Vesicles were prepared from DOPC/POPC lipids (1:1 by mass) to a stock concentration of 20 mg/ml and extruded to a final diameter of 200 nm. The CF reaction was performed in triplicate using the L1110 system at 2x volume with a total of 2 μg of the KvAP plasmid and either 400 μg, 40 μg or 4 μg of the vesicle suspension. The reaction was incubated for 1 hour at 37∘C under light agitation (1,200 RPM). His-tagged protein was purified as described in section 3.1.8 and run on an SDS page gel as detailed in section 3.1.6

The data in Fig 5.9 a) shows the results when 4 μg of PC/PG vesicles were added to the CF system. It is clear from the gel image that while a number of high molecular weight residual proteins are shown in lane 10, there appears to be no proteins in the region of interest on the gel. The result when 40 μg of PC/PG vesicles was added to the CF system is shown in Fig 5.9 b). Similar to in part a), the figure shows the proteins washed off the beads are seen in lane 2 and non-specifically bound proteins boiled off the beads are shown in lane 10. It is clear from the image that there are no intense bands in the elution lanes 4-10 and no proteins in the region of interest for KvAP. The same outcome was observed when the amount of vesicles supplied to the CF system was increased to 400 μg as shown in Fig 5.9 c).

In summary, the data in this subsection shows that the presence of vesicles did not assist with the CF expression of KvAP.

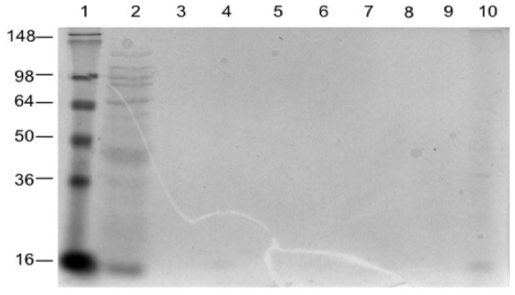

Figure 5.8: Dependence of KvAP expression yield on the amound of DNA template. The CF reaction was incubated with 6 μg of the DNA template per volume for 1 hour at 37 °C under light agitation (1,200 RPM). His-tagged protein was purified and run on an SDS PAGE gel. The image shows that no KvAP was detected in any of the lanes on the gel.

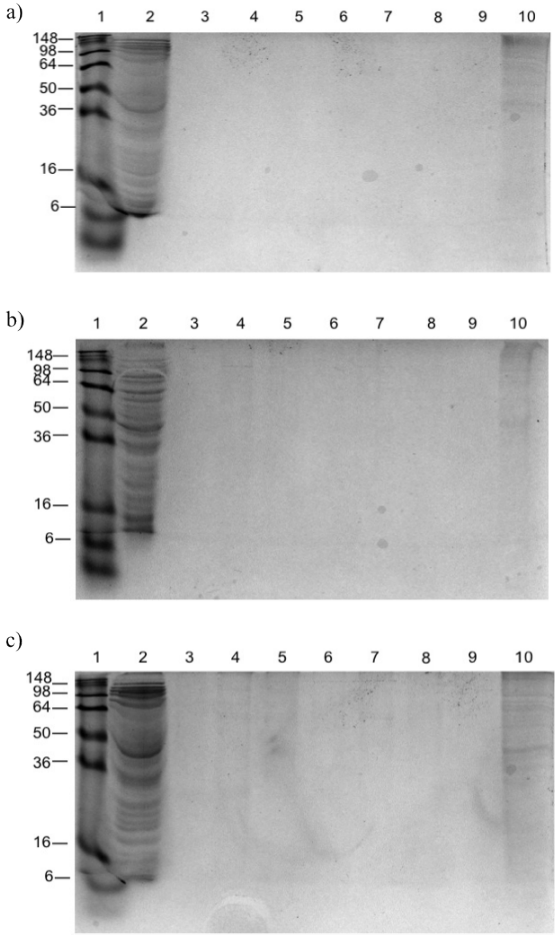

Figure 5.9: Dependence of KvAP expression yield on the presence of lipid vesicles. The CF reaction was performed using the L1110 system at 2x volume with a total of 2 μg of the KvAP plasmid and either a) 400 μg, b) 40 μg or c) 4 μg of the vesicle suspension. The gel images, supported by the intensity plots supplied with the figure, indicate that no KvAP was expressed.

5.3 Cell-free expression of a pore domain of the hERG potassium channel

This subsection describes the CF expression of the hERG$_{S5-S6}$ pore domain. The full-length channel is discussed in section 2.4.3.

5.3.1 Western blotting of CF expressed His-tagged hERG$_{S5-S6}$

This part of the study describes how the method developed to express and purify KcsA in section 5.1 was adopted to express and purify hERG$_{S5-S6}$.

The CF expression reaction was performed at 2x volume with a total of 2 μg of the DNA encoding the hERG$_{S5-S6}$ construct. The reaction was performed for 2 hours at 37 °C when using the L1130 system, and under agitation (1,200 RPM) for 1 hour at 37 °C using the L1110 system. His-tagged protein was purified as detailed in subsection 3.1.8 and run on an SDS page gel as detailed in section 3.1.6 and Western blotting was performed by Maïwenn Beaugrand, (University of Southampton) as described in section 3.1.7.

The expected molecular weight of the hERG$_{S5-S6}$ construct, can be calculated from the pore domain sequence to be ∼18 kDa. No proteins in this region were detected when the DNA encoding the hERG$_{S5-S6}$ pore domain was added to the L1130 system, most likely due to the plasmid containing a trc promoter sequence instead of a T7. However a clear band at ∼ 16 kDa was observed when the process was repeated using the L1110 system, as shown in Fig 5.10 a).

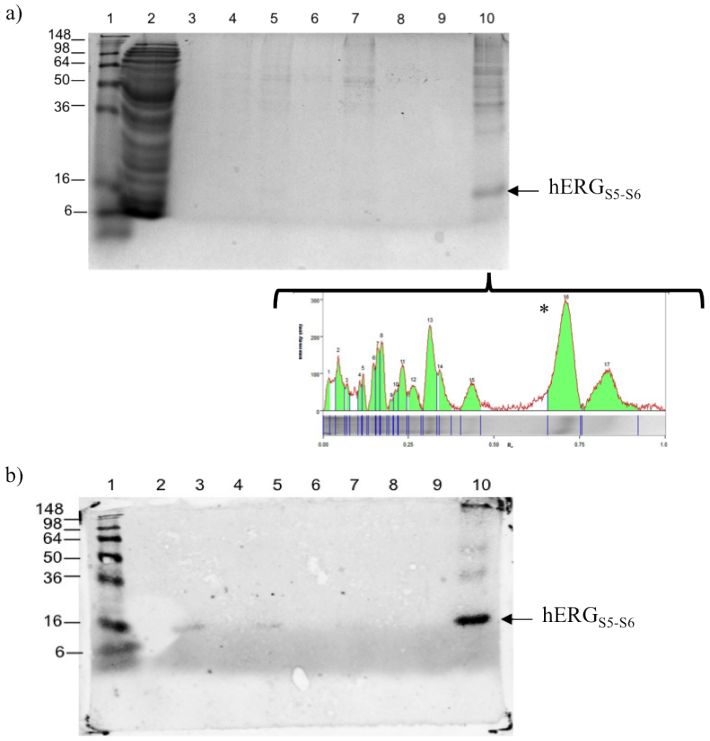

Figure 5.10: Western blotting of CF expressed hERG$_{S5-S6}$. 2 μg of the hERG$_{S5-S6}$ DNA template was incubated with 2 volumes of the CF expression mixture for 1 hour at 37 °C under light agitation. The protein was performed in duplicate, purified and run on SDS PAGE gels. One gel was Coomassie stained a), and the other used for Western blotting b). A band indicated by the arrow at ∼16 kDa in lane 10 of the stained gel in part a) indicates the presence of the hERG$_{S5-S6}$, as confirmed by the presence of a band in the same position in the Western blot in part b).

Table 5.7: Summary of the bands of interest extracted from Fig 5.10 a)

ID	Lane	Band no.	Mol. Wt (kDa)	Relative front	Volume (int)	Band %
Lysozyme	1	7	16.0	0.67	1.0 x 10^6	11.9
$hERG_{S5-S6}$	10	16	12.1	0.71	1.3 x 10^6	30.9

The gel shows a large amount of protein washed off the beads in lane 2 and low concentrations of high molecular weight proteins in lanes 4-7. A distinct band in the expected region for the hERG contruct is present in lane 10 at ∼16 kDa, and is indicated on the supplied intensity profile with an asterisk. Analysis of the gel image, summarised in Table 5.7, indicated that the molecular weight of the highlighted band (band 16) has a molecular weight of 12.1 kDa. To help verify the presence of the $hERG_{S5-S6}$ construct, a Western blot was performed with an unstained duplicate of the SDS PAGE gel shown in part a). An image of the probed blotting paper, captured with an infrared scanner, is shown in Fig 5.10 b). The image shows an intense band in lane 10 at approximately the same ∼16 kDa position observed on the SDS PAGE gel in part a) of the figure and two less intense bands at the same location in lanes 3 and 5. The signal observed is highly indicative of the $hERG_{S5-S6}$, as the primary antibody used in the assay was specific for the affinity tag introduced to the construct. The result is also supported by the absence of a band in the same position in the Western blot attempted for KvAP as shown in part b) of Fig 5.7.

In summary, this subsection shows that the $hERG_{S5-S6}$ pore domain was successfully expressed in a cell-free system.

5.3.2 Dependence of $hERG_{S5-S6}$ expression yield on the amount of DNA template

In this part of the study the CF expression of the $hERG_{S5-S6}$ pore domain was investigated in the presence of different amounts of DNA. This was shown to be important in the previous section for the CF expression of KcsA, where more protein was expressed in the presence of more of the DNA template.

The CF expression reaction was performed at 2x volume with a total of 0, 6 and 12 μg of the DNA encoding the $hERG_{S5-S6}$ construct. The reaction was under light agitation (1,200 RPM) for 1 hour at 37°C using the L1110 system. His-tagged

protein was purified as detailed in section 3.1.8 and run on an SDS page gel as detailed in section 3.1.6

The data in Fig 5.11 a) shows the outcome when no DNA was added to the L1110 system. The gel image shows the proteins washed off the beads in lane 2, however no other proteins are visibly detectable on the gel until lane 10, containing the non-specifically bound proteins boiled off the beads. The presence of several high molecular weight proteins in this lane is consistent with previous observations when attempting to express KvAP in section 5.2. While the absence a band at ∼16 kDa is also in line with the conclusions drawn from Figs 6.8 and 6.9, that a band in this position relates to the $hERG_{S5-S6}$ pore domain.

Fig 5.11 b) shows the result when the DNA supplied to the system was increased to 6 μg. The gel image shows a band at ∼16 kDa in lane 10 as indicated by the intensity plot in the figure, but there are no proteins visibly detectable in lanes 3-9. Analysis of the data indicates that the band in lane 10 corresponds to a protein 16.9 kDa in size, as highlighted in Table 5.8. The values may appear slightly higher than observed previously due to the curvature of the bands.

The data in Fig 5.11 c) shows the result when the amount of the $hERG_{S5-S6}$ DNA template was increased to 6 μg per volume of the reaction mixture. The amount of protein washed off the beads in lane 2 is comparable to previous gels however it is interesting to note that there are few detectable proteins in lane 10. This is different from previous observations, where bands at high molecular weight were commonly detected. While the number of proteins observed in lane 10 is small, a faint band at ∼16 kDa is still distinguishable as clarified by the intensity plot. Analysis of the gel image suggests that the molecular weight of the band of interest in lane 10 was 13.3 kDa, which is close to the value of 12.1 kDa obtained for the $hERG_{S5-S6}$ pore domain in Fig 5.11 b). The data is summarised in Table 5.8.

Table 5.8: Summary of the bands of interest extracted from Fig 5.11 a)

Data from Fig 5.11 part b)						
ID	Lane	Band no.	Mol. Wt (kDa)	Relative front	Volume (int)	Band %
Lysozyme	1	7	16.0	0.55	2.9 x 10^6	13.6
$hERG_{S5-S6}$	10	9	16.9	0.53	0.5 x 10^6	14.7
Data from Fig 5.11 part c)						
Lysozyme	1	7	16.0	0.48	0.9 x 10^6	9.4
$hERG_{S5-S6}$	10	5	13.3	0.52	0.2 x 10^6	8.8

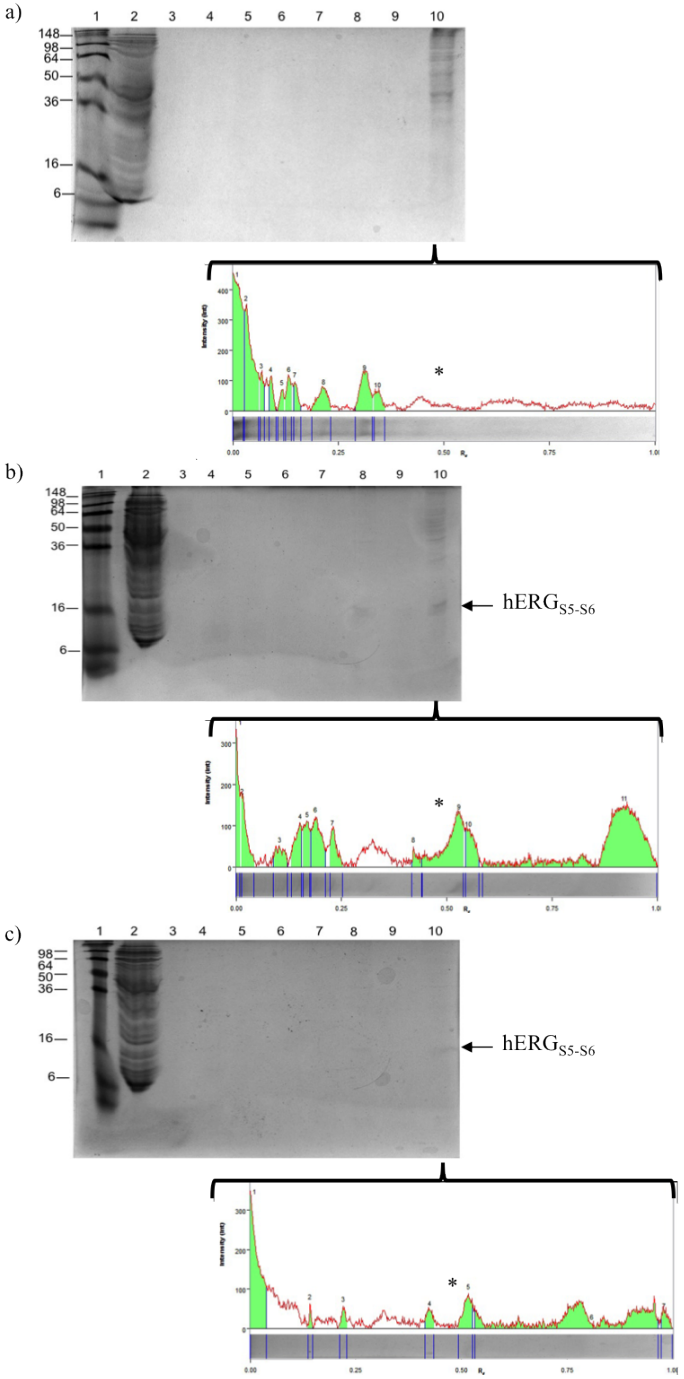

Figure 5.11: Dependence of hERG$_{S5-S6}$ expression yield on the amount of DNA template. SDS PAGE of Ni-NTA purified CF expressed hERG$_{S5-S6}$ expressed in the presence of a) 0 μg, b) 3 μg and c) 6 μg of KcsA DNA per volume of the CF system. The appearance of a band at ~16 kDa in lane 10, which is not present in part a), is shown in parts b) and c) of the figure and indicated by the asterisk on the intensity plots provided. The data indicates that the yield of CF expressed hERG$_{S5-S6}$ is inhibited by an increase in the supply of the DNA template.

In summary, the data shows that $hERG_{S5-S6}$ was expressed but indicates that more of the $hERG_{S5-S6}$ pore domain was expressed when 1 μg of the DNA template was added to the CF system compared to when 3 μg and 6 μg of the DNA template was supplied.

5.4 Summary

As protein expression was difficult to verify directly from the CF mixture by gel electrophoresis (3.1.11 & 3.1.13), a His affinity tag was introduced to the DNA template (3.1.1) to facilitate affinity purification and Western blotting of CF expressed ion channels.

It was found that Western blotting attempted directly from the CF mixture led to problems with the specificity of the antibodies in section 5.1.1, possibly due to the large number of proteins loaded onto the gel. The CF expression of KcsA was subsequently demonstrated after purification from the CF mixture, enabling CF expressed KcsA to be visualised on an SDS PAGE gel next to a control (section 5.1.2). Further to optimisation, the amount of KcsA expressed with 1 μg of DNA supplied to the system was approximated to be 400 ng per 50 μl reaction volume, which is significantly higher yield than the 50-250 ng range specified by the manufacturer (Promega, 2009). This method was also used to show the dependency of the CF yield of KcsA on the presence of DNA or lipids in sections 5.1.3 and 5.1.4. Here, an increase in the amount of DNA supplied to the system to 6 μg was approximated to yield 3.5 μg per 50 μl volume of the CF mixture, while 1 μg of the DNA template supplied in the presence of vesicles yielded approximately 3.7 μg of KcsA, independent of the concentrations added. The latter is in agreement with previous reports in the literature, discussed in section 2.3.1.

The methods developed for expressing KcsA were also attempted with the full-length KvAP channel in section 5.2 but expression of this template was not confirmed, possibly due to the large size of the protein, the lack of optimum expression conditions or as a result of error in the preparation of the DNA template. The method was however shown to work on the $hERG_{S5-S6}$ pore domain, the expression of which was confirmed on an SDS PAGE gel and by Western blotting after purification from the CF mixture in section 5.3.1. Expression of the $hERG_{S5-S6}$ template was not enhanced by increasing the supply of the DNA template, while the effect of adding vesicles remains to be determined.

Verifying the CF expression of KcsA and hERG$_{S5-S6}$ and identifying some of the factors which affect protein yield is an important step towards achieving single channel measurements, which is the focus of the following chapter.

Chapter 6

Electrophysiology of cell-free expressed ion channels

As discussed in Chapter 1, the overall aim of this work was to determine whether the CF expression and electrical characterisation of ion channels could be coupled in microdroplets.

With this motivation, the stability of interdroplet bilayers formed in the presence of different commercial CF mixtures was studied in Chapter 4, where it was found that diluting the system and adding vesicles stabilised the interdroplet bilayer to allow for single-channel measurements to take place. The capability of the CF system to express ion channels was then verified in Chapter 5 through the expression of the KcsA channel (section 5.1) and the hERG pore domain (section 5.3). Interestingly it was shown that increasing the amount of DNA (section 5.1.3) to the mixture, or adding vesicles (section 5.1.4), led to an enhanced yield of KcsA expressed, however the same effect was not observed for the hERG pore domain and attempts to express KvAP were unsuccessful as outlined in section 5.2.

With the bilayer stability addressed and the expression of ion channels confirmed, this part of the thesis concentrates on demonstrating that CF expressed ion channels can spontaneously insert into interdroplet bilayers for electrophysiological characterisation. This phenomenon, discussed in section 2.3.2, should enable single-channels to be measured directly from the CF system without protein purification or reconstitution. The effect is discussed in the first part of the chapter with CF expressed KcsA and in the second half of the chapter with CF expressed hERG_{S5-S6}. The demonstration of single-channel activity in each case shows that both channels are capable of self-inserting into the bilayer directly from the CF

mixture, which has only been previously achieved with the small viral channel Kcv (Syeda et al., 2008) as discussed in section 2.3.3.

6.1 Electrophysiology of CF expressed KcsA in interdroplet bilayers

As discussed in section 2.4.1, KcsA is a pH gated channel that activates when the intracellular pH falls to 4.0 or below. As an initial control it was therefore first determined whether any channel activity could be detected when one droplet contained the CF system incubated with 1 μg of the un-tagged KcsA DNA template (section 3.1.1) and when the second droplet (representing the intracellular side of the cell), contained buffer at pH 7.0.

The CF reaction was incubated at 37 °C for 2 hours before a 2 μl droplet was taken from the completed reaction mixture and used to form an interdroplet bilayer using manual manipulation as described in section 3.2.5.4. Current measurements were performed as described in section 3.2.1.

Three repeats of the experiment are shown in Fig 6.1 a) to c) where the data shows that the baseline remains stable, with no channel activity detected, for the duration of each 30 minute recording. The stability of the bilayer is evident from the zooms of the highlighted regions in the figure, while the capacitance measurements confirm that the bilayer remained in contact at the end of the 30 minute recording. The capacitance measured for a) was 100 pF which, assuming a specific capacitance of 0.5 μF/cm^2, roughly equates to a bilayer diameter of 160 μm. For part b) the capacitance measured was 90 pF, corresponding to an approximate bilayer diameter of 151 μm, while for part c) the capacitance was 80 pF, which gives an approximate bilayer diameter of 143 μm.

In the absence of single-channel activity under these conditions the experiment was performed without DNA supplied to the CF system and with the second droplet containing 150 mM KCl at pH 4.0. Three repeats of the experiment are shown in Fig 6.2 where, consistent with the findings in Chapter 4, the bilayer is shown to fail in <15 min in each case. The recordings show that no single channel activity was observed before the bilayer failed.

Single-channel activity was observed when the experiment was repeated with 1 μg of DNA. Recordings under different holding potentials are shown in Fig 6.3, where

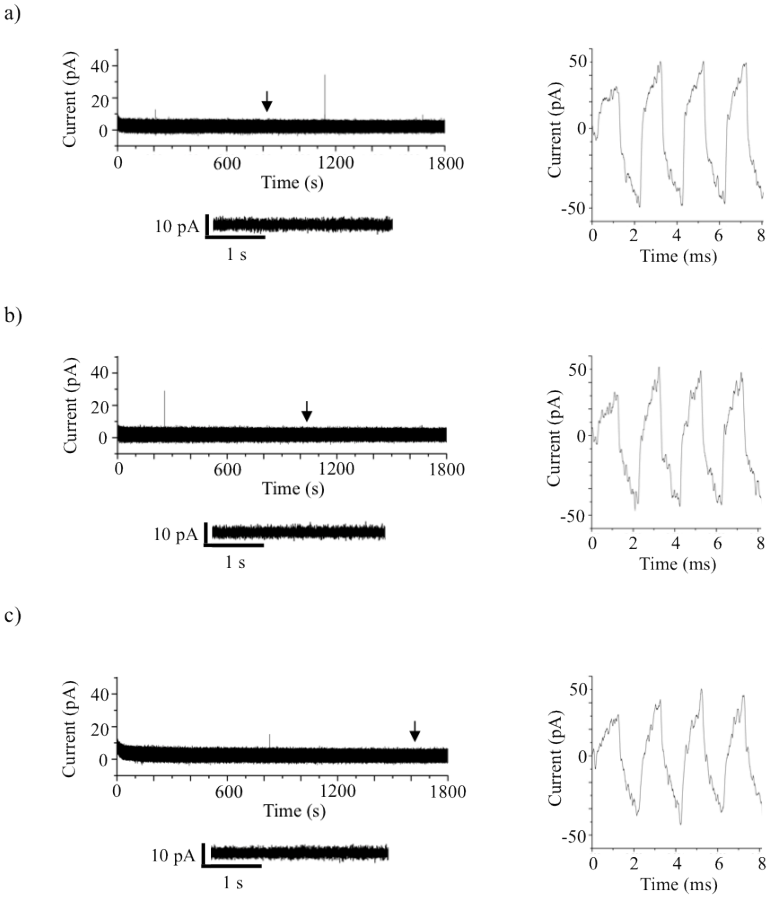

Figure 6.1: Electrophysiology of CF expressed KcsA at pH 7.0. Interdroplet bilayers were formed from one 2 μl droplet of the cell-free system incubated with 1 μg of the DNA template for 2 hours at 37 °C and a second 2 μl droplet containing 150 mM KCl at pH 7.0. Three repeats of the experiment at 100 mV are shown in parts a)-c). The traces show that the bilayer was stable for the duration of each experiment and no channel activity was observed, as indicated by the zoomed region of each sample. The capacitance measurementsshow that the bilayer remained intact at the end of the 30 minute recordings. The figure shows that no single channel activity was observed when the second droplet contained buffer at pH 7.0

a 30 s segment of each recording is shown in part i), a histogram of the data is shown in part ii) and two zooms are provided in the remaining two parts of the figure. The recording shown in a) part i), where a holding potential of 125 mV was applied, shows that the baseline is stable before a brief burst of current fluctuations appear in the baseline. It is notable that the intensity of these events appears to be equal at ∼15 pA as shown by the histogram in part ii). A zoom of the region is shown in part iii) and reveals a non-periodic flickering in the baseline. Analysis of the burst reveals that the average amplitude of the events was 16 ±2.1 pA, the

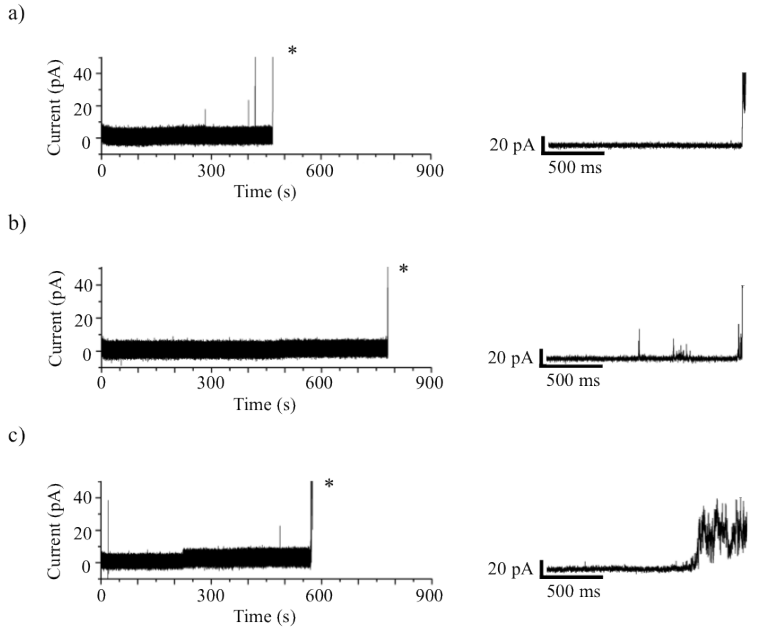

Figure 6.2: Electrophysiology of interdroplet bilayers formed with a 2 μl droplet of the cell-free expression mixture incubated for 2 hours at 37 °C with no DNA and a 2 μl droplet of 150 mM KCl at pH 4.0. Three repeats of the experiment are shown in parts a)-c) of the figure. In part a) the baseline appears stable with a few low intensity spikes before the bilayer fails at ∼8 minutes, indicated by the saturation of the current (*). The bilayer also fails after ∼12 minutes In part b) and after ∼ 9 minutes in part c). The zooms reveal the final stages leading to bilayer failure. The figure shows that no channel activity was observed when no DNA was added to the CF system

dwell time was 1.49 ms and the P_o was 0.54. The second zoom shows another burst from a separate region of the trace, where the openings and closings appear to occur less rapidly. The average amplitude of the openings was 15.3 ±1.7 pA the dwell time was 1.09 ms and the P_o was 0.42. Both values for P_o match closely with the flicker mode described for KcsA gating by Chakrapani et al. (2007), while the average opening amplitude is close to the value reported for KcsA at 125 mV by LeMasurier et al. (2001).

Recordings obtained when the holding potential was held at 100 mV are shown in part b) of the figure. The activity of the bilayer is indicated from the short spikes in the baseline in part i) which appear at approximately the same intensity, at ∼12.5 pA according to the histogram in b) part ii). A zoom of the activity is shown in i) where the activity in the bilayer appears as infrequent openings and closings in the baseline. The average amplitude of the openings was 13 ±1.8 pA, the dwell time was 3.06 ms and the P_o was 0.11. The zoom in part iv) shows a another burst

of activity from an independent experiment using the same conditions. In this example the activity appears as an opening in the baseline which rapidly closes.

The average amplitude of the openings in this case was 13 ±1.6 pA, the dwell time was 1.91 ms and the P_o was 0.68. A P_o of 0.11 is consistent with the low P_o mode as described by Chakrapani, while value of 0.68 is also in line with the high P_o mode described by the same author (Chakrapani et al., 2007). The average amplitude of the openings is also close to published values (LeMasurier et al., 2001). The low P_o mode was also observed when the holding potential was adjusted to 75 mV.

The activity shown in Fig 6.3 c) part i) appears similar to that shown in the previous figure, where the openings appear as brief, non-periodic spikes in the baseline. The histogram in part ii) shows that the amplitude of the openings was ∼10 pA. This is supported from analysis of the insert shown in c) part iii), where the average amplitude was shown to be 9.7 ±1.0 pA, the dwell time was 2.24 ms and the P_o was 0.22. A second burst of activity shown in c) part iv) of the figure reveals an average opening amplitude of 9.5 ±1.2 pA, a dwell time of 1.97 ms and a P_o of 0.14.

Fewer openings in the baseline were observed when the holding potential was reduced to 50 mV as shown in d). The activity in the baseline shown in part i) appears similar to the previous figures however both the frequency and the intensity of the events appears to be comparatively less, as indicated by the histogram in part ii) which suggests an opening amplitude of ∼6 pA. A magnified region of the trace is shown in part iii), which shows the activity as slightly longer but less frequent openings in the baseline.

Single-channel analysis of the burst reveals an average opening amplitude of 6.5 ±0.91 pA, a dwell time of 0.59 ms and a P_o of 0.15. The second zoom in d) part iv), obtained from a separate region of the recording shows similar gating to the zoom in part iii). The average amplitude of the channel openings was 6.7 ±1.1 pA, the dwell time was 0.81 ms and the P_o was 0.16.

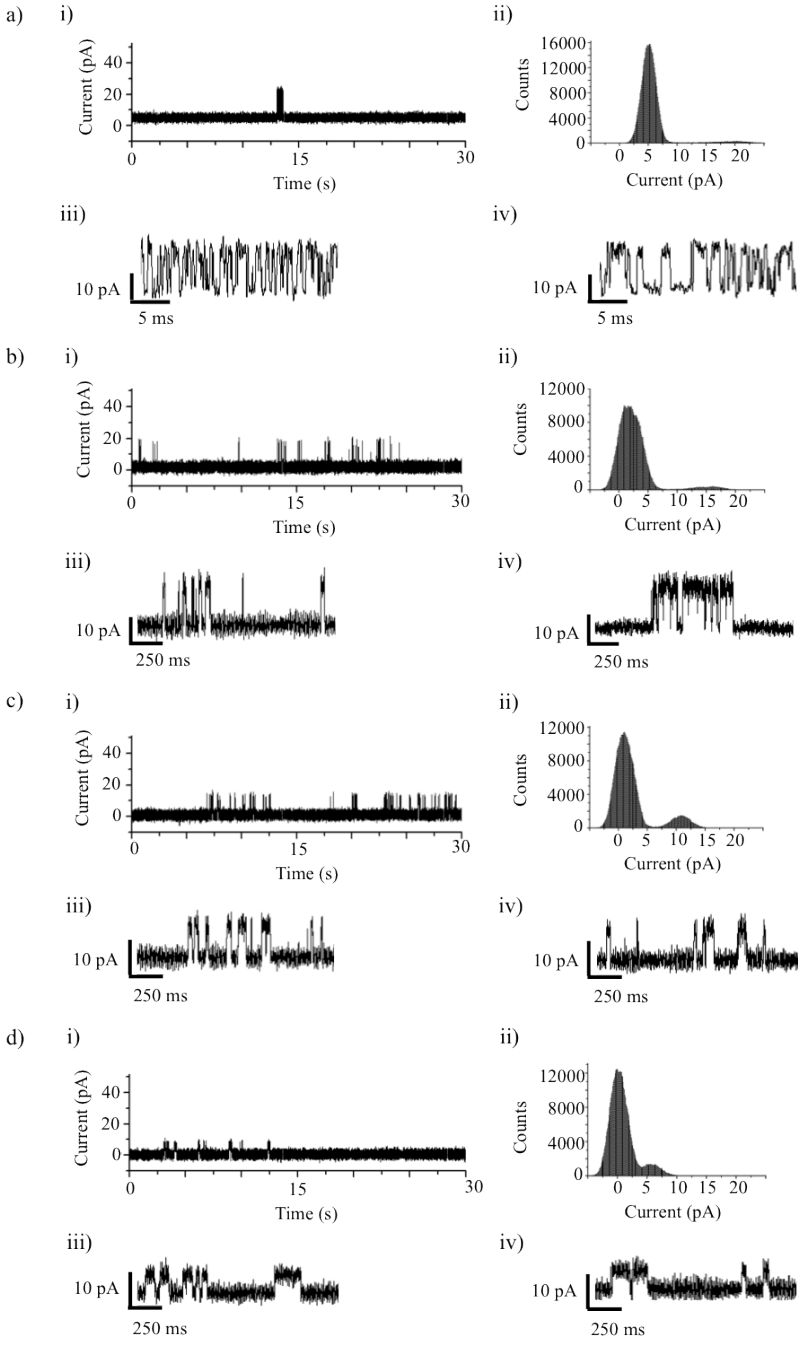

Figure 6.3: Electrophysiology of CF expressed KcsA in interdroplet bilayers at positive potentials. Interdroplet bilayers were formed with one droplet containing the CF expression system incubated with 1 μg of DNA at 37 °C and a second droplet containing 150 mM KCl at pH 4.0. Recordings were obtained at a) 125 mV, b) 100 mV, c) 75 mV and d) 50 mV. A 30 s sample of each condition is shown in part i) of the figure, revealing discrete activity in the baseline. The histogram in part ii) indicates the intensity of the openings. A zoomed region of the trace in part i) is shown in part iii) while another region of the recording, or an excerpt from an independent measurement is shown in part iv). The figure shows gating behavior as previously described for KcsA.

Data obtained under negative potentials are shown in Fig 6.4, where three recordings obtained at -100 mV are shown in a). The traces show that the bilayer fails in $\leq$ 3 minutes in each case, resulting in the droplets merging as indicated by the saturation of the current. In part i) the baseline is seen to briefly fall to ∼-20 pA before returning to ∼0 and suddenly fusing after 40 seconds.

The insert reveals that a small amount of low intensity noise is detected in the baseline before the current saturates. In a) part ii) the baseline is slightly offset at ∼5 pA and gradually returns to ∼0 pA. With the exception of two low-intensity

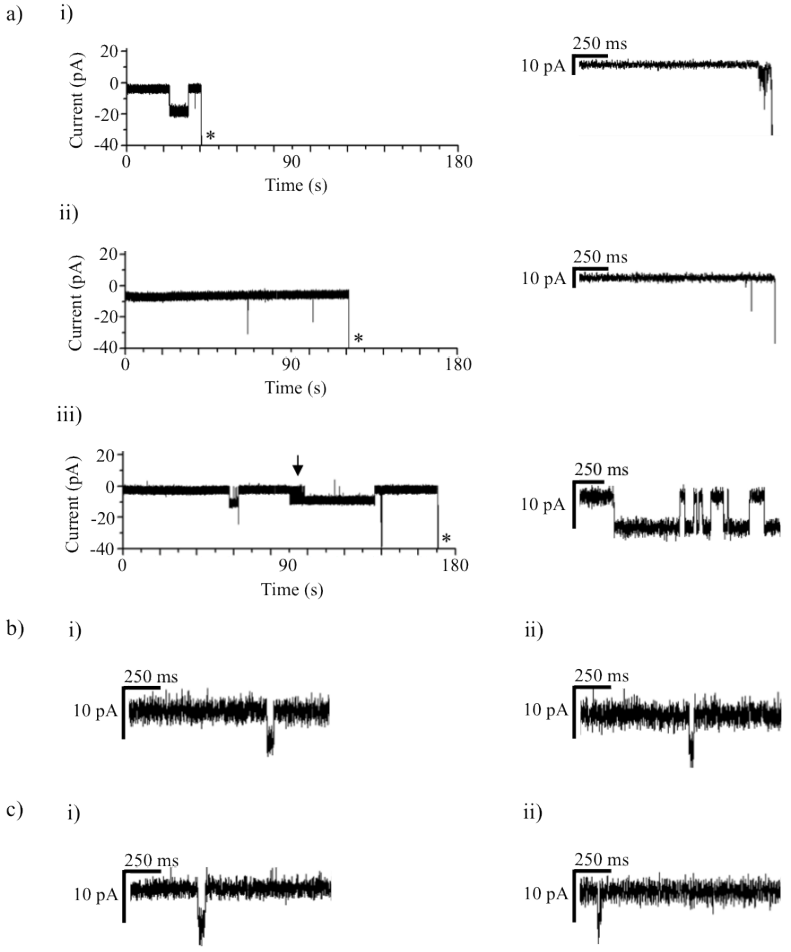

Figure 6.4: Electrophysiology of CF expressed KcsA in interdroplet bilayers at negative potentials. Interdroplet bilayers were formed with one droplet containing the CF expression system incubated with 1 μg of DNA at 37 °C for 2 hours and a second droplet containing 150 mM KCl at pH 4.0. Recordings were obtained at a) -100 mV, b) -50 mV and c) -25 mV. a) Shows that the bilayer fails in $\leq$ 3 minutes at -100 mV but that it is possible to obtain single-channel activity in this timeframe. Parts b) and c) show two examples of individual events at -50 mV and -25 mV respectively. The figure shows that the channel shows weak outward rectification by comparison to the data obtained at positive potentials.

spikes, the baseline appears stable for the duration of the recording before the bilayer suddenly fails after 120 s. The zoom shows one low intensity spike in the recording before the current rapidly saturates. The recording in a) part iii) shows two bursts of discrete activity in the baseline before the bilayer rapidly fails after 170 s. The magnified segment of the trace shows a stable opening in the baseline followed by fast gating events. Analysis of the openings revealed an average amplitude of 7.1 ±0.7 pA which is in line with what has been reported previously by LeMasurier et al. (2001) and is significantly less than the value of ∼13 pA which was obtained when the channel was recorded under forward bias.

Part b) of the figure shows two separate segments of a different recording when the holding potential was increased to -50 mV. Both examples show a single opening in the baseline, which is common to observe with KcsA electrophysiology at negative potentials (LeMasurier et al., 2001). The amplitude of the opening in part i) of the figure was measured to be 5.6 ±1.1 pA, while the amplitude of the event shown in part ii) was calculated to be 6.4 ±1.4 pA. Both values are close to, but remain less than, the average amplitudes measured at forward bias. Part c) of the figure shows two separate regions of a recording obtained at -25 mV. Part i) and part ii) each show a single opening in the baseline, measured to be 4.3 ±1.6 pA and 4.9 ±1.1 pA respectively.

The data from Figs 6.3 and 6.4 can be combined to form a current/voltage relation shown in 6.5. The data confirms that the channel behaves as a weak outward rectifier, as shown by the greater amount of current passed at positive potentials compared to negative potentials, which is indicative of KcsA behavior (LeMasurier et al., 2001).

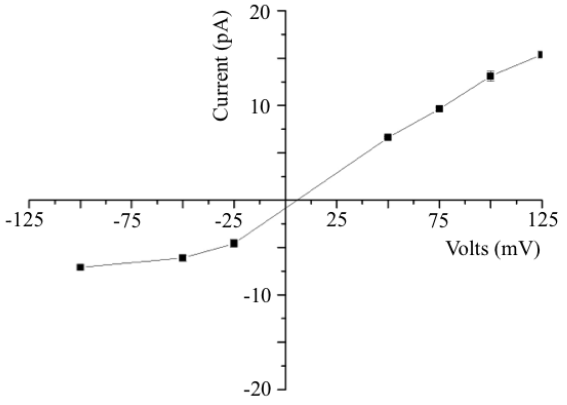

Figure 6.5: I/V curve of cell-free expressed KcsA characterised in interdroplet bilayers without purification. The plot reveals that the channel shows outward rectification, as expected for KcsA gating.

In summary, the data in this subsection shows that single-channel measurements of CF expressed KcsA were obtained directly from the CF mixture, without purification or reconstitution. This demonstrates both the functionality of the CF expressed channel, and its capability to spontaneously self-insert into the interdroplet bilayer for characterisation.

6.2 KcsA inhibition by TEA

Single-channel measurements of CF expressed KcsA were obtained in the previous subsection where the characteristics of the channel were shown to closely match those previously reported in the literature. To demonstrate this further, measurements were repeated in the presence of different amounts of tetraethyl ammonium (TEA), a quaternary ion which is known to block the channel as discussed in section 2.4.1.

The TEA was added to the second droplet at concentrations of a) 25 mM and b) 50 mM as described by Kutluay et al. (2005). The data is shown in Fig 6.6, where two examples are shown for each condition. The channel appears to be predominantly in the open position in a) part i) before brief closing and opening events are seen to occur. Analysis of the burst reveals that the average amplitude of the events was 8.1 $\pm$1.7 pA, which is close to 8.2 $\pm$1.7 pA found for the second insert in a) part ii). Both values are significantly lower than $\sim$13 pA found when no TEA was added and are in-line with what was reported previously (Kutluay et al., 2005).

The amplitude of the openings was further reduced when the TEA concentration was increased to 50 mM as shown in part b). The recording shown in b) part i), for example, shows what appears to be a burst of quick gating akin to the flicker mode. The average amplitude of the channel openings was 6.2 $\pm$1.1 pA, the dwell time was 1.02 ms and the P_o was 0.57. A different region of the same trace is shown in part ii). Specifically, it appears that a channel in the bilayer briefly closes and opens before closing for $\sim$100 ms and briefly opening and closing again. The amplitude of the events was $\sim$6 pA, which fits closely both with the data from part i) and with previously published values (Kutluay et al., 2005).

In summary, the data shows that the TEA inhibits the channel, providing further verification that the observed channel activity is indeed CF expressed KcsA.

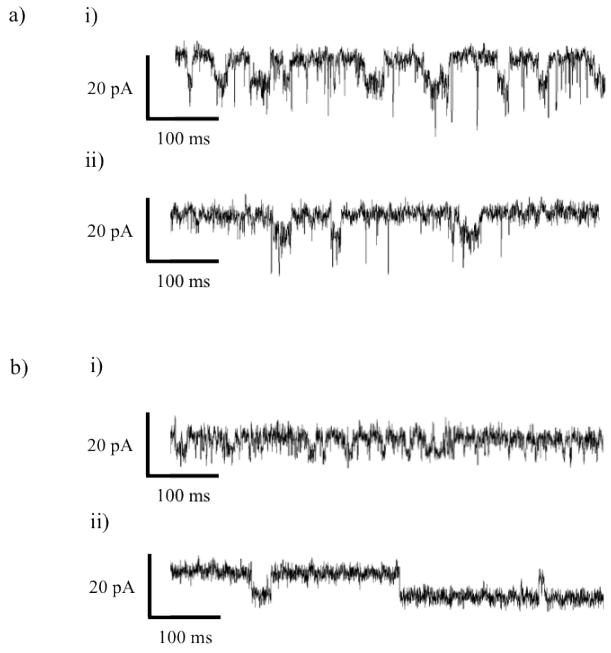

Figure 6.6: Inhibition of CF expressed KcsA by TEA. The figure shows single-channel measurements of interdroplet bilayers formed with a 2 μl droplet of the cell-free expression mixture incubated at 37 °C for 2 hours with 1 μg of the DNA template and a 2 μl droplet of 150 mM KCl, pH 4.0 supplemented with a) 25 mM and b) 50 mM of the quaternary ammonium ion TEA. Recordings were performed at 100 mV. The figure shows that TEA inhibits the channel.

6.3 Electrophysiology of KcsA expressed in the presence of lipid vesicles

In previous parts of this study, the addition of vesicles has been shown to 1) assist with the stabilisaiton of interdroplet bilayers using the unincubated CF mixture (section 4.6) and 2) promote the CF expression of KcsA (section 5.1.4. In addition, vesicles can also serve as a delivery mechanism to the bilayer as discussed in sections 2.1.5 and 2.2.5.

The CF mixture was prepared in triplicate with 1 μg of DNA and incubated at 37°C for 2 hours as described in section 3.1.4, except for the addition of a) 250 μg, b) 25 μg and c) 2.5 μg of DOPC/POPG (1:1 by mass) vesicles (extruded to a final diameter of 100 nm). 2 μl of each preparation was used to form an interdroplet bilayer with a second droplet containing 750 mM KCl, 10 mM HEPES, pH 4.0 using manual manipulation as described in section 3.2.5.4. Single channel measurements were performed as detailed in section 3.2.1 .

A representative measurement for each condition is shown in Fig 6.7. Where 250 μg of vesicles was added to the CF system in part a), the recording shows the baseline current briefly rising to ∼50 pA before later rising again to ∼200 pA where smaller and shorter increases and decreases in the baseline current are observed. The region of the trace shown in part i) reveals a discrete burst of activity in the baseline which resembles single-channel activity. Notably, the brief events show a reduction in the baseline current, suggesting that there is at least one channel held in the open position which momentarily closes. Analysis of the activity reveals that the average amplitude of the closings is 17.3 ±2.0 pA, a dwell time of 4.33 ms and a P_o of 0.84. Similar activity is shown in the zoom in part ii) where two closings and openings appear to occur sequentially, suggesting that several active channels may have inserted into the bilayer. The average amplitude for the first level of closings was 17.6 ±5.7 pA, the dwell time was 1.35 ms while the average amplitude for the second level of openings was 31 ±3.3 pA, with a dwell time of 7.61 ms. The suggestion that two channels are sequentially closing and opening is indicated as 31.2 pA is close to double the value of 17.6 pA, however the amplitude of these openings is lower than what has been reported for KcsA when 750 mM KCl is present on both sides of the bilayer (LeMasurier et al., 2001). This could be due to an artefact or because the KCl concentrations were asymmetric in this case, with 150 mM KCl in the cis (extracellular) side of the bilayer and 750 mM on the trans side. It is also possible the gating seen in the figure is not caused by KcsA at all, however no events of this nature were observed under similar conditions in Chapter 4 when no DNA was added to the CF system.

The recording shown in part b), where 25 μg of vesicles were added to the CF system, shows a similar increase in the bilayer current however the level of the baseline is lower at ∼100 pA compared to part a). Closer inspection of the recording revealed several discrete closings as shown in the zooms in i) and ii) however no bursts of activity were observed. Analysis of the opening shown in part i) reveals an amplitude of 20 pA, while the openings in part ii) were measured at 19 pA and 13 pA respectively. It is possible that the larger openings relate to the single-channel, while the lower value represents the sub-conductance state as described by Cuello et al. (Cuello et al., 1998) however the absence of bursts of gating was unexpected.

When 2.5 μg of vesicles were added to the CF mixture in part c) the baseline was seen to rise to ∼30 pA, far less than what was observed in parts a) and b). The zoom in part i) shows three short bursts of activity in the bilayer, each separated by a brief period of inactivity, which is indicative of KcsA gating behaviour. The

average amplitude of the closings was 20 ±2.5 pA, the dwell time was 3.6 ms and the P_o was 0.74, values that are expected for single-channel KcsA. A continuous burst of gating behaviour is shown in part ii), where the average amplitude of the channel openings was 20 ±2.5 pA, the dwell time was 1.96 ms and the P_o was 0.77.

The large increases in the baseline current seen in the figure are reminiscent to when vesicles were added to the unincubated CF system containing no DNA in Fig 4.9. This indicates that vesicles supplied to the CF system are fusing with the membrane, incorporating KcsA and/or membrane pertubing components from the CF kit with the bilayer. Yet interestingly, this appears to improve when less vesicles are added, implying less incorporation with the bilayer. This the opposite

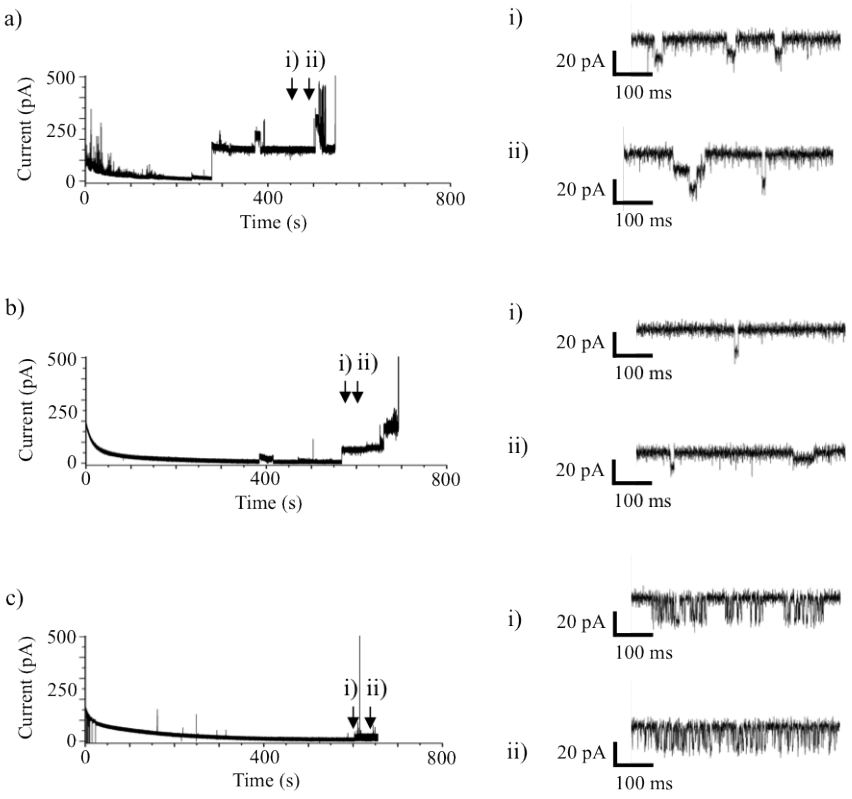

Figure 6.7: Electrophysiology of KcsA expressed in the presence of vesicles. KcsA was expressed with 1 μg of DNA and incubated at 37 °C for 2 hours with a) 250 μg b) 25 μg and c) 0.25 μg of DOPC/POPG (1:1 by mass) vesicles extruded to a final diameter of 100 nm. The indicated regions of each recording are shown in the zooms in i) and ii). Despite the detection of channel activity, the figure shows that stable baslines are difficult to achieve under these conditions and indicates that single channel measurements may be easier to obtain when less vesicles are added to the CF system.

to what was observed in Chapter 4, where the addition of vesicles was found to stabilise the bilayer. It is possible that this effect could be a result of KcsA self-inserting into the vesicles and making them more fusogenic. This is consistent with the observation of channel activity in almost all measurements, the finding that ~3.7 μg of KcsA is expressed per volume of the CF kit in the presence of vesicles (section 5.1.4) and with previous reports with MscL, where macroscopic currents were observed when the channel was expressed in the presence of liposomes (Berrier et al., 2011). The difference in the lifetime of the bilayers compared to Fig 4.9 is exlained by the low pH of the second droplet as detailed in section 4.3.

In summary, the results in this subsection show that the CF mixture incubated with the KcsA template and vesicles leads to the appearance of transient bilayer current fluctuations in single-channel measurements. The data implies that this might be caused by a large number of active KcsA channels in the bilayer, suggesting that the addition of vesicles compromises the control of bilayer insertion.

6.4 Electrophysiology of CF expressed and purified KcsA in interdroplet bilayers

In the previous subsections single-channel measurements of CF expressed KcsA were obtained in interdroplet bilayers formed directly from the CF system, where the channel was shown to be capable of self-inserting into the membrane for characterisation. To identify whether the effect of self-insertion was dependent on the presence of the CF system, the His-tagged protein was expressed and purified and supplied to the bilayer without reconstitution.

The CF reaction was incubated at 2x volume with 3 μg of DNA per volume at 37 °C for 2 hours. The expressed protein was purified as described in section 3.1.5 except that the final elution was performed using 500 mM imidazole containing 150 mM KCl, pH 7.0. The elutions were collected in a PCR tube and used for single channel experiments which were performed as described in section 3.2.1.

The data in Fig 6.8 part a) shows a representative trace of three experiments where an interdroplet bilayer was formed from a 2 μl droplet of purified protein from the CF mixture supplied with no DNA, and a second 2 μl droplet containing 150 mM KCl buffer at pH 4.0. The current trace in part i) shows that the baseline is stable

for the duration of the 15 minute recording with the appearance of only a few low intensity spikes.

A zoom of the indicated region of the recording distinguishes the spikes from channel activity while the capacitance trace in part ii) shows that the bilayer remained intact for the duration of the recording, revealing a capacitance of 250 pF which equates to an approximate bilayer diameter of 252 μm. The data shows that no single channel activity was observed when no DNA was added to the system.

Part b) of the figure shows a representative trace of three independent measurements of an interdroplet bilayer formed from a 2 μl droplet of purified protein from the CF expression mixture incubated with the DNA template, and a second 2 μl droplet containing 150 mM KCl buffer at pH 7.0. The current trace in part i) shows several low intensity spikes in the baseline of varying magnitude, which are distinguished from channel activity by the zoom provided. The bilayer was intact for the duration of the 15 minute recording as shown from the capacitance trace in part ii), revealing a capacitance of 400 pF, equating to an approximate bilayer diameter of 319 μm.

A representative trace from three repeats of a third control experiment is shown in Fig 6.8 part c), where an interdroplet bilayer was formed of one droplet of the final elution buffer (500 mM imidazole containing 150 mM KCl, pH 7.0) and a second droplet containing 150 mM KCl buffer at pH 4.0. The current measurement in part i) of the figure shows some current spikes in the baseline, which do not resemble channel activity as indicated by the zoom. The capacitance recording shown in part ii) of the figure confirms that the bilayer remained in contact at the end of the 15 minute recording, revealing a capacitance of 325 pF which equates to an approximate bilayer diameter of 288 μm.

Measurements of CF expressed and purified KcsA are shown in Fig 6.9 under different positive holding potentials, where interdroplet bilayers were formed from one 2 μl droplet of purified protein from the CF mixture, and a 2 μl droplet of 150 mM KCl buffer at pH 4.0.

Part a) of the figure shows segments of two separate measurements obtained at 125 mV where in both cases the channel appears predominantly open with rapid closing and opening events. The histogram in part iii) is taken from the measurement in part i) and reveals an average opening amplitude of $\sim$20 pA. This value is in line with the results obtained from the analysis of the burst, revealing an average

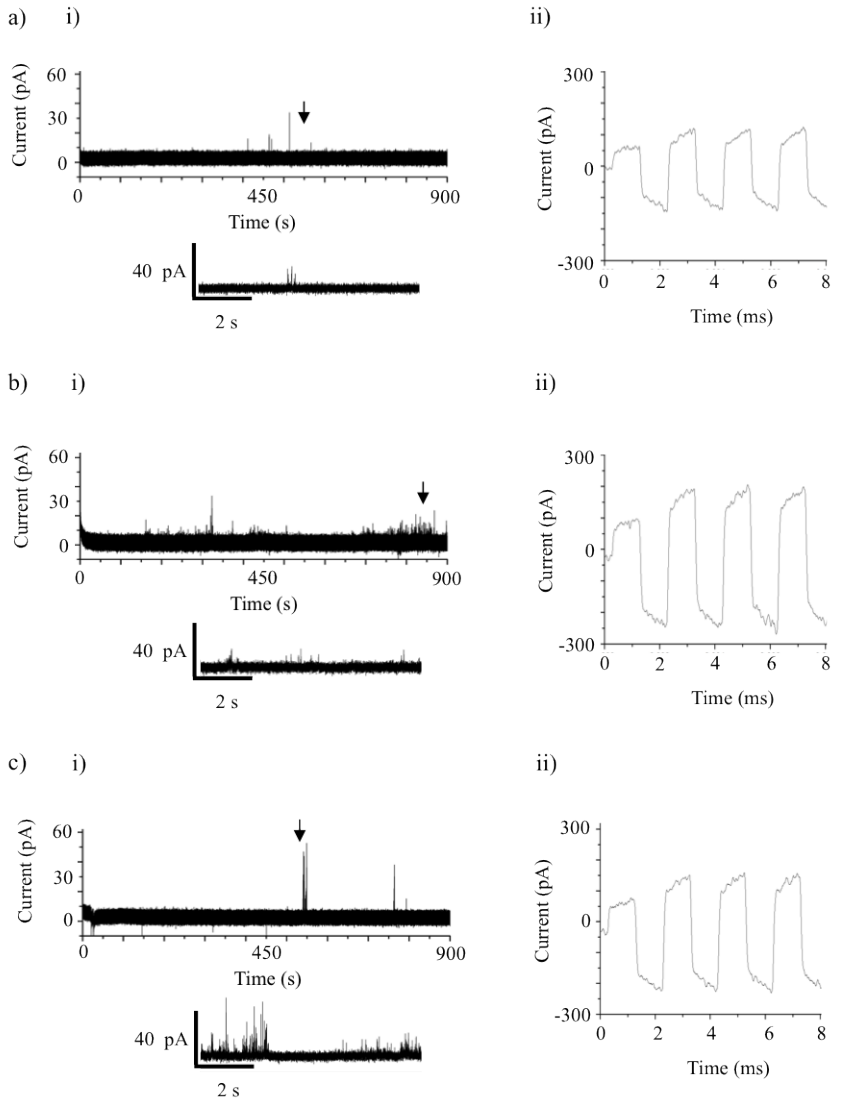

Figure 6.8: Negative control experiments for cell-free expressed and purified KcsA. a) Electrophysiology of interdroplet bilayers formed from one 2 l droplet of protein purified from a CF mixture incubatted with no DNA, and a 2 μl droplet of 150 mM KCl buffer at pH 4.0. b) Electrophysiology of interdroplet bilayers formed from one 2 μl droplet of protein purified from a CF mixture incubated with 3 μg of the His-tagged KcsA DNA template and a 2 μl droplet of 150 mM KCl buffer at pH 7.0. c) Electrophysiology of interdroplet bilayers formed from one 2 μl droplet of elution buffer (500 mM imidazole, 150 mM KCl, pH 7.0) and a 2 μl droplet of 150 mM KCl buffer at pH 4.0. The inserts are magnified regions of the recording that are indicated by the arrow. Measurements were performed in triplicate using a holding potential of 100 mV. The data shows that no single channel activity is detected in any of the recordings. The capacitance traces in part ii) of the figure confirm that the bilayer remained intact at the end of the 15 minute recordings.

amplitude of 20 ±1.7 pA with a dwell time of 8.49 ms and a P_o of 0.93. Analysis of the burst shown in part ii) of the figure shows an average amplitude of 19 ±0.96 pA, a dwell time of 6.33 ms and a P_o of 0.90. Both values for the open probability are consistent with those for the high P_o state of the channel as described by Chakrapani (Chakrapani et al., 2007) however the average opening amplitudes in each case are ∼4 pA higher than those reported in the previous subsection for unpurified protein and by (LeMasurier et al., 2001). This could be a result of fact that the measurement was obtained at an elevated baseline, as indicated by the histogram in part iii), yet how this would lead to a higher opening amplitude is unclear.

Two independent measurements at 100 mV are shown in part b) of Fig 6.9, where the segment shown in i) shows relatively long openings followed by brief closings. It is notable that the openings and closings seem to appear more rapidly toward the end of the trace. The histogram in iii) indicates that the amplitude of the events is approximately 13 pA. A different type of gating behavior is shown in the example provided in part ii) where the channel appears to be predominately in the open state and rapidly closes. Analysis of the measurement in part i) reveals an average amplitude of 13 ±0.98 pA, a dwell time of 12.84 ms and a P_o of 0.46. Meanwhile analysis of the burst in part ii) returned an average amplitude of 15 ±1.2 pA a dwell time of 7.36 ms and a P_o of 0.88. The values are ∼1 pA higher than the measurements obtained for the unpurified protein without the HN tag under the same holding potential.

Part c) of Fig 6.9 shows two separate measurements performed at 75 mV. In the example provided in part i) the channel appears to stay open with brief gating events, similar to the activity observed previously. While in part ii) the gating is observed as discrete openings and closings. The average amplitude for the events in part i) was 9.2 ±0.96 pA, the dwell time was 5.64 ms and the P_o was 0.87. The same measurements for ii) returned a value of 8.7 ±1.2 pA for the average opening amplitude, a dwell time of 3.19 ms and a P_o of 0.52. Both values for the average opening amplitude are ∼1 pA less than those reported in the previous subsection.

Measurements performed at 50 mV are shown in part d) of Fig 6.9. In i) and ii) the channel appears to be predominantly held in the open state with brief gating events. However it is also clear that under these conditions it can be challenging to separate the low amplitude gating events from the noise already present in the baseline. This difficulty is also illustrated by the histogram in part iii) where two

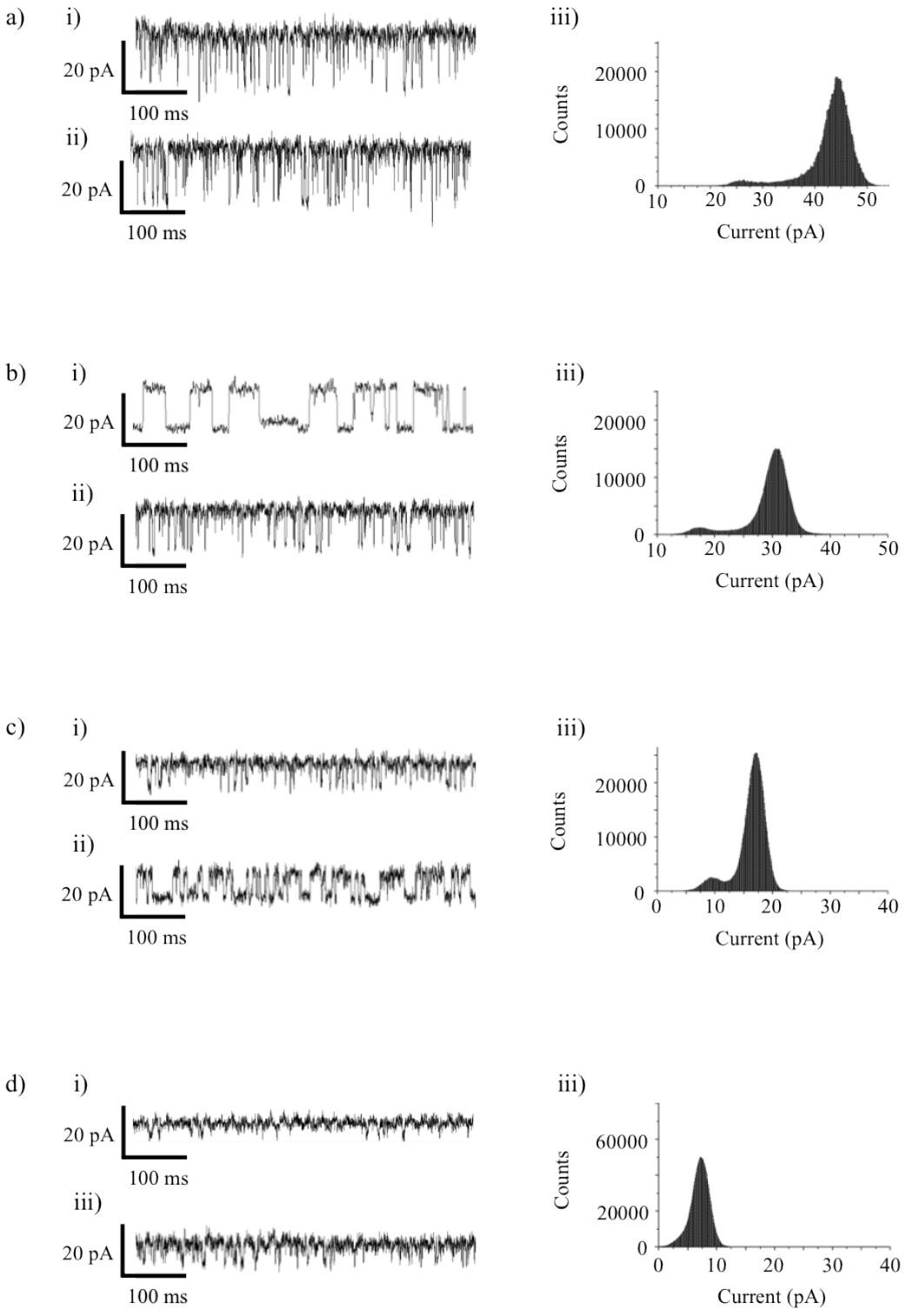

Figure 6.9: Electrophysiology of cell-free expressed and purified KcsA in under positive holding potentials. Measurements were performed at a) 125 mV, b) 100 mV, c) 75 mV and d) 50 mV with the second 2 μl droplet containing 150 mM KCl buffer at pH 4.0. Gating events are observed under each condition as seen from the examples in i) and ii). The histograms in iii) are taken from the measurement shown in part i) of the figure.

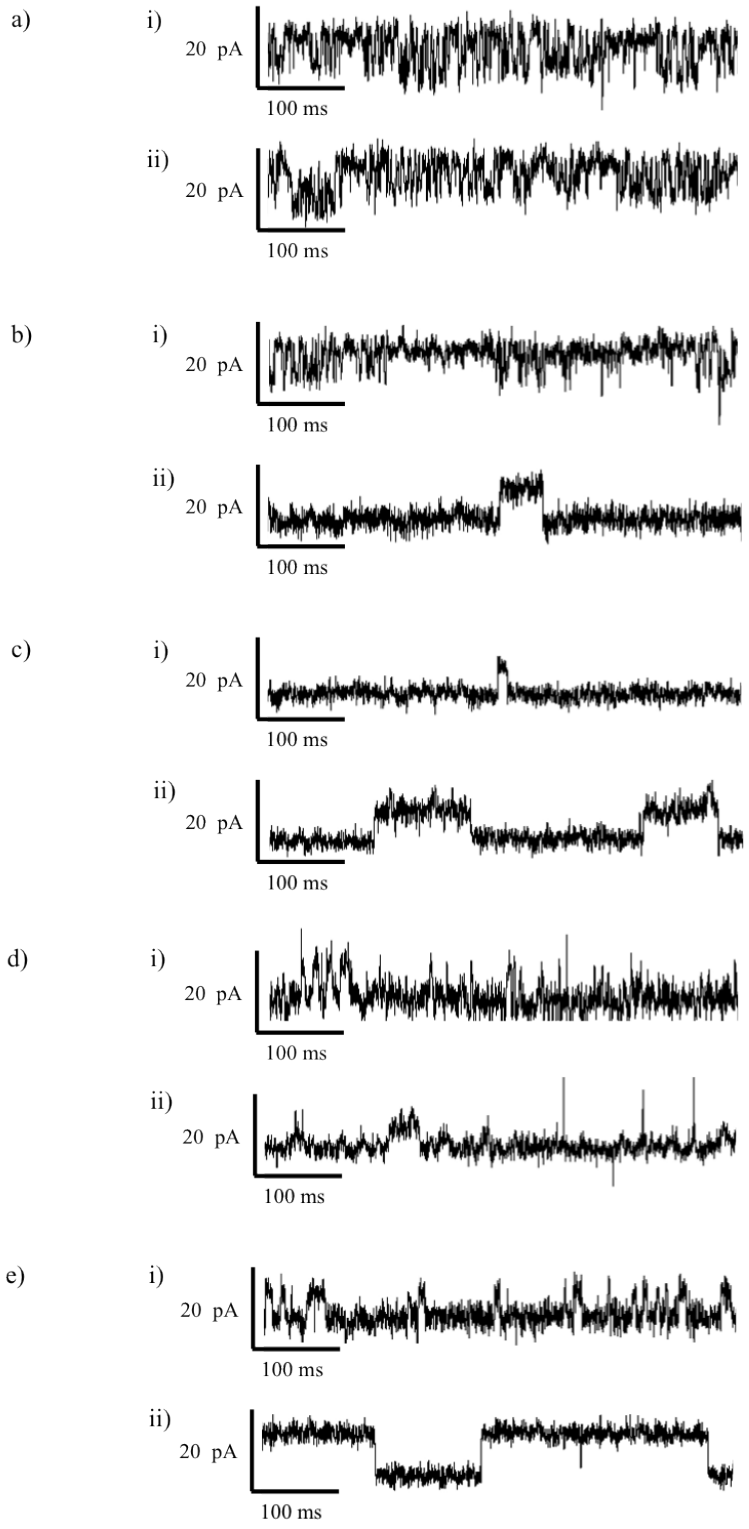

Figure 6.10: Electrophysiology of cell-free expressed and purified KcsA in interdroplet bilayers under negative holding potentials. Measurements were performed at a) -125 mV, b) -100 mV, c) -75 mV, d) -50 mV and e) -25 mV with the second 2 μl droplet containing 150 mM KCl buffer at pH 4.0. The traces show that the channel exhibits slight outward rectification.

populations of openings are difficult to clearly identify. Single-channel analysis of the data returned an average amplitude of 5.0 ±0.79 pA a dwell time of 2.29 ms and a P_o of 0.84 for the measurement in part i) and an average amplitude of 6.7 ±1.1 pA a dwell time of 3.09 ms and a P_o of 0.85 for the measurement in part ii). The data is close to the value of ∼6.5 pA obtained previously for unpurified KcsA at 50 mV.

To further characterise the CF expressed and purified KcsA, measurements of the channel were performed under negative holding potentials as shown in Fig 6.10. Part a) of the figure shows two measurements obtained at -125 mV. In each case the activity is seen as rapid opening and closing events, without a notable inactive period.

Other reports of KcsA measurements obtained at negative potentials suggests that this is less common for the channel under these conditions where single, less frequent, openings and closings in the baseline tend to be observed (LeMasurier et al., 2001). Analysis of the data reveals an average opening amplitude of -9.1 ±1.6 pA for part i) and -8.4 ±1.3 pA for part ii), values which are noticeably less than the results obtained for the channel at positive potentials and close to those reported previously (LeMasurier et al., 2001).

The data in part b) of 6.10 shows two separate measurements performed at -100 mV. The example in part i) shows a burst of openings of in the baseline separated by a period of inactivity. The average amplitude of the events was -8.1 ±1.4 pA, which is similar to the value obtained with unpurified protein in the previous subsection. The value is also similar to average amplitude of the opening in part ii), which was -8.1 ±1.8 pA. The intensity of the single event shown in part c) of the figure was measured to be -7.3 ±0.3 pA when the holding potential was increased to -75 mV. A separate region of the same trace is presented in ii) where the two gating events in the baseline were measured to have an average amplitude of -7.7 pA ±1.4 pA.

Two separate measurements at -50 mV are shown in c), where a number of brief events are shown in part i) and a single, longer event in part ii). The average amplitude of the openings in i) was -6.8 ±1.9 pA, while in part ii) the average amplitude of the openings was -6.1 ±1.3 pA. The values are close to what was obtained for the unpurified protein in the previous subsection. Part d) of the figure shows two separate measurements obtained when the holding potential was changed to -25 mV. Several low amplitude openings are shown in i) with an average amplitude of -4.8 ±1.4 pA, while two longer events are shown in ii). The average

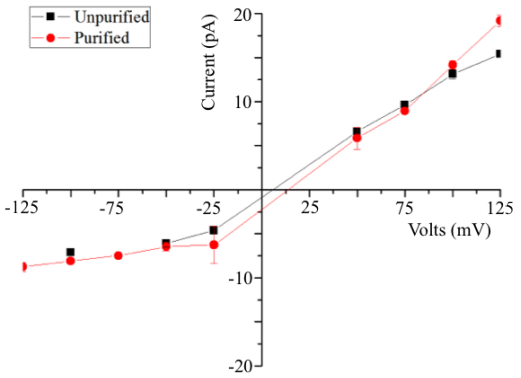

Figure 6.11: I/V curve of cell-free expressed and purified KcsA characterised in interdroplet bilayers. The values from the I/V curve shown in the previous subsection with unpurified KcsA is shown for comparison (black Squares). The plot reveals that the purified protein also shows weak outward rectification and the values from both data sets appear closely in line.

amplitude of the events shown in ii) was 7.7 pA, which was higher than what was expected compared to the data obtained from the unpurified protein.

The I/V data obtained for the purified KcsA is shown in Fig 6.11 (red circles) alongside what was obtained in the previous subsection where measurements were performed without purification (black squares). It is clear from the figure that the purified protein displays similar outward rectification to what was obtained with the unpurified protein. With the exception of a small deviation at -25 mV and 125 mV, the figure shows close similarity between the two values.

Similarity was also observed when the CF expressed His-tagged KcsA protein was studied without purification as shown by the measurement at 100 mV in Fig 6.12. The trace shows discrete openings and closings in the baseline before remaining open with rapid closing events. Single channel analysis of the burst reveals an average opening amplitude of 12 pA ±1.7 pA a dwell time of 5.57 ms and a P_o of 0.35, values which are close to those observed in both data sets.

The response of the purified channel to the blocker TEA was also studied as shown in parts b) and c) of Fig 6.12 where measurements of purified CF expressed KcsA were obtained at 100 mV with 1 mM and 10 mM of TEA respectively. When 1 mM TEA was used the amplitude of the openings were found to reduce to 8.1 ±2.2 pA, while when the amount of TEA was increased to 10 mM the average amplitude of single openings was found to reduce to 3.8 ±0.9 pA. The data shows that TEA inhibits the channel, unexpectidly at a lower concentration of the blocker compared to what was required in the previous subsection for unpurified KcsA.

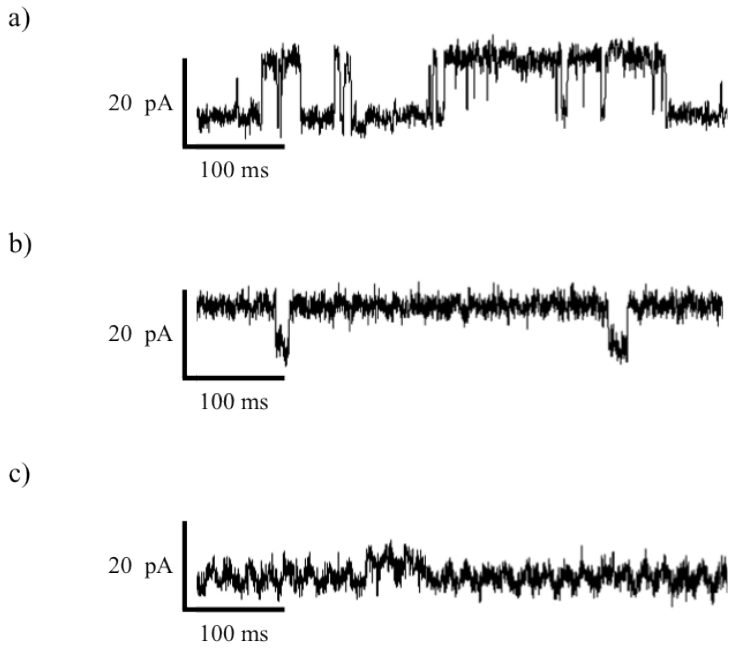

Figure 6.12: Electrophysiology of cell-free expressed HN tagged KcsA without purification and with purification in the presence of TEA. a) Interdroplet bilayers formed from one 2 μl droplet of the cell-free system incubated with 1 μg of the HN- tagged DNA template for 2 hours at 37 °C and a second 2 μl droplet containing 150 mM KCl at pH 4.0. The measurement was performed without purification under a holding potential of 100 mV. The trace shows single channel activity comparable to what was found in the previous subsection. b)-c) Electrophysiology of interdroplet bilayers formed with one 2 μl droplet of purified KcsA and a second 2 μl droplet containing 150 mM KCl buffer at pH 4.0 and b) 1 mM TEA and 10 mM TEA. The measurements shows inhibition of the channel by TEA.

In summary, the data in this subsection shows that the I/V characteristics of CF expressed and purified KcsA closely match that of the KcsA obtained directly from the CF system without purification. This verifies the measurements obtained in the previous sections and suggests that the presence of the CF system is not required for the spontaneous insertion of the channel into the bilayer. Control experiments indicate that the presence of 500 mM imidazole did not destabilise the interdroplet bilayers, however it is unclear whether any residual molecules/surfactant remains from the CF mixture.

6.5 Electrophysiology of CF expressed hERG$_{S5-S6}$ in interdroplet bilayers

Further to demonstrating the CF expression of the hERG$_{S5-S6}$ pore domain in section 5.3, this subsection addresses the functionality of the channel and its capability to self-insert into an interdroplet bilyer directly from the CF mixture, without purification or reconstitution.

The hERG$_{S5-S6}$ construct was expressed using the L1110 system as described in section 5.3.1. A 2 μl droplet of the completed reaction mixture was used to form an interdroplet bilayer with a second droplet containing 150 mM KCl buffer at pH 7.0 by manual manipulation as described in section 3.2.5.4. Single channel measurements were obtained as detailed in section 3.2.1.

Single channel recordings of the CF expressed hERG$_{S5-S6}$ pore domain over a range of holding potentials between 50 mV and 125 mV, with an interval of 25 mV, are shown in Fig 6.13. The 30 second example of a recording at 50 mV in a) part i) of the figure shows discrete fluctuations in the baseline current that are magnified in the inserts, iii) and iv). The appearance of the events as negative spikes from an elevated baseline seems to indicate that the channel is held in the open state with brief closing and opening events. This is depicted in the histogram, where a far greater number of data points are shown at a peak of ∼26 pA compared to the second population of data points at ∼21 pA. This value of ∼5 pA for the channel opening is close to the 4.9 ± 0.64 pA obtained from ClampFit analysis, which also generated a dwell time of 0.38 ms and an open probability of 0.05.

A similar form of gating behavior is shown in the measurement in part b), obtained from the same recording at 75 mV. In this case, the histogram in part ii) of the figure shows the two populations of data points more distinctly at ∼30 pA and ∼39 pA indicating an average channel opening of ∼ 9 pA. Intraburst analysis of the trace revealed a similar value of 8.8 ±1.6 pA, a dwell time of 1.37 ms and an opening probability of 0.07.

The data in part c) shows a 30 second segment of low intensity bilayer activity at 100 mV, resolved as individual openings and closings in the baseline from the zooms shown iii) and iv). Both the open and the closed state of the channel is detectable from the histogram shown in part b) of the figure, where the closed state appears at ∼4 pA compared to the open state at ∼8 pA, meaning that the average amplitude of the channel openings was ∼4 pA. This is close to the value

provided from burst analysis, which produced a figure of 3.7 pA ±0.4 pA for the average amplitude of the channel openings, a mean open time of 0.3 ms and a P_o of 0.03. The observation of channel openings with such low amplitude was unexpected compared to the larger events obtained observed at 50 mV and 75 mV in parts a) and b) of the figure, however these appear to be closer in magnitude to the value of 10 pS reported using patch clamping, as detailed in section 2.4.3 (Kiehn et al., 1996). Channel openings closer to the values obtained in parts a) and b) were also observed at 125 mV in part d) of Fig 6.13, where an average opening amplitude of 8.6 ± 1.4 pA was measured. The dwell time for these events was 0.7 ms, while the P_o was calculated to be 0.16.

The interpretation that the channel activity attributes to the $hERG_{S5-S6}$ pore domain is supported by the fact that events of this magnitude were not previously observed under any of the previous conditions investigated in this study. The occurrence of the gating events with both sides of the bilayer at pH 7.0 also means that the channel activity can be clearly distinguished from the KcsA measurements obtained in Chapter 5. The appearance of ∼10 seconds of continuous activity visible in the traces in Fig 6.13 a) part is also distinctly different from the short bursts of channel activity separated by periods of inactivation observed for KcsA. It is unclear whether this is due entirely or at all to the removal of the voltage-sensing domain of the $hERG_{S5-S6}$ construct resulting in it being constitutively active.

Interestingly a second large conductance gating mode for the channel was separately recorded when single channel measurements of the $hERG_{S5-S6}$ pore domain were obtained. A 30 second segment of a recording is provided in Fig 6.14 a) part i) and shows two bursts of events at an elevated baseline, separated by a closing event of approximately one channel opening. Magnified regions of the activity are shown in parts iii) and iv) of the figure and show discrete, non periodic, openings and closings in the baseline of approximately the same amplitude, indicative of single-channel activity. The three levels are clearly depicted in the histogram in part ii) of the figure, where three distinct populations of events are noticeable. Here, the peak at ∼260 pA represents the data points obtained when at least two channels were open, while the peak at ∼235 pA corresponds to when at least one channel was open and one channel was closed. The data points at ∼206 pA arise when both of the observed channels are closed, however it is unclear whether this still remains as an open state for other channels held in the open position as might be suggested by the elevated baseline.

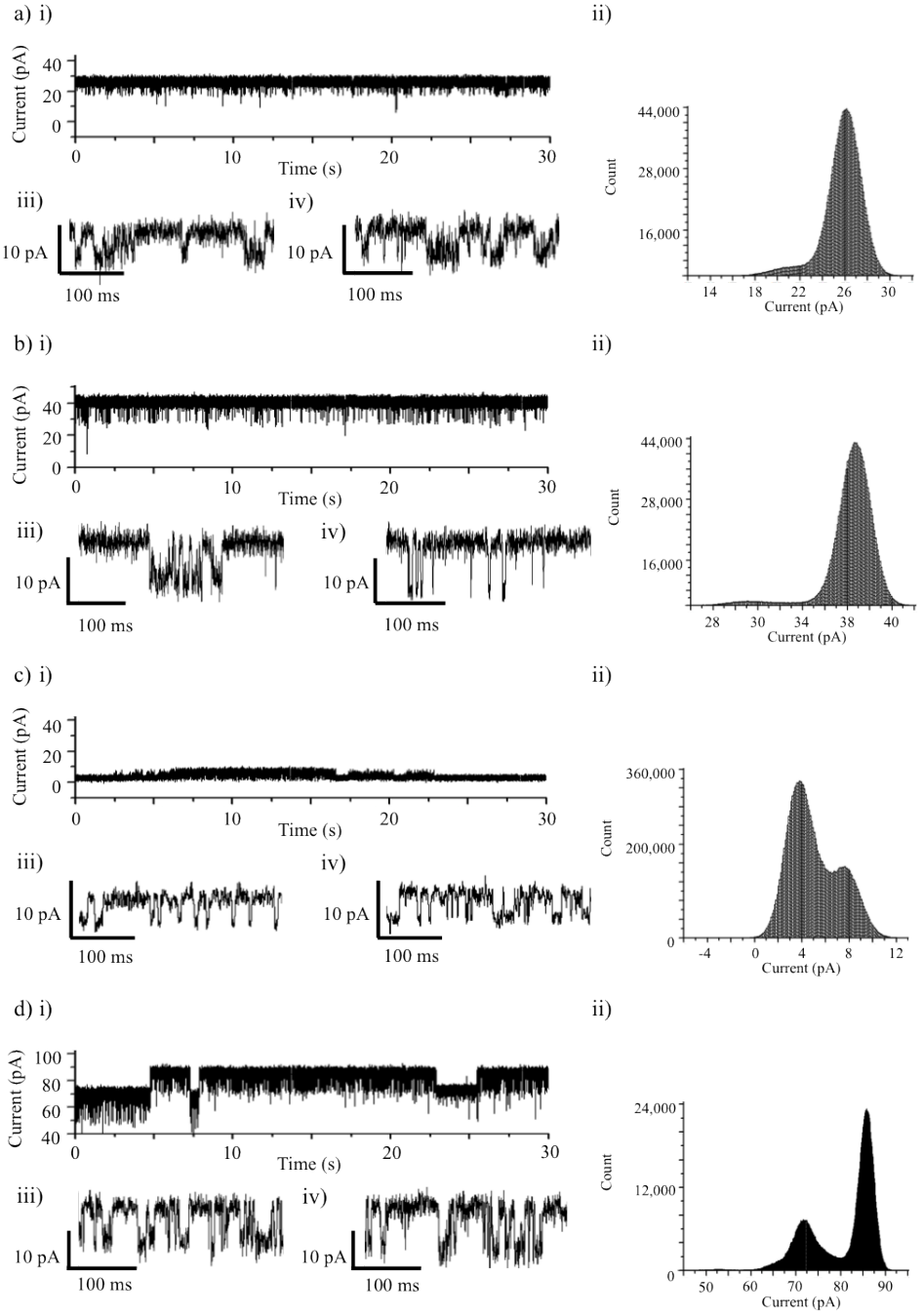

Figure 6.13: Single channel recordings of cell-free expressed hERG$_{S5-S6}$ in interdroplet bilayers without purification. Measurements were obtained at a) 50 mV, b) 75 mV, c) 100 mV and d) 125 mV. A 30 second sample of each recording is shown in part i), the distributions of the data in the form of a histogram in parts ii) and two magnified regions of the trace in parts iii) and iv). The recordings reveal discrete openings and closings in the baseline with magnitudes of approximately 5, 9, 4 and 9 pA respectively. The appearance of gating activity as negative facing events indicates that the channel is constitutively open as would be expected with the S1-S5 voltage sensor removed

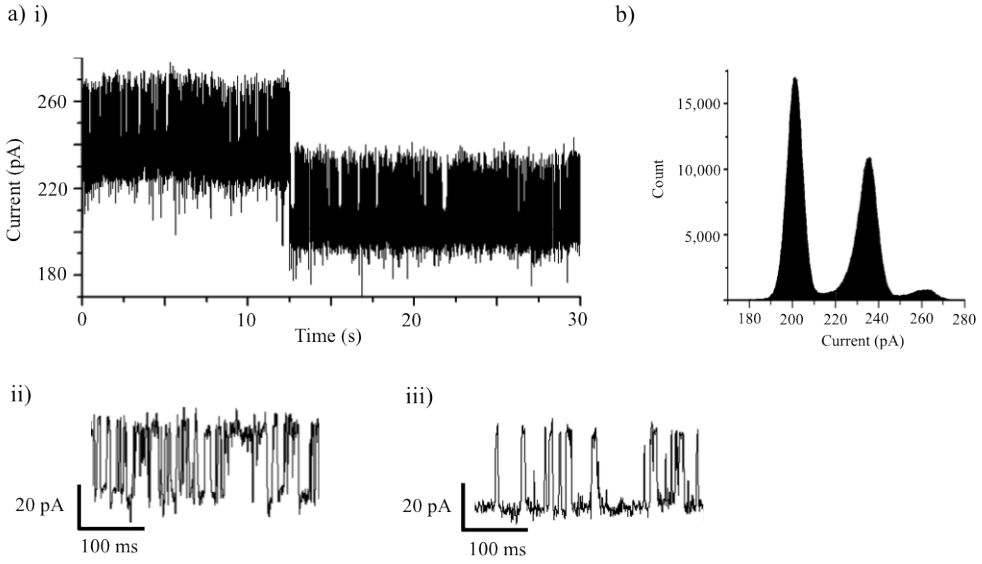

Figure 6.14: Large-conductance single channel recordings of cell-free expressed hERG$_{S5-S6}$ in interdroplet bilayers without purification. a) i) A 30 second segment of a recording obtained at 100 mV, the channel activity is visible as large fluctuations in the baseline at elevated current levels. The two bursts are separated by a closing event approximately equal to the magnitude of the channel openings. Magnified regions of the recording in ii)-iii) reveal discrete openings and closings in the baseline. The data points are represented in the histogram in b), revealing three distinct populations at ∼260 pA, ∼235 pA and ∼206 pA. Analysis of the recording revealed an average opening amplitude of 24.3 pA ± 2.9 pA.

Analysis of the activity revealed an average opening amplitude of 24.3 ±2.9 pA, a mean open lifetime of 1 ms and an open probability of 0.07. The large conductance open state for the hERG$_{S5-S6}$ pore domain was unexpected, particularly since a small number of full-length hERG studies using the patch clamp technique suggest a conductance of approximately 10 pS. In this example, a current amplitude of 0.3 pA at -40 mV and 100 mM KCl was obtained with an average open time of 3.2 ms, or an amplitude of ∼1 pA at -120 mV (Vandenberg et al., 2012; Kiehn et al., 1996). This suggests that the low conductance state for the hERG$_{S5-S6}$ pore domain is most likely more relevant than the large conductance state. As transitions between the two conductance states did not typically occur in a single experiment, it could be suggested that the low and high conductance current events result from different conformations of the bilayer incorporated hERG$_{S5-S6}$ pore domain, which in the absence of the flanking voltage sensor and C-terminal domains may not have a single open state.

In summary, this section shows that single channel measurements of the hERG$_{S5-S6}$ pore domain can be obtained directly from CF expressed protein without

purification or reconstitution in interdroplet bilayers. This demonstrates that the CF expressed channel is functionally active and that it is capable of spontaneous self-insertion into the bilayer for characterisation.

6.6 Summary

As the CF expression of ion channels was verified in Chapter 5, the focus of this chapter was to identify whether the CF expressed ion channels were functional and capable of self-inserting into an interdroplet bilayer for characterisation without purification from the CF expression mixture. This was shown in section 6.1 for KcsA, and section 6.5 for $hERG_{S5-S6}$ where in both cases, single-channel currents were observed in interdroplet bilayers formed directly from the CF mixture after incubation with the respective DNA template. The KcsA activity closely matched examples reported previously in the literature, including the blockade of the channel by TEA (section 6.2), however it was found that the bilayer failed quickly at negative potentials. The bilayer was also found to become unstable and fail through the appearance of spikes and leakage currents when KcsA was expressed in the presence of vesicles (section 5.1.4), more so than observed when vesicles were supplied to a preincubated CF system in the absence of DNA in 4.6. It was expected that the problem would be improved by diluting the CF mixture, however this resulted in the observation of stable baselines with no channel activity. Instead it was found that single-channel activity could be observed by reducing the amount of vesicles supplied to the system. This implies that the presence of vesicles promoted the expression of KcsA and/or fusion with the bilayer, while the ineffectiveness of dilution suggests that perhaps the presence of the CF system was required in order to achieve self-insertion into the bilayer. To clarify this, CF expressed His-tagged KcsA was purified from the CF mixture in buffer containing 500 mM imidazole and 150 mM KCl (section 6.4). The observation of single-channel activity under these conditions indicates that the mechanism of insertion is not dependent on the presence of the CF system however it is unclear whether any residual surfactant from the expression mixture remained. Thus, this chapter shows that single channel measurements of CF expressed KcsA and $hERG_{S5-S6}$ can be obtained in interdroplet bilayers formed directly from the CF expression mixture, without purification or reconstitution. This demonstrates the functionality of both CF expressed channels and their capability to spontaneously insert into the bilayer for characterisation.

Chapter 7

Conclusion

7.1 Summary

As outlined in Chapter 1, ion channels are important targets for medical research and drug discovery, however the conventional methods for studying ion channels in model membrane systems are limited by the requirement to over-express the channel of interest in cells, which is low-yielding. To obtain a suitable yield, and to account for further losses downstream through protein purification and reconstitution the expression of ion channels in cells is typically performed in a volume of several litres, requiring a substantial amount of time, equipment and lab space.

As explained in section 2.3 it is possible that this could be considerably simplified using CF protein expression, with a commercially available mixture based on either prokaryotic or eukaryotic cell extracts. One distinct advantage of this method is that the reaction can be encapsulated inside a microdroplet. This economises the cost of the reaction mixture and, in principle, allows for the ion channel of interest to be expressed in the presence of an interdroplet bilayer. Under these conditions it has been reported that ion channels can spontaneously insert into lipid bilayers (section 2.3.2), allowing for single-channel electrophysiological measurements to be obtained (section 2.1.4).

While coupling the expression and characterisation of ion channels in microdroplets could significantly improve the throughput of ion channel measurements in bilayers, potentially improving the rate of discovering novel pharmaceutical compounds, progress has been limited by the short lifetime of interdroplet bilayers

containing a pre-incubated CF expression mixture. This was investigated in Chapter 4, where it was found that lipids, high concentrations of proteins and PEG 8,000 caused membrane instability. However it was also shown that the bilayer could be stabilised by diluting the CF expression mixture and adding large concentrations of lipids, supplied to the reaction mixture as vesicles.

The capability of commercial CF systems to express ion channels from custom DNA templates was shown in Chapter 5 through the expression of KcsA and $hERG_{S5-S6}$, which were both identified on SDS PAGE gels after purification. The presence of $hERG_{S5-S6}$ was also verified by Western Blotting (section 5.3.1). Interestingly, for KcsA, it was found that the addition of vesicles to the CF mixture facilitated an increase in the amount of protein expressed, from approximatly 0.4 μg per 50 μl volume of the CF mixture to 3.7 μg. A similar increase in the amount of KcsA expressed was also observed by increasing the amount of KcsA DNA to the CF mixture, however neither effect was observed for $hERG_{S5-S6}$ expression. This shows that the expression conditions are important for controlling the amount of protein expressed and indicates that optimal conditions for protein expression and the yield of the expression may differ from channel to channel. The control measurements in Chapter 6 show that interdroplet bilayers formed with one droplet containing the CF mixture incubated with the KcsA DNA template and a second droplet containing buffer at pH 7.0 were repeatedly stable for the duration of the 30 minute recordings, and were more stable than interdroplet bilayers formed in Chapter 4 with one droplet containing the pre-incubated CF mixture (without DNA) and a second droplet containing buffer at pH 7.0 (average lifetime <10 minutes). It is unclear whether this unexpected increase in the bilayer stability can be attributed to the presence of the CF expressed protein, or whether the exhausted CF system, after incubation with the DNA template, perturbs the bilayer less compared to the pre-incubated mixture. However, it is clear through the appearance of spikes and leakage currents leading to bilayer failure, that the interdroplet bilayers comprised of a CF system incubated with vesicles and the KcsA DNA template (Chapter 6) were less stable than those formed with the unincubated CF system, without DNA, in the presence of vesicles (Chapter 4).

In Chapter 6 it was also shown that single-channel measurements of CF expressed KcsA and $hERG_{S5-S6}$ could be obtained from a 2 μl droplet of the CF expression mixture incubated with the respective DNA template, by forming an interdroplet bilayer with a 2 μl droplet of buffer. These measurements, obtained directly from the undiluted CF mixture, without protein purification or reconstitution,

show that CF expressed proteins can self-insert into interdroplet bilayers *in-situ* for electrical characterisation. The detection of channel activity in these measurements, together with the observation of an increased yield of KcsA expressed in the presence of vesicles in Chapter 5, indicates that the instability observed in this case arises due to a number of active channels inserted into the membrane. It was expected that this would be improved by dilution, however this instead led to the observation of stable baselines devoid of channel activity. This may indicate that the components of the CF mixture is required in order for the channel to spontaneously insert into the bilayer, components of which may have remained when measurements of the purified CF expressed His-tagged KcsA were obtained. While these results indicate that the stabilisation strategy of diluting the CF system and adding high concentrations of vesicles may not be suitable for obtaining ion channel measurements, the results in Chapter 5 imply that this may be optimised by limiting the amount of DNA supplied to the CF system. This in combination with adding more lipids to the oil and a small dilution may allow for the expression and characterisation of ion channels to be fully coupled in microdroplets.

In conclusion, the findings of this study, namely the stabilisation of the bilayer in the presence of the CF system, the demonstration of the CF expression of ion channels and the observation of spontaneous bilayer insertion support the feasibility of coupling the expression and characterisation of ion channels in microdroplets for the development of high-throughput bilayer platforms for ion channel measurements, including drug screening.

7.2 Recommendations for future work

- **Single-channel electrophysiology of different cell-free expressed ion channels by direct incorporation in lipid bilayers**

  The focus of this study was to achieve single channel measurements of CF expressed ion channels without purification. This was achieved with KcsA, a pH gated ion channel, and the pore domain of the voltage-gated ion channel hERG, which were both found to spontaneously self-insert (section 2.3.2) into interdroplet bilayers directly from the CF mixture for electrophysiological measurements. It would therefore be useful to determine whether this phenomenon can also be observed with different ion channels, particularly voltage-gated channels that are relevant to medical research.

- **Investigation of conditions for bilayer incorporation of ion channels from CF mixtures**

  While this study highlighted the spontaneous insertion of ion channels into interdroplet bilayers, the mechanism for bilayer incorporation remains unclear; perhaps ion channels can incorporate with the membrane because it is not completely stable or maybe the presence of the CF system influences the capability of the CF expressed ion channels to self-insert, possibly by surfactant-like properties that destabilise the membrane. It is also feasible that the relatively large bilayer area increases the probability of ion channels randomly fusing with the membrane.

- **Parallel measurements of interdroplet bilayers**

  Recent advances in parallel bilayer platforms, for example Kawano et al. (2013), allow multiple interdroplet bilayers to be measured simultaneously. This is advantageous as it would enable the studies proposed in this section to be investigated more rapidly, while also allowing for more statistically relevant data sets to be obtained. This could be potentially automated using more elaborate versions of the electrokinetic devices shown in Chapter 4 which might include a microfluidic droplet generator, more electrode arrays and integrated Ag/AgCl electrodes for electrophysiological measurements.

7.3 Publications

- Friddin, Mark S., Morgan, Hywel and de Planque, Maurits R.R. (2013) Cell free protein expression systems in microdroplets: stabilization of interdroplet bilayers. *Biomicrofluidics*,7, 014108.

- Friddin, Mark S., Smithers, Natalie P., Beaugrand, Maïwenn, Marcotte, Isabelle, Williamson, Philip T.F., Morgan, Hywel and de Planque, Maurits R.R. (2013) Single-channel electrophysiology of cell-free expressed ion channels by direct incorporation in lipid bilayers. *Analyst*, 138, (24), 7294-7298.

- Friddin, Mark S., Smithers, Natalie P., Lee, Anthony G., Morgan, Hywel and de Planque, Maurits R.R.(2013) Electrophysiology of a cell-free expressed potassium channel in microdroplets without protein purification. *At Advances in Microfluidics and Nanofluidics (AMN2013), Notre Dame, Indiana, US, 24 - 26 May 2013*. Selected as oral presentation but conference not attended.

- Friddin, Mark S., Smithers, Natalie P., Lee, Anthony G., Morgan, Hywel and de Planque, Maurits R.R.(2013) Ion channel characterization with microdroplets of protein expression mixtures. *At 7th IEEE International Conference on Nano/Molecular Medicine and Engineering (IEEE-NANOMED 2013), Phuket, TH, 10 - 13 Nov 2013.*

- Friddin, Mark S., Smithers, Natalie P., Lee, Anthony G., Morgan, Hywel and de Planque, Maurits R.R. (2012) Cell-free expression and electrophysiological measurements of the KcsA channel with interdroplet bilayers. At NanoBioTech 2012, Montreux, CH, 12 - 14 Nov 2012

References

Abraham, M. R., Jahangir, A., Alekseev, A. E., Terzic, A., 1999. Channelopathies of inwardly rectifying potassium channels. FASEB J 13 (14), 1901–10.

Aghdaei, S., 2011. Electrodynamic droplet actuation for lab on a chip system. Ph.D. thesis, University of Southampton, Electronics and Computer Science.

Aghdaei, S., Sandison, M. E., Zagnoni, M., Green, N. G., Morgan, H., 2008. Formation of artificial lipid bilayers using droplet dielectrophoresis. Lab Chip 8 (10), 1617–20.

Aimon, S., Manzi, J., Schmidt, D., Larrosa, J. A. P., Bassereau, P., Toombes, G., 2011. Functional reconstitution of a voltage-gated potassium channel in giant unilamellar vesicles. PLOS ONE 10, 0025529.

Alfaifi, B. Y., 2013. Interdroplet bilayers for ion channel electrophysiology. Master's thesis, University of Southampton, Electronics and Computer Science.

Angenendt, P., Nyarsik, L., Szaflarski, W., Glokler, J., Nierhaus, K. H., Lehrach, H., Cahill, D. J., Lueking, A., 2004. Cell-free protein expression and functional assay in nanowell chip format. Anal Chem 76 (7), 1844–9.

Asmild, M., Oswald, N., Krzywkowski, K. M., Friis, S., Jacobsen, R. B., Reuter, D., Taboryski, R., Kutchinsky, J., Vestergaard, R. K., Schrder, R. L., Srensen, C. B., Bech, M., Korsgaard, M. P. G., Willumsen, N. J., 2003. Upscaling and automation of electrophysiology: Toward high throughput screening in ion channel drug discovery. Receptors and Channels 9 (1), 49–58.

Baranov, V. I., Spirin, A. S., 1993. Gene expression in cell-free system on preparative scale. Methods Enzymol 217, 123–42.

Bayley, H., Cronin, B., Heron, A., Holden, M. A., Hwang, W. L., Syeda, R., Thompson, J., Wallace, M., 2008. Droplet interface bilayers. Mol Biosyst 4 (12), 1191–208.

Berrier, C., Guilvout, I., Bayan, N., Park, K. H., Mesneau, A., Chami, M., Pugsley, A. P., Ghazi, A., 2011. Coupled cell-free synthesis and lipid vesicle insertion of a functional oligomeric channel mscl mscl does not need the insertase yidc for insertion in vitro. Biochim Biophys Acta 1808 (1), 41–6.

Berrier, C., Park, K. H., Abes, S., Bibonne, A., Betton, J. M., Ghazi, A., 2004. Cell-free synthesis of a functional ion channel in the absence of a membrane and in the presence of detergent. Biochemistry 43 (39), 12585–91.

Bezanilla, F., 2005. Voltage-gated ion channels. IEEE Trans Nanobioscience 4 (1), 34–48.

Blicher, A., Wodzinska, K., Fidorra, M., Winterhalter, M., Heimburg, T., 06 2009. The temperature dependence of lipid membrane permeability, its quantized nature, and the influence of anesthetics. Biophysical journal 96 (11), 4581–4591.

Byrne, R., Levin, J., Bladen, H., Nirenberg, M., 1964. The in vitro formation of a dna-ribosome complex. Proceedings of the National Academy of Sciences of the United States of America 52 (1), 140.

Celesia, G. G., 2001. Disorders of membrane channels or channelopathies. Clinical Neurophysiology 112 (1), 2 – 18.

Cens, T., Charnet, P., 2007. Use of xenopus oocytes to measure ionic selectivity of pore-forming peptides and ion channels. In: Molnar, P., Hickman, J. (Eds.), Patch-Clamp Methods and Protocols. Vol. 403 of Methods in Molecular Biology. Humana Press, pp. 287–302.

Chakrapani, S., Cordero-Morales, J. F., Perozo, E., 2007. A quantitative description of kcsa gating ii: single-channel currents. J Gen Physiol 130 (5), 479–96.

Chekulayeva, M. N., Kurnasov, O. V., Shirokov, V. A., Spirin, A. S., 2001. Continuous-exchange cell-free protein-synthesizing system: synthesis of hiv-1 antigen nef. Biochem Biophys Res Commun 280 (3), 914–7.

Cortes, D. M., Cuello, L. G., Perozo, E., 2001. Molecular architecture of full-length kcsa: Role of cytoplasmic domains in ion permeation and activation gating. The Journal of General Physiology 117 (2), 165–180.

Craig, D., Howell, M. T., Gibbs, C. L., Hunt, T., Jackson, R. J., 1992. Plasmid cdna-directed protein synthesis in a coupled eukaryotic in vitro transcription-translation system. Nucleic Acids Res 20 (19), 4987–95.

Creasy, M. A., Leo, D. J., 2010. Non-invasive measurement techniques for measuring properties of droplet interface bilayers. Smart Materials and Structures 19 (9), 094016 (7 pp.)–094016 (7 pp.).

Cuello, L. G., Jogini, V., Cortes, D. M., Perozo, E., 2010. Structural mechanism of c-type inactivation in k+ channels. Nature 466 (7303), 203–208.

Cuello, L. G., Romero, J. G., Cortes, D. M., Perozo, E., 1998. ph-dependent gating in the streptomyces lividans k+ channel. Biochemistry 37 (10), 3229–3236.

Curran, M. E., Splawski, I., Timothy, K. W., Vincen, G., Green, E. D., Keating, M. T., 1995. A molecular basis for cardiac arrhythmia: {HERG} mutations cause long {QT} syndrome. Cell 80 (5), 795 – 803.

Curtis, H., Cole, K., 1940. Membrane action potentials from the squid giant axon. Journal of Cellular and Comparative Physiology 15, 147–157.

Curtis, H., Cole, K., 1942. Membrane resting and action potentials from the squid giant axon. Journal of Cellular and Comparative Physiology 19, 135–144.

de Planque, M. R., Aghdaei, S., Roose, T., Morgan, H., 2011. Electrophysiological characterization of membrane disruption by nanoparticles. ACS nano 5 (5), 3599–3606.

de Planque, M. R. R., Mendes, G. P., Zagnoni, M., Sandison, M. E., Fisher, K. H., Berry, R., Watts, A., Morgan, H., 2006. Controlled delivery of membrane proteins to artificial lipid bilayers by nystatin-ergosterol modulated vesicle fusion. Nanobiotechnology, IEE Proceedings - 153 (2), 21–30.

Demarche, S., Sugihara, K., Zambelli, T., Tiefenauer, L., Voros, J., 2011. Techniques for recording reconstituted ion channels. Analyst 136, 1077–1089.

DeVries, J. K., Zubay, G., 1967. Dna-directed peptide synthesis. ii. the synthesis of the alpha-fragment of the enzyme beta-galactosidase. Proceedings of the National Academy of Sciences of the United States of America 57 (4), 1010.

Doyle, D. A., Cabral, J. M., Pfuetzner, R. A., Kuo, A., Gulbis, J. M., Cohen, S. L., Chait, B. T., MacKinnon, R., 1998. The structure of the potassium channel: Molecular basis of k+ conduction and selectivity. Science 280 (5360), 69–77.

Dunlop, J., Bowlby, M., Peri, R., Vasilyev, D., Arias, R., 2008. High-throughput electrophysiology: an emerging paradigm for ion-channel screening and physiology. Nat Rev Drug Discov 7 (4), 358–68.

Farre, C., Stoelzle, S., Haarmann, C., George, M., Brggemann, A., Fertig, N., 2007. Automated ion channel screening: patch clamping made easy. Expert Opinion on Therapeutic Targets 11 (4), 557–565.

Fertig, N., Meyer, C., Blick, R. H., Trautmann, C., Behrends, J. C., 2001. Microstructured glass chip for ion-channel electrophysiology. Phys Rev E Stat Nonlin Soft Matter Phys 64 (4 Pt 1), 040901.

Finkel, A., Wittel, A., Yang, N., Handran, S., Hughes, J., Costantin, J., 2006. Population patch clamp improves data consistency and success rates in the measurement of ionic currents. Journal of Biomolecular Screening 11 (5), 488–496.

Freischmidt, A., Meysing, M., Liss, M., Wagner, R., Kalbitzer, H. R., Horn, G., 2010. Limiting factors of the translation machinery. Journal of Biotechnology 150 (1), 44 – 50.

Friddin, M. S., Morgan, H., de Planque, M. R. R., 2013a. Cell-free protein expression systems in microdroplets: Stabilization of interdroplet bilayers. Biomicrofluidics 7 (1), 014108.

Friddin, M. S., Smithers, N. P., Beaugrand, M., Marcotte, I., Williamson, P. T. F., Morgan, H., de Planque, M. R. R., 2013b. Single-channel electrophysiology of cell-free expressed ion channels by direct incorporation in lipid bilayers. Analyst 138, 7294–7298.

Friddin, M. S., Smithers, N. P., Lee, A. G., Morgan, H., de Planque, M. R., 2013c. Electrophysiology of a cell-free expressed potassium channel in microdroplets without purification. At advances in Microfluidics and Nanofluidics, Notre Dame, Indiana, USA.(Selected for oral presentation but not attended).

Friddin, M. S., Smithers, N. P., Lee, A. G., Morgan, H., de Planque, M. R. R., 2012. Cell-free expression and electrophysiological measurements of the kcsa channel with interdroplet bilayers. At NanoBioTech 2012, Montreux, CH, 12-14 Nov.

Friddin, M. S., Smithers, N. P., Lee, A. G., Morgan, H., de Planque, M. R. R., 2013d. Ion channel characterization with microdroplets of cell-free expression mixtures. At 7th IEEE International Conference on Nano/Molecular Medicine and Engineering, Phuket, Thailand, 10-13 November 2013.

George, A. L., 8 2005. Inherited disorders of voltage-gated sodium channels. The Journal of Clinical Investigation 115 (8), 1990–1999.

Goren, M. A., Nozawa, A., Makino, S., Wrobel, R. L., Fox, B. G., 2009. Cell-free translation of integral membrane proteins into unilamelar liposomes. Methods Enzymol 463, 647–73.

Hahn, G. H., Asthana, A., Kim, D. M., Kim, D. P., 2007. A continuous-exchange cell-free protein synthesis system fabricated on a chip. Anal Biochem 365 (2), 280–2.

Hardin, J., Bertoni, G. P., Kleinsmith, L. J., 2011. Becker's World of the Cell. Pearson; 8 edition.

He, M., Taussig, M. J., 2001. Single step generation of protein arrays from dna by cell-free expression and in situ immobilisation (pisa method). Nucleic Acids Res 29 (15), E73–3.

He, M., Wang, M. W., 2007. Arraying proteins by cell-free synthesis. Biomol Eng 24 (4), 375–80.

Heginbotham, L., LeMasurier, M., Kolmakova-Partensky, L., Miller, C., 1999. Single streptomyces lividans k+ channels: Functional asymmetries and sidedness of proton activation. The Journal of General Physiology 114 (4), 551–560.

Heron, A. J., Thompson, J. R., Mason, A. E., Wallace, M. I., 2007. Direct detection of membrane channels from gels using water-in-oil droplet bilayers. J Am Chem Soc 129 (51), 16042–7.

Hille, B., 2001. Ion Channels of Excitable Membranes. Sinauer Associates, Inc.; 3rd Edition edition.

Hirano, M., Onishi, Y., Yanagida, T., Ide, T., 2011. Role of the kcsa channel cytoplasmic domain in ph-dependent gating. Biophysical Journal 101 (9), 2157 – 2162.

Hodgkin, A., A.F, H., 1945. Resting and action potentials in single nerve fibres. Journal of Physiology 2, 176–195.

Hodgkin, A., A.F, H., Katz, B., 1952. Measurement of current-voltage relations in the membrane of the giant squid axon of loligo. Journal of Physiology 116, 424–428.

Holden, M. A., Needham, D., Bayley, H., 2007. Functional bionetworks from nanoliter water droplets. Journal of the American Chemical Society 129 (27), 8650–8655.

Hovijitra, N. T., Wuu, J. J., Peaker, B., Swartz, J. R., 2009. Cell-free synthesis of functional aquaporin z in synthetic liposomes. Biotechnol Bioeng 104 (1), 40–9.

Hughes, M. P., 2000. Ac electrokinetics: applications for nanotechnology. Nanotechnology 11 (2), 124.

Hwang, W. L., Chen, M., Cronin, B., Holden, M. A., Bayley, H., 2008. Asymmetric droplet interface bilayers. J Am Chem Soc 130 (18), 5878–9.

Ide, T., Ichikawa, T., 2005. A novel method for artificial lipid-bilayer formation. Biosens Bioelectron 21 (4), 672–7, ide, Toru Ichikawa, Takehiko Evaluation Studies England Biosensors & bioelectronics Biosens Bioelectron. 2005 Oct 15;21(4):672-7. Epub 2005 Jan 26.

Jacobson, K., Sheets, E. D., Simson, R., 1995. Revisiting the fluid mosaic model of membranes. Science 268 (5216), 1441–1442.

Jiang, Y., Lee, A., Chen, J., Ruta, V., Cadene, M., Chait, Brian, T., Mackinnon, R., 2003. X-ray structure of a voltage-dependent k+ channel. Nature 423, 33–41.

John, V. H., Dale, T. J., Hollands, E. C., Chen, M. X., Partington, L., Downie, D. L., Meadows, H. J., Trezise, D. J., 2007. Novel 384-well population patch clamp electrophysiology assays for ca2+-activated k+ channels. Journal of Biomolecular Screening 12 (1), 50–60.

Junge, F., Haberstock, S., Roos, C., Stefer, S., Proverbio, D., Dotsch, V., Bernhard, F., 2011. Advances in cell-free protein synthesis for the functional and structural analysis of membrane proteins. N Biotechnol 28 (3), 262–71.

Junge, F., Schneider, B., Reckel, S., Schwarz, D., Dotsch, V., Bernhard, F., 2008. Large-scale production of functional membrane proteins. Cell Mol Life Sci 65 (11), 1729–55.

Kalmbach, R., Chizhov, I., Schumacher, M. C., Friedrich, T., Bamberg, E., Engelhard, M., 2007. Functional cell-free synthesis of a seven helix membrane protein: in situ insertion of bacteriorhodopsin into liposomes. J Mol Biol 371 (3), 639–48.

Katzen, F., 2008. Cell-free protein expression of membrane proteins using nanolipoprotein particles. Biotechniques 45 (2), 190.

Katzen, F., Chang, G., Kudlicki, W., 2005. The past, present and future of cell-free protein synthesis. Trends Biotechnol 23 (3), 150–6.

Katzen, F., Peterson, T. C., Kudlicki, W., 2009. Membrane protein expression: no cells required. Trends Biotechnol 27 (8), 455–60.

Kawano, R., Tsuji, Y., Sato, K., Osaki, T., Kamiya, K., Hirano, M., Ide, T., Miki, N., Takeuchi, S., 2013. Automated parallel recordings of topologically identified single ion channels. Scientific Reports 3.

Khnouf, R., Beebe, D. J., Fan, Z. H., 2009. Cell-free protein expression in a microchannel array with passive pumping. Lab Chip 9 (1), 56–61.

Khnouf, R., Olivero, D., Jin, S., Coleman, M. A., Fan, Z. H., 2010. Cell-free expression of soluble and membrane proteins in an array device for drug screening. Anal Chem 82 (16), 7021–6.

Kiehn, J., Lacerda, A. E., Wible, B., Brown, A. M., 1996. Molecular physiology and pharmacology of herg: Single-channel currents and block by dofetilide. Circulation 94 (10), 2572–2579.

Kigawa, T., Yabuki, T., Matsuda, N., Matsuda, T., Nakajima, R., Tanaka, A., Yokoyama, S., 2004. Preparation of escherichia coli cell extract for highly productive cell-free protein expression. J Struct Funct Genomics 5 (1-2), 63–8.

Kim, H.-C., Kim, D.-M., 2009. Methods for energizing cell-free protein synthesis. Journal of Bioscience and Bioengineering 108 (1), 1 – 4.

Kinpara, T., Mizuno, R., Murakami, Y., Kobayashi, M., Yamaura, S., Hasan, Q., Morita, Y., Nakano, H., Yamane, T., Tamiya, E., 2004. A picoliter chamber array for cell-free protein synthesis. J Biochem 136 (2), 149–54.

Kistler, J., Stroud, R., 1981. Crystalline arrays of membrane-bound acetylcholine receptor. Proceedings of the National Academy of Sciences 6, 3678–3682.

Kitta, M., Tanaka, H., Kawai, T., 2009. Rapid fabrication of teflon micropores for artificial lipid bilayer formation. Biosens Bioelectron 25 (4), 931–4.

Klammt, C., Schwarz, D., Fendler, K., Haase, W., Dotsch, V., Bernhard, F., 2005. Evaluation of detergents for the soluble expression of alpha-helical and beta-barrel-type integral membrane proteins by a preparative scale individual cell-free expression system. FEBS J 272 (23), 6024–38.

Klein, S. A., Wilk, S. J., Thornton, T. J., Posner, J. D., 2008. Formation of nanopores in suspended lipid bilayers using quantum dots. Journal of Physics: Conference Series 109 (1), 012022.

Kuschel, M., 2000. Protein sizing and analysis using the agilent 2100 bioanalyzer and protein 200 labchip® kit. Agilent Technologies, 1–8.

Kutluay, E., Roux, B., Heginbotham, L., 2005. Rapid intracellular {TEA} block of the kcsa potassium channel. Biophysical Journal 88 (2), 1018 – 1029.

Laemmli, U., 1970. Cleavage of structural proteins during the assembly of the head of bacteriophage t4. Nature 227, 680–685.

Lamborg, M. R., Zamecnik, P. C., 1960. Amino acid incorporation into protein by extracts of *E. coli*. Biochimica et biophysica acta 42, 206–211.

Laszlo, K., Bennett, P. B., Uebele, V. N., Koblan, K. S., Kane, S. A., Neagle, B., Schroeder, K., 2003. High throughput ion-channel pharmacology: Planar-array-based voltage clamp. ASSAY and Drug Development Technologies 1, 127–135.

Laub, K. R., Witschas, K., Blicher, A., Madsen, S. B., Lckhoff, A., Heimburg, T., 2012. Comparing ion conductance recordings of synthetic lipid bilayers with cell membranes containing {TRP} channels. Biochimica et Biophysica Acta (BBA) - Biomembranes 1818 (5), 1123 – 1134.

Le Pioufle, B., Suzuki, H., Tabata, K. V., Noji, H., Takeuchi, S., 2008. Lipid bilayer microarray for parallel recording of transmembrane ion currents. Anal Chem 80 (1), 328–32.

Lederman, M., Zubay, G., 1967. Dna-directed peptide synthesis i. a comparison of t_2 and *Escherichia coli* dna-directed peptide synthesis in two cell-free systems. Biochimica et Biophysica Acta (BBA)-Nucleic Acids and Protein Synthesis 149 (1), 253–258.

LeMasurier, M., Heginbotham, L., Miller, C., 2001. Kcsa: It's a potassium channel. The Journal of General Physiology 118 (3), 303–314.

Long, S., Tao, Xiao, C. B. E., Mackinnon, R., 2007. Atomic structure of a voltage-dependent k^+ channel in a lipid membrane-like environment. Nature 450, 376–382.

Long, S. B., Campbell, E. B., MacKinnon, R., 2005. Crystal structure of a mammalian voltage-dependent shaker family k^+ channel. Science 309 (5736), 897–903.

Maramont, G., 1949. Studies on the axon membrane; a new method. Journal of Physiology 34, 351–382.

Marius, P., de Planque, M. R., Williamson, P. T., 2012. Probing the interaction of lipids with the non-annular binding sites of the potassium channel kcsa by magic-angle spinning nmr. Biochimica et Biophysica Acta (BBA)-Biomembranes 1818 (1), 90–96.

Marius, P., Zagnoni, M., Sandison, M. E., East, J. M., Morgan, H., Lee, A. G., 2008. Binding of anionic lipids to at least three nonannular sites on the potassium channel kcsa is required for channel opening. Biophysical journal 94 (5), 1689–1698.

Martín, M., Albanesi, D., Alzari, P. M., de Mendoza, D., 2009. Functional¡ i¿ in vitro¡/i¿ assembly of the integral membrane bacterial thermosensor desk. Protein expression and purification 66 (1), 39–45.

Mathes, C., 2006. Qpatch: the past, present and future of automated patch clamp. Expert Opinion on Therapeutic Targets 10 (2), 319–327, pMID: 16548779.

Matthaei, H., Nirenberg, M. W., 1961. The dependence of cell-free protein synthesis in e. coli upon rna prepared from ribosomes. Biochem Biophys Res Commun 4, 404–8.

Matthies, D., Haberstock, S., Joos, F., Dtsch, V., Vonck, J., Bernhard, F., Meier, T., 2011. Cell-free expression and assembly of {ATP} synthase. Journal of Molecular Biology 413 (3), 593 – 603.

McQuillen, K., Roberts, R. B., Britten, R. J., 1959. Synthesis of nascent protein by ribosomes in escherichia coli. Proceedings of the National Academy of Sciences of the United States of America 45 (9), 1437.

Mei, Q., Fredrickson, C. K., Jin, S., Fan, Z. H., 2005. Toxin detection by a miniaturized in vitro protein expression array. Analytical chemistry 77 (17), 5494–5500.

Mei, Q., Khnouf, R., Simon, A., Fan, Z. H., 2010. Protein synthesis in a device with nanoporous membranes and microchannels. Lab on a Chip 10 (19), 2541–2545.

Montal, M., Mueller, P., 1972. Formation of bimolecular membranes from lipid monolayers and a study of their electrical properties. Proceedings of the National Academy of Sciences 69 (12), 3561–3566.

Moritani, Y., Nomura, S.-i. M., Morita, I., Akiyoshi, K., 2010. Direct integration of cell-free-synthesized connexin-43 into liposomes and hemichannel formation. FEBS Journal 277 (16), 3343–3352.

Neher, E., Sakmann, B., 1976. Single-channel currents recorded from membrane of denervated frog muscle fibres. Nature 260 (5554), 799–802.

Noireaux, V., Bar-Ziv, R., Godefroy, J., Salman, H., Libchaber, A., 2005. Toward an artificial cell based on gene expression in vesicles. Phys Biol 2 (3), P1–8.

Noireaux, V., Libchaber, A., 2004. A vesicle bioreactor as a step toward an artificial cell assembly. Proc Natl Acad Sci U S A 101 (51), 17669–74.

Noireaux, V., Maeda, Y. T., Libchaber, A., 2011. Development of an artificial cell, from self-organization to computation and self-reproduction. Proc Natl Acad Sci U S A 108 (9), 3473–80.

Overington, John, P., Al-Lazikani, B., Hopkins, Andrew, L., 2006. How many drug targets are there? Nature Reviews Drug Discovery 5, 993–996.

OShaughnessy, T., Hu, J., Kulp, JohnL., I., Daly, S., Ligler, F., 2007. Laser ablation of micropores for formation of artificial planar lipid bilayers. Biomedical Microdevices 9 (6), 863–868.

Patnaik, R., Swartz, J., et al., 1998. E. coli-based in vitro transcription/translation: in vivo-specific synthesis rates and high yields in a batch system. Biotechniques 24 (5), 862–868.

Periasamy, A., Shadiac, N., Amalraj, A., Garajov, S., Nagarajan, Y., Waters, S., Mertens, H. D., Hrmova, M., 2013. Cell-free protein synthesis of membrane (1,3)-β-d-glucan (curdlan) synthase: Co-translational insertion in liposomes and reconstitution in nanodiscs. Biochimica et Biophysica Acta (BBA) - Biomembranes 1828 (2), 743 – 757.

Peterman, M. C., Ziebarth, J. M., Braha, O., Bayley, H., Fishman, H. A., Bloom, D. M., 2002. Ion channels and lipid bilayer membranes under high potentials using microfabricated apertures. Biomedical Microdevices 4 (3), 231–236.

Piccolino, M., 1998. Animal electricity and the birth of electrophysiology: the legacy of luigi galvani. Brain Research Bulletin 46 (5), 381 – 407.

Poulos, J. L., Nelson, W. C., Jeon, T. J., Kim, C. J., Schmidt, J. J., 2009. Electrowetting on dielectric-based microfluidics for integrated lipid bilayer formation and measurement. Applied Physics Letters 95 (1).

Poulos, J. L., Portonovo, S. A., Bang, H., Schmidt, J. J., 2010. Automatable lipid bilayer formation and ion channel measurement using sessile droplets. J Phys Condens Matter 22 (45), 454105.

Price, C. E., Kocer, A., Kol, S., van der Berg, J. P., Driessen, A. J., 2011. In vitro synthesis and oligomerization of the mechanosensitive channel of large conductance, mscl, into a functional ion channel. FEBS letters 585 (1), 249–254.

Promega, 2009. E.Coli T7 S30 Extract System for Circular DNA. Promega Corporation, 2800 Woods Hollow Road, Madison, WI 53711-5399. USA.

Proverbio, D., Roos, C., Beyermann, M., Orbn, E., Dtsch, V., Bernhard, F., 2013. Functional properties of cell-free expressed human endothelin a and endothelin b receptors in artificial membrane environments. Biochimica et Biophysica Acta (BBA) - Biomembranes 1828 (9), 2182 – 2192.

Punnamaraju, S., Steckl, A. J., 2011. Voltage control of droplet interface bilayer lipid membrane dimensions. Langmuir 27 (2), 618–26.

Rigaud, J.-L., Levy, D., Mosser, G., Lambert, O., 1998. Detergent removal by non-polar polystyrene beads. European Biophysics Journal 27 (4), 305–319.

Robelek, R., Lemker, E. S., Wiltschi, B., Kirste, V., Naumann, R., Oesterhelt, D., Sinner, E.-K., 2007. Incorporation of in vitro synthesized gpcr into a tethered artificial lipid membrane system. Angewandte Chemie International Edition 46 (4), 605–608.

Roberts, R. B., 1958. Microsomal particles and protein synthesis. Pergamon Press.

Rogers, N., 2010. The structure of a voltage gated potassium channel. Ph.D. thesis, University of Southampton, School of Biological Sciences.

Roos, C., Kai, L., Proverbio, D., Ghoshdastider, U., Filipek, S., Dötsch, V., Bernhard, F., 2013. Co-translational association of cell-free expressed membrane proteins with supplied lipid bilayers. Molecular membrane biology 30 (1), 75–89.

Ruta, V., Jiang, Youxing, Lee, A., Chen, J., Mackinnon, R., 2003. Functional analysis of an archaebacterial voltage-dependent k+ channel. Nature 422, 180–185.

Sandison, M. E., Morgan, H., 2005. Rapid fabrication of polymer microfluidic systems for the production of artificial lipid bilayers. Journal of Micromechanics and Microengineering 15 (7), S139.

Sanguinetti, M. C., Tristani-Firouzi, M., 2006. herg potassium channels and cardiac arrhythmia. Nature 440, 463–469.

Sarles, S. A., Leo, D. J., 2010a. Physical encapsulation of droplet interface bilayers for durable, portable biomolecular networks. Lab Chip 10, 710–717.

Sarles, S. A., Leo, D. J., 2010b. Regulated attachment method for reconstituting lipid bilayers of prescribed size within flexible substrates. Analytical Chemistry 82 (3), 959–966.

Schindler, H., 1980. Formation of planar bilayers from artificial or native membrane vesicles. FEBS Letters 122 (1), 77–79.

Schmidt, D., Cross, S. R., MacKinnon, R., 2009. A gating model for the archeal voltage-dependent k+ channel kvap in {DPhPC} and pope:popg decane lipid bilayers. Journal of Molecular Biology 390 (5), 902 – 912.

Schmidt, D., Jiang, Q.-X., Mackinnon, R., 2006. Phospholipids and the origin of cationic gating charges in voltage sensors. Nature 444, 775–779.

Schmidt, D., MacKinnon, R., 2008. Voltage-dependent k+ channel gating and voltage sensor toxin sensitivity depend on the mechanical state of the lipid membrane. Proceedings of the National Academy of Sciences 105 (49), 19276–19281.

Schow, E. V., Freites, J. A., Nizkorodov, A., White, S. H., Tobias, D. J., 2012. Coupling between the voltage-sensing and pore domains in a voltage-gated potassium channel. Biochimica et Biophysica Acta (BBA) - Biomembranes 1818 (7), 1726 – 1736.

Schrempf, H., Schmidt, O., Kummerlen, R., Hinnah, S., Muller, D., Betzler, M., Steinkamp, T., Wagner, R., 1995. A prokaryotic potassium ion channel with two predicted transmembrane segments from streptomyces lividans. The EMBO Journal 21, 5170–5178.

Schroeder, K., Neagle, B., Trezise, D. J., Worley, J., 2003. Ionworks ht: A new high-throughput electrophysiology measurement platform. Journal of Biomolecular Screening 8 (1), 50–64.

Schwarz, D., Dotsch, V., Bernhard, F., 2008. Production of membrane proteins using cell-free expression systems. Proteomics 8 (19), 3933–46.

Schweet, R., Lamfrom, H., Allen, E., 1958. The synthesis of hemoglobin in a cell-free system. Proceedings of the National Academy of Sciences of the United States of America 44 (10), 1029.

Seddon, A. M., Curnow, P., Booth, P. J., 2004. Membrane proteins, lipids and detergents: not just a soap opera. Biochimica et Biophysica Acta (BBA) - Biomembranes 1666 (12), 105 – 117.

Sigworth, F. J., 2 1994. Voltage gating of ion channels. Quarterly Reviews of Biophysics 27, 1–40.

Sobhanifar, S., Reckel, S., Junge, F., Schwarz, D., Kai, L., Karbyshev, M., Lohr, F., Bernhard, F., Dotsch, V., 2010. Cell-free expression and stable isotope labelling strategies for membrane proteins. J Biomol NMR 46 (1), 33–43.

Spirin, A. S., 2004. High-throughput cell-free systems for synthesis of functionally active proteins. Trends Biotechnol 22 (10), 538–45.

Spirin, A. S., Swartz, J. R., 2008. Cell-free protein synthesis : methods and protocols. Wiley-VCH, Weinheim.

Studer, A., Demarche, S., Langenegger, D., Tiefenauer, L., 2011. Integration and recording of a reconstituted voltage-gated sodium channel in planar lipid bilayers. Biosensors and Bioelectronics 26 (5), 1924 – 1928.

Suzuki, H., Tabata, K., Kato-Yamada, Y., Noji, H., Takeuchi, S., 2004. Planar lipid bilayer reconstitution with a micro-fluidic system. Lab Chip 4 (5), 502–5.

Syeda, R., Holden, M. A., Hwang, W. L., Bayley, H., 2008. Screening blockers against a potassium channel with a droplet interface bilayer array. J Am Chem Soc 130 (46), 15543–8.

Tao, H., Santa Ana, D., Guia, A., Huang, M., Ligutti, J., Walker, G., Sithiphong, K., Chan, F., Guoliang, T., Zozulya, Z., et al., 2004. Automated tight seal electrophysiology for assessing the potential herg liability of pharmaceutical compounds. Assay and drug development technologies 2 (5), 497–506.

Thompson, J. R., Heron, A. J., Santoso, Y., Wallace, M. I., 2007. Enhanced stability and fluidity in droplet on hydrogel bilayers for measuring membrane protein diffusion. Nano Lett 7 (12), 3875–8.

Tissieres, A., Schlessinger, D., Gros, F., 1960. Amino acid incorporation into proteins by escherichia coli ribosomes. Proceedings of the National Academy of Sciences of the United States of America 46 (11), 1450.

van Dalen, A., van der Laan, M., Driessen, A. J., Killian, J., de Kruijff, B., 2002. Components required for membrane assembly of newly synthesized k+ channel kcsa. {FEBS} Letters 511 (13), 51 – 58.

Vandenberg, J. I., Perry, M. D., Perrin, M. J., Mann, S. A., Ke, Y., Hill, A. P., 2012. herg k+ channels: Structure, function, and clinical significance. Physiological Reviews 92 (3), 1393–1478.

Varnier, A., Kermarrec, F., Blesneac, I., Moreau, C., Liguori, L., Lenormand, J. L., Picollet-Dhahan, N., 2010. A simple method for the reconstitution of membrane proteins into giant unilamellar vesicles. Journal of Membrane Biology 233 (1-3), 85–92.

Warmke, J. W., Ganetzky, B., 1994. A family of potassium channel genes related to eag in drosophila and mammals. Proceedings of the National Academy of Sciences 91 (8), 3438–3442.

Whittaker, J., 2013. Cell-free protein synthesis: the state of the art. Biotechnology Letters 35 (2), 143–152.

Woodbury, D. J., 1999. Nystatin/ergosterol method for reconstituting ion channels into planar lipid bilayers. Methods Enzymol 294, 319–39.

Woodbury, D. J., Miller, C., 1990. Nystatin-induced liposome fusion. a versatile approach to ion channel reconstitution into planar bilayers. Biophys J 58 (4), 833–9.

Xu, J., Guia, A., Rothwarf, D., Huang, M., Sithiphong, K., Ouang, J., Tao, G., Wang, X., Wu, L., 2003. A benchmark study with seal chip planar patch-clamp technology. Assay and drug development technologies 1 (5), 675–684.

Yamamoto, T., Fujii, T., Nojima, T., 2002. Pdms-glass hybrid microreactor array with embedded temperature control device. application to cell-free protein synthesis. Lab Chip 2 (4), 197–202.

Yildiz, A. A., Kang, C., Sinner, E.-K., 2013. Biomimetic membrane platform containing herg potassium channel and its application to drug screening. Analyst.

Zagnoni, M., Sandison, M. E., Marius, P., Morgan, H., 2009. Bilayer lipid membranes from falling droplets. Anal Bioanal Chem 393 (6-7), 1601–5.

Zawada, J., 2012. Preparation and testing of e. coli s30 in vitro transcription translation extracts. In: Douthwaite, J. A., Jackson, R. H. (Eds.), Ribosome Display and Related Technologies. Vol. 805 of Methods in Molecular Biology. Springer New York, pp. 31–41.

Zou, A., Curran, M. E., Keating, M. T., Sanguinetti, M. C., 1997. Single herg delayed rectifier k+ channels expressed in xenopus oocytes. American Journal of Physiology - Heart and Circulatory Physiology 272 (3), H1309–H1314.

Zubay, G., 1973. In vitro synthesis of protein in microbial systems. Annual review of genetics 7 (1), 267–287.